

For Reference

NOT TO BE TAKEN FROM THIS ROOM

Ex libris
UNIVERSITATIS
ALBERTAENSIS



BRUCE PEEL SPECIAL COLLECTIONS LIBRARY
UNIVERSITY OF ALBERTA LIBRARY

REQUEST FOR DUPLICATION

I wish a photocopy of the thesis by

LAW, TEAN CHIE (author)

entitled DEFORMATIONS OF EARTH DAMS DURING CONSTRUCTION

The copy is for the sole purpose of private scholarly or scientific study and research. I will not reproduce, sell or distribute the copy I request, and I will not copy any substantial part of it in my own work without permission of the copyright owner. I understand that the Library performs the service of copying at my request, and I assume all copyright responsibility for the item requested.



Digitized by the Internet Archive
in 2021 with funding from
University of Alberta Libraries

<https://archive.org/details/Law1975>

THE UNIVERSITY OF ALBERTA

RELEASE FORM

NAME OF AUTHOR TEAN-CHIE LAW.....

TITLE OF THESIS DEFORMATIONS OF EARTH DAMS DURING
CONSTRUCTION.....

DEGREE FOR WHICH THESIS WAS PRESENTED Ph.D......

YEAR THIS DEGREE GRANTED 1975.....

Permission is hereby granted to THE UNIVERSITY OF
ALBERTA LIBRARY to reproduce single copies of this
thesis and to lend or sell such copies for private,
scholarly or scientific research purposes only.

The author reserves other publication rights, and
neither the thesis nor extensive extracts from it may
be printed or otherwise reproduced without the author's
written permission.

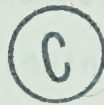
THE UNIVERSITY OF ALBERTA

FACULTY OF GRADUATE STUDIES AND RESEARCH

DEFORMATIONS OF EARTH DAMS

DURING CONSTRUCTION

by



TEAN-CHIE LAW

A THESIS

SUBMITTED TO THE FACULTY OF GRADUATE STUDIES AND RESEARCH
IN PARTIAL FULFILMENT OF THE REQUIREMENTS FOR THE DEGREE
OF DOCTOR OF PHILOSOPHY

DEPARTMENT OF CIVIL ENGINEERING

EDMONTON, ALBERTA

FALL, 1975

THE UNIVERSITY OF ALBERTA
FACULTY OF GRADUATE STUDIES AND RESEARCH

The undersigned certify that they have read, and recommend to the Faculty of Graduate Studies and Research for acceptance, a thesis entitled "Deformations of Earth Dams During Construction " submitted by Tean-Chie Law in partial fulfilment of the requirements for the degree of Doctor of Philosophy in Civil Engineering.

IN MEMORY OF MY WIFE

ABSTRACT

The thesis deals with finite element analysis of deformations and stresses during constructions of earth dams. Mica dam in British Columbia, Canada was used as a prototype model for the study. Particular attention was given to important geotechnical factors that influence results of such types of analysis.

Laboratory studies on stress-strain behaviour, pore pressure response and drainage characteristics of compacted soils were conducted under high pressures. The studies showed that water content, density and gradation of the material have considerable effects on their behaviour. Under the high pressures used it was observed the degree of grain breakage of the core material was relatively small.

The importance of considering stress path dependency of stress-strain behaviour of soil in deformation analysis is discussed. Analysis with elastic moduli derived from conventional triaxial test data overestimated the field deformations. Stress path followed in oedometer test described closely the field condition in Mica Dam as indicated by the close agreement between analytical solutions and measured deformations.

In addition to two parameters used in isotropy theory, three more elastic parameters are required to describe the cross-anisotropic behaviour of compacted soil. Comparison of

analyses with isotropic and anisotropic elastic parameters showed that the calculated deformations for a model dam did not differ greatly. It was indicated that the isotropic theory can be used satisfactorily in deformation analysis for the range of anisotropic properties expected in compacted soil.

The influence of relative stiffness between core and shells on the core settlement was studied. The important role played by load transfer in nonhomogeneous dams was indicated. Unfavourable low stresses in the core as the result of significant load transfer between soft core and stiff shells were discussed. Significant differences could result between the pore pressure analyses with and without considering load transfer in nonhomogeneous dam.

Pore pressures in the core partially dissipated during construction of earth dams. Procedures for analyzing construction deformations including those associated with pore pressure dissipation were developed. The usefulness of the procedures in practice was tested by analyzing the deformations in Mica Dam. Reasonably good agreement was obtained between analytical results and observed behaviour.

ACKNOWLEDGEMENTS

The investigations reported in this thesis were carried out at the Department of Civil Engineering, University of Alberta, under the supervision of Professor Z. Eisenstein. The author is indebted to Professor Z. Eisenstein for his continued guidance, support, and encouragement throughout the period of this study.

Sincerest thanks are expressed to Professor N. R. Morgenstern, Professor D. W. Murray and Dr. A. V. G. Krishnayya with whom the author had many stimulating and highly rewarding discussions. The suggestions given by Professor S. Thomson on the form and presentation of the thesis are greatly appreciated.

The author is grateful to CASECO Consultants for providing access to the detailed field data of Mica Dam and to British Columbia Hydro Power Authority for permission to use these data in this study.

Thanks are due to Messrs. J. V. Simmons and W. D. Roggensack for their discussions and assistance with various aspects related to the research. The assistance of Mr. S. Tan in the preparation of the thesis is appreciated.

The assistance of Messrs. A. Muir, O. Wood, G. Cyre and R. F. Howells of the Department of Civil Engineering in the experimental and computational work is gratefully acknowledged.

The author is grateful to the University of Alberta and National Research Council of Canada for providing him financial support throughout the period of the study.

The research work reported in this thesis has been carried out under a Special Project Grant from the National Research Council of Canada.

The thesis was typed by Mrs. Marilyn Wahl, whose careful work is appreciated.

The author wishes to express his most sincere gratitude to his parents for their continued encouragement.

Thanks are due to the staff in Student Union's Day Care Center for providing the necessary care to his son, and especially thanks to Mrs. Dianne Dalley, the director of the center, for her assistance in the arrangement. Without their help, this study would not have been possible.

TABLE OF CONTENTS

CHAPTER		PAGE
I	INTRODUCTION	1
	1.1 The Need for Predicting Deformation . . .	1
	1.2 Significance of the Study	2
	1.3 Possible Consequences of Deformation in Earth and Rockfill Dams	3
	1.4 Modes of Deformations in Earth and Rockfill Dams	5
	1.5 Brief Review of Previous Studies	6
	1.6 Purposes of the Present Investigation . .	10
	1.7 Outline of the Thesis	11
II	LABORATORY STUDIES ON STRESS-STRAIN BEHAVIOR OF SOILS	17
	2.1 Introduction	17
	2.2 Brief Review of Constitutive Models . . .	19
	2.3 Formulations of Stress-Strain Behavior .	28
	2.4 Stress Path Dependency of Stress-Strain Behavior	32
	2.5 Derivation of Elastic Moduli	33
	2.6 The Need for High Pressure Tests	37
	2.7 Experimental Equipment	38
	2.7.1 Oedometer Compression Cell	38
	2.7.2 Isotropic Compression Cell	41
	2.7.3 Kneading Compactor	43
	2.7.4 Recording System	44

CHAPTER	PAGE
2.8 Description of the Soil Tested	44
2.9 Sample Preparation	47
2.10 Laboratory Tests	48
2.10.1 Compression Tests Performed . .	48
2.10.2 Oedometer Compression Partial Dissipation Test	51
2.10.3 Oedometer Compression Drained Test	53
2.10.4 Isotropic Compression Partial Dissipation Test	54
2.11 Some Aspects of Stress-Strain Relationships	54
2.11.1 Effective Stress in Compacted Soil	54
2.11.2 Total Stress-Strain Relationship	55
2.11.3 Parameters for the Stress-Strain Functions	56
2.12 Discussion of Test Results	58
III SOME FACTORS INFLUENCING STRESSES AND DEFORMATIONS	95
3.1 Scope	95
3.2 Settlement Profile in a Dam During Construction	95
3.3 Finite Element Stress-Deformation Analysis	98
3.4 Load Transfer in a Zoned Dam During Construction	100
3.5 The Use of Two Dimensional Analyses in Deformation Studies	104
3.6 Deformations and Relative Stiffnesses Between Core and Shells	107
3.7 Principal Stress Ratios in a Dam	109

CHAPTER		PAGE
	3.8 The Influence of Anisotropy on Embankment Stresses and Displacements	110
	3.8.1 Stress-Strain Relationships for Anisotropic Soil	111
	3.8.2 Bounding Values on Elastic Parameters	116
	3.8.2 Anisotropic Analysis of a Model Dam	117
	3.8.4 Results of the Analyses	118
IV	PORE PRESSURE AND EFFECTIVE STRESS ANALYSES	136
	4.1 Introduction	136
	4.2 A Brief Review of Methods for Estimating Construction Pore Pressures	137
	4.3 Finite Element Pore Pressure Analysis .	139
	4.4 Considerations of \bar{B} and C_v in the Pore Pressure Analyses	141
	4.5 The Influence of Load Transfer on Construction Pore Pressure	144
	4.6 Consideration of Possible Treatment of Total Deformations	148
	4.7 Discussion of the Assumption of Constant Total Stress During Consolidation . . .	150
	4.8 Effective Stress Analysis of Earth Dam During Construction	152
	4.9 The Accuracy of Procedure Used in Effective Stress Analyses	156
V	ANALYSIS OF DEFORMATIONS IN MICA DAM	168
	5.1 Introduction	168
	5.2 General Description of the Dam	168
	5.3 Field Control Data of Placement Materials	171

CHAPTER	PAGE
5.4 Instrumentation of the Dam	172
5.5 Observed Behaviour During Construction .	174
5.5.1 Effects of Upstream and Down Stream Water Level	174
5.5.2 Bedrock Settlements	176
5.5.3 Pore Pressures in the Dam	177
5.5.4 Embankment Deformations	180
5.6 Finite Element Idealization	182
5.7 Analyses Based on Triaxial Test Data . .	183
5.7.1 Derivation of the Moduli	183
5.7.2 Results of the Analyses and Their Implication	188
5.8 Analyses Based on Oedometer and Isotropic Compression Test Data	190
5.8.1 Total Stress Analysis	190
5.8.2 Analysis of Construction Pore Pressure	193
5.8.3 Effective Stress Analysis	196
5.9 Results of Analyses Based on Oedometer and Isotropic Compression Test Data . .	198
5.9.1 Embankment Deformations	198
5.9.2 The Influences of Bedrock Movements	200
5.9.3 Load Transfer in the Dam	201
5.9.4 Construction Pore Pressures . . .	203
VI CONCLUSIONS AND RECOMMENDATIONS FOR FURTHER RESEARCH	262
6.1 Conclusions	262

CHAPTER	PAGE
6.1.1 Stress-Strain Behaviour of Compacted Soil	263
6.1.2 Pore Pressure Response and Drain- age Chacteristic of Compacted Soil	264
6.1.3 The Simulation of Field Material	264
6.1.4 The Consideration of Stress Path Dependency	265
6.1.5 Anisotropy of a Soil and Dam Deformation	265
6.1.6 Load Transfer in the Zoned Dam .	266
6.1.7 Pore Pressure Dissipation and Deformation During Construction	268
6.2 Recommendations for Further Research .	268
BIBLIOGRAPHY	271
APPENDICES	283
APPENDIX A: LABORATORY TEST RESULTS	284
APPENDIX B: FINITE ELEMENT COMPUTER PROGRAM FOR TOTAL OR EFFECTIVE STRESS ANALYSIS	311
B.1: Description of the Program . .	311
B.2: Input Data Procedure	313
B.3: Listing of Program	325
APPENDIX C: DETAILS OF MV GAUGE INSTALLATION AND FIELD BEDROCK MOVEMENT DATA	348
APPENDIX D: DERIVATION OF EMBANKMENT SETTLE- MENT EXCLUDING THE BEDROCK MOVEMENT	359
APPENDIX E: HYPERBOLIC STRESS-STRAIN RELATION- SHIP PROGRAM	362

LIST OF TABLES

TABLE		PAGE
1.1	Summary of Core Material Properties and Placement Procedures for Some Major Rockfill Dams	13
1.2	Summary of Methods of Placement of Rockfill for Some Major Rockfill Dam	14
1.3	Relationship Between Embankment Compression and Soil Type	15
2.1	Summary of Compression Tests Performed . . .	49
2.2	Test Results of Sample OW-3	57
2.3	\bar{B} values determined from Oedometer Compression Partial Dissipation Tests	63
2.4	C_v Values Determined from Oedometer Compression Partial Dissipation Tests	65
3.1	Values of Elastic Parameters for Anisotropy Analyses	122
5.1	Basic Data for Mica Dam	205
5.2	Statistics for Water Content and Density in Mica Dam	206
5.3	Representation of Dam Fill from Material Used in Triaxial Test	207
5.4	Values of Hyperbolic Stress-Strain Parameters Used in the Analysis	208
5.5	Poisson's Ratios Used in Total and Effective Stress Analyses	209
5.6	\bar{B} values Used in the Analysis	210
5.7	Comparison of C_v values Derived from Various Tests	211
5.8	Comparison Between r_u and \bar{B}	212

LIST OF FIGURES

FIGURE		PAGE
1.1	Modes of Load Transfer	16
2.1	Illustration of Elastic Moduli Derivation . .	70
2.2	Oedometer Compression Cell	71
2.3	Set-up for Oedometer Compression Test	72
2.4	Isotropic Compression Cell	73
2.5	Set-up for Deformation Measurements in Isotropic Compression Cell	74
2.6	General View of Kneading Compaction Machine .	75
2.7	Close-up View of the Specimen During Compaction	75
2.8	Grain Size Distribution Curves for Mica Till Tested	76
2.9	Water Content-Density Relationship for Mica Till for Different Compaction Tests	77
2.10	Comparison of Compaction Methods	78
2.11	Set-up for Isotropic Compression Test	79
2.12	Total Stress-Strain Curve for the Analysis . .	80
2.13	Determination of Parameters for Oedometer Compression Stress-Strain Function	81
2.14	Variation of Stiffness With Water Content for Mica Till in Oedometer Compression Test . . .	82
2.15	The Influence of Gradation on Stress-Strain Behaviour of Mica Till	83
2.16	Variation of Stiffness with Maximum Grain Size for Mica Till in Oedometer Compression Test .	84
2.17	Grain Size Curves for Mica Till Before and After High Pressure Oedometer Compression Test . . .	85

FIGURE		PAGE
2.18	Comparison of Stress-Strain Curves for Mica Till with Modified Proctor and Kneading Compactions at Low Water Content	86
2.19	Comparison of Stress-Strain Curves for Mica Till with Standard Proctor and Kneading Compactions at High Water Content	87
2.20	Comparison on Predicted and Experimental Stress-Strain Curves of Till with Low Water Content	88
2.21	Comparisons on Predicted and Experimental Stress-Strain Curves of Till with High Water Content	89
2.22	Coupling Effective Stress-Strain Curves of Mica Till with Low Water Content	90
2.23	Coupling Effective Stress-Strain Curves of Mica Till with High Water Content	91
2.24	Coupling Total Stress-Strain Curves of Mica Till with Low Water Content	92
2.25	Coupling Total Stress-Strain Curves of Mica Till with High Water Content	93
2.26	Ratios of Lateral Strain to Vertical Strain in Isotropic Compression Tests	94
3.1	Broad Continuously Placed Fill	123
3.2	Settlement Profile of a Continuously Placed Fill	123
3.3	Settlement Curves at Various Stages of Construction	124
3.4	Finite Element Idealization of a Zoned Dam .	125
3.5	Maximum Major Principal Stresses Near the Base of the Core for Different Ratios of Moduli of Core to Shell	126
3.6	Maximum Settlements in the Center of the Core for Different Ratios of Moduli of Core to Shell	127
3.7	Maximum Outward Displacements of the Slope Surface for Different Ratios of Moduli of Core to Shell	128

FIGURE		PAGE
3.8	Stress Paths for Soil Elements in a Dam During Construction	129
3.9	Axial Stress-Strain Curves of a Soil Under Different Types of Compression	130
3.10	Finite Element Idealization of a Model Dam . .	131
3.11	The Influence of G_v on Embankment Displacements and Shear Stresses	132
3.12	The Influence of E_H on Embankment Displacements and Shear Stresses	133
3.13	The Influence of v_{HH} on Embankment Displacements and Shear Stresses	134
3.14	The Combined Influence of E_H and v_{HH} on Embankment Displacements and Shear Stresses	135
4.1	Pore Pressure Set-Up in the Center of an Earth Dam During Construction	158
4.2	Pore Pressure Set-Up in the Center of the Core During Construction ($E_{shell} = 5E_{core}$; $E_{shell} = 10E_{core}$)	159
4.3	Pore Pressure Profiles in Central Core at the End of Construction for Different Degrees of Load Transfer	160
4.4	Scheme of Possible Treatment of Total Deformation in Finite Element Analysis	161
4.5	Scheme of Analysis of Consolidation Movements	162
4.6	Height Versus Time Relationship Used in the Analysis	163
4.7	Analysis Procedures for Newly Placed Layer . .	164
4.8	Analysis Procedures for Every Additional Layer	165
4.9	Rectangular Clay Core With Side Drains	166

FIGURE		PAGE
4.10	The rate of Surface Settlement for Rectangular Core With Two-Dimensional Pore Pressure Dissipation	167
5.1	Location of Mica Dam	213
5.2	General Arrangement of Mica Dam	214
5.3	Fill Arrangement in Mica Dam	215
5.4	Embankment Construction Progress in 1969, Mica Dam	216
5.5	Embankment Construction Progress in 1970, Mica Dam	217
5.6	Embankment Construction Progress in 1971, Mica Dam	218
5.7	Embankment Construction Progress in 1972, Mica Dam	219
5.8	Variation of Fill Elevation at Mica Dam Core With Time	220
5.9	Statistical Gradation Envelopes for Till and Sand and Gravel in Mica Dam	221
5.10	Location of Vertical and Near-Vertical Movement Gauges	222
5.11	Piezometric Observations in Shells and River Overburden	223
5.12	Piezometric Observations in Core Foundation	224
5.13	Bedrock Movements as the Boundary Displacements in the Analysis of Mica Dam	225
5.14	Locations of Piezometers in the Core of Mica Dam	226
5.15	Piezometric Observations in the Core	227
5.16	The Variations of Pore Pressure With Overburden Pressure in Mica Dam	228

FIGURE		PAGE
5.17	Settlement Profiles Measured in MV8 at the Beginning and the End of Shutdown Seasons . .	229
5.18	Settlement Profiles Measures in MV15 at the Beginning and the End of Shutdown Seasons . .	230
5.19	Vertical Stress-Strain Relationship for Sand and Gravel in Zone M2	231
5.20	Vertical Stress-Strain Relationships for River Overburden Sand	232
5.21	Vertical Stress-Strain Relationship for Sand and Gravel in Zone M2DI	233
5.22	Finite Element Idealization of Mica Dam for 2D Analyses	234
5.23	Gradation Curves of Materials Used in Triaxial Tests	235
5.24	Drained Triaxial Stress-Strain Relationships for Sand and Gravel in Zone M2	236
5.25	Drained Triaxial Stress-Strain Relationships for River Overburden Sand	237
5.26	Drained Triaxial Stress-Strain Relationships for Sand and Gravel in Zone M2DI	238
5.27	Consolidated Undrained Triaxial Stress-Strain Relationships for Mica Till at Optimum Water Content	239
5.28	Undrained Triaxial Stress-Strain Relationships for Mica Till at Modified Optimum Water Content	240
5.29	Settlements Calculated with Triaxial Test Data for MV8 and MV9, Mica Dam	241
5.30	Settlements Calculated with Triaxial Test Data for MV10 and MV5, Mica Dam	242
5.31	Settlements Calculated with Triaxial Test Data for MV11 and MV12, Mica Dam	243
5.32	Horizontal Movements Calculated with Triaxial Test Data	244

FIGURE		PAGE
5.33	Stress-Strain Curves for Core in Total Stress Analysis	245
5.34	Stress-Strain Curves Used in Total and Effective Stress Analysis for Sand and Gravel	246
5.35	C_v Determined from Triaxial Dissipation Tests for Mica Till	247
5.36	Direct Permeability Test Results for Mica Till	248
5.37	Variation of Core Fill Elevation with Time in the Analysis	249
5.38	Stress-Strain Curves for Core in Effective Analysis	250
5.39	Settlements from Total and Effective Stress Analysis for MV8 and MV9	251
5.40	Settlements from Total and Effective Stress Analyses for MV10, MV11 and MV12	252
5.41	Settlements from Total and Effective Stress Analyses for MV5 and MV7	253
5.42	Calculated Horizontal Movements in Mica Dam .	254
5.43	Overburden Stresses and Calculated Major Principal Stresses on a Horizontal Plane in Mica Dam	255
5.44	Major Principal Stresses Calculated for the Center of the Core of Mica Dam	256
5.45	The Influences of Bedrock Settlements on the Calculated Embankment Settlements	257
5.46	The Influences of Bedrock Settlements on the Calculated Horizontal Movements	258
5.47	Major Principal Stresses Calculated from 2D and 3D Analyses for the Core	259
5.48	Hydraulic Fracture Mechanism Postulated by Kjaernsli and Torblaa (1968)	259

FIGURE		PAGE
5.49	Observed and Calculated Pore Pressure for PE24, PE25 and PE26	260
5.50	Observed and Calculated Pore Pressures for PP21 and PP20	261

CHAPTER I

INTRODUCTION

1.1 The Need for Predicting Deformations

In the application of soil mechanics, a distinction is commonly made between deformation problems and failure problems. Deformation problems are those requiring the computation of the displacements which the soil mass will exhibit under a given load. In the case of failure problems, attention is directed primarily to the ultimate shear failure of the soil.

In the past, most soil bodies or soil structures with complex interactions have been designed against failure. Without knowing the complex constitutive relationships of the soil, the geotechnical engineer can conveniently perform limit equilibrium analyses and obtain a factor of safety which will ensure that only some fraction of the available shear strength is mobilized. While the consideration of displacements is excluded from the limit equilibrium analysis, the deformations are still controlled empirically by the factor of safety (Morgenstern, 1968).

The distinction between deformation problems and failure problems is actually artificial. The major aim of all design calculations is essentially the limitation or control of the displacements of the soil mass. The most

rational approach to the design would be based upon displacements since either local or overall displacements limit the utility of an engineering structure. Moreover, displacements can be measured directly in the field. The control and measurement of stresses may be regarded as an indirect approach to the displacements and failure may be considered as an extreme displacement condition.

Before design criteria, in terms of allowable displacements and related stresses, can be developed for a variety of problems a better understanding of general stress-strain behavior of soils is necessary.

1.2 Significance of the Study

With the increasing widespread acceptance and adaptation of rockfill concepts, a greater degree of diversification developed in design and construction practices of dams. The type of materials that comprise the core sections of water retaining embankments also vary within wide limits. As a consequence of this the physical properties of the material included in the zones of an embankment may vary widely from, one dam to another. The differences in the physical properties of materials placed in various dams and in the methods of placement are evident in Tables 1.1 and 1.2.

Because of the preceding factors there is an increasing need to improve our understanding of the behavior of dams. The effect on the behavior of differences in the stress-strain relationships including compressibility properties of

the materials, in an embankment are of particular concern. Different stress-strain properties of various materials in an embankment, in addition to other factors, may result in relative displacements and in a transfer of load from one material to another or from one location to another. The occurrence and effects of load transfer need to be understood not only for design, but also for an evaluation of the behaviour of the embankment during critical construction periods. Advancement in our understanding of the factors which influence the behaviour of embankments can only be made from an analysis and interpretation of data obtained from instruments installed in dams.

1.3 Possible Consequences of Deformation in Earth and Rockfill Dams

Sherard et al. (1963) have summarized some of the major courses which lead to the failure or damage of a dam, among which cracking has been considered as important. Cracking of several earth and rockfill dams and in some cases, subsequent failures caused by erosion of soil through the cracks have been reported in the literature (Marsal and Ramirez, 1967; Patrick 1967; Pope 1967; Gordon and Duguid, 1970). The development of most type of cracks is the result of excessive deformation or differential settlement which occurred in the dam. Because of the nature of earth and rockfill dams, materials of different compressibility have been used within the dam. As a result, the problems due to

differential settlement are pronounced. Detailed studies have been done by Covarrubias (1969), Lowe (1970) and Krishnayya (1973(a)), hence no attempt will be made in this thesis to classify cracks in earth and rockfill dams.

In order to illustrate the close correlation between deformation and cracking, the formation of certain types of cracks are briefly described as follows:

(a) Transverse cracks are caused by differential settlement between adjacent lengths of the embankment, usually between the portion located at the abutment and the portion in the centre of the valley. The worst cracking develops when the foundation under the higher portions is compressible and the abutments consist of steep and relatively incompressible rock.

(b) Longitudinal cracks are generally produced by two types of differential movement. In dams with rolled-earth cutoffs which are much less compressible than the natural foundation soil underlying the slopes, longitudinal cracking may be caused by the tendency of the slopes to settle more than the crest. Dams with central cores of rolled earth and upstream and downstream shells of dumped quarried rock frequently develop cracks near the crest at the junction between the core and the dumped rock sections because the rock shells continue to compress appreciably after construction while the rolled core does not.

(c) Interior cracks may occur in dams with narrow

vertical central cores of compressible impervious material. During construction the core tends to compress more under the weight of the overlying fill than the shells do, so that a part of the weight of the core is transferred to the shells by shear stresses and arching. Within the core, vertical stresses on horizontal planes at various elevations may be very low. This arching effect combined with variable shear strengths developing on the vertical planes separating the core and shells, can conceivably result in horizontal cracks in the core.

1.4 Modes of Deformations in Earth and Rockfill Dams

Lowe (1972) and Wilson (1973) have described modes of deformations which are of interest to engineers. For completeness the modes of deformations are further classified as follows:

- (a) Classification based on direction
 - (i) Vertical deformation
 - (ii) Upstream-downstream movement (movement normal to the dam axis)
 - (iii) Cross-valley deformation (deformation parallel to the dam axis)
- (b) Classification based on loading condition
 - (i) Deformation under compacted weight of embankment materials (mainly during construction)

- (2) Creep under constant load
- (3) Deformation under water load of reservoir
- (4) Deformation under effect of saturation
- (5) Deformation under rapid drawdown.

In the investigation that forms the basis of this thesis only deformations during construction have been considered.

1.5 Brief Review of Previous Studies

Gould (1953) summarized the compressibility during construction of the impervious sections of more than 20 large earth dams in the Western United States. He noted that for stresses below a value of approximately 100 psi, the compaction water content had the greatest influence on compressibility. Embankments constructed with relatively low average water contents showed low initial strains in the compression curves while those constructed with a water content at or above standard Proctor optimum were characterized by high initial strains. However, for pressures exceeding about 100 psi, he observed that the compressibility was more or less independent of the compaction water content and was governed by the gradation and plasticity of the embankment soil. As seen in Table 1.3, the embankments can be grouped roughly according to their soil properties in order of increasing compressibility. As part of his

observations, Gould also concluded that the compression in the central portions of the dam, where the measuring devices were installed, took place essentially in a vertical direction, as though the material had complete lateral restraint. While this study gave much valuable information, it revealed little about the influence of the type and intensity of the compactive effort on compressibility of the embankment.

Nonveiller and Anagnosti (1961) proposed a plastic equilibrium analysis to study the stresses and deformations in a narrow clay core supported by less compressible rockfill shells. The analysis disregards the stresses and deformations existing under elastic equilibrium conditions, and hence it is less suitable for use in investigating dam behaviour under working loads.

Goodman and Brown (1963) were the first to consider the differences between incremental construction and instantaneous loading in the stress analysis of embankments. They did not, however, evaluate the deformations of the system in their analysis.

Clough and Woodward (1967) used the finite element method to do a comprehensive study on the differences between "switch-on-gravity" and "sequence" analyses. A standard embankment was analyzed by considering it to be constructed in a single lift or in 10 lifts. They found the single step analysis gives a satisfactory approximation to the stresses

in most respects, but the displacements were found to be quite strongly affected by the construction process. The horizontal displacement results were similar in both cases, but the vertical displacements for the two cases demonstrate entirely different deformation mechanisms. The single lift vertical displacements were seen to be largest at the top, due to the fact that these were merely the integrated strains developed over the full height. On the other hand, the incremental analysis showed zero vertical displacement at the top and the maximum vertical displacements at midheight. Clough and Woodward concluded that displacements to be expected during the construction of an embankment can be predicted only if the analysis is carried out sequentially following the construction history. In their analysis, they did not consider pore pressure effects.

Squier (1967) undertook a comprehensive study of deformations measured in four rockfill and earth dams. He noticed that the movements in the core were influenced by load transfer. Various modes of load transfer (Fig. 1.1) may exist in an embankment as a result of a relative displacement between the core and the shells. In the dams of his study, load transfer occurred primarily from the core to the rock shells during and after construction, but prior to reservoir storage. During reservoir storage, because of saturation and displacement of the upstream shell, load transfer occurred from the shell to the core.

Kulhawy et al. (1969) employed nonlinear, stress-displacement, stress-strain relationships for the tangent modulus and tangent Poisson's ratio of embankment materials to study the performance of earth and rockfill dams. The stress-strain parameters required were determined from the results of laboratory triaxial tests with volume change measurements. The effectiveness of the procedure was checked against the measurements in Otter Brook Dam during construction and the observed and calculated movements were found to be in good agreement. Since the stress-strain behavior of soil is also path dependent, this approach may not be used for stress paths deviating significantly from the conventional triaxial stress path.

Penman, et al. (1971) performed finite element analyses to predict the deformations in Scammonden Dam during construction. In their analysis, they employed constant values of Young's modulus and Poisson's ratio. These values were derived from the results of one-dimensional compression tests on the embankment material. Despite the simplification of nonlinear behaviour of the material, the method gave fairly good agreement between the calculated values of settlement and horizontal movement and those measured during construction.

Wilson (1973) reviewed the performances of several earth and rockfill dams and reported that the compressibility of a rockfill increases as the uniformity and average size of

the rock increases, and as the quality of the rock decreases. The compressibility of dumped rockfill is greater than that of compacted rockfill. He suggested in order to minimize the settlement during and after construction, the shells of a dam should be constructed of well graded, unweathered, hard rock or of sand and gravel. The fill should be spread in layers, watered or sluiced, and well compacted.

Lefebvre et al.(1973) investigated the accuracy with which two-dimensional analyses may be used to study stresses and movements in dams in V-shaped valleys. By comparing the results of two-dimensional analyses and of three-dimensional analyses of hypothetical dams in valleys with three different vally-wall slopes, they concluded that for dams in valleys with valley walls inclined at 3:1 or flatter, plane strain analyses of the maximum transverse section will provide reasonably accurate results for both stresses and displacements.

1.6 Purposes of the Present Investigation

A brief review of previous studies in section 1.5 has indicated that a completely satisfactory procedure to deal with deformation problems in earth dams is not yet available. Since a need for certain improvements is obvious, the present investigation was undertaken with the following objectives:

(1) To investigate laboratory procedures to determine the stress-strain relationships of soils which would simulate field conditions and which would be applicable in design practice.

(2) To perform analytical studies that contribute to an understanding of the influence of various factors on deformations and stresses in dams and to verify such studies using the data derived from the observation of a real dam.

(3) To develop a procedure for a more reasonable prediction of the deformations in earth dams during construction.

1.7 Outline of the Thesis

The thesis is organized in following sequence:

Chapter II describes the laboratory studies on the stress-strain behaviour of soils. Investigations of the influence of water content, density (relative to the method of compaction), gradation and maximum grain size on the compressibility of Mica Till are discussed. Compressibility and drainage characteristics of the Mica Till under high pressures are reported. Procedures for obtaining elastic moduli from oedometer and isotropic compression tests are proposed.

Chapter III describes the parametric studies carried out to investigate the relationship between relative magnitude of core and shell moduli and the degree of load transfer

The differences in deformation and stress results obtained from analyses with and without considering anisotropic properties of embankment materials are examined.

Chapter IV describes a procedure developed for analyzing the deformations in earth dams during construction. The influences of the pore pressure dissipation on deformations are considered in the procedure through calculated effective stress changes.

Chapter V illustrates the applicability of the procedure developed in Chapter IV in practice. This is done by verifying it against the case history of a prototype model, namely Mica Dam.

In Chapter VI, the conclusions from the investigations are made.

TABLE 1.1
(After Squier 1967)
SUMMARY OF CORE MATERIAL PROPERTIES AND PLACEMENT PROCEDURES
FOR SOME MAJOR ROCKFILL DAMS

Dam	Type ¹	Country (Date)	Core Material Properties		Placement Procedure	
			Description	Shear Strength C (T/M ²) ϕ		
Gepatsch	cc	Austria (1964)	Talus and Boulder Clay (-No. 200, 15 - 25%)	1.0 29°	$t_i^2 = 30$ cm	40T r-t ³ 6 passes
El Infiernillo	cc	Mexico (1963)	Clay (CL to CH)	7.0 14°	$t_i = 15$ cm	15T Sf ³
Göschenen	cc	Switzerland (1960)	Sand and Gravel and Clay	- 40°	$t_f = 25$ cm	40T r-t 8 passes
Messaure	cc	Sweden (1962)	Moraine	- 45°	$t_i = 25$ cm	Tractor
Miboro	sc	Japan (1960)	Disintegrated Granite and clay	3.0 35°	$t_i = 20$ cm	20T Sf 12 passes
Brownlee	sc	U.S.A. (1958)	Clay (CL)	10-17 17°	$t_i = 15$ cm	Sf 12-16 passes

¹cc - central core sc - sloping core ³r-t = rubber-tired rolled,
²t_i = initial layer thickness, Sf = sheepsfoot
t_f = final layer thickness

TABLE 1.2
(After Squier 1967)
SUMMARY OF METHODS OF PLACEMENT OF ROCKFILL FOR
SOME MAJOR ROCKFILL DAMS

Dam (Height, m)	Type ¹	Country (Date)	Designation	Methods of Placement		Sluiced
				Layer Thickness	Compaction	
Gepatsch (153)	cc	Austria (1964)	Compacted	2m	Vibratory roller 4 passes	no
El Infiernillo (148)	cc	Mexico (1963)	Compacted	1m	D-8 Tractor 4 passes	no
			Dumped	2m	Dumped, spread by tractor	no
Göschenenalp (155)	cc	Switzerland (1960)	Compacted	2 to 3m	Hauling and spreading equipment	no wetted
Messaure (101)	cc	Sweden (1962)	Compacted	1 to 1.5m	Tractors	2:1 ²
Miboro (130)	sc	Japan (1960)	Dumped	4 to 8m	---	3:1
Brownlee (122)	sc	U.S.A. (1958)	Compacted	0.4 to 0.5m	50T r-t ³ , 3 passes	Yes
			Dumped	15 to 45m	---	4:1
² Ratio of volume of water applied to volume of rockfill 3 50 ton rubber-tired roller ¹ cc - central core, sc - sloping core						

TABLE 1.3

(After Gould 1953)

RELATIONSHIP BETWEEN EMBANKMENT COMPRESSION AND SOIL TYPE

Embankment Soil Type	Approximate Range of Measured Compression (Vertical)	
	At 10 psi (%)	At 100 psi (%)
Silty Gravel and Coarse Silty Sand (GM & SM)	0.2 - 0.3	0.9 - 1.4
Fine Silty Sand and Silt of Low Plasticity (SM - ML)	0.2 - 0.5	1.3 - 2.1
Clayey Sands and Gravels (GC - SC)	0.3 - 0.8	1.9 - 3.3
Clay of Low to Medium Plasticity (CL & CL-ML)	0.2 - 1.1	2.8 - 4.2

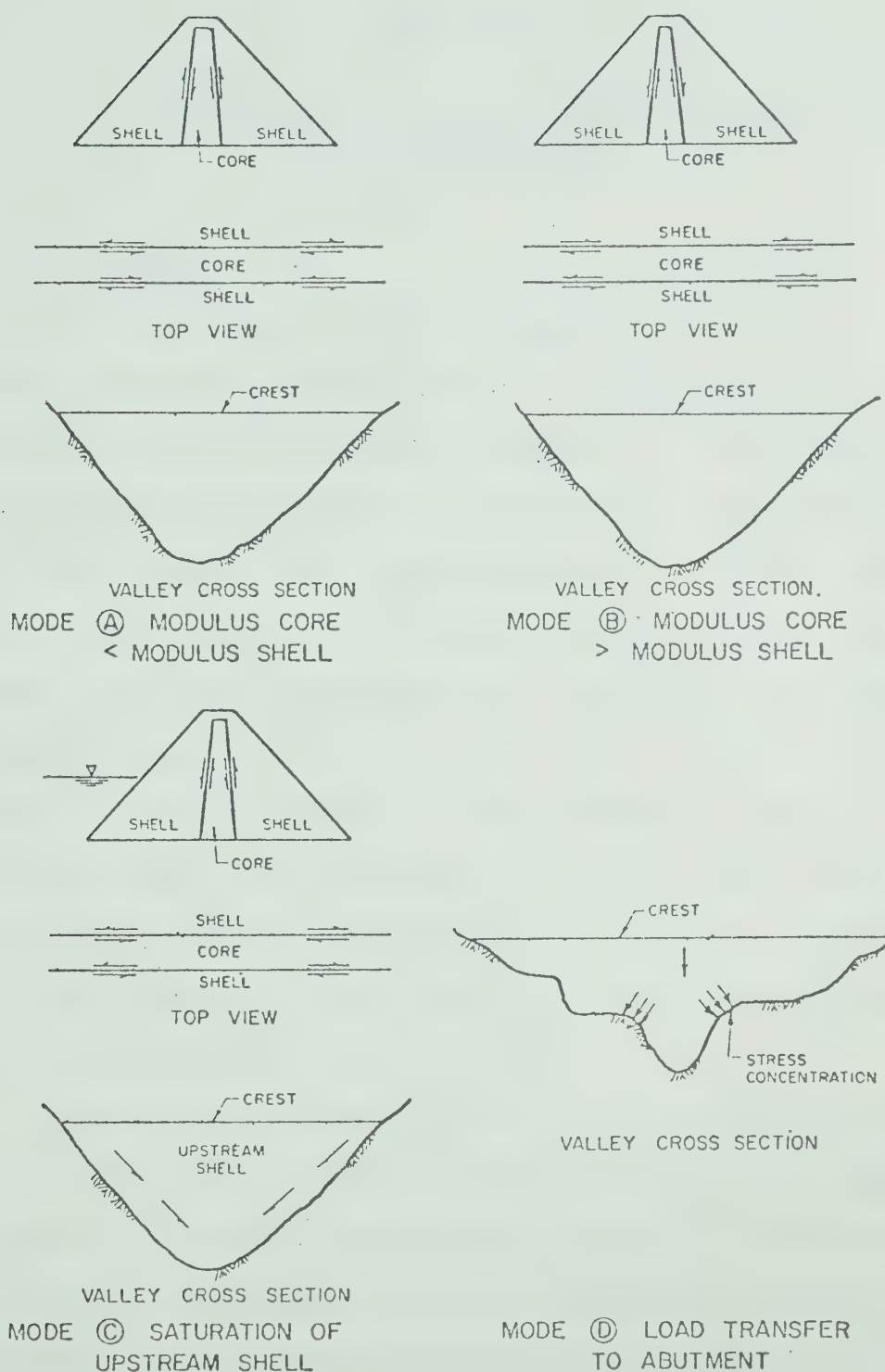


Fig. 1.1 Modes of Load Transfer
(after Squier, 1967)

CHAPTER II

LABORATORY STUDIES ON STRESS-STRAIN BEHAVIOR OF SOILS

2.1 Introduction

In an analysis of the deformation of a soil structure, the most relevant material property to be defined is the stress-strain behavior of the soil. The finite element method, introduced to geotechnical engineering in about 1966, has provided the geotechnical engineer with a powerful analytical tool to solve various deformation problems involving complex boundary conditions and material non-homogeneity. However, the accuracy of predicting soil deformations with the finite element method depends mainly on how accurately the constitutive relationships for the soil involved is modelled. In their state-of-the-art reports Desai (1972), Duncan (1972) and Eisenstein (1974) repeatedly emphasized this point.

As a result of the particulate nature of the skeleton of a soil, the stress-strain behavior is much more complex than those for man-made engineering materials, such as steel and polymers. The amount of strain caused by stress in a soil depends on the composition, void ratio, past stress history of the soil, and the stress path followed during the history of loading. Volume changes also take place due

to factors such as pure shear and rotation of principal stress axes. A general constitutive law which can describe or define behavior of soil under any possible states of stress and deformation is very difficult to derive and is not yet available.

Although a general constitutive law for soils is not yet available, various constitutive models have been proposed by a number of authors. Some of these models are briefly reviewed in this chapter. There are generally two different approaches used in such models: (1) utilizing only elastic theory (2) utilizing plastic theory. In the elastic models, attempts are made mainly to account for nonlinearity observed between stress and strain in soils. The models which use the plasticity approach have more variations which are based mainly on the type of yield function and the type of flow rule. It is interesting to note that the majority of these approaches employ some form of empirical curve fitting process. In nonlinear elastic models, curve fitting is used to simulate the stress-strain curves so that stiffness parameters may be determined at any stress level. In plasticity models a flow rule is usually determined by a curve fitting technique (Audibert, 1972). Because of this curve fitting process and path dependent nature of stress-strain response of soils, the accuracy of describing the deformation behaviour of soil structure with these models, in particular, nonlinear elastic models is highly dependent

on how close the laboratory test simulates the field situation. With the consideration of previous comments, the oedometer compression test was used to study the stress-strain response of Mica Till in this investigation.

It is thought that loading conditions in the core of Mica Dam during construction followed a K_0 (no-lateral-strain) path to a large extent

Although a few plasticity models (Roscoe and Burland, 1968) have been demonstrated that adequately simulate certain classes of soil behavior observed in laboratory tests, no comparison has been made with field observations in dams. The proof of the adequacy of nonlinear elastic approaches has come from the successful use of these models in analyses of observed field behavior (Kulhawy and Duncan, 1970; Eisenstein et al., 1972; Nobari and Duncan, 1972). In view of this, a nonlinear elastic model (or incremental elastic model) is used to describe the soil behavior in this study.

2.2 Brief Review of Constitutive Models

Desai (1972) and Duncan (1972) have reviewed various constitutive models proposed for soils. In this section, an attempt is made to discuss briefly some important aspects of several models; such as the number of parameters needed to define the model and the advantages and limitations of the model.

Linear elastic models. Only two elastic parameters, viz. Young's modulus and Poisson's ratio or bulk modulus and shear modulus, are needed to describe the stress-strain response of a material. The advantage of the model is simplicity of application. However, because the stress-strain response of soil is strongly affected by the state of stresses and strains, it is rather difficult to determine appropriate constant values for the elastic parameters. Despite this limitation, an interesting practical use of the linear elastic model has been demonstrated by Penman et al., (1971), Cole and Burland (1972) and Simmons (1974).

Incremental elastic models using Young's or shear modulus and Poisson's ratio. In these models, the loading sequence is broken into small steps and for each load increment, a linear elastic constitutive law is employed. The elastic modulus is calculated by determining a tangent to a stress-strain curve for a given stress level. Poisson's ratio may be varied as well.

The main achievement of these models is the close simulation of the nonlinear stress-strain response of a soil. The disadvantages are that dilatancy and strain softening behaviour cannot be modelled, since these would require use of a Poisson's ratio greater than 0.5 and a negative modulus respectively. Elastic theory is simply invalid for these two cases.

In the application of the technique just described, several forms of representation of stress-strain curves were employed. These are described briefly as follows:

(a) Bilinear Representation

The actual stress-strain curve of a soil is represented by two straight lines. The soil has a relatively large value of Young's modulus before failure, and a relatively small value (close to zero) after failure. This form of representation has been used in several finite element analyses (e.g. Dunlop, et al. 1968; Dunlop and Duncan, 1970; D'Appalonia and Lambe, 1970; Palmer and Kenney, 1971). The disadvantage of this procedure is that the stresses in some soil elements inevitably are found to exceed the assigned strength values before the value of the modulus is reduced.

(b) Hyperbolic Function Representation

The nonlinear stress-strain curve of soil is represented by a hyperbola approaching a straight asymptote. This hyperbolic representation was proposed by Konder and his co-workers (Konder, 1963; Konder and Zelasko 1963) and subsequently used in finite element analyses by several researchers (e.g. Kulhawy et al., 1969; Duncan and Chang, 1970; Clough and Duncan, 1971). In the procedure, the value of Young's modulus for a given stress level is defined as a tangent to the corresponding hyperbolic curve. In analyses

using this model, the effects of confining pressure on the stress-strain behavior are also introduced. The effects are represented by using empirical equations to express the variations of hyperbolic parameters with confining pressure (Duncan and Chang, 1970).

In this model, tangent Poisson's ratio varying with the stress level was sometimes introduced. By applying a similar formulation procedure as for Young's modulus to the volume change data from triaxial tests, Kulhawy et al. (1969) had used varying tangent Poisson's ratio values in their analyses.

A total of eight parameters is needed to describe completely the variations of tangent Young's modulus and tangent Poisson's ratio. These can all be determined from conventional triaxial tests with volume change measurements.

The advantages of the model are the nonlinear stress-strain behaviour of soil is approximated better than with bilinear representation, and the variations of tangent Poisson's ratio with the stress level may be incorporated into the analysis. The limitation of the model is that it is strictly valid for loading conditions similar to that in conventional triaxial tests and thus a more general path dependency of the stress-strain curve may not be resolved with this model.

(c) Spline Function Representation

A spline function was proposed by Desai (1971) for use in representing the nonlinear stress-strain curve of soil in finite element analyses. The nonlinear tangent Young's modulus and Poisson's ratio were calculated as the first derivatives of the bicubic splines which described the conventional triaxial test data with volume change measurements (Desai and Abel, 1972). While this model has the same limitation as the hyperbolic function model, it exhibits the advantage of being able to represent the actual experimental data to any desired degree of accuracy.

(d) Digital Representation

In the digital representation, a number of closely spaced points on an experimentally obtained stress-strain curve are given as input. The modulus, which is calculated by considering two adjacent points (chord slope), approximates the tangent modulus. Krishnayya (1973(a)) employed this procedure to represent triaxial test results, and hence to determine the nonlinear shear modulus and Poisson's ratio used in the analysis of cracking of earth dams.

The advantage of the procedure is that no approximation is involved in representing the actual stress-strain relationship. Moreover, if the test data are expressed in invariant forms for the derived moduli (Krishnayya, 1973(a)), the procedure may be used for various tests

(e.g. plane strain test, constant stress ratio triaxial test) with stress paths other than the conventional triaxial stress path. The disadvantage of the procedure is that it involves greater computational effort than function representation methods.

Incremental elastic models using bulk modulus and shear modulus. The stress-strain response system in a soil mass, idealized as an elastic body, can generally be separated into two distinct components, namely, volumetric and deviatoric. The volumetric stress and strains, and deviatoric stress and strain are uniquely related by bulk modulus and shear modulus respectively. The use of bulk modulus (K) and shear modulus (G) has the advantage over the use of Young's modulus (E) and Poisson's ratio (ν) is that the distinct behaviour of these two components can be more appropriately characterized. This advantage is even clearer in describing the soil behaviour after failure. The reduction in shear resistance with relatively no change in compressibility behaviour can be conveniently described by a low shear modulus and a constant bulk modulus. However, for the model using E and ν , if the value of E is reduced to represent the soil behaviour after failure while the value of ν is maintained constant, the compressibility of the soil is inevitably overestimated. The models utilizing bulk and shear moduli had been employed by Clough and Woodward (1967) and Girijavallabhan and Mehta (1969) in their finite element analyses, and by Morgenstern and Tamuly Phukan (1969)

in the study of stress-strain behavior of sandstone.

In the study of stress level dependencies of bulk and shear moduli of a sand, Domaschuk and Wade (1969) performed the isotropic compression and pure shear (constant mean normal stress) triaxial compression tests. The same procedure may be useful for obtaining the parameters needed in current stress-strain models. The limitation is that constant mean normal stress triaxial compression tests are not so easily performed as conventional triaxial tests. Unless a servo control mechanism is introduced, continuous attention is needed to maintain constant mean normal stress by reducing σ_3 (cell pressure) and increasing σ_1 during the test.

Audibert (1972) did a comprehensive laboratory testing program to study the capability of the bulk modulus - shear modulus model. It was concluded that the model can adequately describe the soil behaviour under a variety of stress path loadings.

Elasto-plastic models. In these models, generalized Hooke's law is used to describe the stress-strain relationship of soil before yielding. After yielding, it is assumed that the soil becomes perfectly plastic and the principle of normality holds. In order to characterize the behaviour of a general type of soil in which yielding is affected by both deviatoric and volumetric components of stresses, the extended Mohr-Coulomb failure criterion postulated by Drucker and Prager (1952) is usually used.

This yield function takes the following form:

$$f = \alpha J_1 + J_{D2}^{\frac{1}{2}} = k \quad (2.1)$$

where α , k are material constants, J_1 is first stress invariant and J_{D2} is second invariant of stress deviation.

The use of this technique in two dimensional finite element analysis for excavations in rock has been illustrated by Reyes and Deere (1966) and Chang et al. (1972).

The advantage of elasto-plastic models over models reviewed previously is better descriptions of the deformation behaviour after yielding. However, as discussed by Pariseau et al. (1970) because of dependence of yield on the volumetric component of stress and the application of the principle of normality, the models are limited to those materials which increase in volume upon yielding.

Elastic-work hardening plastic models. These models were mainly developed by Roscoe et al. (1958) and Roscoe and Burland (1968) as the results of comprehensive work at Cambridge University in the area of constitutive equations for soils. As of this date, the theories suggested for normally consolidated clays are more advanced than for granular materials. Two models named "Cam Clay" and "Modified Cam Clay" were presented for describing the general stress-strain behaviour of normally consolidated or slightly overconsolidated clays which exhibit a decrease in volume

upon the application of shear. In the Cambridge theory, several assumptions regarding the elastic or recoverable behaviour of clays are made. First, the bulk modulus of a soil is assumed to vary linearly with volumetric stress. Secondly, Roscoe et al (1958) assumed that the soil is rigid-plastic in shear. Third, it is assumed that there is never any recoverable energy associated with shear distortion. As a result, if the stress state of a soil sample lies wholly within an elastic region the only strain that occurs is volumetric.

By comparing these models with other elasticity approaches, it becomes clear that current procedures treat many of the facets of the constitutive behaviour of soil more rigorously. However as far as is known, only Smith and Kay (1971) have introduced these models in finite element formulations and used them to predict the soil behaviour in a laboratory test with reasonable accuracy. No examples are available that shows the use of these models for real earth structures. The ability of these models to describe the soil behaviour in full scale structures is unknown at this time.

2.3 Formulations of Stress-Strain Behaviour

The strains experienced by an element of soil are the result of strain within and relative motions among the many particles forming the element. Formulations of stress-strain behaviour of a soil element have often been based on an understanding of the mechanism of particulate system response to stress. Since some previous studies are considered to be useful in explaining the stress-strain function employed in present investigations they are reviewed in the following paragraphs.

Brandt (1955) studied the behaviour of granular materials under hydrostatic stress by modelling the materials with various packings of spheres. Hertz's contact theory was considered applicable at each contact in these models. The theory (Timoshenko and Goodier, 1957) indicates that the centers of two perfectly linear elastic spheres in contact under a normal force, N , will approach one another by an amount ΔL , given by:

$$\Delta L = 2 \left[\frac{3}{4} \frac{(1-\nu^2)}{E} \frac{N}{R^{\frac{1}{2}}} \right]^{\frac{2}{3}} \quad (2.2)$$

where R is radius of spheres, ν is Poisson's ratio and E is Young's modulus of the material comprising the spheres.

The result of using this theory, was the formulation of a proportional relationship between the volumetric strain in granular material and the two-thirds power of the external hydrostatic pressure. This relationship may be simply

expressed as:

$$\frac{\Delta V}{V} = C P^{\frac{2}{3}} \quad (2.3)$$

where $\Delta V/V$ is the volumetric strain, C is a constant related to the proportion of the material and P is the hydrostatic pressure.

Ko and Scott (1967) performed hydrostatic compression tests on Ottawa sand and studied the validity of Hertz's contact theory. They found the measured volumetric strain, which was believed to be mainly the result of contact deformations between the sand grains, increased less rapidly than the two-thirds power function. It was explained that this behaviour occurred as a result of the increased number of contacts between grains continuously being created as the stress was increased.

In a study regarding the elastic behavior of sand, El-Sohby (1969) postulated that elastic deformation of two elastic bodies in contact was generally proportional to the applied force raised to some power ' m '. The value of m depended mainly on the rate of increase of the area of contact (El-Sohby, 1964). If the rate of increase of contact area was similar to that of point contact between two spheres, $m = \frac{2}{3}$. Based on this postulate he expressed the axial strain, ϵ_{aea} , in a mass of nonyielding and noncrushing particles of sand caused by a raise in axial pressure from σ_{a0} to σ_a as:

$$\epsilon_{aea} = S_{aea} (\sigma_a^m - \sigma_{ao}^m) \quad (2.4)$$

where S_{aea} is elastic compressibility factor in the axial direction and m is the average elastic power factor. Using the same principle as eq. (2.4) for radial elastic strains, the elastic volumetric strains, V_e , under axial symmetry stress conditions was further derived as:

$$V_e = S_{aea} \sigma_{ao}^m \left[\left(\frac{\sigma_a}{\sigma_{ao}} \right)^m - 1 \right] (1 + 2\mu_{ra}) + 2 S_{rer} \sigma_{ro}^m \left[\left(\frac{\sigma_r}{\sigma_{ro}} \right)^m - 1 \right] (1 + \mu_{ar} + \mu_{rr}) \quad (2.5)$$

where μ_{ra} , μ_{ar} , μ_{rr} are coefficients of the functions of packing characteristics, S_{rer} is the elastic compressibility factor in the radial direction, σ_{ro} is the initial radial pressure and σ_r is the radial pressure. For material having equal elastic compressibility factors in three principal directions and stresses under constant stress ratio conditions, a simplified form of equation (2.5) can be obtained. This relationship takes the following form:

$$V_e = S \left(\frac{R^m + 2}{3} \right) \sigma_{ro}^m \left[\left(\frac{P}{P_o} \right)^m - 1 \right] \quad (2.6)$$

$$\text{where } S = 3 S_{aea} (1 + 2\mu_{ra}) = 3 S_{rer} (1 + \mu_{ar} + \mu_{rr})$$

$$R = \frac{\sigma_a}{\sigma_r} = \frac{\sigma_{ao}}{\sigma_{ro}}$$

$$P = \frac{(\sigma_a + 2\sigma_r)}{3}$$

R is constant stress ratio, P is applied mean normal pressure, and P_0 is initially applied mean normal pressure.

In the studies outlined so far, only the volumetric component of total strain was discussed. However, in soil under stress, the total strain generally consists of slip strain which is plastic or irrecoverable strain and elastic strain which is recoverable. A comprehension review regarding the mechanisms of these two strain components was given by Rowe (1971). Taking these two components into consideration, he presented a stress-strain relationship for granular material stressed under an axisymmetrical constant stress ratio condition as follows:

$$\epsilon_{1R} = (1 + f) \left(\frac{\sigma_1'}{E} \right)^m \left[S_1 - 2\mu_{13} S_3 \frac{1}{R^m} \right] \quad (2.7)$$

where ϵ_{1R} is the total major principal strain, σ_1' is effective major principal stress, R is ratio of effective major principal stress to effective minor principal stress, f is ratio of slip strain to elastic strain during constant R stress path, E is Young's modulus of the mineral comprising the soil particle, S_1, S_3 are coefficients of the non-linear elastic strain equation due to a stress change in the principal stress direction 1 or 3 only, μ_{13} is a coefficient which as a function of packing characteristics, and m is an elastic power factor. The coefficients S , μ and m are functions of the soil structure which are usually treated as constants during a stress path. As reported by Rowe (1971), the values of m and S for some

sands such as dense Welland River sand were found not to vary significantly even between tests at different R . Thus, if $R \leq K$ at constant R condition, where $K = \tan^2 \left(45 + \frac{\phi_f'}{2} \right)$ and ϕ_f' is equivalent angle of friction between particles and f is constant for a given material at a particular void ratio, then equation (2.7) can be expressed as:

$$\epsilon_{1R} = C \left(\frac{\sigma_1'}{E} \right)^m \quad (2.8)$$

where

$$C = (1 + f) \left[S_1 - 2\mu_{13} \frac{S_3}{R^m} \right] = \text{constant.}$$

It may be noted that the stress-strain relation in the oedometer test can be expressed by substituting the value of f at $R = \frac{1}{K_0}$ in above equations. For $R > K$ condition, f deviates from being constant and tends to increase with pressure.

2.4 Stress Path Dependency of Stress-Strain Behaviour

The deformation response of soils is path dependent. This fact has been illustrated by Lambe (1969, p. 133, 134) with stress-strain curves obtained from triaxial tests using various loading conditions. For a material with this behaviour, stresses, strains, and deformations should be determined by proper integration along the path of loading. Within a soil mass under load, different elements may undergo different

stress paths. Ideally, tests for determining material parameters should embrace all possible stress paths which would eventually occur. This requirement may be impractical due to the complexity of a general constitutive model and the limitations of testing techniques. Thus, tests following one stress path which can characterize the behaviour of most of the soil mass are usually performed. The importance of considering stress path dependency of the stress-strain behaviour of soil in predicting deformations has been repeatedly emphasized by Lambe (1964), Desai (1972), Duncan (1972) and Eisenstein (1974).

2.5 Derivation of Elastic Moduli

The procedures for deriving nonlinear elastic moduli have been developed and used in analysis by several researchers (Kulhawy et al., 1969, Kirshnayya, 1972(a)). These procedures were essentially established to use conventional triaxial test data. However, in some cases the elastic moduli derived from the tests other than conventional triaxial tests are needed and the previous procedures cannot be directly applied. In the present study, stress-strain behaviour during oedometer compression test is of major interest. Thus, the procedure of deriving moduli from this test has to be developed. Plane strain test was not considered in the present study due to the fact that such apparatus is seldom available in practice. Even if the apparatus is available, high pressure testing is difficult to be performed. Furthermore, due to modern compaction technique the stress state in the major part of the

dam is perhaps closer to that under one-dimensional rather than plane strain condition.

In the oedometer compression test, the elastic moduli of the sample can be completely determined if the radial stress is measured during the test. Bishop and Henkel (1957) have suggested a method of performing one-dimensional compression tests in conventional triaxial cell in which the radial stress could be measured. This procedure is acceptable for a low pressure range but is less ideal for a test with high sustained loading. An oedometer in which the radial stress could be measured during compression under high pressure was presented by Brooker and Ireland (1965). A somewhat similar approach was attempted in the present study, but for simplicity the strain gauge attached to the cell, rather than pressure chamber, was used to measure the radial stress. However, it was found that the radial stress could not be measured as successfully as expected. In order to achieve complete determination of elastic moduli another set of stress-strain relationships is needed. The isotropic compression test on nearly identical samples was therefore used.

From section 2.3, it is clear that the stress-strain relationship in a constant stress ratio test is a power function. Although all the formulations were derived for granular materials, it was thought that for Mica till which contains a small percentage of clay sizes, the same principle might also hold. The general expressions for the oedometer compression test and isotropic compression test results may be presented

as follows:

$$\text{Oedometer compression test: } \epsilon_1 = C_D \left(\frac{\sigma_1'}{P_a} \right)^a \quad (2.9)$$

$$\text{Isotropic compression test: } \epsilon_v = C_K \left(\frac{\sigma'}{P_a} \right)^b \quad (2.10)$$

where ϵ_1 is the vertical strain, ϵ_v is the volumetric strain, σ_1' is the effective vertical stress, σ' is the effective isotropic stress, and C_D , C_K , a , b are constants. The term P_a denoting atmospheric pressure, is introduced so that C_D , C_K are pure numbers. For practical purposes, the constants C_D , C_K , a and b are more conveniently determined from compression test data rather than evaluated from the physical meaning of the components involved in the constants. Equation (2.9) can be transformed into logarithmic form as follows:

$$\log \epsilon_1 = \log C_D + a \log \left(\frac{\sigma_1'}{P_a} \right) \quad (2.11)$$

Constants C_D and a can be easily determined by drawing a straight line through ϵ_1 vs $\left(\frac{\sigma_1'}{P_a} \right)$ data plotted on a log-log scale. A similar procedure can be used to determine C_K and b .

By differentiating equation (2.9), the tangential constant modulus can be expressed as a function of vertical stress as:

$$E_C' = \frac{d\sigma_1'}{d\epsilon_1} = \frac{(P_a)^a}{a C_D} \times \frac{1}{(\sigma_1')^{a-1}} \quad (2.12)$$

Assuming that samples having the same volumetric strains are under the same mean stress, the mean stress corresponding to a given σ_1' in the oedometer compression test can be evaluated by

equating ϵ_1 and ϵ_v in equations (2.9) and (2.10). This assumption describes closely real soil behavior for the case where volumetric strain due to shear is not dominant, for example, dense soil under one-dimensional compression. The applicability of this assumption on the test samples will be discussed in a later section.

The equation which may be used to evaluate the mean stress corresponding to σ_1' can be expressed as follows:

$$\sigma' = p_a \sqrt[b]{\frac{C_D}{C_K} \left(\frac{\sigma_1'}{p_a}\right)^a} \quad (2.13)$$

The tangential bulk modulus as a function of isotropic stress can be obtained by differentiating eq. (2.10).

$$K' = \frac{d\sigma'}{d\epsilon_v} = \frac{(p_a)^b}{b C_K} \times \frac{1}{(\sigma')^{b-1}} \quad (2.14)$$

Using eq. (2.12), (2.13) and (2.14), the effective constrained modulus and bulk modulus at a particular σ_1' stress level can be evaluated. It may be noticed that eq. (2.12) and (2.14) are only valid for non-zero stress states. Subsequently effective Young's modulus and Poisson's ratio can be determined simply from Hooke's law:

$$E' = \frac{9K' (E_C' - K')}{E_C' + 3K'} \quad (2.15)$$

$$\nu' = \frac{3K' - E_C'}{E_C' + 3K'} \quad (2.16)$$

The preceding procedure may be described more clearly by the schematic illustration shown in Fig. 2.1. The results of oedometer and isotropic compression tests on identical samples are presented with a common coordinate for strain. The use of the common coordinate for strain is acceptable because the axial strain (ϵ_1) in an oedometer compression test and volumetric strain (ϵ_v) in an isotropic compression test are both equal to strain invariant, $3\epsilon_{oct}$. In Fig. 2.1, for a known magnitude of effective major principal stress, oa , the tangential constraint modulus, E_c' can be obtained from the tangent to the oedometer compression stress-strain curve presented in the upper quadrant. From the same curve, the axial strain or strain invariant, ob , corresponding to the same stress can be determined. For the same strain the tangential bulk modulus, K' , and the mean stress, oc , which corresponds to the stress level in the oedometer compression test, can be evaluated from the isotropic compression stress-strain curve presented in the lower quadrant.

2.6 The Need for High Pressure Tests

The increasing use of high earth dams requires that soil engineers provide information on the strength-deformation and drainage characteristics of soils under high pressure. In the case of Mica Dam, which rises about 650 ft. above the river bed and some 800 ft. above the lowest point in the underlying bedrock channel, the normal

stresses existing near the base of the embankment are much higher than those usually encountered in soil engineering practice. Since the deformation and drainage characteristics of some soils under high pressure may be significantly different than those under low pressure, it is unreasonable to use information obtained from low pressure tests and extrapolate them to high pressures. It is known that grain breakage causes crushing and leads to strain in addition to the strains occurring in soil with rigid particles. Moreover the coefficient of consolidation may vary with the stress level. High pressure testing is especially important for studying the influence of grain breakage on the stress-strain behaviour of soil and the value of the coefficient of consolidation at high pressures.

2.7 Experimental Equipment

2.7.1 Oedometer Compression Cell

The cell is a modified form of the Rowe consolidation cell (Rowe and Barden, 1966), and is illustrated in Fig. 2.2. The view of the cell during testing is shown in Fig. 2.3. It is designed to test specimens 4 inches in diameter and 4.5 inches in length. Since this is the standard sample size prepared by many available compaction machines, its use avoids the disturbance caused by trimming. The major parts of the cell are constructed with stainless steel in order to minimize the deformation of the cell under high pressures and to prevent the rusting of the parts in contact with water.

The main modification of the cell is the addition of an almost frictionless boundary between the soil and the ring. This is done by adding a teflon sleeve and a greased rubber membrane as shown on Fig. 2.2.

A uniform vertical load is applied to the sample by means of air pressure acting on water or mercury covering the belofram jack. The air pressure generating system is adopted because of the simplicity in operation and maintainence of the pressure as high as 750 psi for a considerable period of time. The required pressure is controlled by an air regulator and the actual pressure is measured by a 2000 psi transducer to an accuracy of 0.5 psi. The disadvantage of the system is its potentially explosive nature. However, by exercising considerable care during the tests avoiding any sudden release of the high pressure, and performing the tests in an isolated room no accident has occurred throughout this investigation. The use of a top chamber filled with water was found effectively to minimize the diffusion of air through the belofram and into the soil. This arrangement was used for most of the tests.

The vertical settlement is measured at the center of the sample by means of a rod attached to the jack and passing out through the top cover to an LVDT. With this set-up, the settlement can be measured to an accuracy of 0.0002 in. Two rolling 'o' rings are used to prevent the leakage through the spacing between the rod and cover and also to provide a frictionless guide during its movement. As a safety precaution,

a dial gauge was sometimes added in order to have immediate detection of any unexpected movement resulting from failure of the pressure system.

Top and base drainage can be controlled through the drainage control valves attached to the base plate and top cover of the cell. The top drainage outlet is provided by a tube sealed through the jack and leading directly to the top drainage control valve. Pore water pressures can be measured at the base with a high air entry ceramic stone. A stone having the same air entry value as those used on the piezometers was installed. The air entry value is 2 bars. In order to have proper comparisons with the observed piezometer readings, the pressures are registered by a transducer connected to the stone and are measured to an accuracy of 0.2 psi. This arrangement provides full control of drainage, undrained pore pressures and back pressures.

There are several important features which make this hydraulic loading system more attractive for the present study. These features are as follows:

(a) It is simpler to provide higher loads for large diameter samples than conventional dead load systems.

(b) The sample is not subject to vibration effects magnified by a lever system.

(c) Drainage can be controlled. The load can be applied with the drain closed, allowing a full development of the undrained pore pressure. The dissipation stage can be started from an equilibrium pore pressure condition at a

chosen time.

(d) Back pressure can be easily applied.

(e) Any change in water content of the test specimen due to evaporation is prevented.

2.7.2 Isotropic Compression Cell

The cell is a standard triaxial cell modified for high pressure testing. It is shown in Fig. 2.4. The conventional transparent perspex cylinder is replaced by a steel cylinder 0.25 in. thick, reinforced with three stainless steel straps.

Due to the high confining pressure used, measurements of the total volume change of the sample, would inevitably encounter some difficulties. The standard volume change indicator with transparent perspex cannot withstand the pressure. In the mercury displacement method, the movement of the mercury surface cannot be viewed with a cathetometer because of the opaque steel cylinder used for the cell. The simplest solution, adopted in this study, was to measure vertical and lateral deformations by LVDTs inside the cell. The lateral strain measuring device used is a modification of the lateral strain indicator described by Bishop and Henkel (1957) for performing compression tests on 4" dia. samples under zero lateral strain. The modification is made by replacing the diaphragm mercury indicator by an L.V.D.T. of 24 volts. A thin wire is tied to the lower end of the core of L.V.D.T. while the upper end is supported by a spring. The relative

movement of two curved metal pads which bear lightly on the surface of the membrane sealing the sample is magnified twice by the hinged ring which embraces the sample and is imparted to the thin wire, stretching across the two ends of the ring. The wire causes a vertical movement of the core of L.V.D.T. equivalent to twice the amount of the lateral displacement of the specimen. The vertical displacement is measured by an L.V.D.T. of 24 volts with the plunger resting on the upper cap of the sample. The vertical and lateral deformations can be measured to an accuracy of 0.00001 and 0.00004 inches respectively. After vertical and lateral strains are obtained the volumetric strain at any pressure may be calculated by adding twice the lateral strain to the vertical strain. A view of deformation measurement set-up on the specimen is shown in Fig. 2.5

Hydraulic oil is used to fill the chamber. Water is not used because it is considered as a conducting medium which may influence the voltage signal once water is forced in the L.V.D.T. gauge under high pressure. As a consequence, standard latex membranes cannot be used since they would deteriorate in contact with the hydraulic oil. Furthermore, latex has insufficient strength to resist the punching effect of the soil particles under high pressure. Membranes comprised of 1/32" thick neoprene were finally used successfully throughout the tests. In order to have the membrane properly sealed on the top cap and at the base, steel

bands pressing the membrane against 'o' rings recessed into grooves around the perimeter of the cap and base were used. Diffusion of air through the membrane is checked by measuring the air pressure built up inside the membrane which enclosed an undeformable dummy sample. No significant build-up pressure was measured for the duration of the tests performed.

Same as in oedometer compression cell, top and base drainage can be controlled. Pore water pressures can be measured at the base in which is 2 bars air entry ceramic stone.

2.7.3 Kneading Compactor

The kneading compactor used in this investigation is a model CS1000 electronic-hydraulic kneading compactor manufactured by Cox and Sons of Sacramento, California. The general view of the machine and the view during soil compaction are shown in Figures 2.6 and 2.7 respectively. The compactor is basically designed for bituminous compaction in which tamper foot heat can be controlled. For embankment material compaction, temperature control is not an important issue, however several other features made this machine attractive. These are:

(a) The ram pressure can be controlled easily and varied from 0 to 1000 psi.

(b) The number of compactive tamps applied to the specimen can be pre-selected and varied.

(c) The amount of time the ram applies pressure to the specimen can be adjusted.

(d) The amount of movement of the table between tamps of the ram can be controlled. Table rotation can be varied from 6° to 72° increments for each 360° of table rotation.

(e) The time interval between tamps of the ram can be adjusted.

Using this compacting device, nearly identical samples can be made at any time if the same initial conditions (moisture content, etc.) are maintained.

2.7.4 Recording System

The voltage outputs from the L.V.D.T.s are scanned, amplified and recorded by an automatic digital voltmeter (Hewlett-Packard Testmobile Model 3440 A with Model 5050B digital recorder). The readings can be taken at intervals of time ranging from one second to one hour. The pressures are measured by transducers and read with strain gauge bridges.

2.8 Description of the Soil Tested

Mica Till, which is the main soil investigated in this study, has the following properties:

Liquid Limit	18%
Plastic Limit	13%
Plasticity Index	5%
Specific Gravity	2.80

The gradation curve for the material passing the 3/4" sieve is shown in Fig. 2.8 and designated as gradation No. 1. As a convenience this designation is also used for natural material passing 3/8" and No. 4 sieves without reworking. The gravel sizes of Mica Till are mainly granitic gneiss and quartz with some friable schist. Mica flakes are present in the fines.

In order to study the influence of gradation, several specimens were prepared from material with gradation No. 2. This gradation curve is also shown in Fig. 2.8. The material consisted of particles smaller than 3/4". The soil was artificially mixed in such a way that the percentages in weight finer than each selected sieve size were the same as those of the mean gradation curve of the core fill.

Water content and density relationships for the till for different compaction tests are shown in Fig. 2.9. In this figure, it is noteworthy that two pairs of average water content and density values measured in three seasons of core fill fall closer to the water content and density relationship for samples compacted by kneading compactor in 7 layers with 70 tamps of 150 psi pressure per layer. The better correlation between kneading compaction method with the field compaction than dynamic (conventional) compaction has been discussed by Wilson (1950) and Zegarra (1958). In his discussion, Zegarra (1958) compared the

line-of-optimums developed in the field compaction tests with sheepsfoot and rubber-tired rollers with those obtained from laboratory compaction tests on the same soil using dynamic compaction and Harvard or kneading compaction. The line-of-optimums was defined as the line which joins the peaks of water content-density curves for the different compaction efforts. From the comparison as shown in Fig. 2.10, he concluded that dynamic compaction indicates less obvious relationship to field compaction curves. By coincidence the highest compaction achieved by dynamic compaction (Modified AASHO) had the same numerical value as field compaction by the heaviest rubber-tired roller at maximum coverage. On the other hand, kneading compaction was most likely to duplicate the field compaction using rubber-tired rollers.

While kneading compaction has the flexibility of varying foot pressures and number of blows per layer and thus can achieve different combinations of water content and density, no standard procedure has been established. At the present time, the field compaction is not usually controlled or designed based on a water content -density relationship obtained from kneading compaction. Thus, during the design stage of each project, particular combinations of foot pressure, number of blows per layer and number of layers in kneading compaction corresponding to the field compaction can only be found by performing several compaction tests. Water content and density data recorded from test embankments

would provide very useful information regarding the expected field compaction results in the main dam. The kneading compaction procedure thus established for each project will be most useful for preparing the test specimens to be used in strength-deformation study.

2.9 Sample Preparation

The till was obtained from Wood River Burn borrow area of Mica dam. The soil was forced through the desired maximum (e.g. $3/4"$, $3/8"$, No. 4) grain size sieve and the material passing the sieve was air dried. Twenty-five hundred grams of the air dried soil was mixed with the required quantity of distilled water by weight in a mechanical mixer for at least 5 minutes. About 0.5% more water than required was added to the soil to compensate for the moisture loss during mixing. The soil thus mixed was believed free of lumps before curing. The lumps were broken by hand if necessary. A uniform mixture could frequently be obtained without difficulty. The soil-water mixture was removed from the mixer, placed in plastic bags, sealed and cured in a moist room for a minimum of 24 hours prior to compaction.

The ring of the oedometer compression cell was so designed that it could also be used as a compaction mould. The samples for oedometer compression tests were compacted directly in the ring, thus the disturbance due to extruding was avoided. The ring which was being prepared for compaction was coated with silicon grease on the inner surface of the

teflon sleeve and a standard latex membrane was inserted in the mould and brought into close contact with teflon. The circular plunger, slightly smaller than the inside diameter of the ring, was sometimes used to ease the membrane into place and force it to adhere to the teflon surface. For impact compaction, standard proctor and modified proctor efforts were achieved with the ASTM procedure. For kneading compaction, the foot pressure, tamps per layer and number of layers were varied as noted. To control the uniformity of samples, material required for preparation of one sample was divided into equal parts. Each part was placed in the mould and spread evenly by hand. After compaction of the last layer, the collar was removed and the soil was trimmed off even with the top of the mould. The compacted samples were weighed before curing for density determination. The water contents of the sample were determined from the sample trimmings.

The same procedure as described were used to prepare the samples for isotropic compression tests and almost identical samples in terms of density were obtained as for oedometer compression tests.

2.10 Laboratory Tests

2.10.1 Compression Tests Performed

A summary of compression tests performed in this study is shown in Table 2.1. The test results are presented in Appendix A. The types of tests include oedometer compression partial dissipation test, oedometer compression drained test

TABLE 2.1
SUMMARY OF COMPRESSION TESTS PERFORMED

Name of the Series and type of Test	Name of Sample	Compaction Method	Water Content (%)	Dry Density (pcf)	Gradation Type	Maximum Grain Size	Remark
OW Oedometer Compression Partial Dissipation Test	OW-1	Kneading (150,3,25)	9.00	132.0	No. 1	No. 4	
	OW-2	Standard Proctor	8.95	132.1	No. 1	3/4"	Material having water content close to (69) fill in the core
	OW-3	Standard Proctor	8.81	133.5	No. 2	3/4"	
	OW-4	Kneading (150,7,70)	9.15	134.4	No. 1	3/4"	
	OW-5	Kneading (150,3,25)	8.48	133.9	No. 1	3/4"	
	OW-6	Kneading (150,7,70)	8.90	134.7	No. 1	3/4"	
	OW-7	Modified Proctor	8.30	134.6	No. 2	3/4"	
	OW-8	Modified Proctor	8.55	134.1	No. 1	3/4"	
OD Oedometer Compression Partial Dissipation Test	OD-1	Kneading (150,7,70)	6.47	137.5	No. 1	No. 4	
	OD-2	Kneading (150,7,70)	6.57	137.2	No. 1	3/8"	Material having water content close to (70-72) fill in the core
	OD-3	Kneading (150,7,70)	6.89	139.4	No. 1	3/4"	
	OD-4	Modified Proctor	6.24	140.0	No. 1	3/4"	
	OD-5	Kneading (150,5,25)	7.27	137.0	No. 2	3/4"	
	OD-6	Kneading (150,7,70)	5.90	142.6	No. 2	3/4"	
	OD-7	Kneading (150,7,70)	7.42	139.2	No. 2	3/4"	
	OD-8	Modified Proctor	6.95	139.0	No. 2	3/4"	
S Oedometer Compression Drained Test	S-1	Kneading (150,7,70)	6.14	139.7	No. 1	3/4"	
	S-2	Kneading (150,7,70)	5.80	140.8	No. 1	3/4"	
	S-3	Kneading (150,7,70)	4.55	140.8	No. 1	3/4"	
	S-4	Kneading (150,7,70)	7.96	134.7	No. 1	3/4"	
	S-5	Kneading (150,7,70)	6.43	140.8	No. 2	3/4"	
	S-6	Kneading (150,7,70)	6.53	139.9	No. 2	3/4"	
HW Isotropic Compression Partial Dissipation Test	HW-1	Kneading (150,3,25)	8.89	132.0	No. 1	No. 4	Material having water content close to (69) fill in the core
	HW-2	Standard Proctor	8.48	132.9	No. 1	3/4"	
	HW-3	Kneading (150,3,25)	9.05	133.5	No. 1	3/4"	
HD Isotropic Compression Partial Dissipation Test	HD-1	Kneading (150,7,70)	6.75	136.8	No. 1	No. 4	Material having water content close to (70-72) fill in the core
	HD-2	Modified Proctor	7.03	138.9	No. 1	3/4"	
	HD-3	Modified Proctor	7.01	139.2	No. 1	3/4"	
	HD-4	Kneading (150,5,25)	7.01	138.3	No. 1	3/4"	

and isotropic compression partial dissipation test. The samples were generally prepared at two water contents which were the two different average values measured in the three seasons of core fill of Mica Dam. In order to obtain elastic parameters of the soil with respect to total stresses, it is quite clear that undrained tests have to be performed. For a saturated soil, compression tests other than oedometer and isotropic compression are usually used. These tests (e.g. triaxial and plane strain tests) essentially impose shear stresses on the specimens and thus shear deformations are measured for undrained stress-strain curves. In compacted or unsaturated soil, volume change usually occurs under undrained oedometer or isotropic compression test. Hence, the results from these tests may also be used for deriving the elastic parameters with respect to total stresses. Compression partial dissipation tests performed in this study are mainly undrained tests but with the difference that pore pressures are partially dissipated when the specimens are loaded to certain stress levels. These stress levels for the case of earth dams can correspond to the maximum load at the end of each construction season. In oedometer or isotropic compression tests, undrained loading will gradually bring unsaturated soil to full saturation after which no further volume change occurs. With partial dissipation in the test, this condition may be prevented.

Elastic parameters with respect to effective stresses are most conveniently derived from drained tests. However,

with pore pressure measurements in partial dissipation tests described earlier, volume change and effective stress relationship for unsaturated soil can be obtained. These relationships may also be used for deriving elastic parameters with respect to effective stresses.

2.10.2 Oedometer Compression Partial Dissipation Test

Before setting up the test specimens, the high air entry porous stone at the base of the cell was saturated with water. This was accomplished by applying pressurized water on top of the stone and occasionally flushing out the bubbles from the base drainage line connected to the bottom of the stone (Fredlund, 1972). After saturation of the stone the base drainage line was filled with water and connected to a reservoir with a slight water head difference. Due to this head difference, the top of the stone was always covered with a thin film of water before starting the test. A saturated filter paper was used between the stone and the base of the specimen. The specimen compacted in the ring was then removed from the moist room after curing for one day. The ring with the specimen was seated on the base as shown in Fig. 2.2. In the final position, the inner surface of lower 0.5 in of the ring was tight against the side of pedestal and the bottom of the specimen rested directly on top of the filter paper. An 'O' ring recessed into the groove around perimeter of the pedestal was used to prevent any

leakage between the ring and the pedestal.

At the top of the specimen, a saturated filter paper and a coarse porous stone were used. In addition, the specimen was sealed by a plunger with a membrane and belofram. During the sealing, particular attention was taken to minimize the amount of air trapped between the sample and the seal. The top chamber was subsequently assembled and filled with water. The top drainage line was also filled with water but no flow was allowed. After setting up the vertical L.V.D.T., the top and base drainage control valves were checked to be in the closed position. The specimen was now ready for testing.

All the tests were performed in the environment controlled room at 65°F and 50% relative humidity. The variations in temperature and the relative humidity were $\pm 1^\circ\text{F}$ and $\pm 2\%$ respectively. The purpose of conducting the test in an environment controlled room was to avoid the effects of environment fluctuation on the air pressure system, stress-strain properties of the specimens and the measuring devices.

Step loadings were applied in the test, and increments of 100, 200, 400, 600 and 750 psi were used. Only at 200, 400, 600 and 750 psi, was partial dissipation allowed after undrained loading. During undrained loading, the pore pressures were monitored by the transducer. The pressures were read with a strain gauge bridge and multiplied by an

appropriate calibration factor. Each loading was maintained until no significant change in pore water pressure was observed. This usually happened within 30 minutes after the application of the load. However, as a standard procedure (Bishop and Henkel, 1957) each undrained loading was maintained for 30 minutes prior to application of the next loading, pore pressure and L.V.D.T. readings were recorded. During the dissipation stage, the zero time was set when the top drainage control valve was opened. The valve was closed at the time when the percentage of pore pressure dissipated was about the same as that measured in the fill during a work stoppage period. The next undrained load was applied immediately after the top drainage control valve was closed.

2.10.3 Oedometer Compression Drained Test

In the drained test, the set-up was generally the same as that described in section 2.10.2. Only some features relating to drainage were different. Because this type of test was performed in the early stage of investigation, no pore pressure measurement was attempted. Hence instead of a high air entry porous stone, the coarse porous stone was used at the base of cell. During the test, the top and base drainage lines were kept open.

The same loading increments as described in section 2.10.2 were used. Each load was maintained until there was no significant change in the measured vertical deformation.

The amount of time to reach that condition varied with water content and magnitude of the loading. The maximum time was set at 24 hours.

2.10.4 Isotropic Compression Partial Dissipation Test

The pore pressure measuring system and the high air entry porous stone at the base of the isotropic compression cell were saturated using the same procedures as those outlined in section 2.10.2. The lateral strain measuring device and the vertical L.V.D.T. were set on the specimen after it was properly sealed with the neoprene membrane. The top drainage line was filled with water before the test. The initial readings for L.V.D.T.s measuring lateral and vertical deformations were recorded at the time after the cell was filled with hydraulic oil but before the pressure was applied. The same pressure system as for the oedometer compression tests was used.

The loading sequences in the test were the same as those in the oedometer compression partial dissipation test.

The general view of the test set-up is shown in Fig. 2.11.

2.11 Some Aspects of Stress-Strain Relationships

2.11.1 Effective Stress in Compacted Soil

In the present studies, the effective stress in compacted soil is, unless specifically stated otherwise,

generally defined as the difference between total stress and pore water pressure. Although more refined effective stress theories for unsaturated soil (Bishop et al., 1960, Matyas et al., 1968 and Fredlund, 1973) are available, the use of these theories in field problems may be premature. The error in simplified effective stress theory has been discussed by Bishop et al. (1964). As indicated for the case of a dam where the fill is compacted near the optimum water content and has a high degree of saturation, the error due to neglecting the difference between pore air pressure and pore water pressure is relatively small. The error will increase as the molding water content decreases.

2.11.2 Total Stress-Strain Relationship

Due to the dissipation of pore pressures at certain stress levels in oedometer and isotropic compression partial dissipation tests, additional strains occur under these constant stresses. The curves relating stresses and strains in the tests are thus discontinuous. In Fig. 2.12, a stress-strain curve from an oedometer compression partial dissipation test can be represented diagrammatically by a solid line and as shown, the curve is discontinuous at stresses $(\sigma_1)_a$, $(\sigma_1)_b$ and $(\sigma_1)_c$. In the derivation of elastic parameters with respect to total stresses, total stress-strain relationships

during undrained loading are mainly of interest. Thus, a total stress-strain curve required for total stress analysis should exclude the strains due to pore pressure dissipation under constant load. The derivation of this curve from the test results is illustrated diagrammatically in Fig. 2.12. For stress $(\sigma_1)_a$, undrained strain, $O_1 P_1'$, is obtained by subtracting the strain caused by pore pressure dissipation, $P_1' P_1$, from the measured total strain, $O_1 P_1$. For stress $(\sigma_1)_b$, the corresponding undrained strain, $O_2 P_3'$, is obtained by subtracting the sum of strains due to pore pressure dissipations up to this stress level, that is $P_1' P_1$ plus $P_2 P_3$, from the measured total strain, $O_2 P_3$. The same procedure is used to determine the undrained strain, $O_3 P_5'$, for the stress $(\sigma_1)_c$. The resulting total stress-strain curve for the analysis is obtained by fitting a smooth curve through the origin O and the points P_1' , P_3' and P_5' . This curve is illustrated in the same figure with a dashed line.

2.11.3 Parameters for the Stress-Strain Functions

Stress-strain relationships for the soils under stress conditions in oedometer and isotropic compression tests have been discussed in section 2.5. In order to illustrate the determination and to illustrate the typical values of the parameters involved in the power functions, the results of an oedometer compression partial dissipation test are discussed. The values of effective major principal

stresses and major principal strains of test sample OW-3 are listed in the first and second columns respectively of Table 2.2.

TABLE 2.2
TEST RESULTS OF SAMPLE OW-3

σ_1' (psi)	ϵ_1	$\frac{\sigma_1'}{P_a}$
60	0.030	4.08
100	0.037	6.80
260	0.050	17.69
480	0.059	32.65
660	0.063	44.90

The values in column $\frac{\sigma_1'}{P_a}$ are obtained by dividing the values in the first column by $P_a = 14.7$ psi. After plotting the corresponding values of $\frac{\sigma_1'}{P_a}$ and ϵ_1 on log-log scales, it is noted that the points may be represented by a straight line as shown in Fig. 2.13. For constants a and C_D in the equations $\epsilon_1 = C_D \left(\frac{\sigma_1'}{P_a}\right)^a$, the values can be obtained from the slope of the line, which is $\frac{\Delta \log \epsilon_1}{\Delta \log \left(\frac{\sigma_1'}{P_a}\right)}$,

and the value of ϵ_1 for $(\frac{\sigma_1'}{p_a}) = 1$ respectively. In the present case, a is 0.298 and C_D is 0.021. The tangential constrained modulus at any stress level greater than zero can be evaluated from equation (2.12) from these parameters. As an example, the E_C' value calculated for σ_1' equal to 200 psi is 14680 psi.

2.12 Discussion of Test Results

The behaviour of compacted soil is fundamentally controlled by compositional factors such as water content, density and structural arrangement of soil particles. For a specific water content, the density and structure of compacted soil are determined by gradation, maximum grain size and the compaction method. The stress-strain response of a compacted soil is inevitably related to these factors. In the following paragraphs, the effects of these factors are discussed based on the test results obtained in this investigation. In addition to the previous aspects some relevant soil behaviour observed in the tests is also discussed.

The effect of water content. Using stiffness as a general term for the ratio of effective major principal stress increment and major principal strain increment in the present discussion, it can be seen from Fig. 2.14 that the stiffness of Mica Till in an oedometer compression test decreases as the molding water content increases. This behaviour may be explained by the theory concerning the effects of compaction

on soil structure (Seed and Chan, 1959). The soil compacted at low water content tends to form a flocculated structure while that compacted at high water content tends to be dispersed. As the result of the flocculated structure, the soil, compacted at low water content are less compressible than those at high water content.

The effect of gradation. As stated in section 2.8, two different sample gradations were prepared for the till having a maximum grain size of $3/4$ ". The stress-strain curves of these soils from oedometer compression tests are shown in Fig. 2.15. From this figure, it can be seen that gradation 2 material is more compressible than the material of gradation 1. Since gradation 2 material was somewhat step graded, it might be expected that the total contact area of the particles was less and hence the higher stress per contact induced more compression.

The effect of maximum grain size. The variation of stiffness with maximum grain size for Mica Till in an oedometer compression test is presented in Fig. 2.16. From this figure, it can be noticed that the stiffness increases with a decrease in maximum grain size in the range of sizes tested. Rowe (1962) performed shear tests on quartz sands with different grain sizes ranging from coarse sand to coarse silt, the results obtained indicated that friction angle also increases as the grain size decreases. This finding was

explained by Lamb (1964, p. 67) as the larger particles were able to roll more easily than the smaller particles due to their center of gravity being further away from the plane of shear. Based on this postulate, it simply meant that there were more rolling strains or slip strains in samples comprised of larger particles than in those having smaller particles. Thus, the observed variation of stiffness in the present tests, which is a direct function of strain, may well be explained by the same postulate. However, samples with maximum grain size as in the field (10" or larger) were not tested, it is by no means implied that the observed stiffness variational behaviour can be extended to the field size. As maximum grain size increases from the sizes tested to the field sizes the well graded effect also increases and may become significant.

Particle breakage. The significance of particle breakage under high stresses for certain soils has been reported by several researchers (Lee and Seed, 1967, Vesic and Clough, 1968). The strain resulting from this breakage always adds to rigid particle slip strain and elastic strain. In order to assess the degree of particle breakage for Mica Till tested in the laboratory the material was sieved before and after each test. Typical grain size curves before and after oedometer compression tests are shown in Fig. 2.17. From this figure, it may be concluded that particle breakage is not very significant in Mica Till even under pressures as

high as would exist in the dam. Since under certain stress levels the degree of particle breakage depends mainly on the gradation and the crushing strength of the grains (Marsal, 1972), the previous observation may be expected for Mica Till which is well graded and consists of grains with high strength.

The effect of compaction method. The comparisons of effective stress-strain curves from oedometer compression tests for Mica Till prepared with Proctor and kneading compaction are shown in Figures 2.18 and 2.19. Some differences can be observed between the curves for the samples prepared using these two procedures. At a low water content which is near the modified Proctor optimum and for samples having similar initial conditions (water content and density), the one prepared in 7 layers and compacted with 70 tamps of 150 psi pressure per layer (kneading compaction (150,7,70)) is less compressible than that prepared with modified Proctor compaction. Slightly higher shear strength of the sample prepared with kneading compaction to the density and water content near the modified Proctor optimum as compared to that prepared with the modified Proctor compaction was also observed by Seed and Chan (1959). At high water contents, which are near standard Proctor optimum, however, the sample prepared with standard Proctor compaction is slightly less compressible than that prepared with kneading compaction (150, 7, 70). From these observations, it appears that

somewhat stronger or more flocculated structures are formed by kneading compaction (150, 7, 70) and standard Proctor compaction at low and high water contents respectively.

Pore pressure response and drainage characteristics.

In oedometer compression partial dissipation tests, the pore water pressures in the samples were monitored throughout the tests. The results of the tests can be used for deriving the stress-strain relationships of the samples and also for studying the pore pressure response and drainage characteristics of the materials. As might be expected, during first undrained loading, the higher pore pressure ratio \bar{B} was generally measured in samples having a higher water content.

From the test results, the influence of coarse particle fraction on \bar{B} value might also be studied. Comparing the samples having about the same water content and compacted with same compactive effort it was noticed that the sample with larger maximum particle size or with gradation 2, which in turn had the higher coarse particle fraction, had a higher \bar{B} value during the first undrained loading. It might be noted the degrees of saturation for the samples in comparison were more or less the same.

The influence of pore pressure dissipation on subsequent undrained pore pressure response has been discussed by Bishop (1957). The \bar{B} values determined on wetter materials in the present studies during each undrained loading stage are listed in Table 2.3. From this table, it can be noted that \bar{B} values of samples with gradation 2 generally decrease

TABLE 2.3
 \bar{B} VALUES DETERMINED FROM OEDOMETER COMPRESSION
 PARTIAL DISSIPATION TESTS

Sample No.	Water Content %	Gradation Type	\bar{B}				Percentage of Pore Pressure Dissipation After Each Loading Stage		
			First Loading 0-200psi	Second Loading 200-400psi	Third Loading 400-600psi	Fourth Loading 600-750psi	First Dissipation	Second Dissipation	Third Dissipation
OW-2	8.95	1	0.26	0.15	0.08	0	21	29	25
OW-3	8.81	2	0.52	0.37	0.25	0.16	40	48	42
OW-4	9.15	1	0.59	0.62	0.67	-	22	34	-
OW-5	8.48	1	0.59	0.56	0.72	0.69	22	26	45
OW-6	8.90	1	0.61	0.57	0.65	0.16	20	33	61
OW-7	8.30	2	0.65	0.53	0.48	0.11	37	45	61
OW-8	8.55	1	0.77	0.76	0.81	0.61	20	23	53

in subsequent stages while those of gradation 1 generally increase. During the tests, it was observed that the percentage of pore pressure dissipation of gradation 2 materials was more than that of gradation 1 materials for the same period of time. This observation can be illustrated by the values of coefficient of consolidation (C_v) listed in Table 2.4. The C_v values were calculated from the theoretical relationship between the percentage of pore pressure dissipation at the base of the sample and the time factor (Bishop and Henkel, 1957). Although this relationship was used by Bishop and Henkel for triaxial samples, it is valid for samples under any strain condition with top drainage only. In Table 2.4, gradation 2 materials have higher C_v values than gradation 1 materials. The coarser particle structures of gradation 2 might increase the perviousness of the samples.

Bishop (1957) had shown that there was a correlation between the percentage of pore pressure dissipation and the pore pressure ratio. It was indicated that the higher the percentage of pore pressure dissipated, the lower the \bar{B} value would be in subsequent undrained loading stages. However, whether the subsequent \bar{B} value would be higher or lower than previous values depended on whether the percentage of pore pressure dissipated was above or below a certain value for a particular soil. In the present studies, it was observed that if about the same percentage of pore pressure

TABLE 2.4

C_v VALUES DETERMINED FROM OEDOMETER COMPRESSION

PARTIAL DISSIPATION TESTS

Sample No.	Water Content (%)	Gradation Type	Compaction Method	Value of C _v (ft ² /month)
OW-2	8.95	1	Standard Proctor	114 [200 psi] 128 [400 psi] 115 [600 psi]
OW-3	8.81	2	Standard Proctor	210 [200 psi] 259 [400 psi] 245 [600 psi]
OW-4	9.15	1	Kneading (150,7,70)	138 [200 psi] 175 [400 psi]
OW-6	8.90	1	Kneading (150,7,70)	131 [200 psi] 176 [400 psi] 139 [600 psi]
OW-8	8.55	1	Modified Proctor	123 [200 psi] 167 [400 psi] 146 [600 psi]
(150,7,70) Foot pressure = 150 psi, 7 layers, 70 tamps per layer				
[200 psi] Total vertical stress value to which test result applies				

dissipation measured in the fill during stoppage was dissipated in the tests for higher water content Mica Till, the subsequent \bar{B} value would generally not be lower than the previous value. This observation, however, might not be considered as the behavior to be expected in the field. The percentage of pore pressure dissipation measured during stoppage was only part of the total dissipation in one season, since some pore pressures had dissipated during construction.

Assumption Used in Elastic Moduli Derivation

For studying the applicability of the assumption made on mean stress in section 2.5, it seems valuable to compare the oedometer stress-strain relationship predicted with experimental isotropic compression curve and that determined from the test. The prediction may be made with the following relationships:

$$\sigma_1' = 3\sigma' (1 + 2K_0)$$

$$\text{and } \epsilon_1 = \epsilon_v$$

$$\text{where } K_0 = 1 - \sin\phi' \text{ (Jaky, 1944).}$$

If the assumption that samples having the same volumetric strain are under the same mean stress is reasonable, the predicted oedometer stress-strain curve should closely resemble the experimental one. In Figs. 2.20 and 2.21 the

comparisons between predicted and experimental curves for till samples with low and high water contents are shown. From these figures, reasonably good agreement may be noted.

Variations of Poisson's ratio. In the isotropic compression tests, the samples were prepared identically in terms of water contents and compaction methods as the six samples tested in oedometer compression. With these pairs of test results a study of the variations of Poisson's ratio derived by the coupling method described in section 2.5 may be made. As previously discussed, the mean stress for a σ_1' value in an oedometer compression test might be equal to a σ' value which induced the same volumetric strain in an isotropic compression test. If Poisson's ratio of the material is independent of the stress level, then for any ' volumetric strain, σ_1' in an oedometer compression test and σ' in an isotropic compression test should be related as follows:

$$\frac{1 + \nu'}{3(1 - \nu')} \sigma_1' = \sigma'$$

In figures 2.22 and 2.23 the test results of Mica Till having two different water contents are presented. For each water content, two pairs of test data in terms of effective stresses are shown. As can be seen from the figures the test data do not deviate significantly from a

constant Poisson's ratio. This result may be expected due to ν'/ν' equal to K_0 , the coefficient of earth pressure at rest for the soil under oedometer stress conditions and K_0 is more or less stress level independent during primary loading. The K_0 values calculated from the determined Poisson's ratios are 0.54 and 0.59 for low and high water content samples respectively. It may be interesting to compare these values with those suggested by the formula $K_0 = 1 - \sin\phi'$ (Jaky, 1944). With this formula and the average reported ϕ' value (CASECO REPORT), K_0 was calculated as 0.47. The close agreement in the comparisons may serve to indicate representative Poisson's ratios for the materials were obtained.

A similar study was performed on test data in terms of total stresses. In Figures 2.24 and 2.25, the test results to the beginning of the first pore pressure dissipation are shown. Since the subsequent total stress-strain relationships are related to the dissipated pore pressures, which may not be compatible between two tests, the coupling method may not be used. From these figures it can also be seen that test data do not deviate significantly from a constant Poisson's ratio.

Anisotropic Behavior of Compacted Soil

In isotropic compression tests performed in this study, lateral deformation as well as vertical deformation were

measured. The strains calculated from these measurements may be used to study anisotropic behavior of compacted soil. Under an equal all-round pressure the lateral strain should equal the vertical strain if the soil is elastic and isotropic. This condition can be proved using the basic equations of elasticity. In Fig. 2.26, the ratios of measured lateral strain to vertical strain are plotted against effective isotropic stresses for several test samples. From this figure, it can be noted that the compacted samples exhibit certain anisotropy. The ratios for all the samples are not equal to one but less than one. The results also show that the wetter samples compacted with lower efforts have the ratios closer to unity.

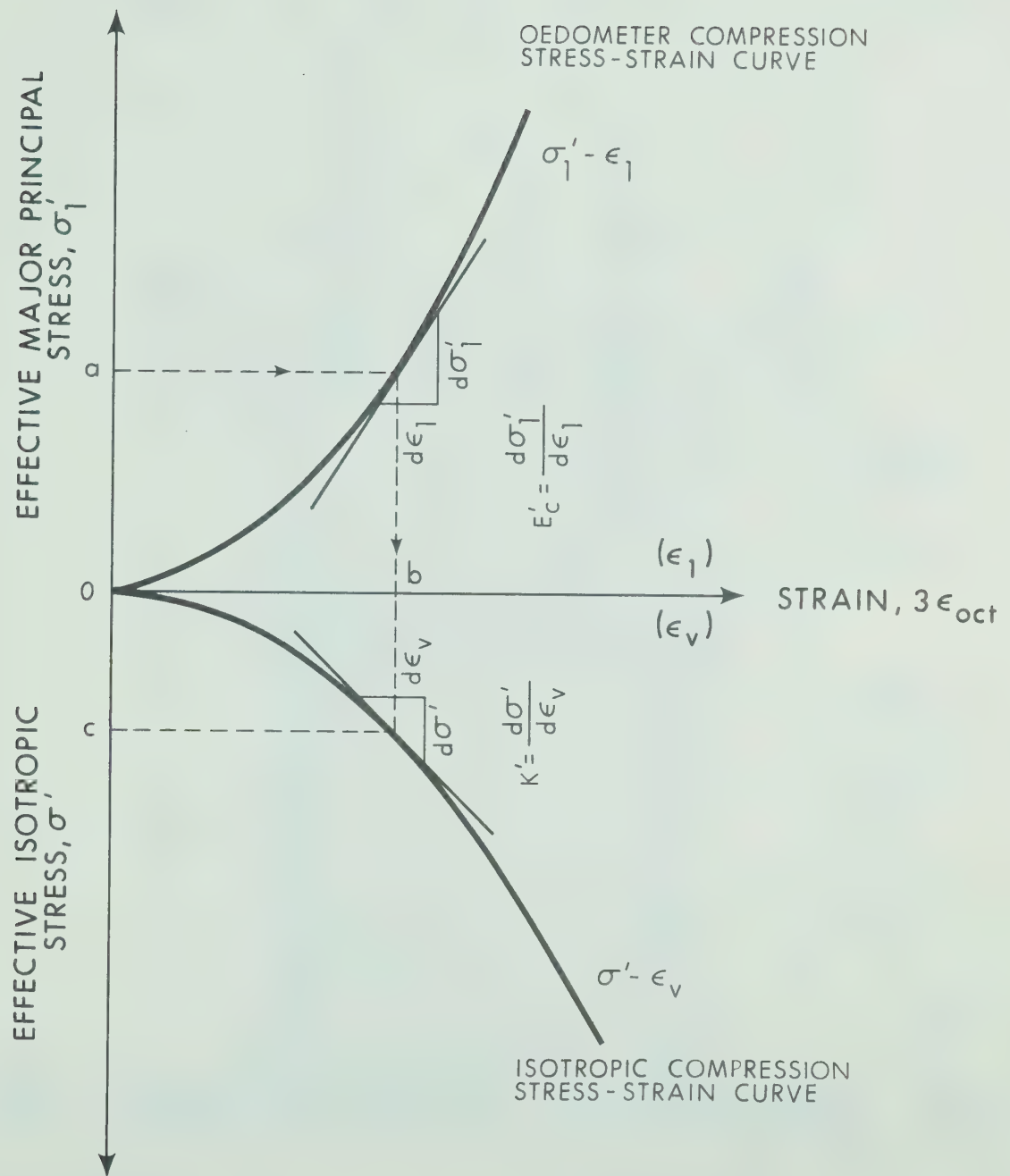


Fig. 2.1 Illustration of Elastic Moduli Derivation

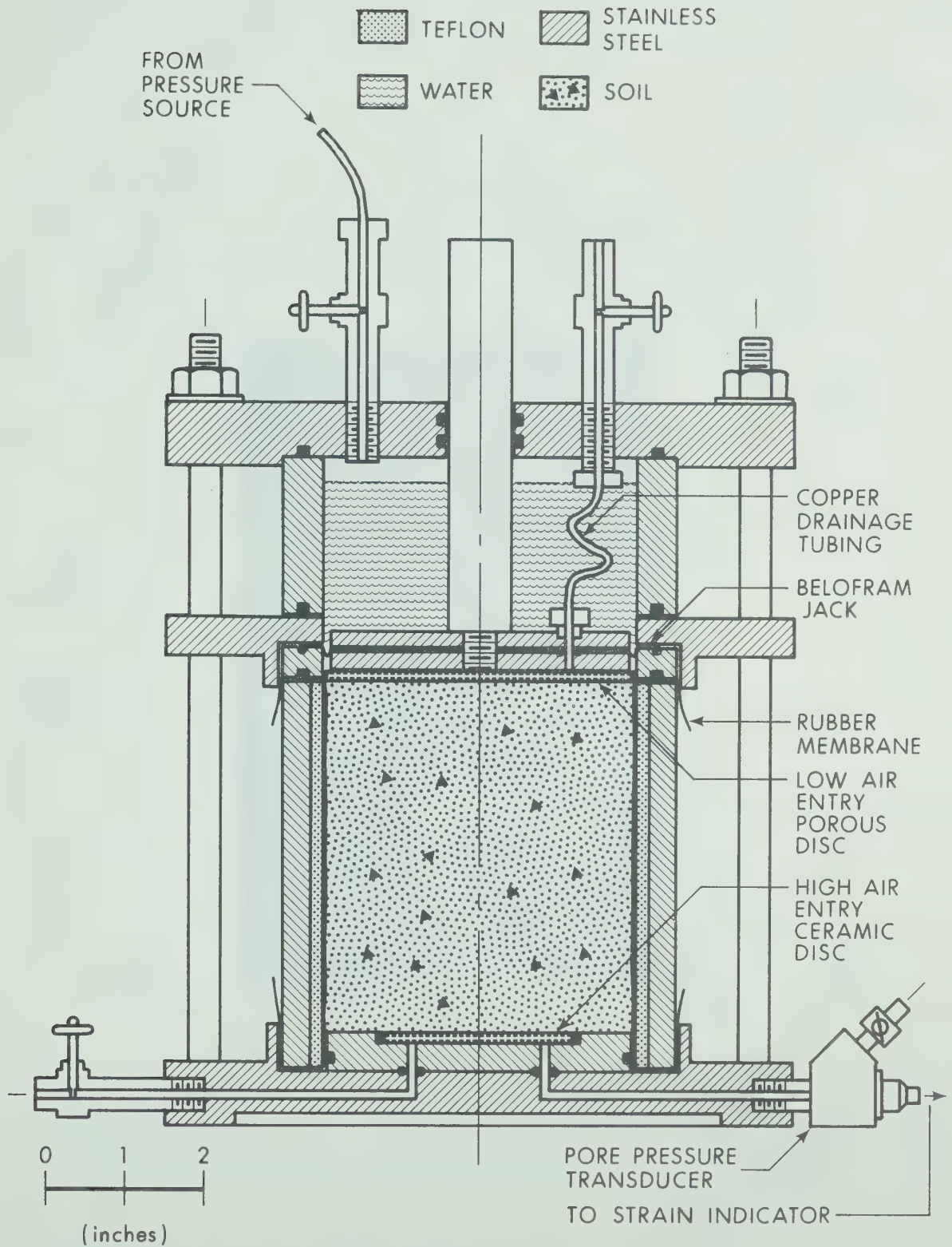


Fig. 2.2 Oedometer Compression Cell

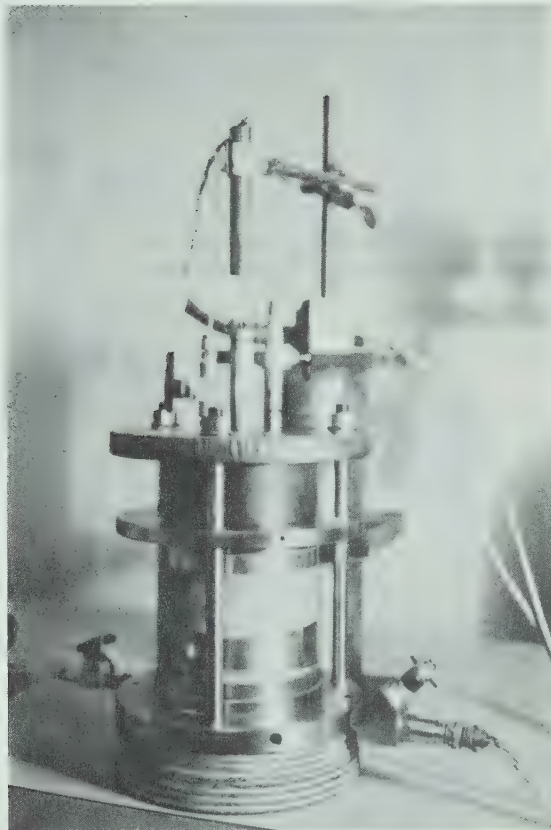


Fig. 2.3 Set-Up for Oedometer Compression Test

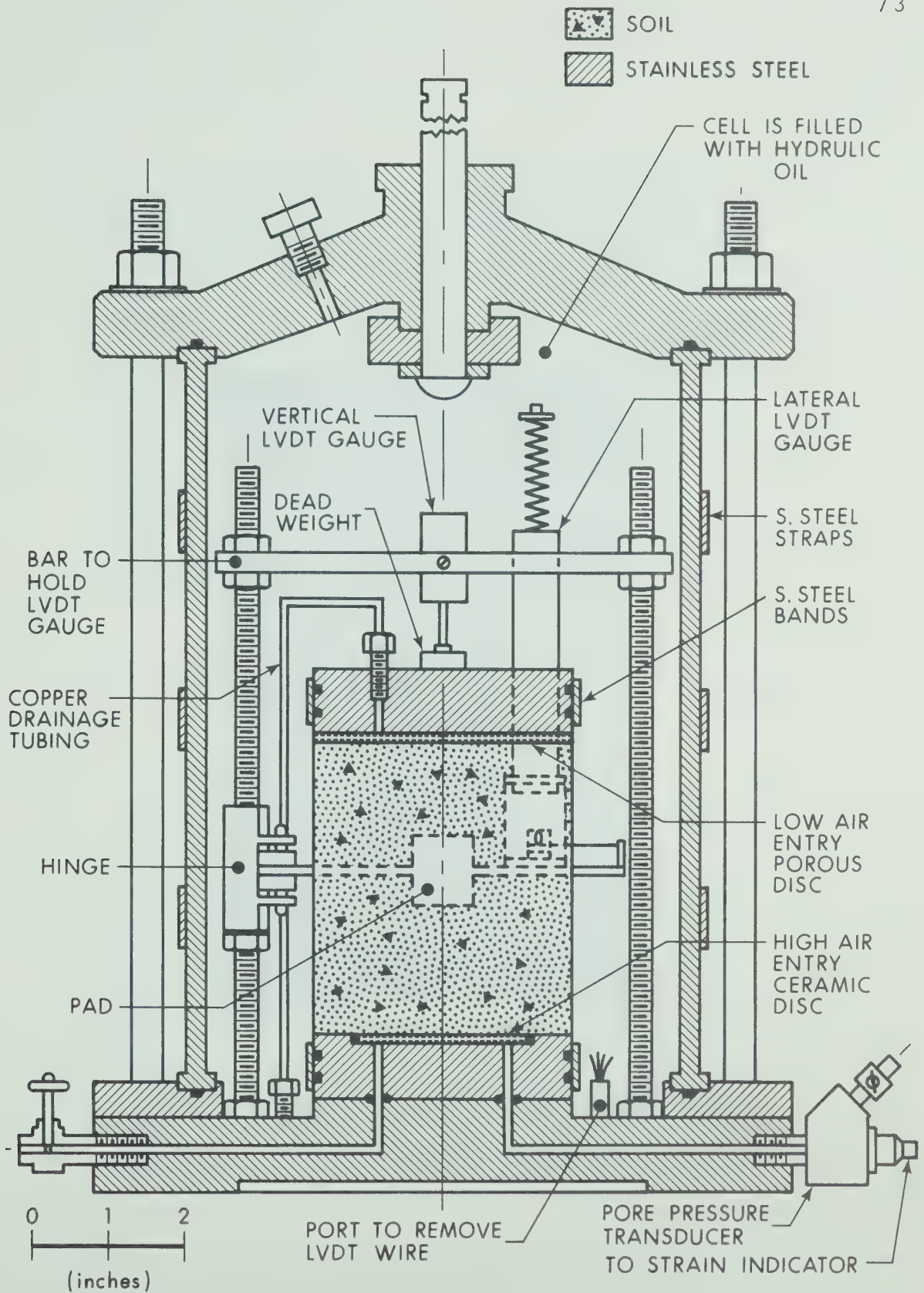


Fig. 2.4 Isotropic Compression Cell



Fig. 2.5 Set-Up for Deformation Measurements
In Isotropic Compression Cell

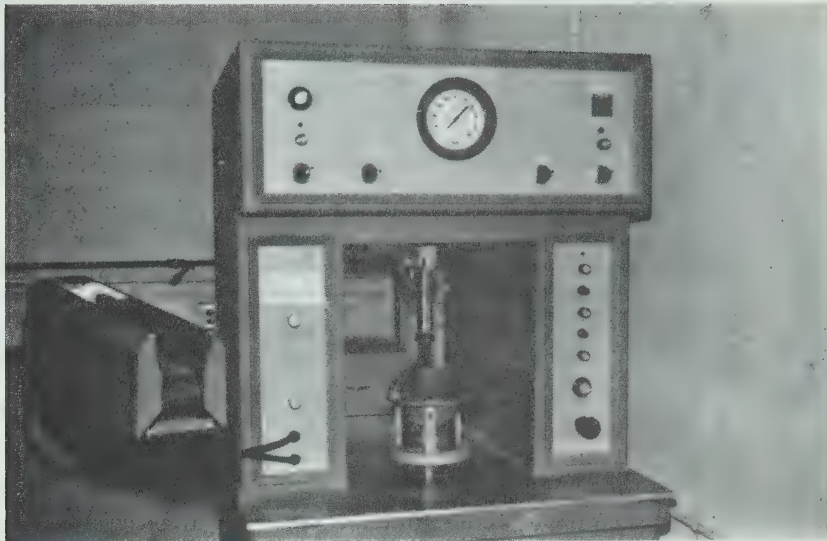


Fig. 2.6 General View of Kneading Compaction Machine

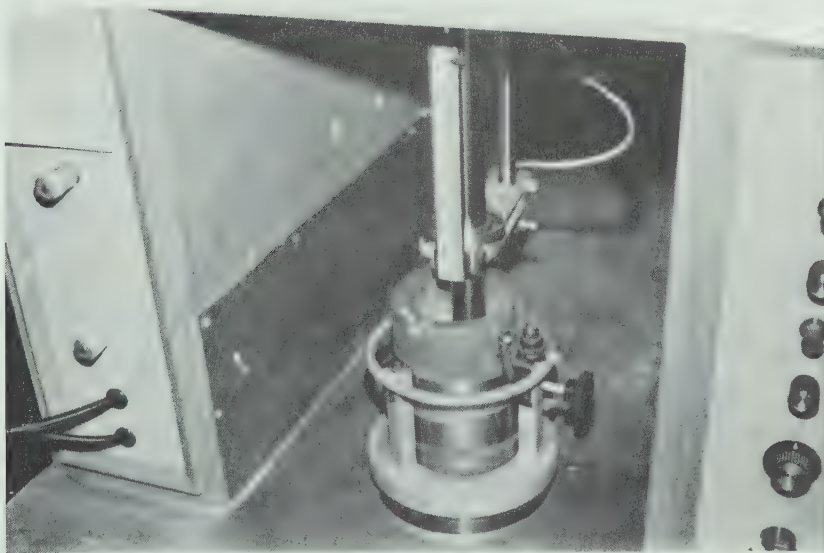


Fig. 2.7 Close-Up View of the Specimen During Compaction

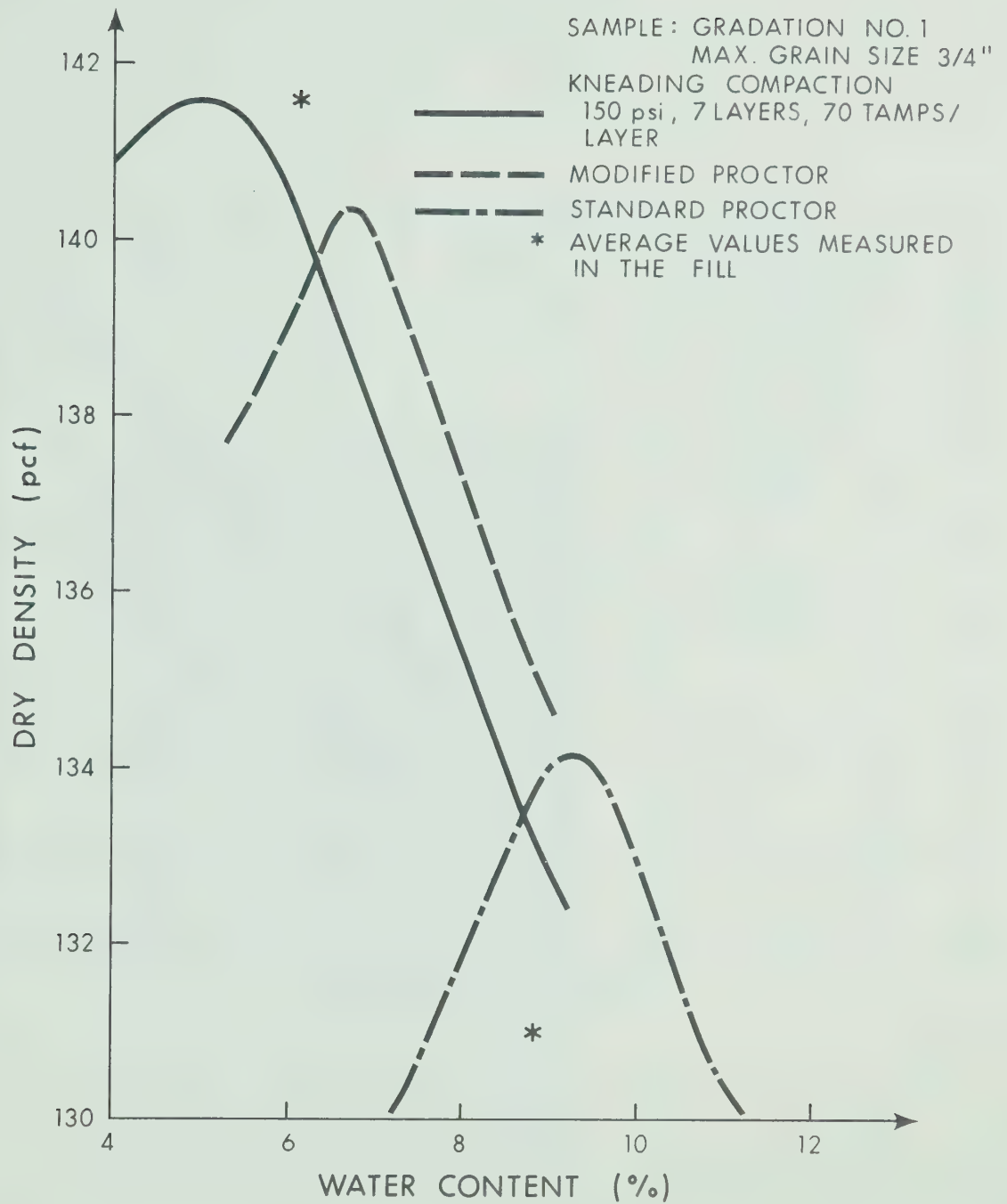


Fig. 2.9 Water Content-Density Relationship for
Mica Till For Different Compaction Tests

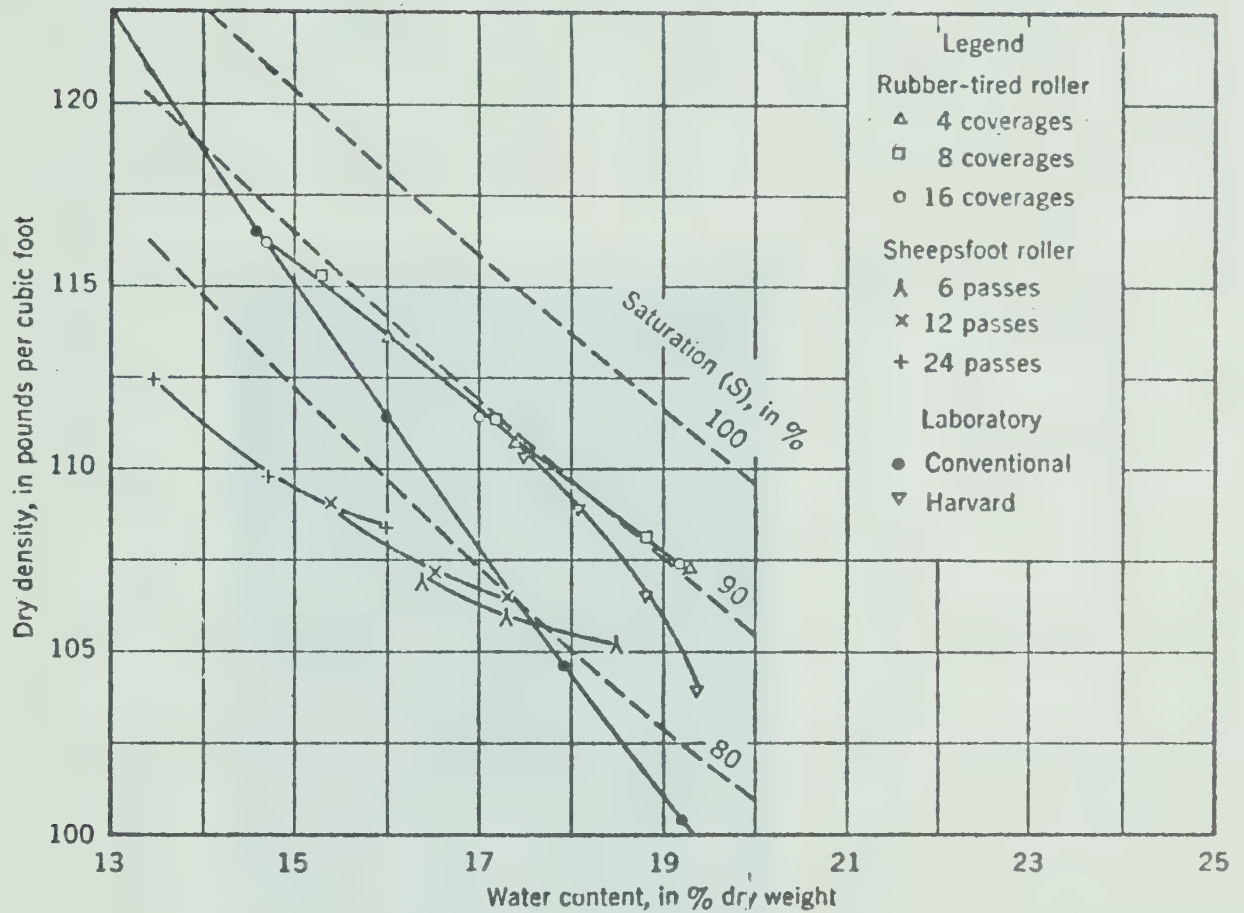


Fig. 2.10 Comparison of Compaction Methods
(after Zegarra, 1958)

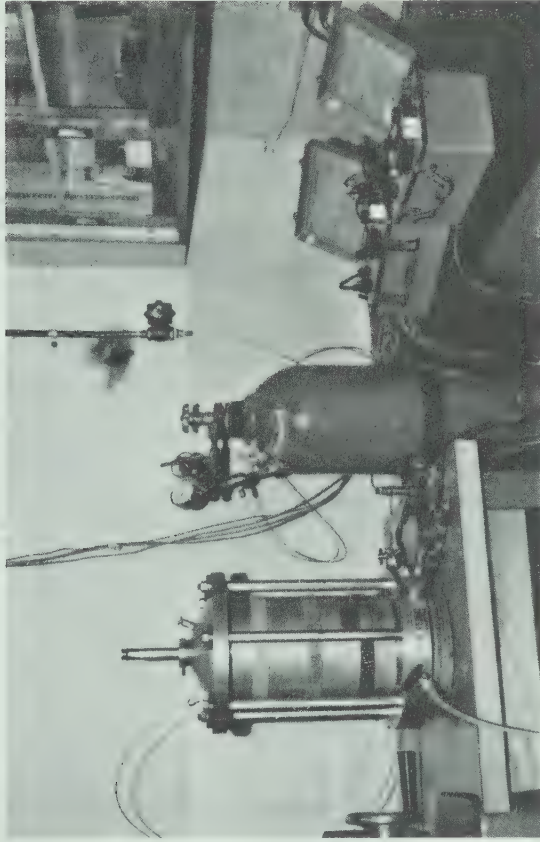


Fig. 2.11 Set-Up for Isotropic Compression
Test

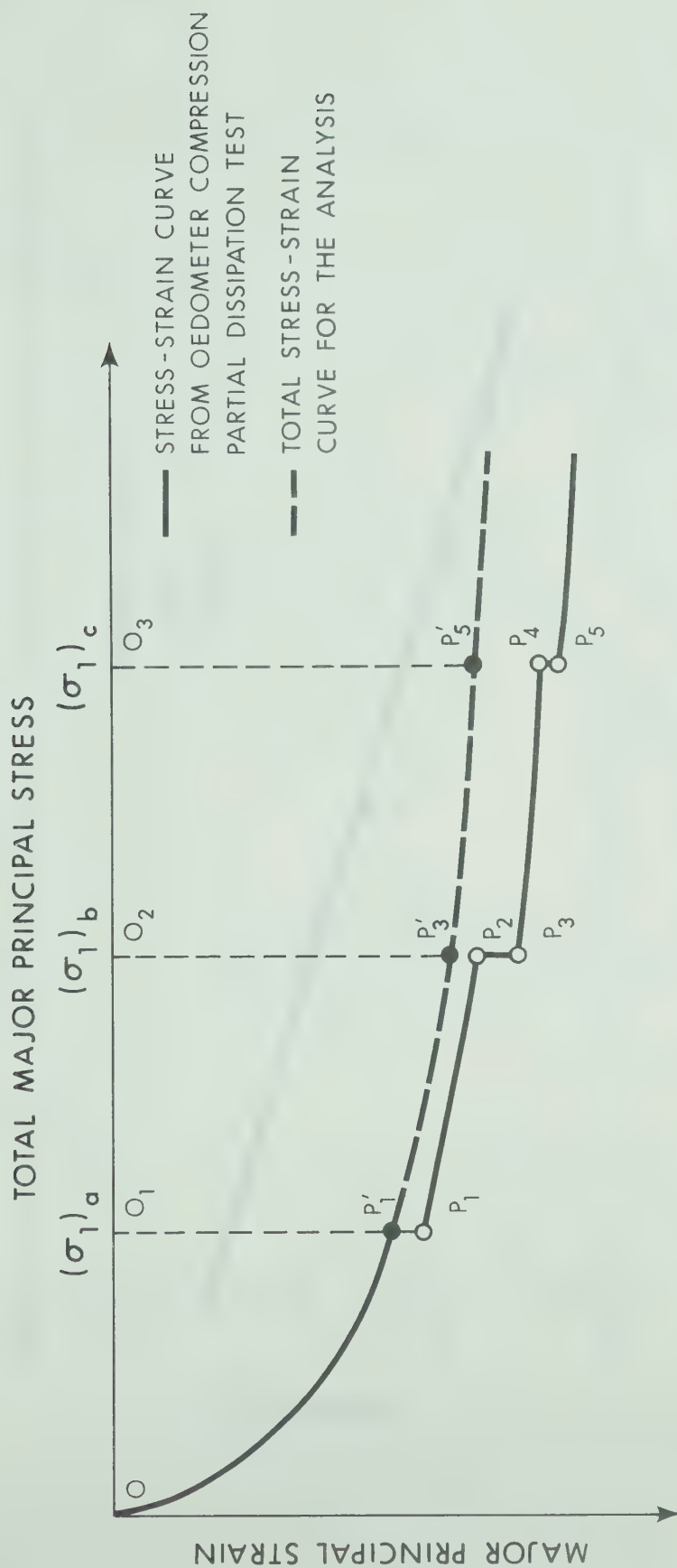


Fig. 2.12 Total Stress-Strain Curve for the Analysis.

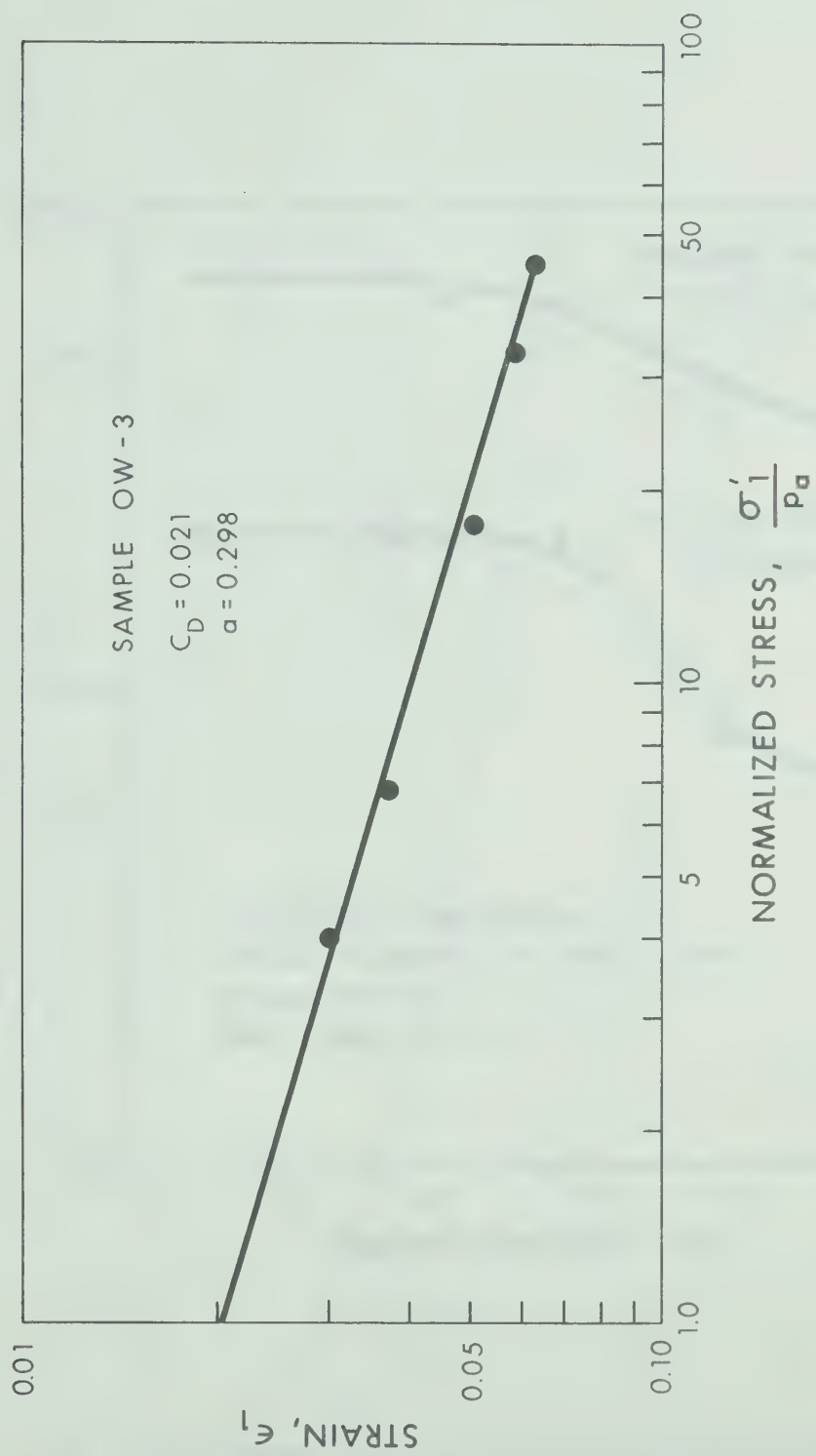


Fig. 2.13 Determination of Parameters for Oedometer Compression Stress-Strain Function

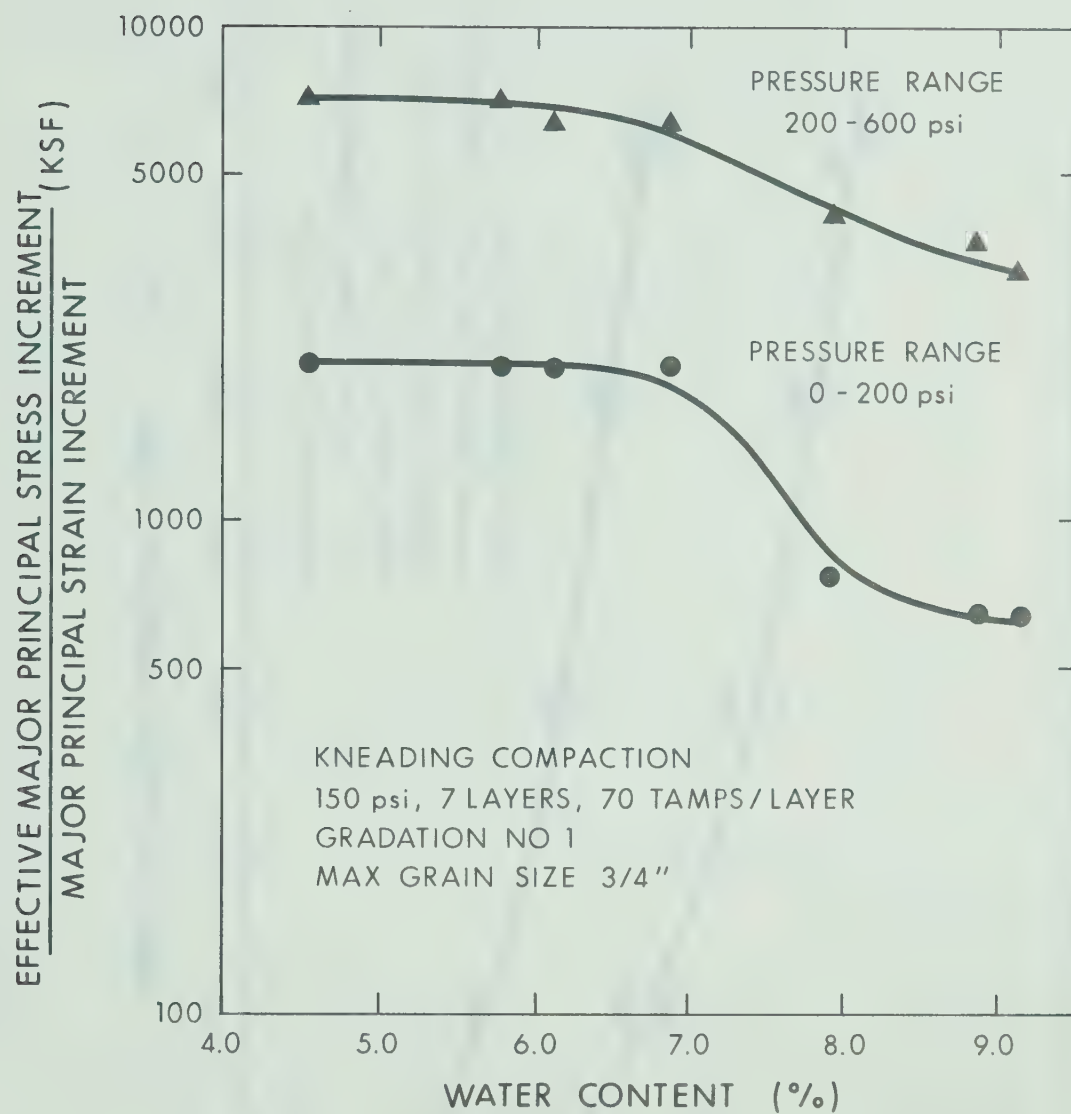


Fig. 2.14 Variation of Stiffness with Water Content for Mica Till in Oedometer Compression Test

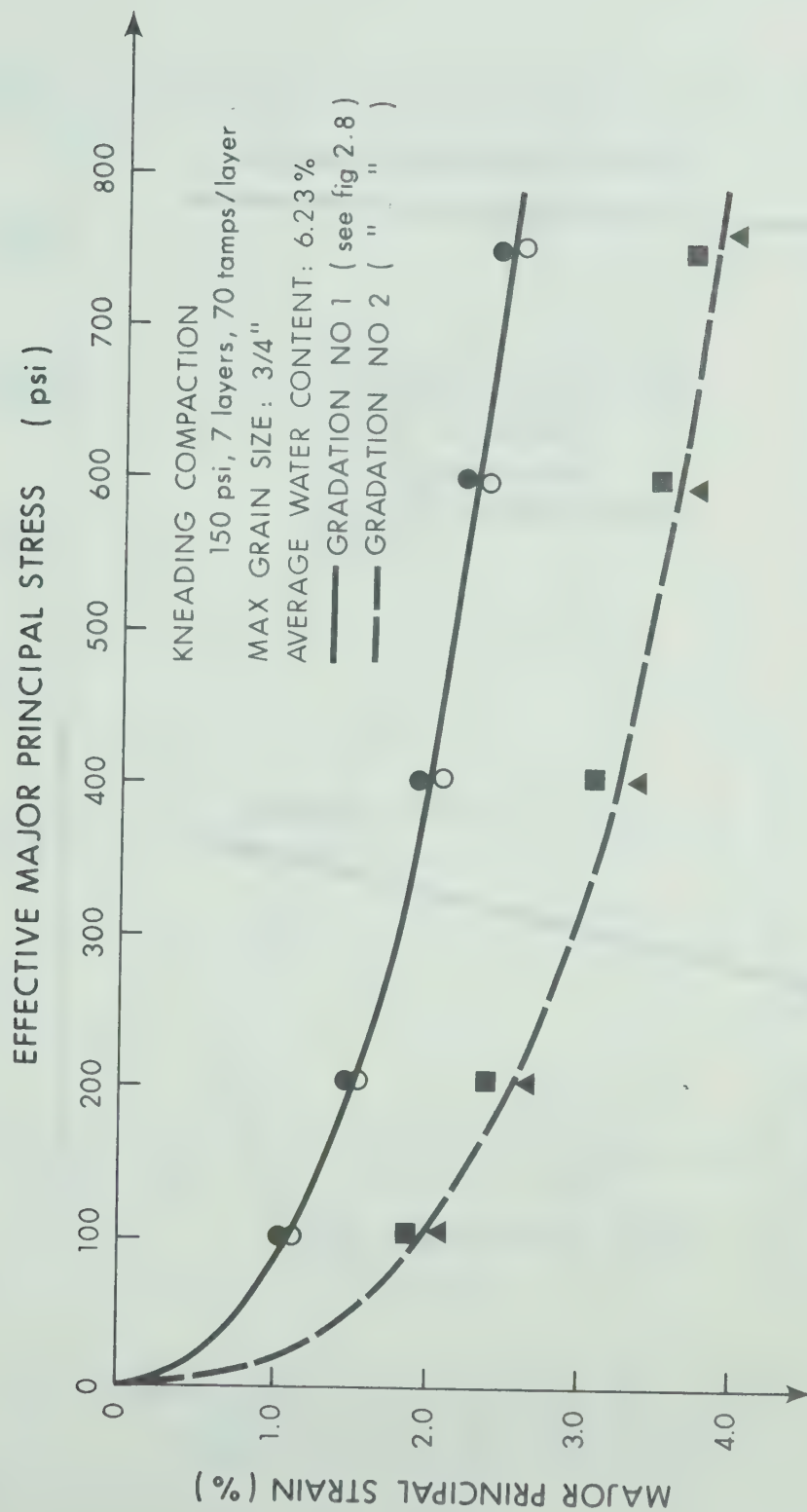


Fig. 2.15 The Influence of Gradation on Stress-Strain Behavior of Mica Till

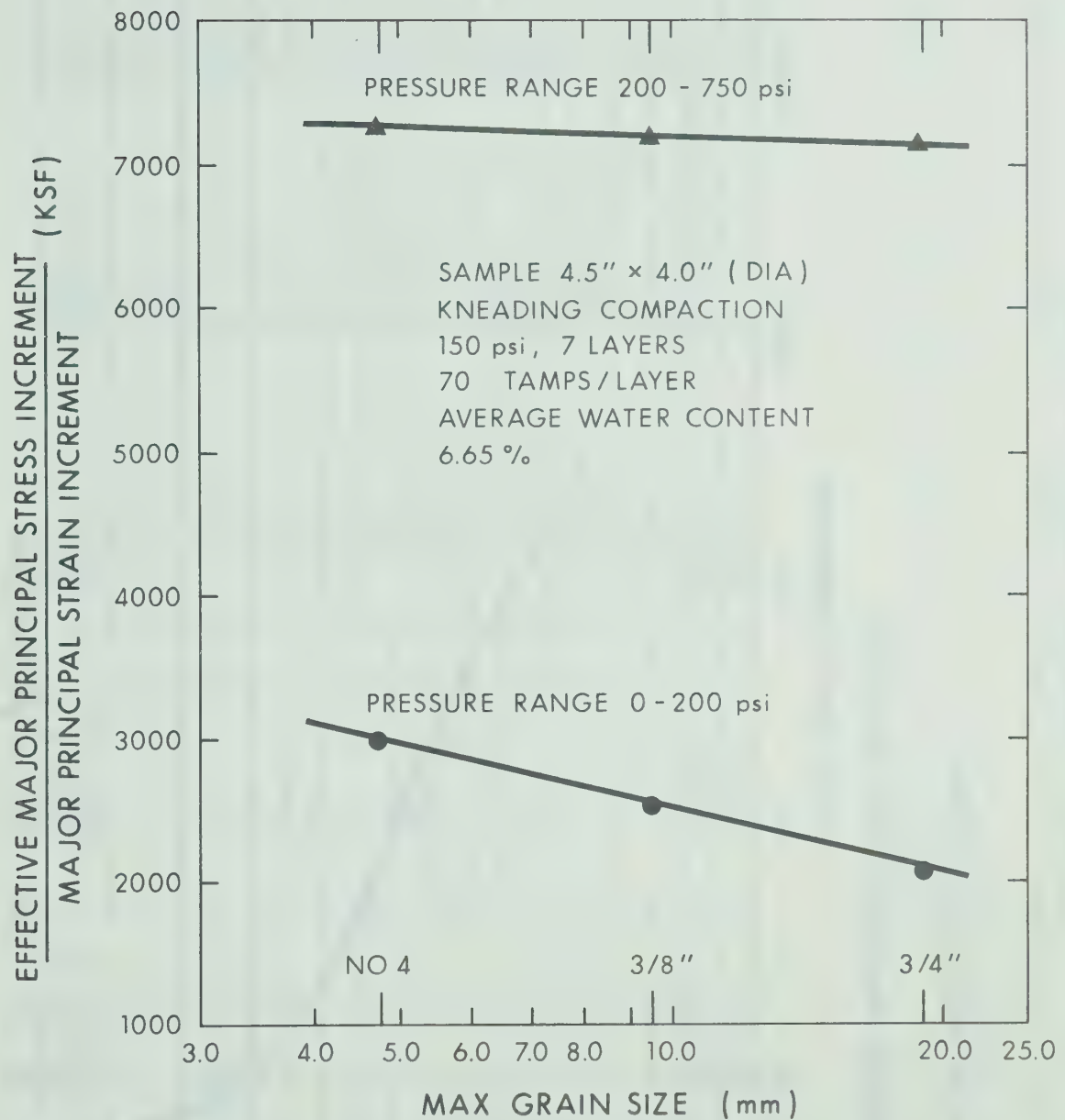


Fig. 2.16 Variation of Stiffness with Max. Grain Size for Mica Till in Oedometer Compression Test

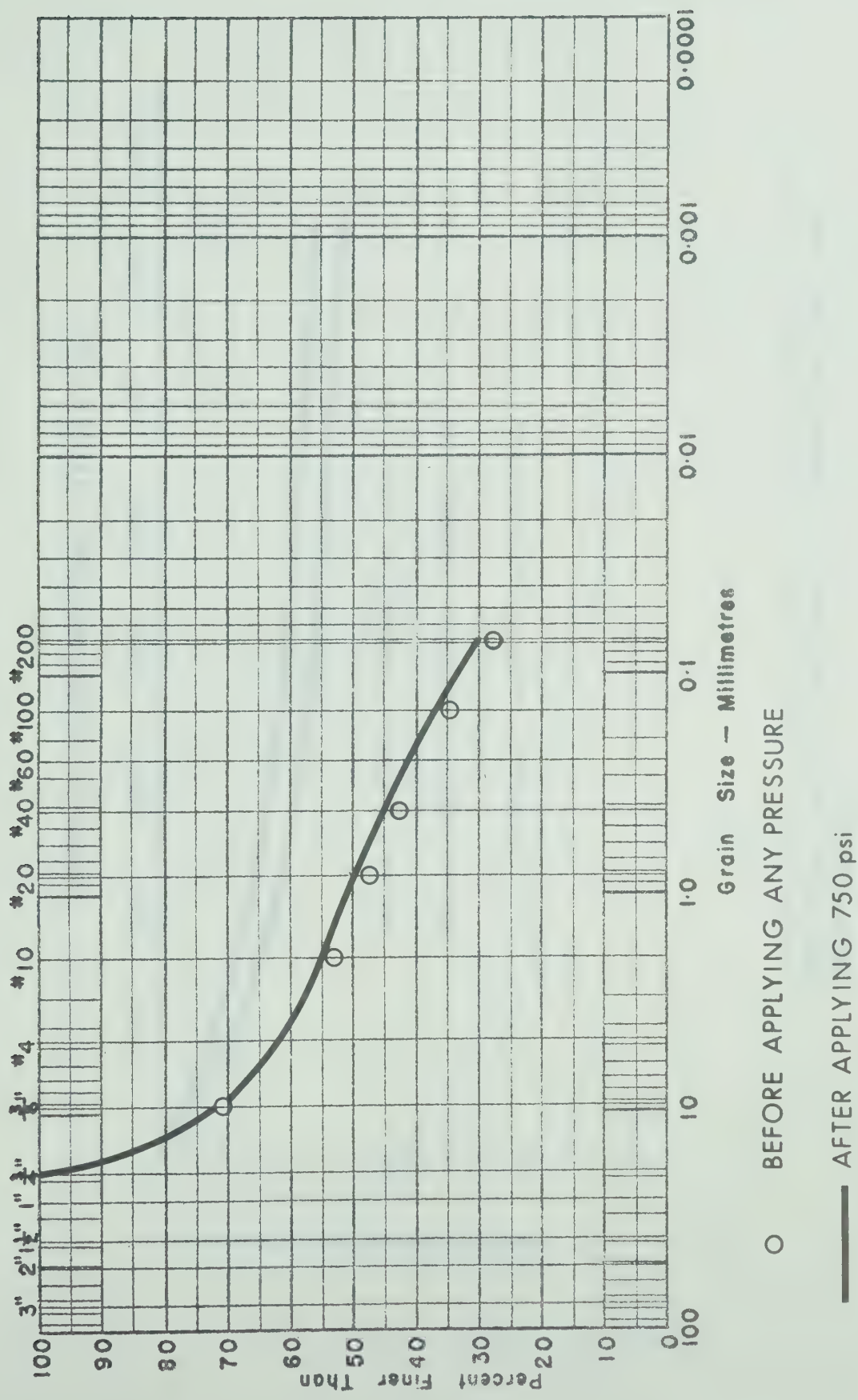


Fig. 2.17 Grain Size Curves for Mica Till Before and After High Pressure Oedometer Compression Test

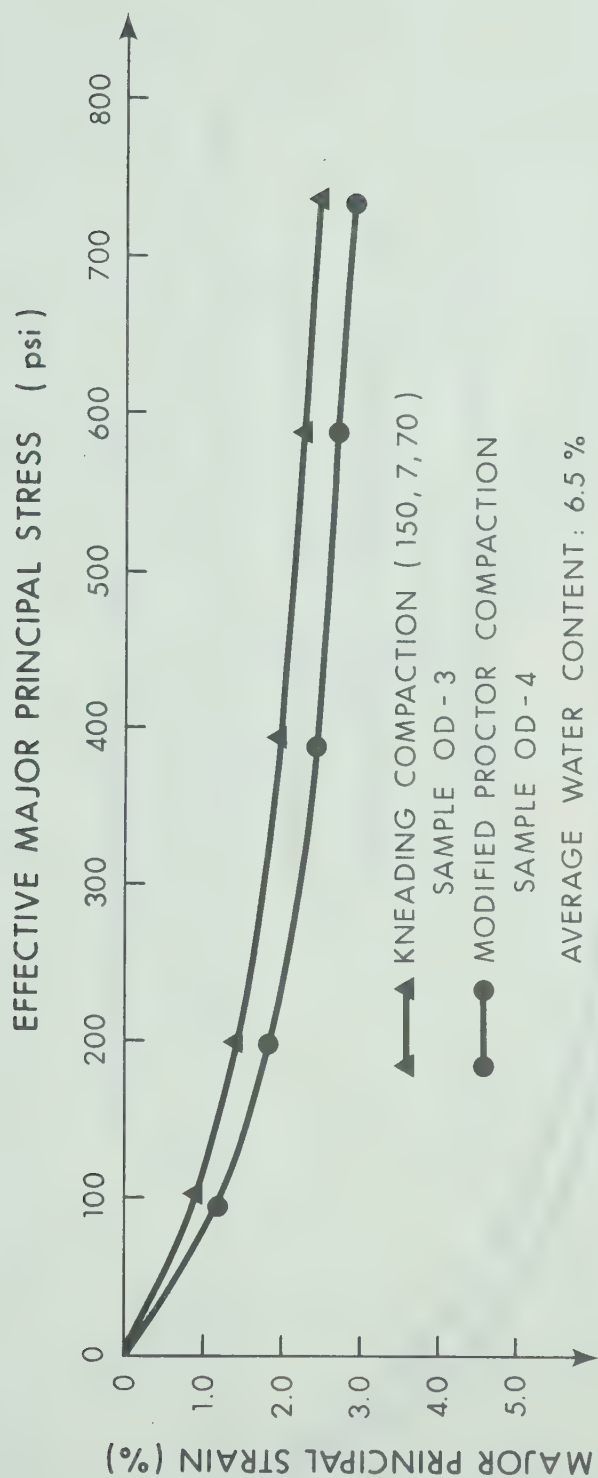


Fig. 2.18 Comparison of Stress-Strain Curves for Mica Till With
 Modified Proctor and Kneading Compaction at Low
 Water Content

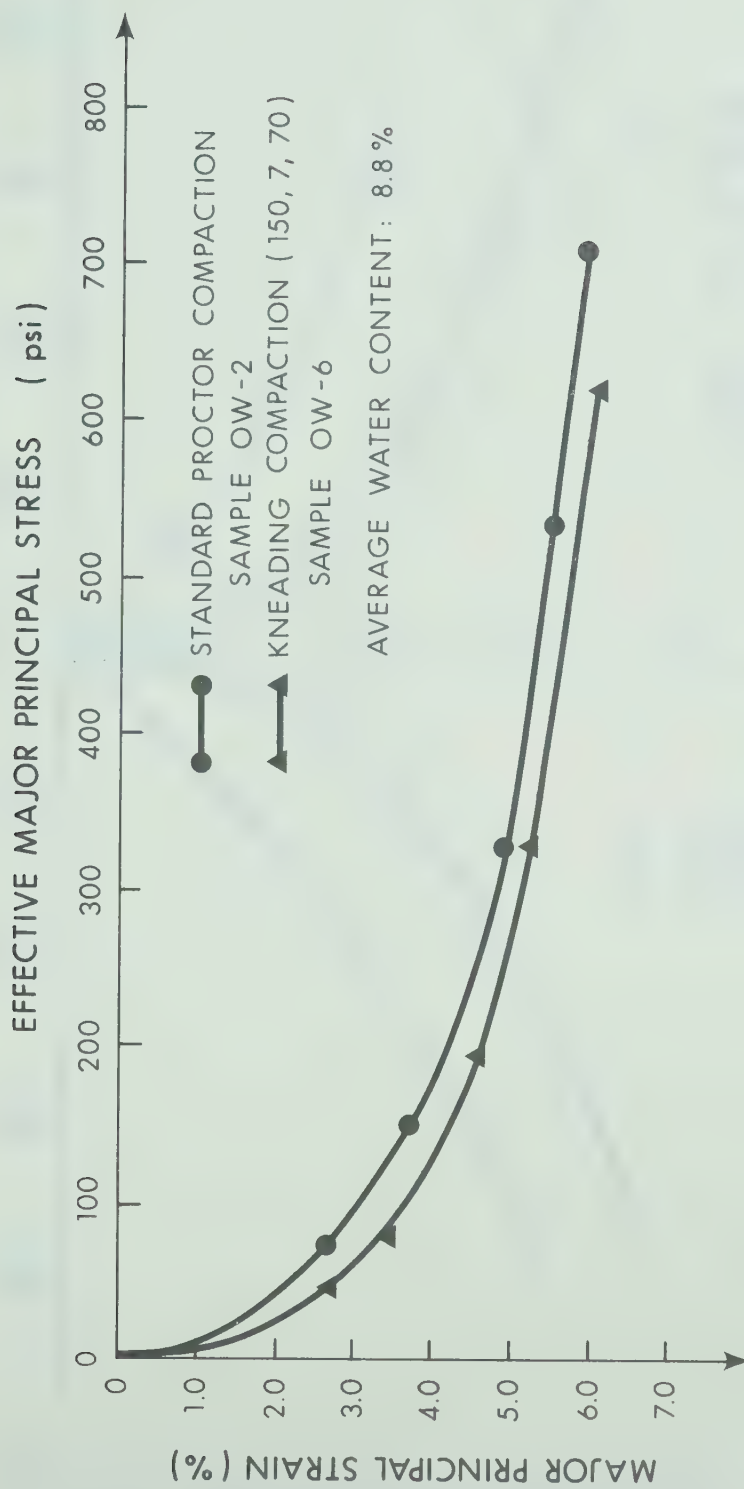


Fig. 2.19 Comparison of Stress-Strain Curves for Mica Till With Standard Proctor and Kneading Compactions at High Water Content

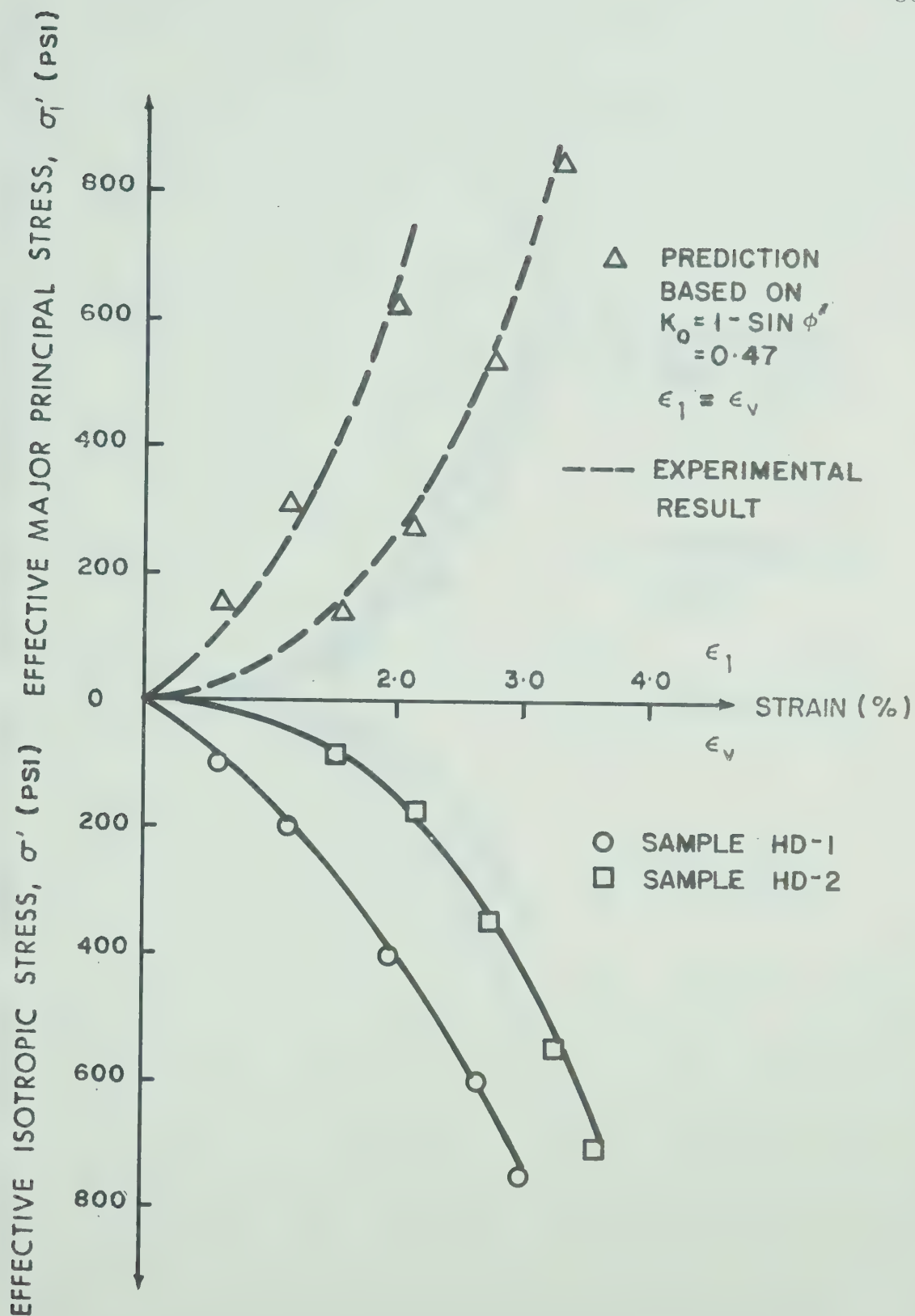


Fig. 2.20 Comparisons on Predicted and Experimental Stress-strain Curves of Till with Low Water Content

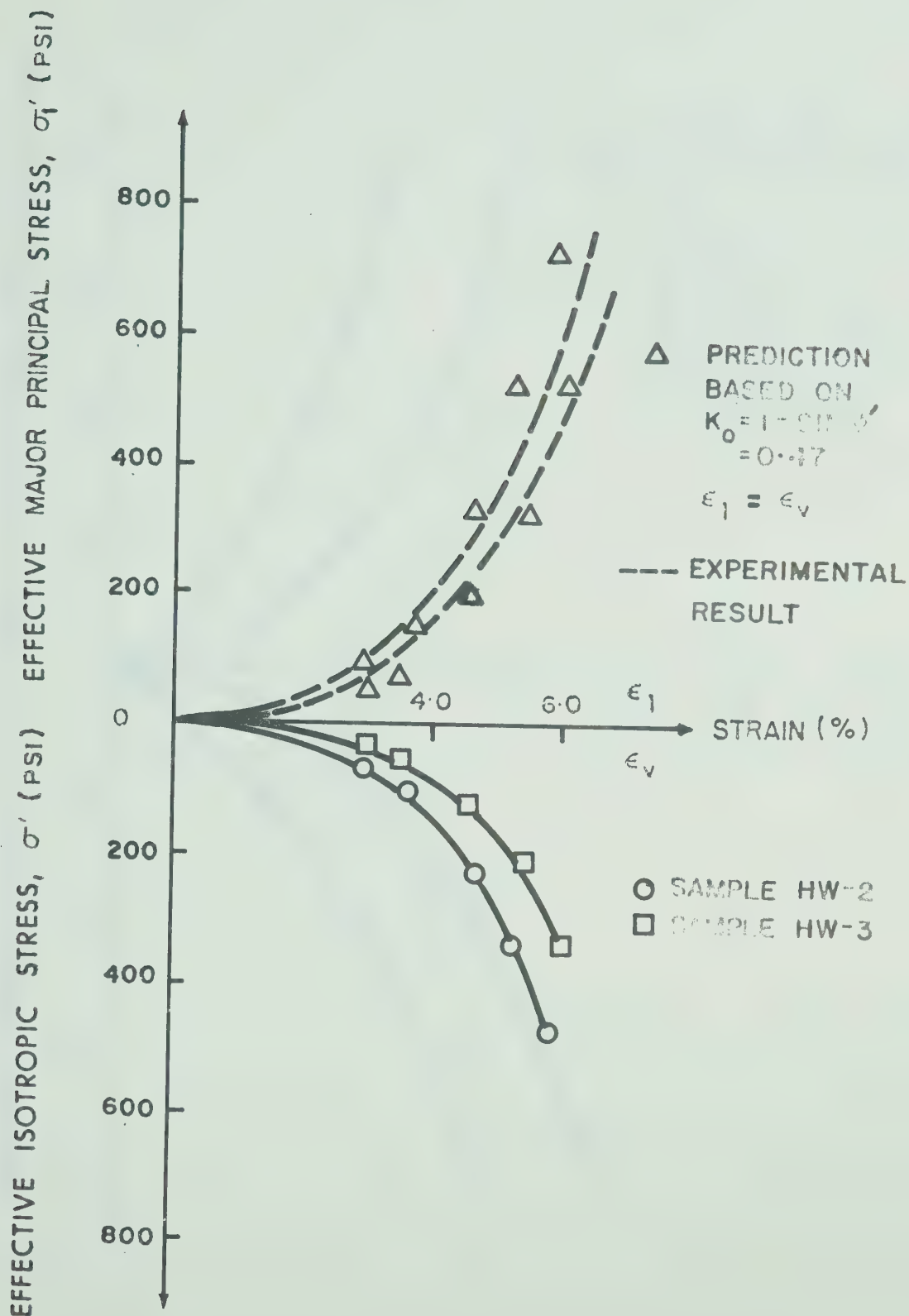


Fig. 2.21 Comparisons on Predicted and Experimental Oedometer Stress-strain Curves of Till With High Water Content

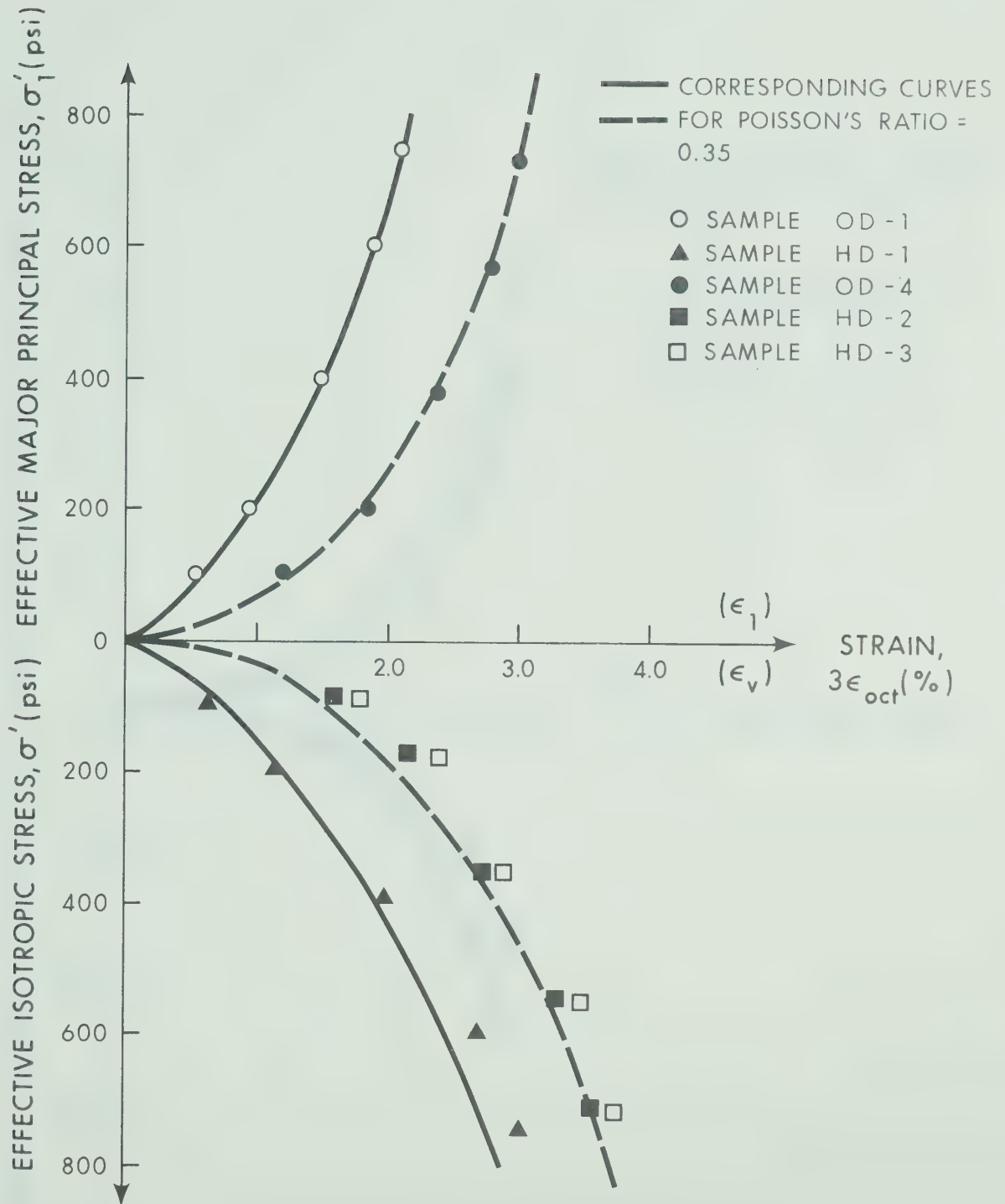


Fig. 2.22 Coupling Effective Stress-Strain Curves of Mica Till With Low Water Content

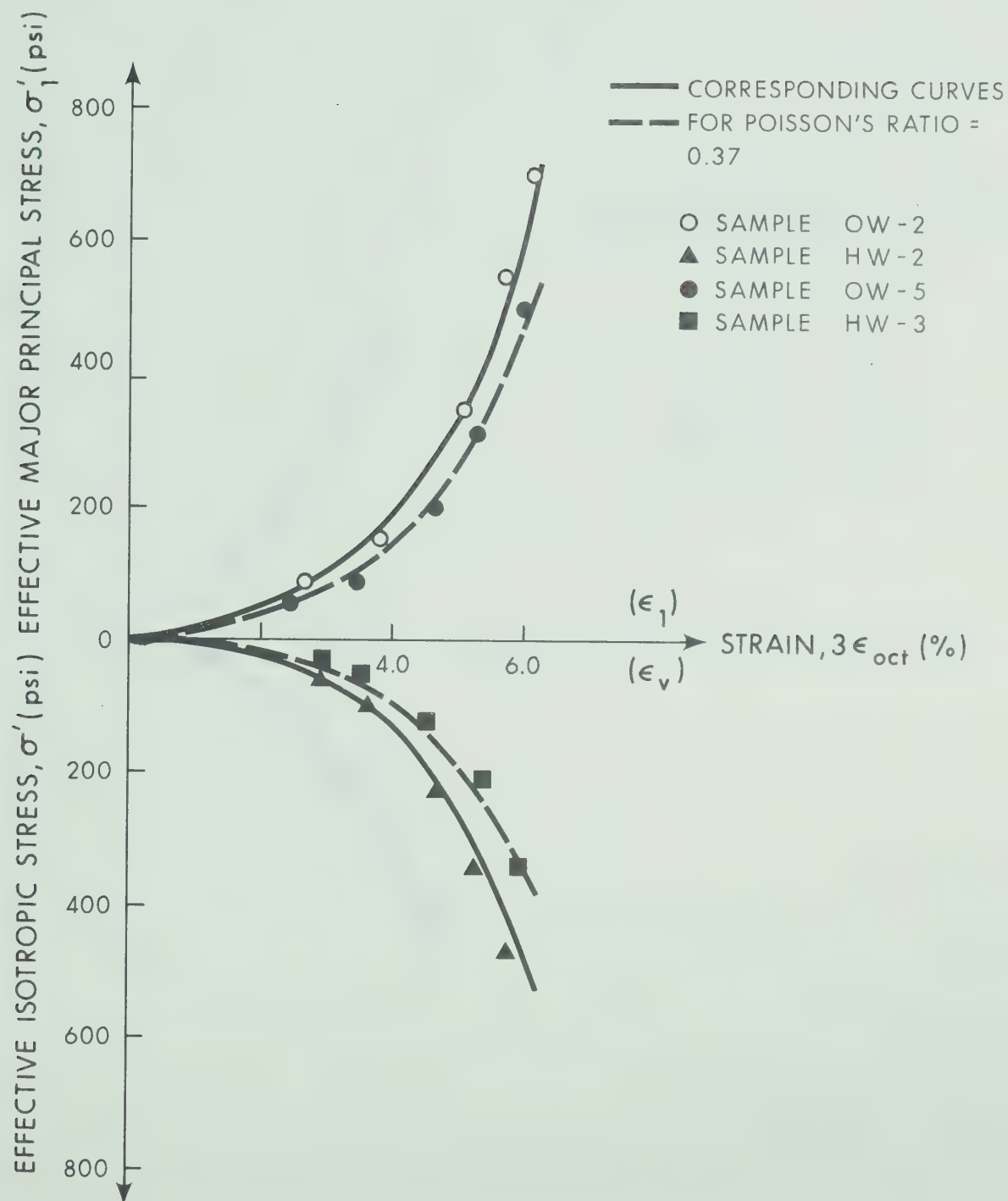


Fig. 2.23 Coupling Effective Stress-Strain Curves of Mica Till with High Water Content

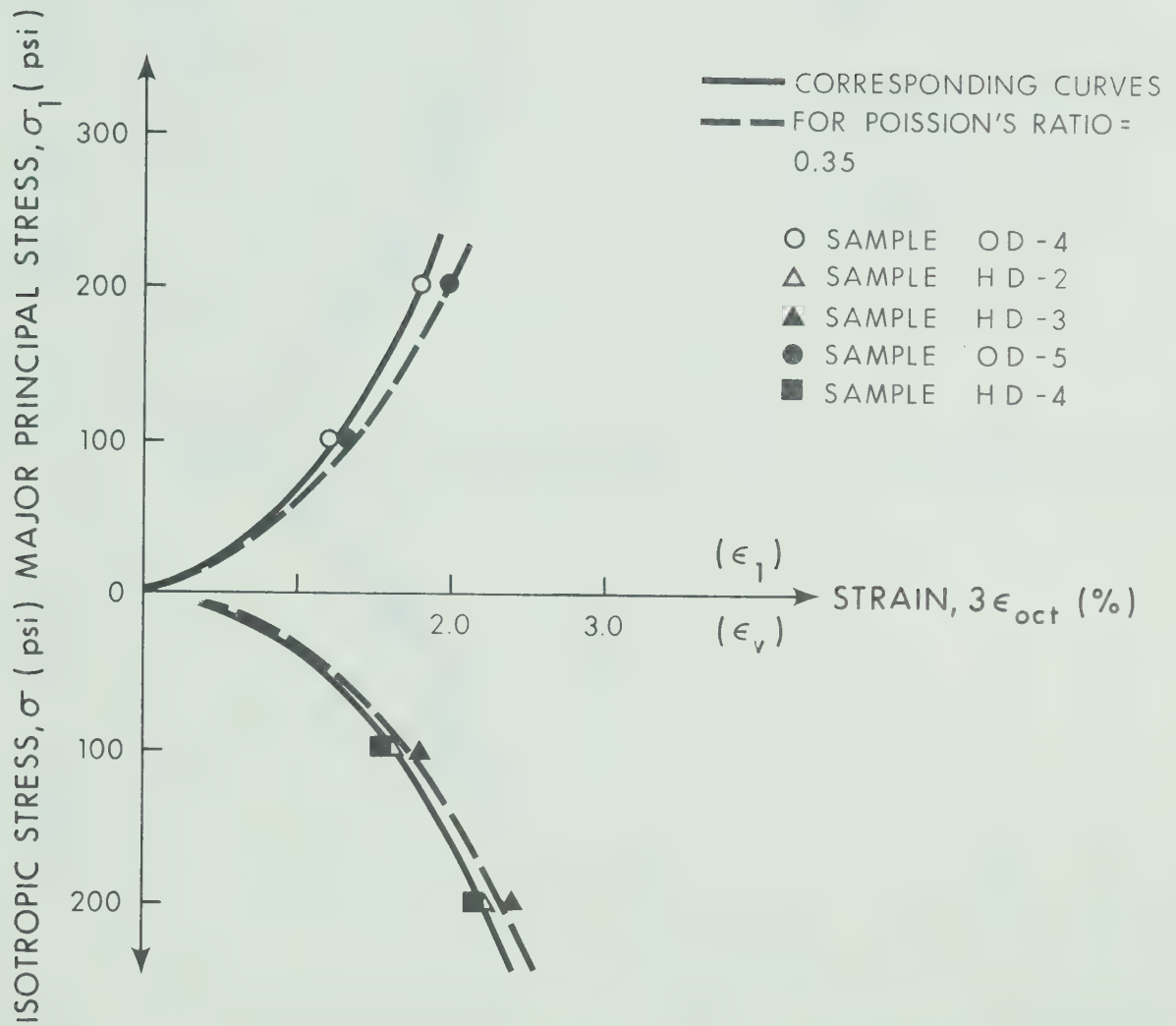


Fig. 2.24 Coupling Total Stress-Strain Curves of Mica Till With Low Water Content

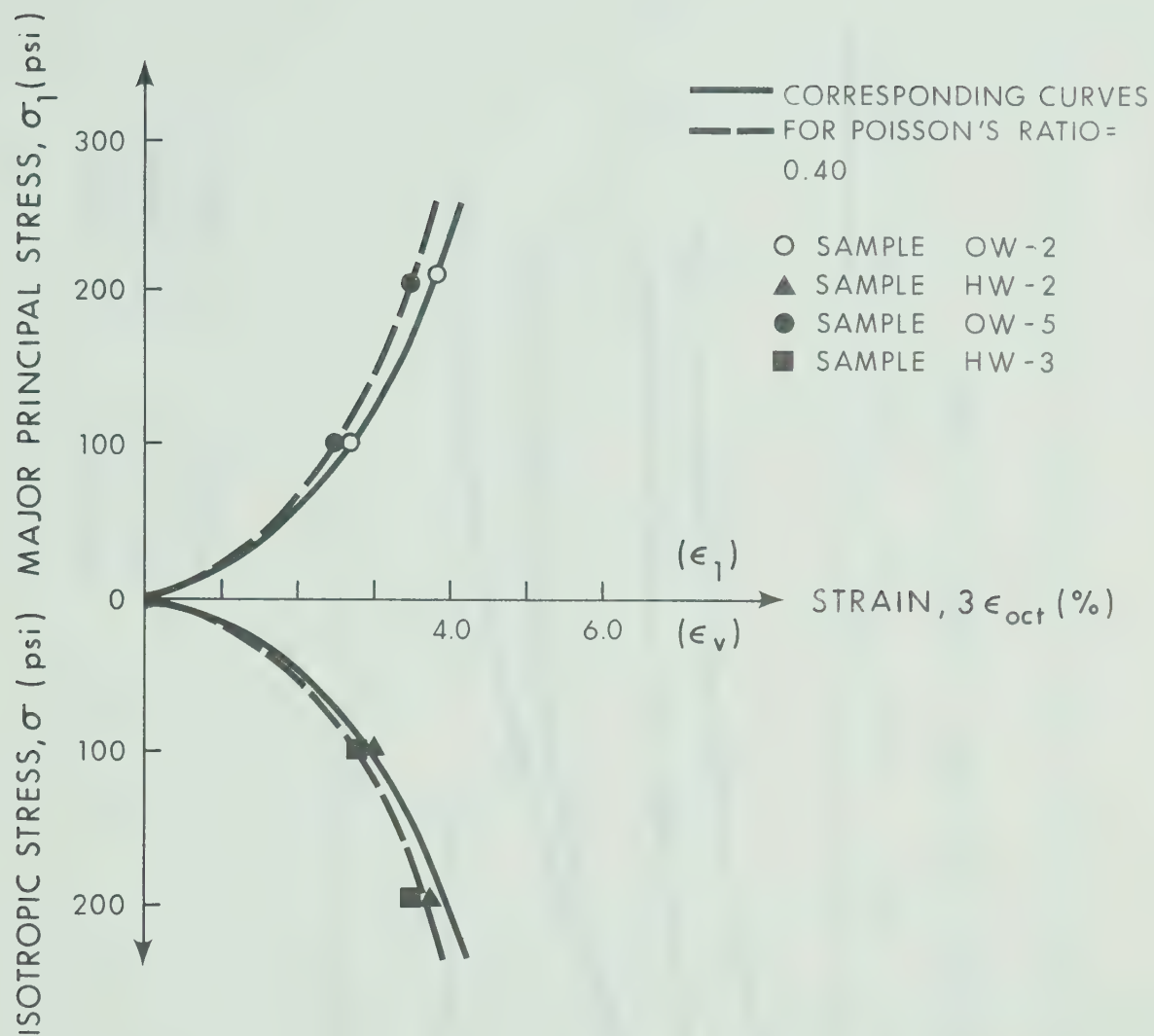


Fig. 2.25 Coupling Total Stress-Strain Curves of Mica Till With High Water Content

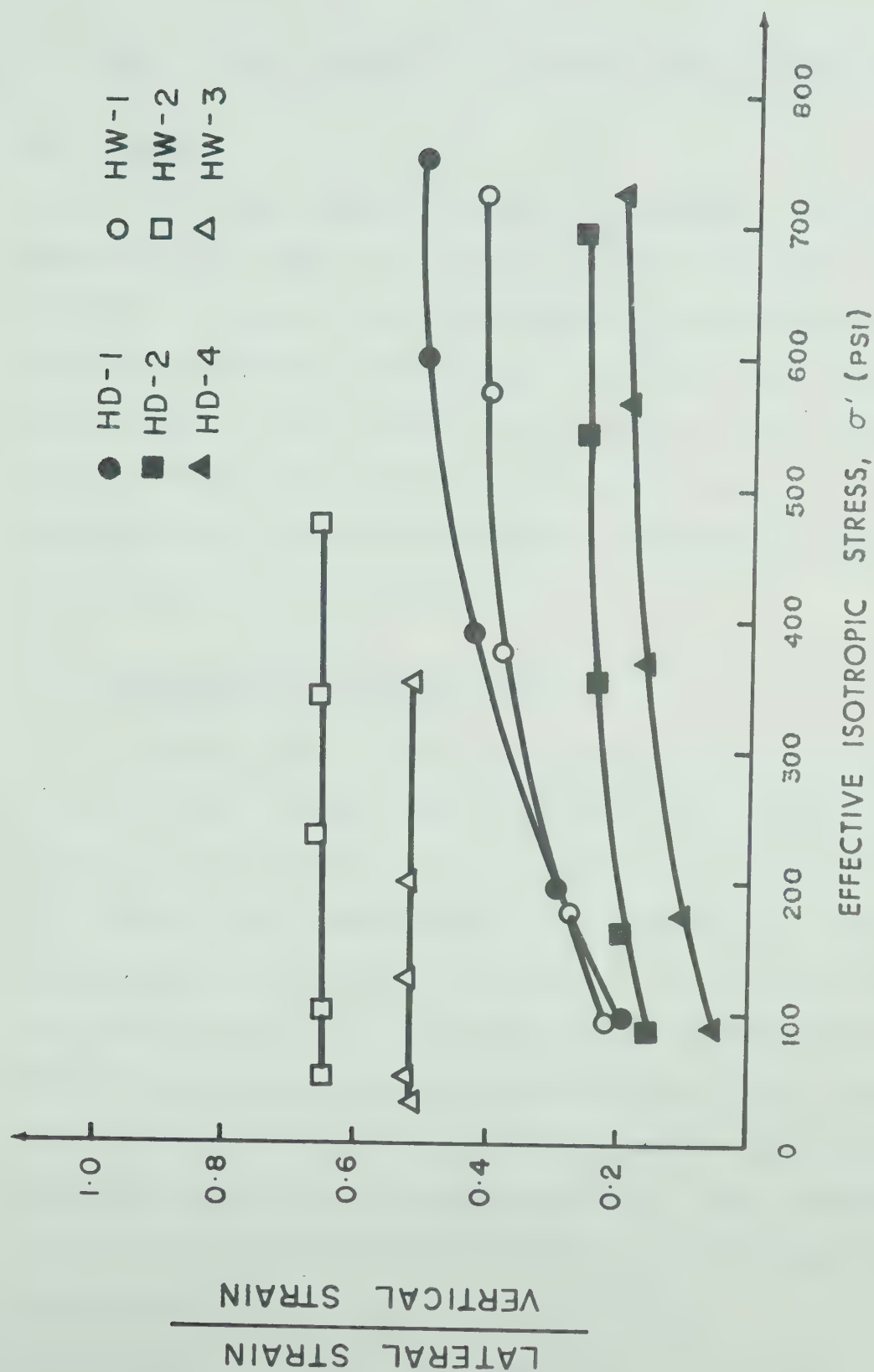


Fig. 2.26 Ratios of Lateral Strain to Vertical Strain in Isotropic Compression Tests

CHAPTER III

SOME FACTORS INFLUENCING STRESSES AND DEFORMATIONS

3.1 Scope

In this chapter a review of the basic settlement mechanism in a dam is presented and the influences of load transfer and anisotropy on stresses and deformations in a dam are examined. The use of two dimensional analyses in the study of deformation is discussed. For convenience and clarity in the sequence of presentation, this chapter considers only those deformations unaffected by pore pressure dissipation.

3.2 Settlement Profile in a Dam During Construction

Since markers used for indicating the settlement in a dam fill are usually placed as the fill is raised, the settlement of a marker at any height of the dam would essentially reflect the compression of the underlying layer caused by the load placed above the marker. The zero settlement datum for each marker is usually established immediately after its placement on the surface of the fill. Thus it is readily apparent that the settlement of the crest immediately after the completion of the dam is zero. This is unlike a 'switch-on gravity' structure which has its maximum settlement at the top.

The basic settlement mechanism in a dam may be studied by considering it as a broad continuously placed fill as shown in Fig. 3.1. Deformations in this broad fill may be regarded as one-dimensional. For simplification, it is assumed that there are no time effects on the settlement and the fill has a constant elastic modulus E_C in a vertical direction. In Fig. 3.1 h is the marker level. The incremental stress at any point within height h due to the fill above the marker level with a thickness dz is:

$$\Delta\sigma_v = \gamma dz$$

The incremental vertical strain at level X within the height h due to this incremental stress is:

$$\Delta\varepsilon_v (X) = \frac{\gamma dz}{E_C}$$

If the fill above the marker is raised from level h to the top of the fill at level H , the total vertical strain at level X is:

$$\varepsilon_v (X) = \int_h^H \frac{\gamma dz}{E_C} = \frac{\gamma(H-h)}{E_C}$$

By integrating this strain for all levels within height h , the total settlement of the marker at level h due to the load from h to the top of the fill is:

$$\delta = \int_0^h \varepsilon_v (X) dX = \frac{\gamma (H-h) h}{E_C} \quad (3.1)$$

From equation (3.1), it is noted that δ is a function not only of the thickness of the compressible layer h , but also the thickness of the fill above the marker $(H-h)$. Thus, the settlement profile showing the settlements at various depths during construction of a dam has a parabolic shape with the maximum value at mid-height of the dam. The typical settlement profile of a continuously placed fill is shown in Fig. 3.2. Although a fill having a constant elastic modulus was considered, a similar situation can also be shown for a material having an elastic modulus that varies with stress level (Naylor and Jones, 1973).

In Fig. 3.2, the settlements are plotted against the heights of reference points in the fill. With the basic definition of strain but without appreciating the settlement mechanism in the continuously placed fill, the slope of the curve may be regarded as the compressive strain of any intermediate layer. However, appreciating the settlement mechanism, it is realized that previous interpretations may not be used in the present case. In Fig. 3.3, δ_2' is the compression of a layer with a thickness h_2 caused by the load $\gamma(H'-h_2)$ while δ_1' is the compression of a layer with thickness h_1 caused by the load $(H'-h_1)$. Settlement δ_2' and δ_1' are functions of two different loads. The ratio $(\delta_1' - \delta_2')/l$ is not related to any single stress and hence it is not the compressive strain of layer A. Consequently, one settlement profile cannot be used to evaluate correctly the elastic modulus of

any intermediate layer in the fill.

The tangential modulus of layer A. however, can be estimated from the two settlement profiles as shown in Fig. 3.3. the incremental strain $[(\delta_1'' - \delta_1') - (\delta_2'' - \delta_2')]/1$ is caused by incremental stress $\gamma(H'' - H')$. The ratio of these incremental stress and strain should indicate the tangential modulus of the layer. For the case where the fill has a constant modulus the use of equation 3.1 indicates that the ratio is equal to modulus E_C .

For a dam project in which a test embankment is constructed during the design stage, it is extremely valuable to employ the previous method for estimating the elastic modulus of the material. Settlement profiles required for the estimation can be obtained from gauges installed in the test embankment. The elastic modulus evaluated in such a way should constitute important parameters to be used for the prediction of deformations in the main dam.

3.3 Finite Element Stress-Deformation Analysis

The finite element stress-deformation analysis in this work were performed by using the computer program given in Appendix B. This program uses constant strain triangular elements each having six degrees of freedom. More refined elements such as quadrilateral elements, each having four constant strain triangular elements (Covarrubias, 1969) or two linear strain triangular elements (Felippa, 1966) are

possible. The less satisfactory results of using constant strain triangular elements usually occur at high shear stress zones. Such zones exist in the dam and are close to the interface between core and shell. In the present investigation, finer mesh was used over expected high shear stress areas. It is believed that this approach eliminated the errors which might otherwise arise from using constant strain elements. As has been shown (Krishnayya, 1973(a)) for soil structure problems accuracies comparable to those obtained with more refined elements can be achieved with the constant strain triangular elements. The equations are solved by Gauss-Seidel iterative procedure. The present program was modified from FENA2D used by Kirshnayya (1973(a)) in the study of the cracking of dams. The following additional facilities were incorporated in the new program.

- (1) The automatic generation of material types.
- (2) The automatic generation of overburden factors for the elements.
- (3) Write or read data to or from tapes.
- (4) The calculation of nonlinear elastic parameters from functional expressions (i.e. hyperbolic function or power function).
- (5) The performance of an "effective stress" analysis with the association of pore pressures analysis.

In this study, several types of stress-deformation analyses were performed. They are incremental linear analysis, non-linear analysis, total stress analysis and effective stress

analysis. In non-linear and incremental linear analyses, the loads were applied in a number of small increments. However, in the former analysis a piece-wise linear relationship between stress and strain was assumed during each increment of load and in the later analysis, constant elastic parameters were used in all the increments. In nonlinear analysis, "average moduli" procedure was used to obtain elastic parameters corresponding to the stress state for each load increment. The details of this procedure have been described by Kirshnayya (1973(a))

Poisson's ratio was not allowed to exceed 0.49 in all the analyses performed. Some elements of the constitutive matrix will become infinite when Poisson's ratio is equal to 0.5. It is widely known that this limitation is inherent in the formulation based on the minimum potential energy principle. Despite this limitation, reasonably good correlations between the results of analysis using maximum Poisson's ratio of 0.49 and field observations have been achieved in a number of cases (e.g., Kulhawy et al., 1969; Chang and Duncan, 1970; Kulhawy and Duncan, 1970), involving nearly incompressible soils ($\nu=0.5$).

3.4 Load Transfer in a Zoned Dam During Construction

The stress conditions in a zoned dam during construction are influenced by two modes of load transfer. These are: (a) load transfer from embankment to abutments (i.e. cross-valley arching) and (b) load transfer between core and shells. In this study, the load transfer is, unless specifically stated otherwise, generally referred to any vertical stress state deviated from

that under one-dimensional uniform compression condition. Load transfer occurs in a dam as a result of a relative displacement or a difference in compressibility of materials. Its existence was evidenced by pressure cell measurements in a number of earth and rockfill dams (e.g. Hölle and Harspranget dams by Löfquist, 1951; Gepatsh dam by Schober, 1967; Scammonden dam by Penman and Mitchell 1970).

Load transfer from embankment to abutments develops due to differences in settlements in the embankment across the valley and higher compressibilities of embankment materials compared to rock abutments. As long as the dam is built in a more or less V-shape valley, regardless of whether the foundation is compressible or incompressible, differential settlements across the valley always exist. Due to the variation in thickness of embankment along the valley walls, settlements in the embankment decrease from a maximum in the center portion of the valley to a minimum at the two edges. The intensity of these differential settlements and hence the intensity of cross-valley arching in a dam is mainly related to the steepness of the valley walls. More significant cross-valley arching is always related to steeper valley walls. The magnitude of cross-valley arching can be studied by a plane strain analysis on a longitudinal (cross-valley) section. In these analyses, the effects of cross-valley arching are separated from combined effects, which include load transfer between core and shell on the actual dam behaviour. In plane strain analyses performed by Lefebvre et al. (1973) for dams in V-shaped valleys with

three different valley wall slopes, it was indicated that major principal stresses in the lower central region of the dam are about 80%, 94% and 96% of overburden pressures for 1:1 (1 horizontal: 1 vertical), 3:1 and 6:1 slopes respectively.

Three dimensional analyses on homogeneous dams with the same material property and the same upstream and downstream slopes but different valley wall slopes are also very useful in the study of cross-valley arching (Lefebvre et al., 1973). The results can clearly show the differences in three-dimensional behaviour relative to 2D due to different degrees of cross-valley arching. However, the major principal stress reductions in the central region of the dam for each geometry should not totally account for the cross-valley arching effects. Load redistribution in transverse direction due to the nearly triangular section also reduces part of the load. This effect can be shown by plane strain analysis on homogeneous transverse section and is referred to in a subsequent discussion. Palmerton (1972) performed a nonlinear three dimensional analysis on a model dam with a central clay core having different elastic properties as compared to the shells. The dam was built in a valley with 1:1 wall slopes. The results of the analyses were compared to those obtained from two dimensional plane strain analyses on the maximum transverse section of the same dam. The comparisons showed that due to cross-valley arching effects the reduction in major principal stresses near the base of the core amounted to 40% of plane strain values.

Load transfer between core and shells, develops due to the difference in the compressibilities of materials in the zones.

As a result of these differences one zone tends to settle more than the other under self weight. The relative displacement mobilizes the shear stress at the interface and hence load is transferred from one zone to another in the embankment. Although load can be transferred from core to shells or from shells to core depending on the relative compressibilities, the former case may be of greater concern to dam designers since near-horizontal fissures may develop through the core. In order to evaluate vertical stresses in the core under arching conditions Nonveiller and Anagnosti (1961) considered the core in a state of plastic equilibrium. While the theory appears to be useful for that state of equilibrium, it cannot be used to evaluate the stresses in elastic equilibrium. Blight (1973) used an effective stress theory to consider the vertical stresses in a narrow core which settled more than the shells. The oversimplifications in the vertical stress distribution pattern across the width of the core and the slopes of the core in this theory may limit the use of the solution.

In order to study the load transfer under various relative stiffnesses or compressibilities between core and shells, a symmetrical half of a typical medium size dam with a central core was used in finite element parametric analyses. The section is shown in Fig. 3.4. In the analysis, the core and the shells had the same unit weight (140 pcf) and the same Poisson's ratio (0.35). The Young's modulus used for the dam when $E_{\text{core}} = E_{\text{shell}}$ was 1000 ksf. Ten lift incremental analyses were performed. From the results of these analyses, which are

shown in Fig. 3.5 it is clearly indicated that when the shell is stiffer, the load is transferred from the core to the shells. As a result the major principal stresses in the core are much less than the overburden pressures. When the core is stiffer, the calculated major principal stresses in the core are generally higher than the overburden pressures due to the load transfer from shell to core. As has been mentioned previously, due to the shape of the transverse section even when the dam was homogeneous ($E_{\text{core}} = E_{\text{shell}}$), the major principal stresses in the core might not be expected to be exactly equal to overburden pressures. In the present case, it is about 90% of the overburden pressures. From the same figure, it can be seen that when E_{shell} is about five times of E_{core} or $E_{\text{core}}/E_{\text{shell}}$ is equal to 0.2 (this is not an uncommon situation and may be expected in zoned dams), the maximum major principal stress near the base of the core can be as low as 50% of the overburden pressure.

3.5 The Use of Two Dimensional Analyses in Deformation Studies

In the previous section, the variations of the magnitude of two modes of load transfer in a zoned dam have been discussed separately. In a real structure, the stress conditions are influenced by both the geometry of the valley and the material properties of core and shells. Thus, it is understandable that more realistic three dimensional stress and displacement results can only be obtained by three dimensional finite element analyses which take into account the combined effect of all the components (Eisenstein et al. 1972(a)). However, it is generally known that 3D analysis

requires considerably more man-time and computer-time compared to 2D analysis. For the case where 2D analysis can provide sufficient accuracy, 2D analysis is still preferred.

Two-dimensional analyses with the assumptions of either plane strain or plane stress conditions on maximum longitudinal sections do not provide correct information regarding the displacements or stresses in a zoned dam. In the analyses, the differences in material properties between core and shells cannot be taken into account. As has been shown earlier, these differences influence significantly the stress distribution in a zoned dam. Even for homogeneous dams, due to the unrealistic boundary conditions imposed the results of plane stress analysis cannot be used to describe the actual behavior (Lefebvre et al. 1973). Plane strain analysis on a maximum longitudinal section of a homogeneous dam can give fairly good results for displacements and stresses in the upper part of the dam. However, differences in stresses as compared to three dimensional case are still significant in the lower portion of the dam (Krishnayya, 1973(a)).

A two dimensional plane strain analysis on a maximum transverse section can provide reasonably accurate results providing the dam is not built in a very steep walled V-shaped valley. Lefebvre et al. (1973) showed, for valley walls inclined at 3:1 (horizontal:vertical) or flatter, that the stresses and displacements obtained from 2D analysis are

not significantly different from 3D results of the same section. For steeper valley walls (e.g. 1:1 slopes), Palmerton (1972) indicated that while stresses from 2D analysis of a zoned dam are less accurate as compared to 3D results, the displacements are in good agreement. The agreement appears to be due to the higher σ_3 values in 2D analysis. A relatively interesting study was performed by Simmons (1974) in the aspect that is presently being discussed. The actual geometry of Mica Dam, which is situated in a valley having walls with a slope of about 2:1, was used in the studies. Remarkably small differences were found in stresses and deformations obtained from 2D and 3D analyses of the main transverse section.

Based on the previous comments and two other reasons described in the following paragraph, two dimensional plane strain analyses performed on maximum transverse section were mainly used in the present study regarding the deformation of a zoned dam. The other reasons are:

- (1) The pore pressure dissipation in a narrow clay core can be incorporated in the 2D stress-deformation analyses in a way which is considerably more feasible compared to 3D analyses. Moreover, from the geometry of the narrow clay core it may be expected that the pore pressure dissipation is mainly two-dimensional and takes

place in transverse sections.

- (2) Deformation results from finite element analysis are sensitive to number of lifts and the simulation of construction sequences used in the analysis. In order to study the representative stress-strain properties of the materials by verifying the analytical results against measurements, it is highly desirable to minimize the errors due to preceding factors. The two dimensional analysis can afford to use a more detailed simulation of construction sequences and number of lifts hence minimizing errors.

3.6 Deformations and Relative Stiffnesses Between Core and Shells

The influence of load transfer on the deformation behavior of earth and rockfill dams has been emphasized by Squier (1970). The case records of two important earth and rockfill dams were shown to indicate clearly this influence. As discussed in a previous section, two dimensional plane strain analyses can be used efficiently to study the deformation in a maximum transverse section of a dam. Deformations in this section are mainly a function of stiffness in the core and shells and their ratio. From the results of the analyses performed on the section shown in Fig. 3.4, the influence of various degrees of core-shell load transfer

on the maximum settlement in the center of the core may be examined. In Fig. 3.6, dimensionless maximum settlements are plotted against ratios of E_{core} and E_{shell} . The E value of 1000 Ksf is used in the presented dimensionless settlements. From this figure, it is seen that the maximum settlement in the core decreases with increasing stiffness of the shells. The amount of reduction was especially significant for the range of E_{shell} equal to five times E_{core} . For the case where core is stiffer than the shells ($E_{\text{core}}/E_{\text{shell}} > 1$) the effect of load transfer from shell to core was outweighed by the effect of the increase in stiffness of the core. As a result, maximum settlement in the core decreases with the increasing $E_{\text{core}}/E_{\text{shell}}$ ratio.

In Fig. 3.7, maximum outward displacements of the slope surface are also plotted against $E_{\text{core}}/E_{\text{shell}}$ ratios. The E value used in the dimensionless displacements is the same as that for the settlements in Fig. 3.6. The increase in core stiffness ($E_{\text{core}}/E_{\text{shell}} > 1$) had only a minor effect on the outward displacements of the slope surface. However, the increase in shell stiffness ($E_{\text{core}}/E_{\text{shell}} < 1$) significantly reduced the outward displacements.

From the previous parametric studies, it is clear that stiff shells can effectively reduce the deformations in a zoned dam. Although an increase in the stiffness of shells alone can also reduce the settlements in the core as the result of load transfer, too high a difference in stiffness between core and shells may affect the safety of the dam.

This is because very low stresses resulting from significant load transfer may facilitate the development of horizontal cracks in the core. The increase in stiffness of shells is preferably accompanied by the increase in core stiffness. In terms of the deformations and safety of the dam the ideal is to maintain the ratio of $E_{\text{shell}}/E_{\text{core}}$ in the range of 2 to 3.

3.7 Principal Stress Ratios in a Dam

The stress conditions in a dam during construction vary from one location to another, e.g. the stress conditions near the slope differ from those in the center of the dam. If K is used to designate the ratio between minor and major principal stress increments, it is found that the K value for most elements of soil in a dam is approximately constant. This condition may be illustrated by the stress analysis results on a transverse section of a model dam. In Fig. 3.8 the calculated minor and major principal stresses resulting from each additional compacted layer of the dam up to its full height are plotted. In two locations of the dam K is constant even though their value differs somewhat for different locations. In a major part of the dam, K values fall within a narrow range and an average of these values may closely represent the values at every part of the dam.

In order to study appropriately the stress-strain behavior of a soil used in the fill of a dam, this constant stress ratio K must be considered in the test. The K value for each particular dam can be estimated from shear strength and factor of safety (Janbu and Hjeltnes, 1965) or a finite

element analysis. Depending on the stress ratio K , the axial stress-strain relationship of a soil under an axisymmetric stress condition would vary. This variation is illustrated in Fig. 3.9 by comparing the experimental stress-strain behavior during isotropic and conventional triaxial compression on identical specimens. The stress states in these two loading paths are the special cases of constant K condition. The values of K in isotropic and triaxial compression are equal to one and zero respectively. The stress-strain curve for the soil having a K value between zero and one may well be expected to lie between those two curves. Since the axial stress-strain curve of the soil is generally used for driving its elastic modulus, there is no doubt that the principal stress ratio would influence the elastic parameters. The variations of elastic parameters with principal stress ratios for two compacted soils was shown by Corotis et al. (1974). It was noted that a higher Young's modulus and a lower Poisson's ratio were derived from the specimen tested under a higher stress ratio K .

3.8 The Influence of Anisotropy on Embankment Stresses and Displacements

Since a compacted earth embankment is placed and rolled in horizontal layers, it might be anticipated that some degree of anisotropy exists. In fact, anisotropic property is indicated in the reported differences in the coefficient of permeability in horizontal and vertical

directions for several completed dams (Sherard et al. 1963). However, due to fewer parameters needed to describe the soil behaviour, studies related to embankment performance so far have always assumed the properties of compacted material to be isotropic.

The simplification is convenient and useful in solving practical problems. The adequacy of assuming isotropy in studies relating to the stresses and displacements of several dams has been reported (Clough and Woodward, 1967; Kulhawy and Duncan, 1970; Eisenstein et al., 1972). However, the general use of this assumption without knowing how much the anisotropy influences the stresses and displacements in the embankment might be questionable. In the following sections, some aspects regarding the stress-strain parameters of an anisotropic material are discussed and a parametric study is conducted on a model dam to investigate the differences in behaviour due to anisotropy. The material is assumed linear elastic in the study.

3.8.1 Stress-Strain Relationships for Anisotropic Soil

It has been shown by Lekhitskii (1963) and many others that thirty-six elastic parameters are used to generalize the linear elastic stress-strain relationships (generalized Hooke's law) of a homogeneous, anisotropic body which has no elements of elastic symmetry. To ensure the existence of the strain-energy function, these parameters are connected by certain relations and hence the number of independent parameters is reduced. Thus, for the most general case of anisotropy, twenty-one elastic parameters are needed to determine the complete stress-strain relation.

The form of anisotropy that usually occurs in construction material is orthogonally-anisotropic. A body of this form of anisotropy has three orthogonal planes of elastic symmetry at each point and nine elastic parameters are needed to describe its elastic stress-strain response. Among all these forms the simplest case, and the one likely to be encountered in geotechnical engineering occurs when the principal axes of anisotropy are everywhere vertical and horizontal and when the properties in all horizontal directions are the same. This kind of anisotropy has generally been referred to as cross-anisotropy or transverse isotropy. Taking horizontal planes as x-y planes and the vertical direction as the z-axis, the stress-strain relationships for cross-anisotropy soil can be expressed as:

$$\begin{aligned}
 \epsilon_x &= \frac{1}{E_H} \sigma_x - \frac{\nu_{HH}}{E_H} \sigma_y - \frac{\nu_{HV}}{E_H} \sigma_z \\
 \epsilon_y &= -\frac{\nu_{HH}}{E_H} \sigma_x + \frac{1}{E_H} \sigma_y - \frac{\nu_{HV}}{E_H} \sigma_z \\
 \epsilon_z &= -\frac{\nu_{HV}}{E_H} \sigma_x - \frac{\nu_{HV}}{E_H} \sigma_y + \frac{1}{E_V} \sigma_z \\
 \gamma_{xy} &= \frac{2(1 + \nu_{HH})}{E_H} \tau_{xy} \\
 \gamma_{yz} &= \frac{1}{G_V} \tau_{yz} \\
 \gamma_{xz} &= \frac{1}{G_V} \tau_{xz}
 \end{aligned} \tag{3.2}$$

where E_H is Young's modulus in the horizontal direction, E_V is Young's modulus in the vertical direction G_V is the shear modulus in a vertical plane, ν_{HH} is Poisson's ratio for strain in any horizontal direction due to a horizontal direct stress at right angles and ν_{HV} is Poisson's ratio for strain in the vertical direction due to a horizontal direct stress. As may be noted there are five independent elastic parameters involved in the relationships. The following equality, which was proved by Love (1892), was introduced in the formulation of the previous equations.

$$\frac{\nu_{VH}}{E_V} = \frac{\nu_{HV}}{E_H} \quad (3.3)$$

where ν_{VH} is Poisson's ratio for strain in the horizontal direction due to a vertical direct stress.

Using the coordinate transformation procedure of Lekhnitskii, (1963), the Young's modulus E_θ for an anisotropic soil with its axis inclined at some angle θ to the horizontal can be expressed as follows:

$$\frac{1}{E_\theta} = \frac{\cos^4 \theta}{E_H} + \frac{\sin^4 \theta}{E_V} + \left(\frac{1}{G_V} - \frac{2\nu_{VH}}{E_V} \right) \cos^2 \theta \sin^2 \theta \quad (3.4)$$

One interesting point emerges from an examination of this equation. It is possible that a material is anisotropic even though it possesses $E_H = E_V = E$ and $\nu_{HH} = \nu_{HV} = \nu$. The modulus, E_θ , will not equal to E or the material will not be isotropic unless $G_V = E/2(1+\nu)$. Since G_V is an independent

parameter, it can have a value which bears no relationship to other parameters. Therefore, although $E_H = E_V$ and $\nu_{HH} = \nu_{HV}$ are necessary to ensure isotropy they are not sufficient.

In view of previous discussions, it might be clear that compression tests on specimens sampled with their axes in horizontal and vertical directions may be used to determine the four independent elastic parameters for anisotropic soil other than G_V . In order to determine G_V reliably, a compression test on specimens sampled with their axes inclined at some angle θ (45° is an obvious choice) is necessary. From this test, E_θ or E_{45° can be determined and hence G_V can be calculated from equation (3.4) with the known values of θ , E_θ , E_V , E_H and ν_{VH} . For an incompressible material, which may represent a soil under conditions of full saturation and no drainage, the independent elastic parameters are reduced from five to three, namely E_V , E_H and G_V . However, compression tests on three specimens as mentioned earlier are still necessary for the determination of these parameters. The other two previous independent parameters are now related to these parameters in the following way:

$$\left. \begin{aligned} \nu_{HV} &= \frac{1}{2} \frac{E_H}{E_V} \\ \nu_{HH} &= 1 - \frac{1}{2} \frac{E_H}{E_V} \end{aligned} \right\} \quad (3.5)$$

These relationships can be conveniently derived by setting the volumetric strain under general stress conditions equal to zero.

By further reviewing the volumetric strain and stress relationship which can be expressed as follows, another interesting behavior of anisotropic material can be observed.

$$\begin{aligned}\epsilon_{\text{oct}} &= \frac{1}{3E_H} [(1-\nu_{HH} - \nu_{HV})(\sigma_x + \sigma_y) + (\frac{E_H}{E_V} - 2\nu_{HV}) \sigma_z] \\ &= K_{\text{an}} \sigma_{\text{oct}}\end{aligned}\quad (3.6)$$

where

$$K_{\text{an}} = \frac{(1-\nu_{HH} - \nu_{HV})(\sigma_x + \sigma_y) + (n - 2\nu_{HV}) \sigma_z}{E_H (\sigma_x + \sigma_y + \sigma_z)}$$

and $n = \frac{E_H}{E_V}$

From this expression, it can be seen that, unlike the bulk modulus of isotropic material, K_{an} depends not only on the elastic parameters but also on the applied stresses. Consequently, σ_{oct} can induce both the same sign and the opposite sign of ϵ_{oct} depending on whether

$$K_{\text{an}} > 0 \quad \text{or} \quad K_{\text{an}} < 0$$

This point implies that dilatant material may be treated by anisotropic elastic theory (Pickering, 1970).

3.8.2 Bounding Values on Elastic Parameters

Since it was assumed that a soil may be treated as an elastic material, the parameters used for describing the stress-strain relationships of anisotropic soil as presented in section 3.8.1 must satisfy the strain energy requirement for that material. It is clearly recognized from thermodynamic considerations that the strain energy of an elastic material should always be positive. By expressing the stress-strain relationships in section 3.8.1 in matrix form as $\{\epsilon\} = [C] \{\sigma\}$, the strain energy per unit volume of anisotropic soil can be evaluated from $\frac{1}{2} \{\sigma\}^T [C] \{\sigma\}$. To ensure this value will be positive, the elastic parameters are bounded on their values as follows (Pickering, 1970).

$$(1) \quad E_H, E_V \text{ and } G_V > 0$$

$$(2) \quad -1 < \nu_{HH} < 1 - 2 (\nu_{HV})^2 \left(\frac{E_V}{E_H} \right)$$

For an incompressible material, the first of the previous two conditions is necessary, while the other condition (Gibson, 1974) is

$$0 \leq \frac{E_H}{E_V} \leq 4$$

3.8.3 Anisotropic Analysis of a Model Dam

The sections shown in Fig. 3.10 represents a symmetrical half of the maximum transverse section of a medium size dam. In order to study the influences of anisotropy this same section was used in all the analyses with different anisotropic elastic properties for the material. Different anisotropic properties were introduced by varying one or two of the five independent parameters discussed previously. In particular, variations of E_H , ν_{HH} and G_V from the values required for isotropic conditions were of particular interest. Parameters E_V and ν_{VH} were kept the same in all the analyses. Instead of ν_{HV} , it is more convenient to consider ν_{VH} as an independent parameter in this section. Details of the values used for each parameter in each analysis are listed in Table 3.1. A total of nine analyses were performed.

In all the analyses, it was assumed that the dam was constructed in ten lifts and had an average density of 140 lb/ft³. The foundation supporting the dam was assumed to be rigid. The section was assumed to be deforming under plane strain conditions. The stress-strain relationships for cross-anisotropic material in plane strain conditions can be derived from the three dimensional relationship discussed in section 3.8.1 by setting zero normal and shear strains relating to the plane normal to x or y direction. In the analyses, the $[D]$ in $[\sigma] = [D][\epsilon]$ relationship can

be expressed as follows (Zienkiewicz and Cheung, 1967).

$$[D] = \frac{E_v}{(1+\nu_{HH})(1-\nu_{HH}-2n\nu_{vH}^2)} \begin{bmatrix} n(1-n\nu_{vH}^2) & n\nu_{vH}(1+\nu_{HH}) & 0 \\ n\nu_{vH}(1+\nu_{HH}) & (1-\nu_{HH}^2) & 0 \\ 0 & 0 & d \end{bmatrix}$$

$$\text{where } n = \frac{E_H}{E_v}, \quad m = \frac{G_v}{E_v}, \quad d = m(1+\nu_{HH})(1-\nu_{HH}-2n\nu_{vH}^2)$$

3.8.4 Results of the Analyses

Results of the analyses are shown in Figs. 3.11 to 3.14. In these figures, the settlements along the centre line of the dam, horizontal movements at a height of 0.4 H and shear stresses along the base of the dam are presented. Horizontal movements at a height of 0.4 H were studied due to the fact that a maximum value occurred about this elevation. From Figs. 3.11 to 3.13 showing individual influences of G_v , E_H or ν_{HH} , it can be noted that settlements decrease and shear stresses along the base of the dam increase with the increasing G_v , E_H or ν_{HH} . Outward horizontal

displacements decrease with increasing G_V and decreasing E_H or ν_{HH} . By considering approximately the same percentage of deviation from an isotropic condition, it was found that the parameter E_H had the most significant effects on the embankment behavior. If E_H is 50% less than the value required for isotropic conditions, the results calculated from isotropic theory will underestimate the actual maximum settlement by about 20% for values of the parameters considered. The maximum outward displacement at a height of $0.4 H$ and the shear stress along the base of the dam will be overestimated by about 100% and 50% respectively.

In an actual cross-anisotropic material, however, the inequality between E_H and E_V is always accompanied by a difference in ν_{HH} and ν_{VH} . Moreover, a value greater than unity for E_H/E_V is quite often accompanied by a value smaller than one for ν_{HH}/ν_{VH} or vice versa. This condition is especially true for an incompressible material. From equation (3.5) presented in section 3.8.1, it is easily verified that if E_H/E_V of an incompressible material is equal to 1.5, then ν_{HH}/ν_{VH} is equal to 0.5. In a cross-anisotropic soil, the relative variations of E_H/E_V and ν_{HH}/ν_{VH} may not be exactly similar to an incompressible material. However, from field evidence, the tendency for similarity has been observed. Seismic tests on a gravel bed beneath the Huskey Tower reported by Clark and Robinson (1971) indicated that ratios of Young's modulus in horizontal and vertical directions

ranging from 1.27 to 1.81 were accompanied by ratios of Poisson's ratio in the same directions ranging from 0.45 to 0.66. Regarding the ratios of Young's modulus in horizontal and vertical directions, a similar range of values had also been measured for London clay (Ward et al. 1959; Ward et al. 1965). Some measured anisotropic properties of compacted soil were discussed in Chapter II. So far, complete data concerning anisotropic stress-strain properties of compacted material has never been reported in the literature.

In spite of this, Skermer (1973) commented that the anisotropy in a dam was likely to have values of $E_H/E_V < 1$ and $\nu_{HH}/\nu_{VH} > 1$.

Since the field evidence seems to indicate that E_H and ν_{HH} do not deviate from isotropic values separately, the combined effect of E_H and ν_{HH} was studied with two sets of values while maintaining G_V at a value equal to $E_V/2(1+\nu_{VH})$. For the first investigation values of $E_H/E_V = 1.5$ and $\nu_{HH}/\nu_{VH} = 0.5$ were chosen and for the second investigation $E_H/E_V = 0.5$ and $\nu_{HH}/\nu_{VH} = 1.5$. The results of the analyses are shown in Fig. 3.14. From these comparisons between results of the first investigation and those of analyses No. 4 ($E_H/E_V = 1.5$, $\nu_{HH}/\nu_{VH} = 1$) and No. 6 ($E_H/E_V = 1$, $\nu_{HH}/\nu_{VH} = 0.5$) of Table 3.1, or from the similar comparisons for the second investigation, it is clear that E_H/E_V has a greater effect on an embankment behaviour than ν_{HH}/ν_{VH} . In the former case, the similar trend of deviation from isotropic behaviour, (i.e. settlements are less than those of isotropic conditions) is observed for first investigation

and analysis No. 4. As compared to the individual effect from E_H or ν_{HH} , the combined effect of E_H and ν_{HH} showed a lesser extent of departure from isotropic behaviour due to anisotropy. For the values investigated as may be observed from Fig. 3.14 the differences were about 10%, 15% and 20% in maximum settlements, maximum outward displacement at a height of 0.4 H and maximum shear stress along the base of the dam respectively.

TABLE 3.1
VALUES OF ELASTIC PARAMETERS FOR ANISOTROPY ANALYSES

Analysis No.	E_v (Ksf)	ν_{vh}	E_H (Ksf)	ν_{HH}	G_v (Ksf)	Remark
1	1000	0.35	1000	0.35	370.4	Isotropy
2	1000	0.35	1000	0.35	500.0	$n = 1^*$, $r = 1^+$
3	1000	0.35	1000	0.35	200.0	$n = 1$, $r = 1$
4	1000	0.35	1500	0.35	370.4	$n = 1.5$, $r = 1$
5	1000	0.35	500	0.35	370.4	$n = 0.5$, $r = 1$
6	1000	0.35	1000	0.175	370.4	$n = 1$, $r = 0.5$
7	1000	0.35	1000	0.525	370.4	$n = 1$, $r = 1.5$
8	1000	0.35	1500	0.175	370.4	$n = 1.5$, $r = 0.5$
9	1000	0.35	500	0.525	370.4	$n = 0.5$, $r = 1.5$

$$* \quad n = \frac{E_H}{E_v} \quad + \quad r = \frac{\nu_{HH}}{\nu_{vH}}$$

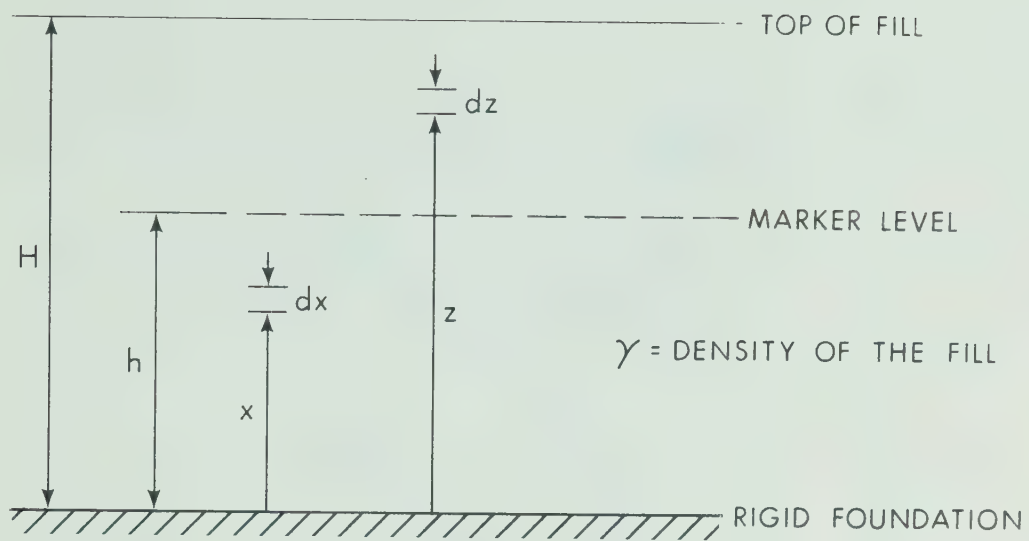


Fig. 3.1 Broad Continuously Placed Fill

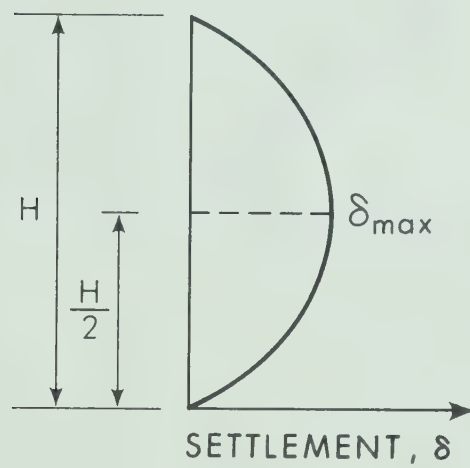


Fig. 3.2 Settlement Profile of a Continuously Placed Fill

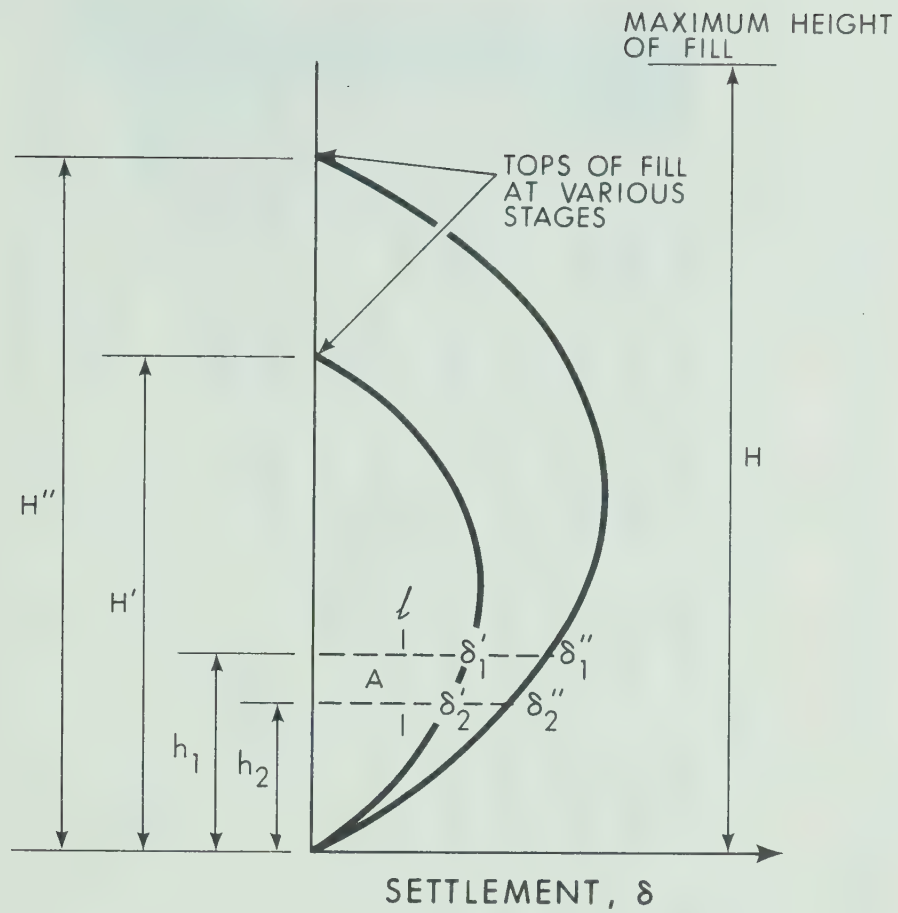


Fig. 3.3 Settlement Curves at Various Stages of Construction

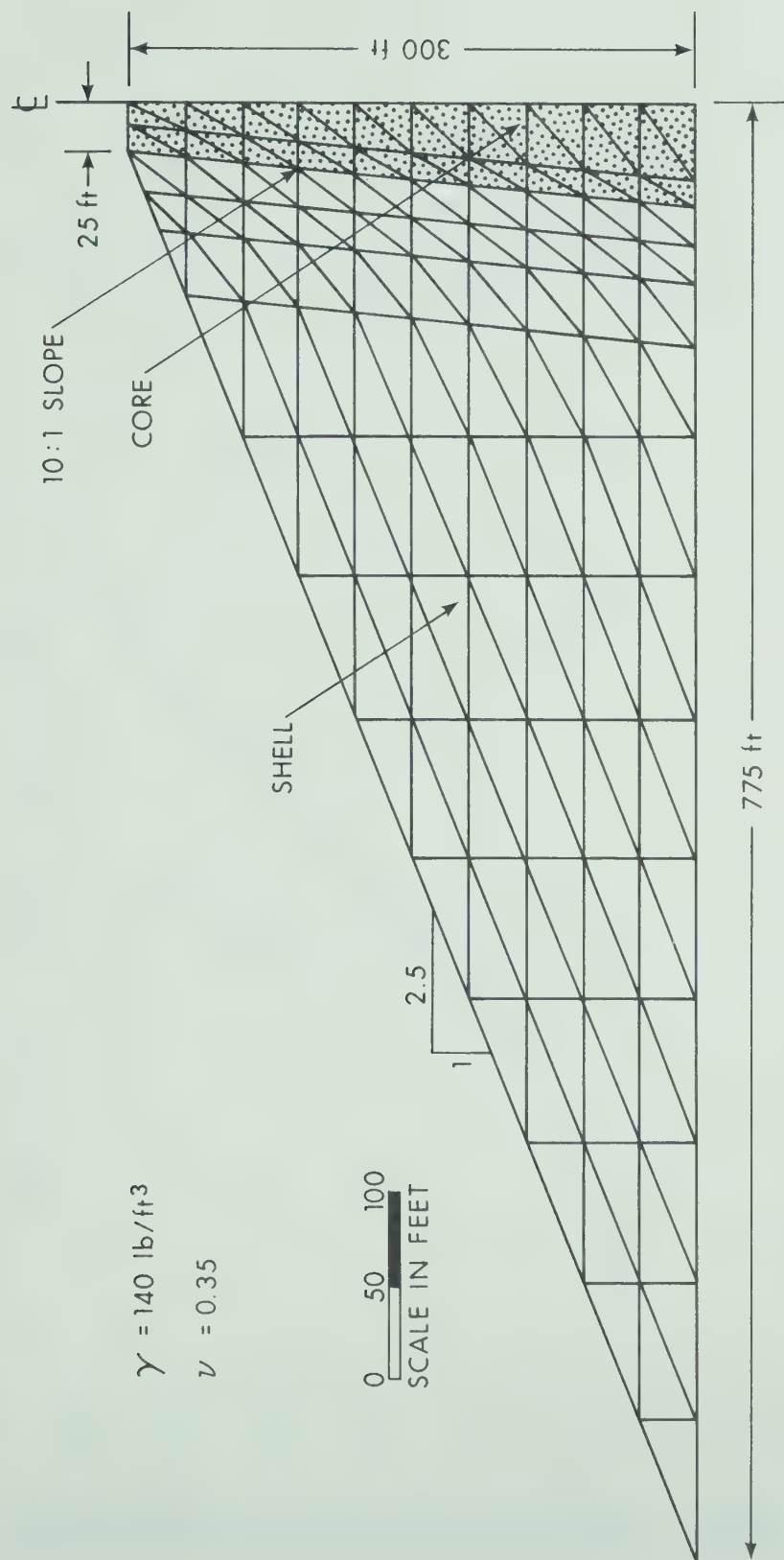


Fig. 3.4 Finite Element Idealization of a Zoned Dam

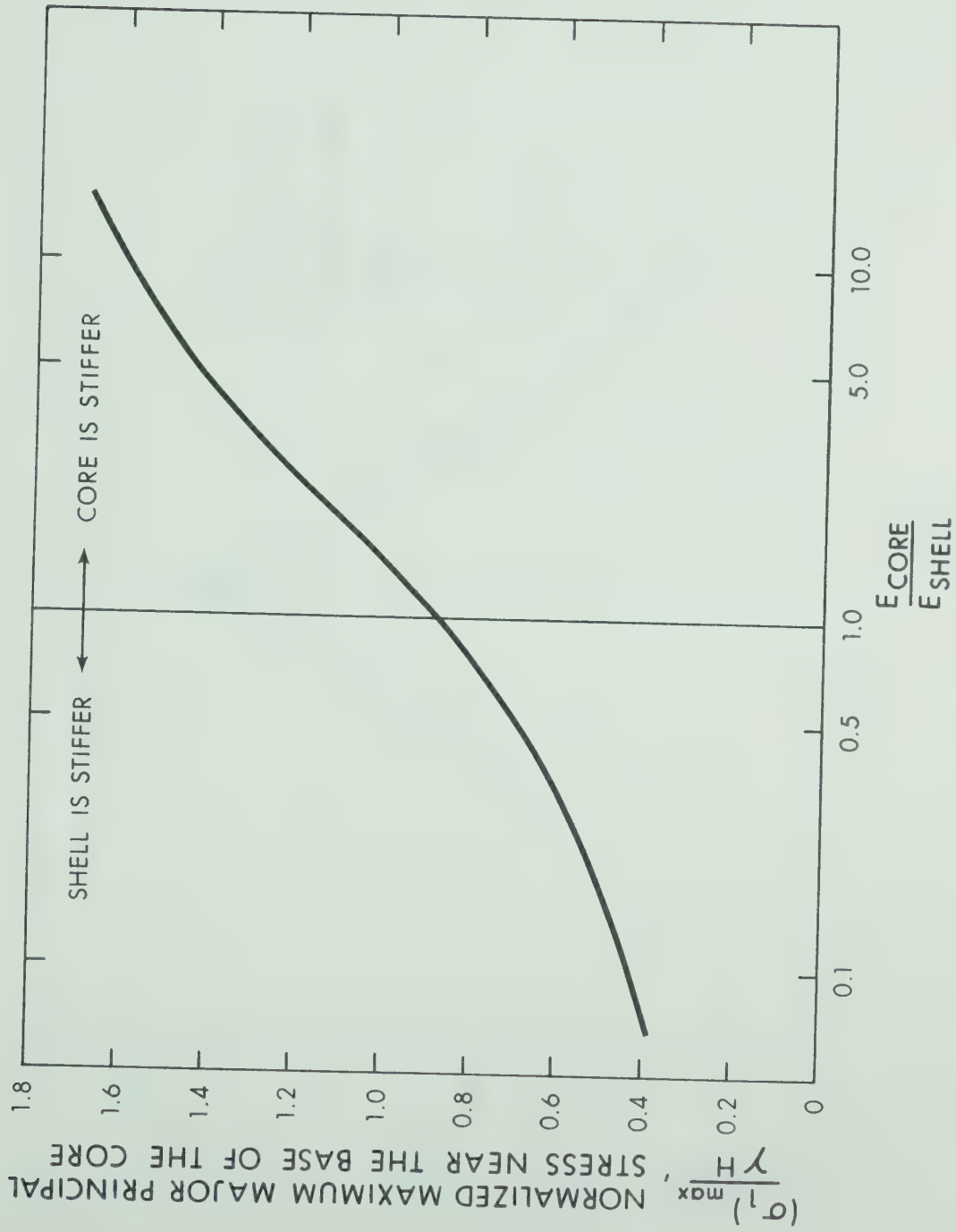


Fig. 3.5 Maximum Major Principal Stresses Near the Base of the Core for Different Ratios of Moduli of Core to Shell

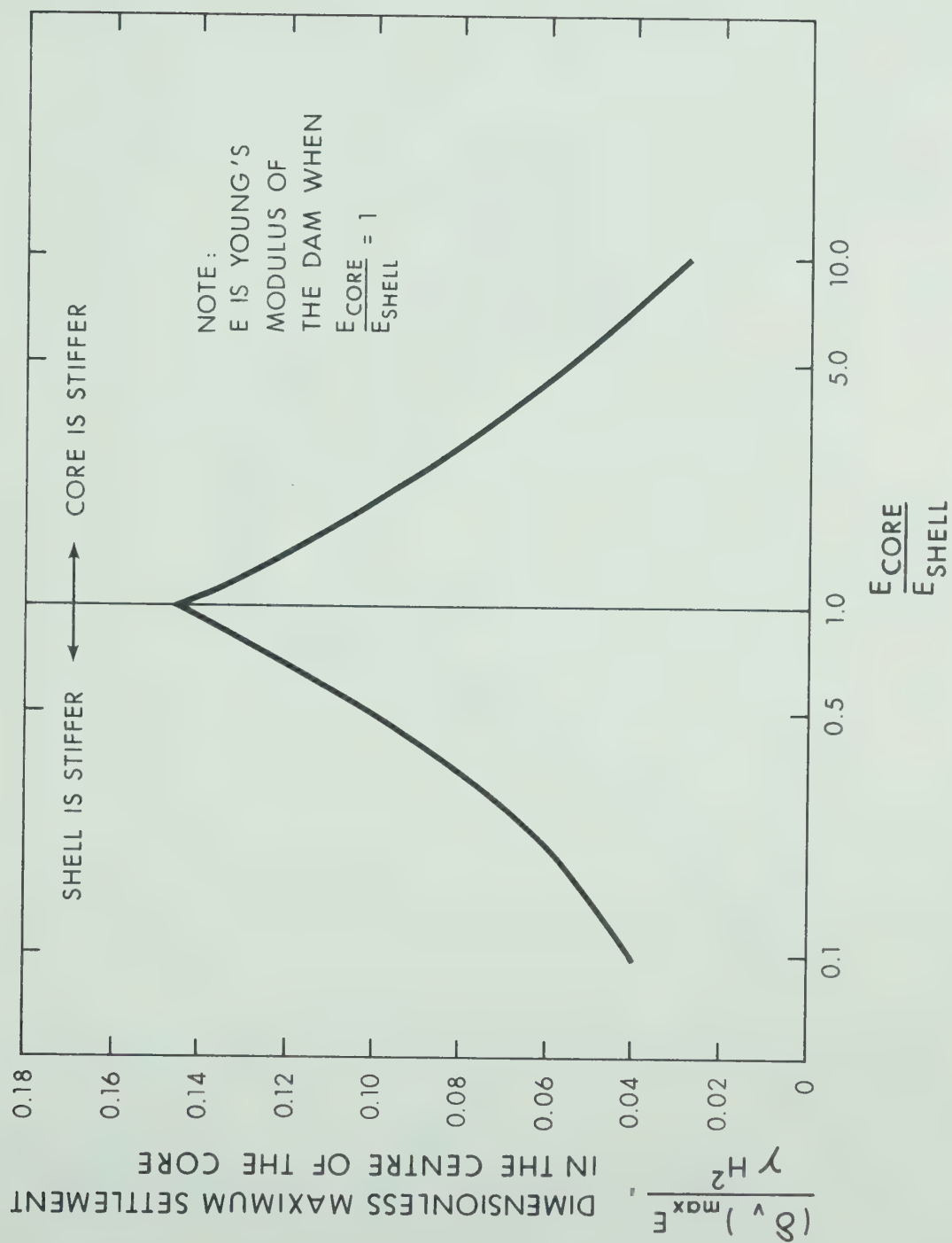


Fig. 3.6 Maximum Settlements in the Center of the Core for Different Ratios of Moduli of Core to Shell

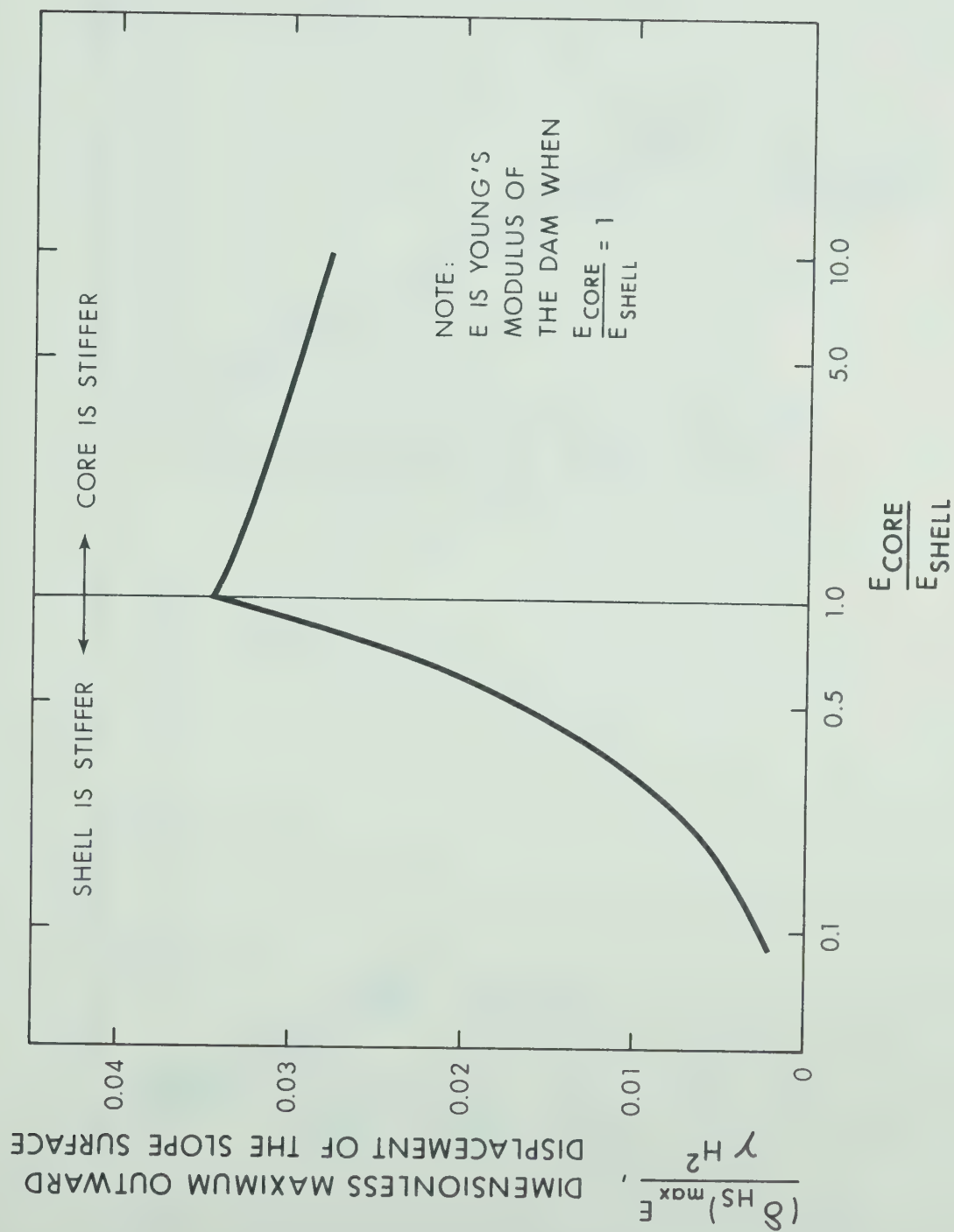


Fig. 3.7 Maximum Outward Displacements of the Slope Surface for Different Ratios of Moduli of Core to Shell

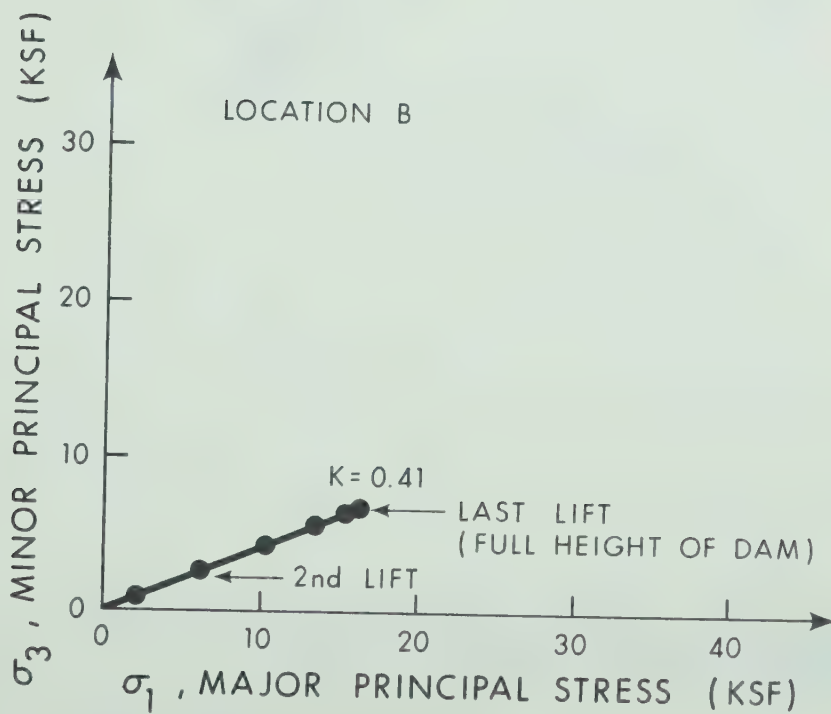
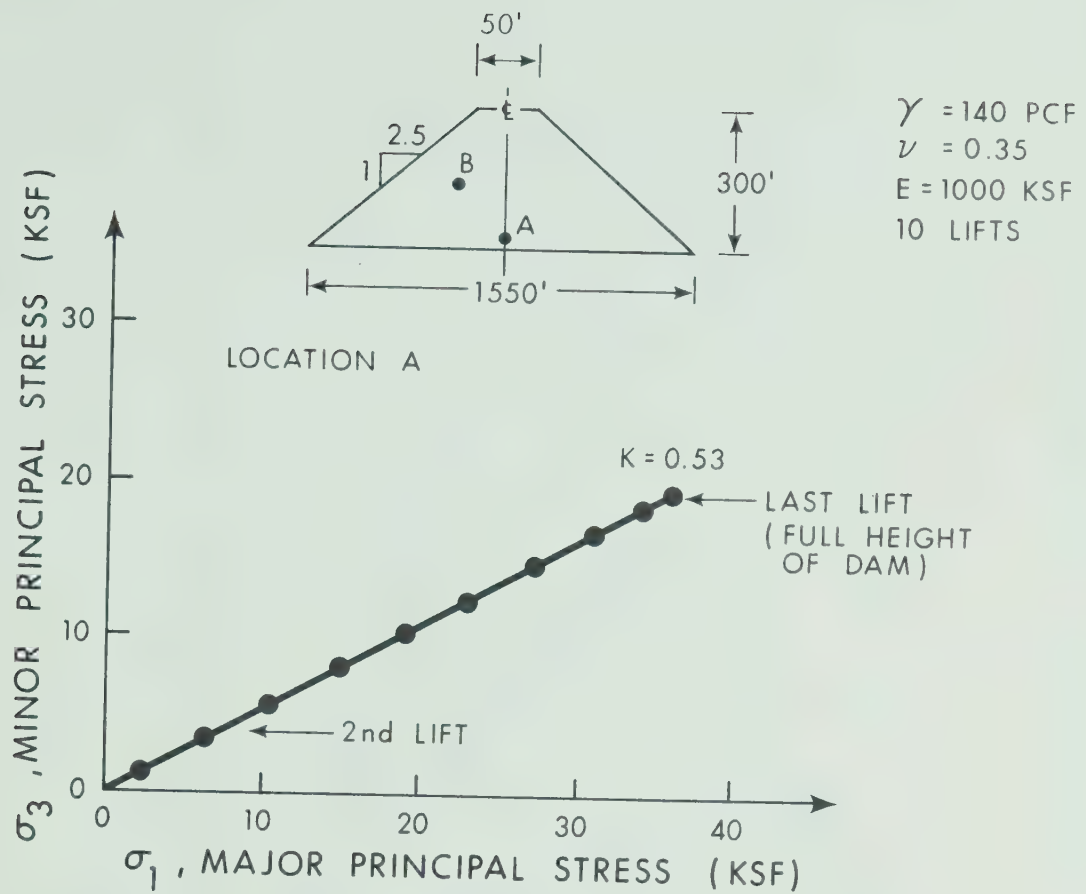


Fig. 3.8 Stress Paths for Soil Elements in a Dam During Construction

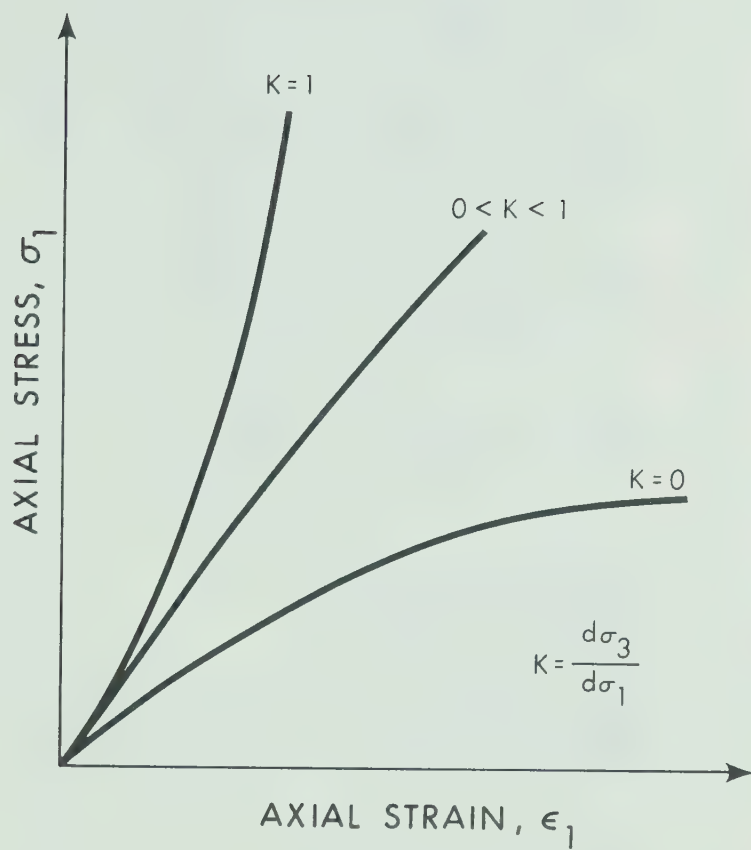


Fig. 3.9 Axial Stress-Strain Curves of a Soil Under Different Types of Compression

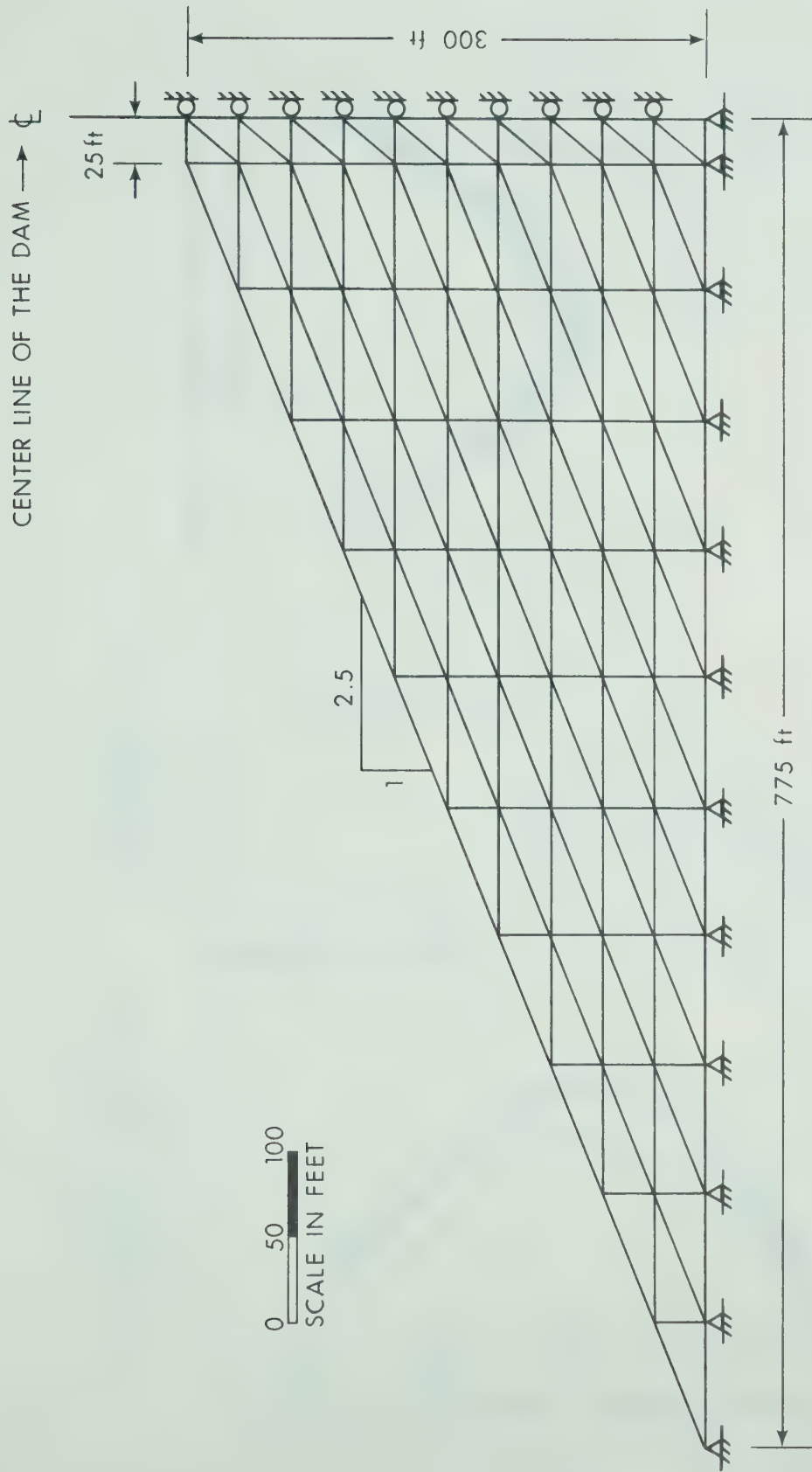


Fig. 3.10 Finite Element Idealization of A Model Dam

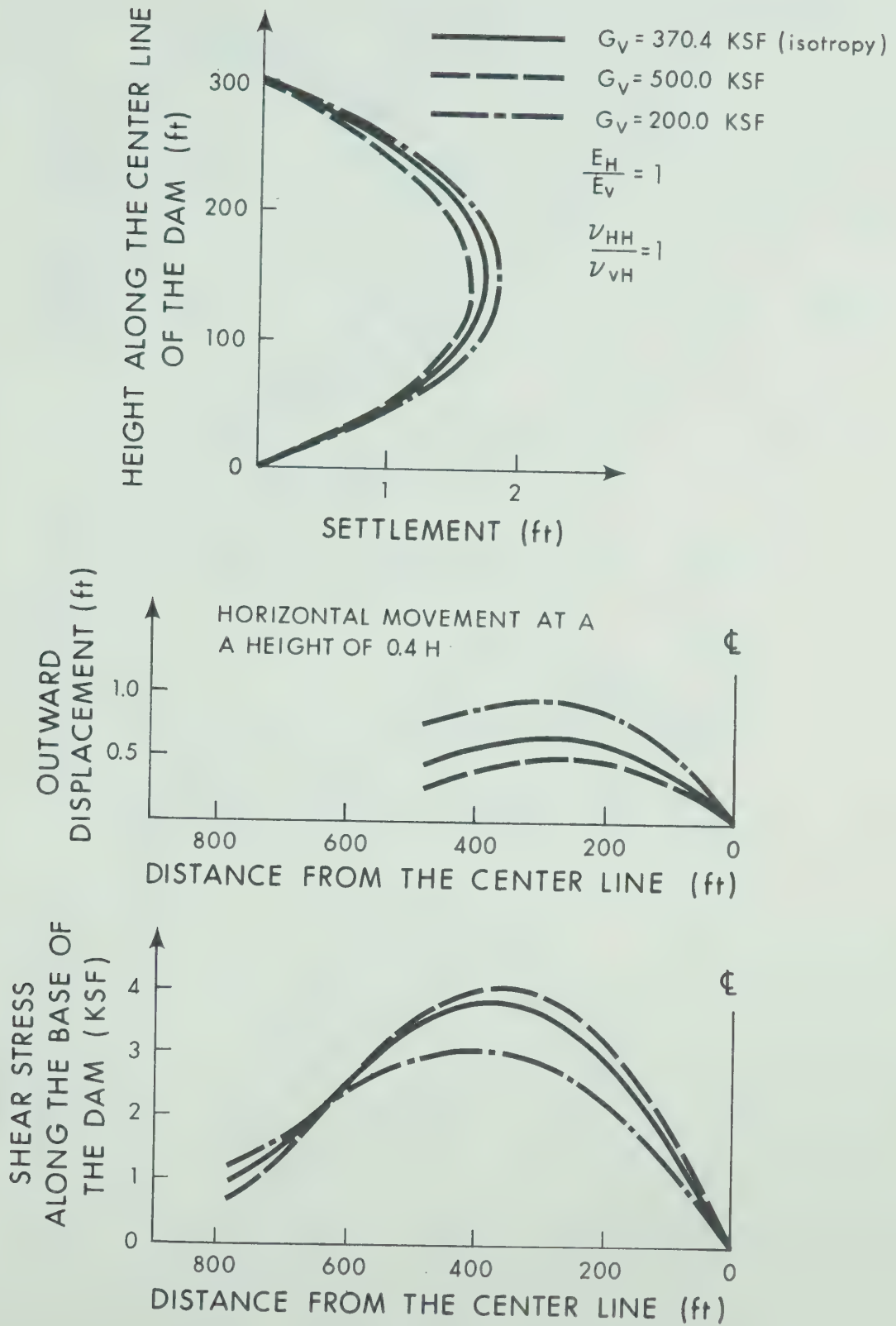


Fig. 3.11 The Influence of G_v on Embankment Displacements and Shear Stresses

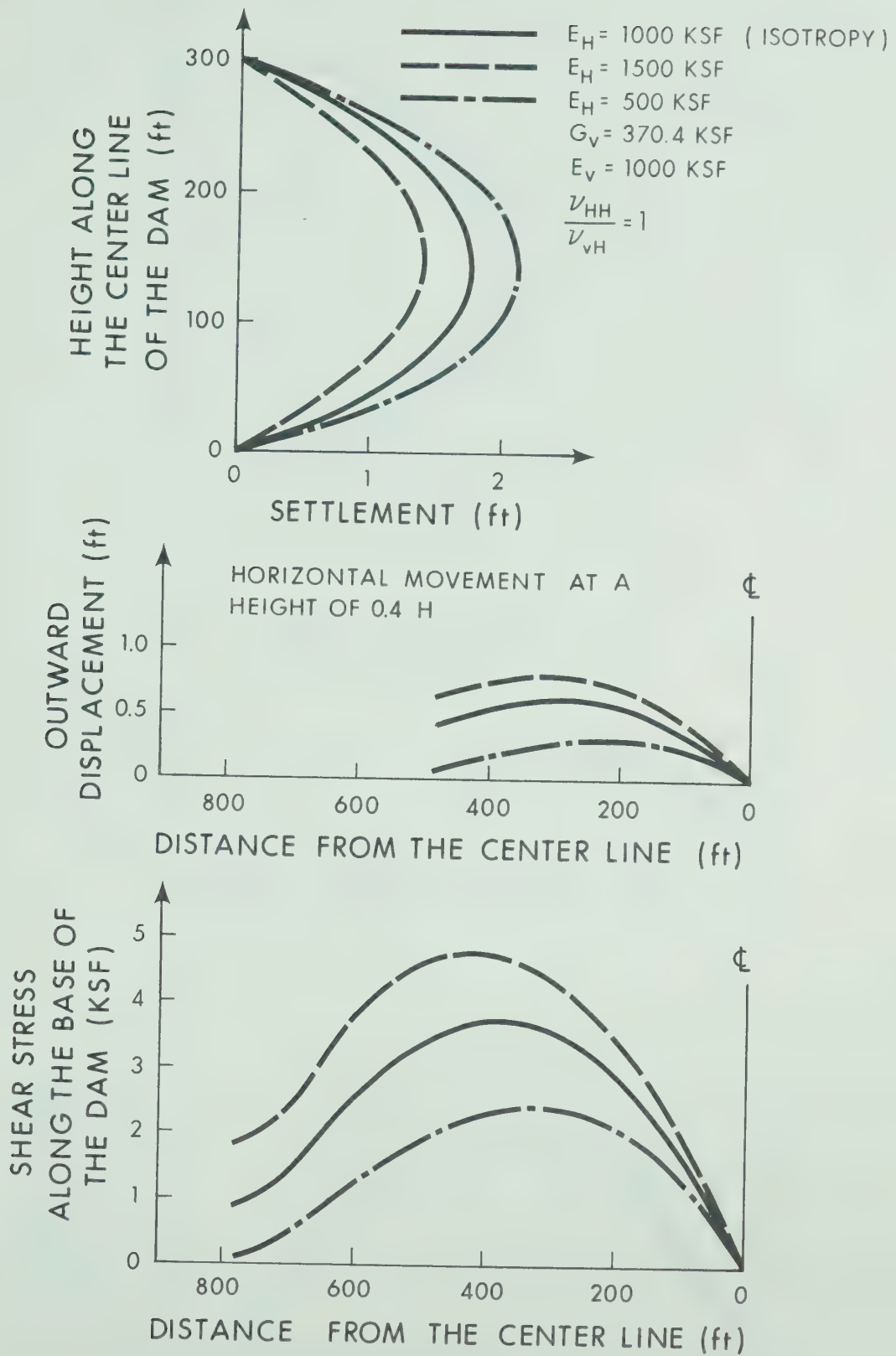


Fig. 3.12 The Influence of E_H on Embankment Displacements and Shear Stresses

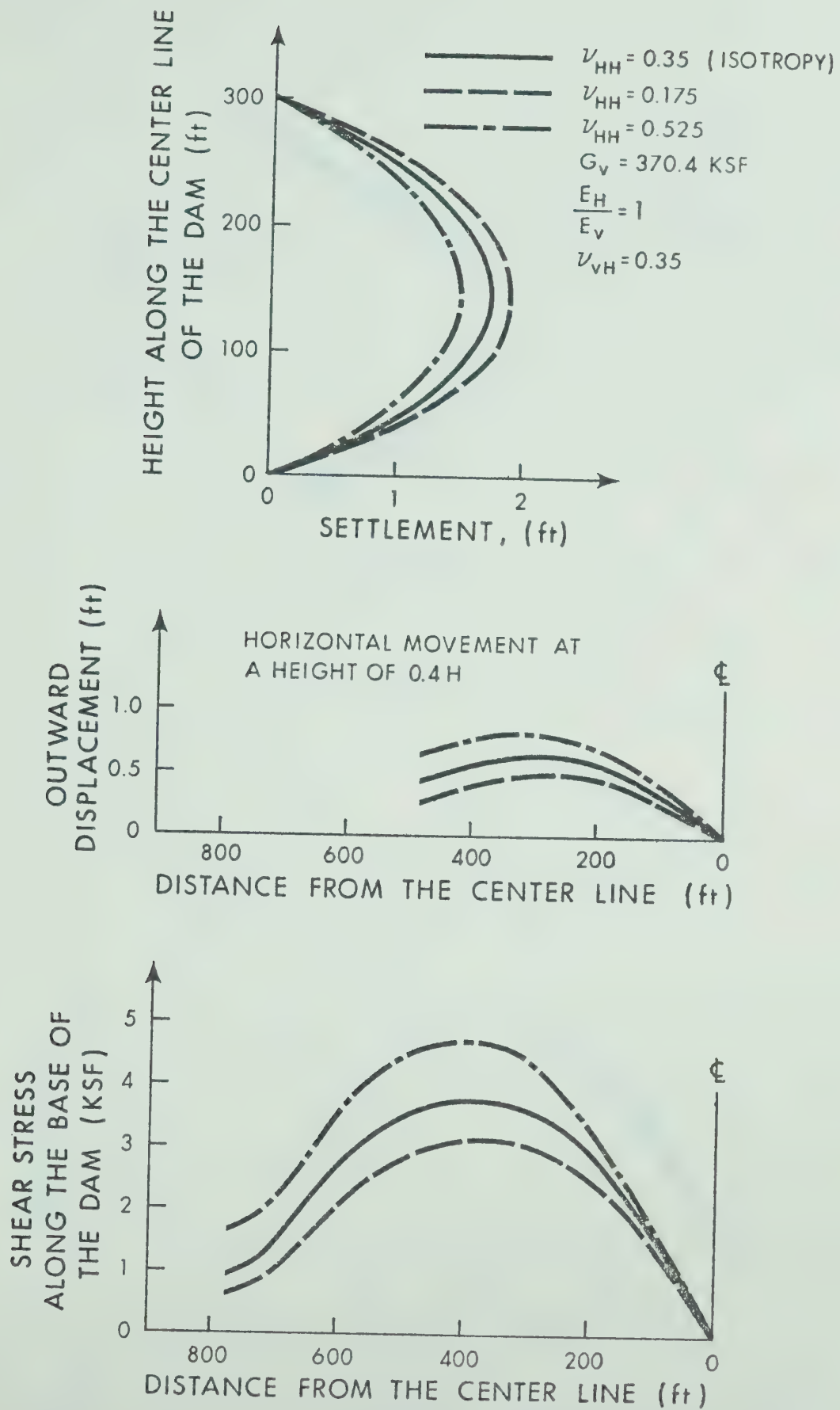


Fig. 3.13 The Influence of ν_{HH} on Embankment Displacements and Shear Stresses

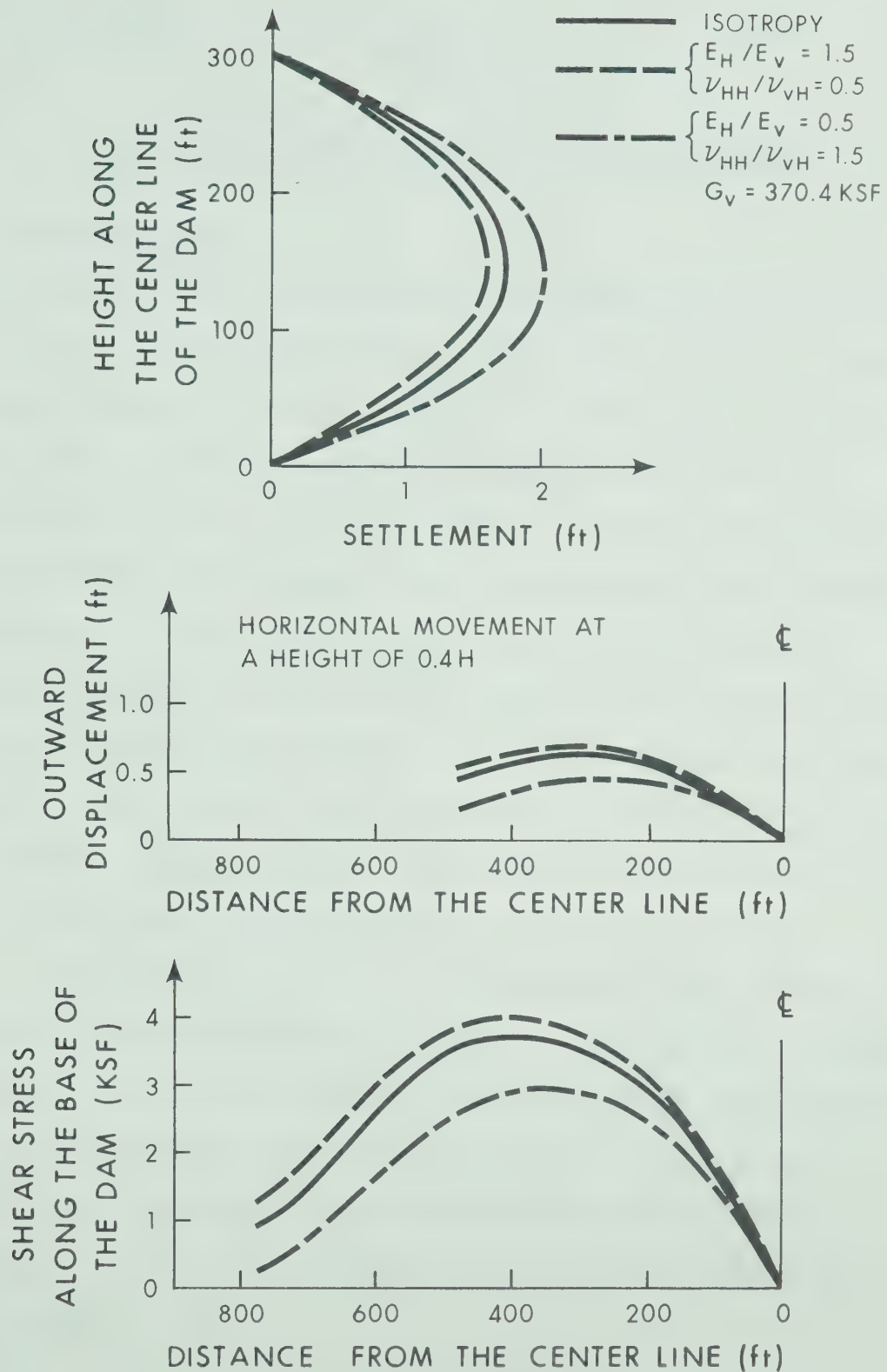


Fig. 3.14 The Combined Influence of E_H and ν_{HH} on Embankment Displacements and Shear Stresses

CHAPTER IV

PORE PRESSURE AND EFFECTIVE STRESS ANALYSES

4.1 Introduction

Estimation of pore pressures generated in an earth dam during construction involves the solution of a moving boundary problem. Several numerical techniques (Gibson, 1958; Koppula, 1970) have been developed to solve this difficult problem. In these methods, total stresses which generate the pore pressures were assumed equal to overburden pressures. As has been discussed previously, vertical stresses in the core may differ significantly from overburden pressures due to load transfer. In this Chapter the significance of this factor on pore pressures in the core is studied with a finite element program (Krishnayya, 1973(b)), which facilitates the incorporation of calculated stresses.

During the construction of an earth dam, excess pore pressures are generated and partially dissipated as the dam is being built. Some deformations take place under relatively undrained conditions and some are due to pore pressure dissipation. In order to evaluate total deformations by summing up these two components, an effective stress analysis is proposed.

4.2 A Brief Review of Methods for Estimating Construction Pore Pressures

A comprehensive review of methods for estimating construction pore pressures in an embankment has been made by Sherman and Clough (1968). These methods, which were described in detail by Sherman and Clough, are mentioned only briefly here. For completeness, some methods which were not included in the previous review are also discussed.

Bruggeman et al. (1939) proposed a method based on the assumption that the time rate of change of the sum of the volumes of moisture and free air in an earth mass is caused by: (1) flow into the unit volume due to percolation; and (2) change in the free-air volume due to changes in pressure and temperature. This time rate of change is equated to the time rate of consolidation, and the integration of this equation provides the solution for the problem of transient pore pressures.

Hilf (1948) utilized the groundwork by Bruggeman et al. (1939) and developed a simplified approach to the estimation of embankment pore pressure during construction. With a condition of no drainage, he postulated that the pore water pressure in a consolidating soil could be related to the amount of compression by combining Boyle's law for the compressibility of air with Henry's law for the solubility of air in water. Although the assumptions used in the development of Hilf's method limit its applicability, the

method eliminated complex mathematical difficulties. Hilf (1956) criticized his own assumption of no surface tension. The assumption of no drainage is overconservative, particularly when internal drainage is provided. Despite the drawbacks inherent in Hilf's method it often enables a reasonable estimate of construction pore pressure to be made with the available data from consolidation and compaction tests.

Bishop (1954) proposed the use of the pore pressure ratio \bar{B} for the determination of pore pressure set up in an earth dam. Since the ratio \bar{B} varied with the principal stress ratio, $\Delta\sigma_3/\Delta\sigma_1$, it was suggested for an accurate determination of the value, a testing procedure should be used in which the principal stress in the tests approximate the actual soil stress during construction of the dam.

Bishop (1957) found the estimation of pore pressure with the assumption of no drainage throughout construction to be overconservative. He pointed out that the pore pressure dissipation during construction shutdown resulted in a two-fold effect on the value of excess pore pressure in a dam. The effect was not only to reduce the excess pore pressure already set up at any stage of construction, but also to reduce the increment of pore pressure which would occur, under undrained conditions, when the subsequent layers of fill were placed. An approach similar to that described by Hilf (1948) was used to provide a solution for such a case.

Bernell and Nilsson (1957) developed electric analogue equipment for the study of transient, two-dimensional flow

problems in earth dams. The equipment permitted an analysis of construction pore pressures at any time during the construction of the dam. The method was essentially for fill placed under wet conditions.

Gibson (1958) considered the pore pressures set-up in an earth dam as a one-dimensional moving boundary problem. In the formulation, pore pressure dissipation during construction was conveniently taken into account when estimating pore pressures.

Koppula (1970) extended Gibson's formulation to include two-dimensional pore pressure dissipation in the case of earth and rockfill dams. Without a stress analysis, the major principal stress increment required in the formulation was approximated by the overburden pressure increment.

4.3 Finite Element Pore Pressure Analysis

From the previous review, it became obvious that the methods available for analyzing construction pore pressure in a dam were based mainly on finite difference formulations. Idealization of a cross-section into a rectangular mesh was generally done in this type of analysis. Although in some instances the accuracy of pore pressure results might not be seriously affected with proper idealization, the actual drainage paths in vertical and horizontal directions were inevitably altered. Moreover, the approximation of major principal stress increments with overburden pressure increments employed by previous methods might be less acceptable for the case when load transfer from core to shell

was significant. An improved formulation was thus felt to be necessary for the present study. A finite element program (FECF 2D), which was then developed by Krishnayya (1973(b)), was used in all the pore pressure analyses in this investigation.

The development of the program was based on the finite element formulation of the heat conduction problems discussed by Wilson et al. (1966). The governing differential equation was:

$$C_v \left(\frac{\partial^2 u}{\partial x^2} + \frac{\partial^2 u}{\partial y^2} \right) = \frac{\partial u}{\partial t} - \bar{B} \frac{\partial \sigma_1}{\partial t}$$

where

C_v - the coefficient of a consolidation of the embankment material

u - the excess pore pressure

σ_1 - the total major principal stress in which the changes occur only due to the changes in the applied loads

\bar{B} - the pore pressure ratio $\left(\frac{\Delta u}{\Delta \sigma_1} \right)$

t - the time variable

Triangular elements with linear pore pressure functions were used in the program. The equations were solved by the Gaussian elimination procedure. The values of C_v and \bar{B} can be changed at any stage of the construction step

by assigning the relevant material properties to the elements. The main improvements achieved in this program are:

(1) Complicated geometry, boundary conditions and the non-homogeneous material distribution can be easily simulated in the analysis.

(2) Simplifying assumptions on the magnitude of major principal stress are not necessary since the stress is obtained from the finite element total stress analysis.

4.4 Considerations of \bar{B} and C_v in the Pore Pressure Analyses

The use of the pore pressure ratio, \bar{B} , for estimating the pore pressures generated in an earth dam was suggested by Bishop (1954). The advantage of using this ratio is that pore pressure can be expressed as a direct function of the major principal stress. Without performing detailed analyses to determine other principal stresses and with the approximation that the overburden pressures be considered as the major principal stresses, pore pressures may be conveniently estimated. However, from the following expressions (Bishop, 1954) for pore pressure ratio,

$$\bar{B} = B[1 - (1 - A)(1 - \frac{\Delta\sigma_3}{\Delta\sigma_1})]$$

or

$$\bar{B} = B \frac{1 - (1 - A)(1 - K)}{1 - B(1 - A)(1 - K)}$$

where K is effective principal stress ratio, $\Delta\sigma_3'/\Delta\sigma_1'$. It is

clear that \bar{B} is a function of principal stress ratio. The test results demonstrating the influence of principal stress ratios on pore pressure ratios have been presented by Bishop (1954). Proper judgement on principal stress ratio expected in the dam is thus necessary in order to determine a \bar{B} value which is suitable for estimating pore pressures.

If the total stress analysis becomes a part of the whole analysis, it is possible that the judgement required in the previous method concerning the principal stress ratio can be eliminated. Subsequently, it may appear the improved results can be obtained with the following (Skempton, 1954) or the similar but more general (Henkel, 1960) expression.

$$\Delta u = B [\Delta \sigma_3 + A (\Delta \sigma_1 - \Delta \sigma_3)]$$

Major and minor principal stress increments obtained from a total stress analysis can be used directly in the above equation. While the preceding argument seems to be valid it will be noted that instead of one, two pore pressure coefficients, A and B, are needed in the equation. Unlike those for saturated soils, B values for unsaturated soils are not equal to one and have to be determined experimentally. The coefficient A whose values vary for different soils, is also determined from the tests.

Since the value of A is not independent of the principal stress ratio, a similar problem as in the determination of \bar{B} will be experienced in the determination of A . In view of these, the application of the latter approach may not gain much accuracy in the results, but it may increase the complexity.

Although incorporation of any one of the two previous expressions can be made in the present finite element program, based on the previous comments, the \bar{B} approach has been formulated for this study. As has been discussed previously the central core in a rockfill dam is more or less under a no lateral strain condition, hence \bar{B} values used in all analyses are determined from no-lateral-strain compression tests.

After the development of the Terzaghi consolidation theory, the value of the coefficient of consolidation has often been referred to as that determined from the oedometer test. As is known, a particular feature of this test is the imposition of a one-dimensional strain condition. If a saturated soil can be regarded as a linear elastic material with constant permeability, it has been shown (Davis and Poulos, 1963) that the values of the coefficient of consolidation determined under different strain conditions may be different. Coefficients of consolidation for three different strain conditions may be expressed as:

$$C_{v1} = \frac{kE'(1 - \nu')}{\gamma_w(1 + \nu')(1 - 2\nu')} \quad \text{or} \quad C_{v1} = \frac{k}{m_v \gamma_w} \quad \text{for one-dimensional strain case}$$

$$C_{v2} = \frac{kE'}{2\gamma_w (1 - 2\nu')(1 + \nu')} \quad \text{for two-dimensional strain case}$$

$$C_{v3} = \frac{kE'}{3\gamma_w (1 - 2\nu')} \quad \text{for three-dimensional strain case}$$

where k is the coefficient of permeability, m_v is one-dimensional compressibility, E' is Young's modulus in terms of effective stress, ν' is Poisson's ratio in terms of effective stress and γ_w is the density of water. From the above expressions, it is noted that three coefficients differ the most when $\nu' = 0$ and the differences decrease as ν' increases. Coefficients of consolidation used in this study are determined from oedometer tests for reasons similar to those for determining \bar{B} .

4.5 The Influence of Load Transfer on Construction Pore Pressure

The influence of load transfer on the total stress distribution in a nonhomogeneous dam has been discussed in previous chapters. As a consequence, construction pore pressures which depend on the magnitude of total stress were inevitably affected by this load transfer. In this section, the same nonhomogeneous dam section as shown in Fig. 3.4 was used to study these influences. Since only two-dimensional analyses on a transverse section were performed, it was assumed that load transfer due to cross-valley arching was less significant for the cases in the study. This assumption may describe closely the actual conditions in a great number of zoned dams except for those in very

steep-walled V-shaped valley (e.g. slopes of 1:1).

In the analyses, it was assumed the model was built at a continuous and uniform rate of 10 ft/month. The dam which was 300 ft. high was represented by ten layers of elements of uniform thickness. The core and shells which might have different modulus values had the same density, $\gamma = 140 \text{ lb/ft}^3$, and Poisson's ratio, $\nu = 0.35$. In order to compare the pore pressures set-up in an earth dam due to different degrees of load transfer, analyses were performed for the following four cases:

(1) Major principal stress increments in the core were equal to overburden pressure increments (i.e. $\Delta\sigma_1 = \gamma\Delta h$). Total stress analysis was not required for this case.

(2) Core and shells had the same modulus, $E_{\text{shell}} = E_{\text{core}} = 1000 \text{ Kips/ft}^2$. Total stresses were obtained from total stress analysis.

(3) The modulus of the shell was five times the modulus of the core, $E_{\text{shell}} = 5E_{\text{core}} = 5000 \text{ Kips/ft}^2$. Total stresses were obtained from the total stress analysis.

(4) The modulus of the shell was ten times the modulus of the core, $E_{\text{shell}} = 10E_{\text{core}} = 10,000 \text{ Kips/ft}^2$. Total stresses were obtained from the total stress analysis.

Two-dimensional dissipation was considered in all four cases. The core was assumed to have a coefficient of consolidation, $C_v = 50 \text{ ft}^2/\text{month}$ and a pore pressure ratio

$\bar{B} = 0.50$. The results of pore pressure analysis for the center of the dam are shown in Figs. 4.1 and 4.2. In Fig. 4.1, slight differences in results for case (i) and (ii) can be noticed. These differences were mainly due to the fact discussed in Chapter III that major principal stresses in the central part of homogeneous dam were not exactly equal to overburden pressures. For the rate of construction of the dam and drainage properties of the core discussed in this investigation, it was found that if there were no load transfer in the core as in case (i), construction pore pressures in the central part of the dam increased continuously. However, for cases (iii) and (iv), total stress increments in the lower part of the dam were significantly less in the later stages of construction. Therefore, pore pressures were dissipated faster than they were generated. As a result, unlike case (i), pore pressures in the lower part of the dam in the later stages of construction were less than those in some previous stages.

In Fig. 4.3 pore pressure profiles at the end of construction for the four cases are presented. From these dimensionless plots, the significant influences of load transfer on pore pressures generated in a dam are obvious. The great differences in results between case (ii) with $E_{shell} = E_{core}$ and case (iii) with $E_{shell} = 5E_{core}$ indicate the comparable importance of the load transfer which occurred at a lower value of the ratio of Young's moduli of core to

shell. In the present study, when $E_{shell} > 5E_{core}$, total stresses in the core were reduced at a decreasing rate and hence the pore pressure results for case (iii) where $E_{shell} = 5E_{core}$ and (iv) where $E_{shell} = 10 E_{core}$ were not greatly different.

An analysis was also performed assuming one-dimensional dissipation and major principal stress increments equal to overburden pressure increments on the same core section. The pore pressure profile at the end of construction ($\frac{m^2 t}{c_v} = 60$) obtained from this analysis are also presented in Fig. 4.3. In the same figure, Gibson's one-dimensional solution (1958, Fig. 3) on the relation between $u/\gamma'h$ and x/h at $\frac{m^2 t}{c_v} = 64$ for constant rate of sedimentation is shown. Although saturated soils were dealt with by Gibson, presentation of pore pressures in normalized forms facilitated the comparison of the two solutions. The pore pressure $\gamma'h$ generated in sediment is comparable to $\bar{B} \gamma h$ in compacted earth dams. As may be seen from the figure, the pore pressure profiles from the two solutions do not differ significantly.

In Fig. 4.3, the great differences between one-dimensional dissipation and two-dimensional dissipation results are also displayed. The importance of the effectivenesses of side drains is thus indicated. The influence of various degrees of effectivenesses of side drains on pore pressure dissipation has been discussed by Koppula & Morgenstern (1972).

No detailed studies are attempted here.

Since load transfer from core to shells rather than the opposite, are the more common situations in most dams, the influence of this type of load transfer on pore pressures set-up has been the main study in this section. From the results of the studies it is pertinent to note that without considering the load transfer in a dam having soft core and rigid shells, the pore pressures will be overestimated. The consequence of this overestimation can either be on the safe side or the unsafe side, hence proper consideration of load transfer is necessary. When a dam has a rigid core and soft shells, load will be transferred from shells to core. Without consideration of the load transfer, pore pressures in the core will be underestimated.

4.6 Consideration of Possible Treatment of Total Deformations

Total deformations in cohesive soil have conventionally been treated as the summation of immediate deformation and consolidation deformation. Immediate deformations are always referred to as the deformations occurring during undrained loading, and consolidation deformations are referred to those taking place as the consequence of dissipation of pore pressure. In several methods (e.g. Skempton and Bjerrum, 1957; Davis and Poulos, 1963) which have been proposed for the analysis of foundation settlement similar principles of obtaining total settlement were suggested. Total settlements at any

time t after the load application is equal to the sum of the immediate settlement or undrained settlement and consolidation settlement occurring at time t measured from the time of application of the load. Although the procedures for obtaining consolidation settlement were different in these methods, the settlement was generally attributed to the effective stress increases resulting from the dissipation of pore pressure.

In finite element analyses, the previous approach of obtaining total deformations may also be introduced. The scheme of the possible treatment is illustrated in Fig. 4.4. In the first stage, total stresses and immediate deformations caused by external load or self weight can be calculated from a standard finite element analysis. In this analysis elastic moduli with respect to total stresses, E and ν , are generally used. With the total stresses and drainage properties of the material known, the pore pressure at any time after the application of the load can be determined from a pore pressure analysis. In this analysis it is usually assumed that total stresses do not change during consolidation. The change in pore pressure from its initial value, u_0 , at any time t_1 can subsequently be evaluated in the second stage. In the third stage, the effective stress increases, which result from the dissipation of pore pressure, are set equal to pore pressure changes. The fourth stage requires converting the changes in effective normal stresses into equivalent

nodal forces. Such forces constitute the loading for the finite element analysis to evaluate consolidation deformations caused by increases in effective stresses. In this analysis, elastic moduli with respect to effective stresses, E' and ν' , in the appropriate stress range are used. After the completion of the four stages, the total deformations at time t_1 can be obtained by adding the immediate deformations calculated in first stage and the consolidation deformations determined in fourth stage. This type of approach has been suggested by Eisenstein (1974) for evaluating the deformations during the "steady seepage" stage.

Regarding the complexity in programming, the approach discussed in this section may be more suitably applied to cases where total stresses do not change with time. The changes include those caused by consolidation and by the application of external loads. It thus seems logical to apply the approach to the analysis of foundation settlement or to calculating deformations in an earth dam during the "steady seepage" stage. In these problems, there is a more or less clear division between the undrained stage and the drainage stage. In the latter stage, total stresses may be assumed to remain more or less constant.

4.7 Discussion of the Assumption of Constant Total Stress During Consolidation

The assumption of constant total stress during consolidation has been considered and subsequently used in the

present study. It is known that the same assumption was generally used in consolidation formulation based on the Terzaghi-Rendulic theory. The inadequate representation of the continuity of the soil mass using this assumption was recognized by Biot (1941) and hence the Biot consolidation theory was developed. A thorough review of the two theories has been presented by Schiffman et al (1969) in which the advantages and limitations of the two theories were discussed. The reasons for using the former approach in this study are as follows:

(1) As the result of the comparison between settlements calculated using the Skempton-Bjerrum method (1957) and those based on the Biot theory, Hwang et al (1972) indicated that the Skempton-Bjerrum method, which does not consider total stress changes during consolidation, can be used for most practical problems.

(2) It is considered important to incorporate the nonlinear stress-strain relationships of soil in the present study. So far, finite element formulations based on Biot theory (e.g., Sandhu and Wilson, 1969; Hwang et al. 1971) have only incorporated linear elastic stress-strain relationships. The complexity involved in those formulations tends to inhibit the incorporation of any more sophisticated stress-strain relationship.

(3) Problems involving incremental loads (e.g., an earth dam during construction) may be formulated easier using the approach considered. The Biot theory has only been used

for single load increment problems (e.g., a foundation problem).

4.8 Effective Stress Analysis of Earth Dam During Construction

During the construction of an earth dam, pore pressures are generated and partially dissipated as the fill is placed. Except for seasonal stoppages (e.g., winter shutdown), it is difficult to draw a clear division between the undrained stage and the drainage stage. As was discussed in section 4.6, the conventional treatment of total deformations may be less convenient to apply to this type of problem. In this case, it may be easier to correlate the deformations with effective stresses at all times. Incremental deformations may be attributed to the changes in effective stress.

The general scheme, which has been described by Eisenstein (1974), of using the effective stress principle in the analysis of deformations in the core is shown in Fig. 4.5. For every construction stage, changes in total stresses, $\Delta\sigma$, are computed by a total stress analysis. With $\Delta\sigma$ and the drainage characteristics of the material, \bar{B} and C_v known, the pore pressure increments, Δu_t for every element and given time interval, can be calculated from a pore pressure analysis. Since the changes in effective stress $\Delta\sigma'_t$ are equal to the changes in pore pressure assuming constant total stress during consolidation, the effective stress changes are subsequently obtained. The displacements components Δv_t can then be calculated from the changes in

effective stress and elastic parameters with respect to effective stresses. More details regarding the procedure of introducing effective stress analysis in the entire dam are shown in Fig. 4.5 to Fig. 4.8. As in the standard incremental analysis, the full height of the dam is divided into several construction layers. The time history of the construction which includes the times to fill the layers and the time period of the shut-down should be known. The height versus time relationship used in the analysis is shown in Fig. 4.6. Referring to Fig. 4.7 and Fig. 4.8, the procedures for each layer may be described as follows:

(1) Finite element analysis is performed to obtain total stresses, σ_{SAA} and σ_{CAA} , in the shells and core of layer A due to self weight. Elastic moduli with respect to total stresses, E and ν , are used in the analysis. The total stresses obtained are assumed constant between time t_0 and t_A , which are the times of starting and completing the placement of layer A. After the total stresses are determined the finite element program (FENCP 2D) which has been described in section 4.3 is used to determine the pore pressure in every element in the core at various times. In order to evaluate deformations, $v_{SAA t_A}$ and $v_{CAA t_A}$, in the shells and core of layer A at time t_A , a finite element analysis is performed with σ_{SAA} and $(\sigma_{CAA} - u_{t_A})$ as the loads in shells and core respectively. Elastic moduli with respect to effective stresses, E' and ν' , are used in the analysis.

(2) When a new layer B is placed on top of layer A, a finite element analysis is performed to obtain the total stress changes, $\Delta\sigma_{SAB}$ and $\Delta\sigma_{CAB}$, in the shells and core of layer A due to the weight of layer B. Elastic moduli with respect to total stresses, E and ν , are used in the analysis. If t_B is the time of completion of layer B, the total stress changes determined are assumed constant between time t_A and t_B . With the total stress changes known, the pore pressure difference, $(u_{tB} - u_{tA})$, between time t_B and t_A can subsequently be determined from a pore pressure analysis. In order to evaluate incremental deformations, Δv_{SABtB} and Δv_{CABtB} , in the shell and core of layer A between time t_A and t_B , a finite element analysis is performed with $\Delta\sigma_{SAB}$ and $(\Delta\sigma_{CAB} - (u_{tB} - u_{tA}))$ as the loads in shells and core respectively. Since no excess pore pressure is generated, $\Delta\sigma_{SAB}$ obtained from total stress analysis is directly used in the shell. Elastic moduli with respect to effective stresses, E' and ν' are used in the analysis.

For each additional layer, procedure (2) is repeated to evaluate the incremental deformations in layer A. Total deformations in layer A when the fill reaches the full height of the dam is obtained by summing the deformations calculated in procedure (1) and all the incremental deformations calculated in procedure (2).

In addition to the reason explained in the first paragraph of this section, another reason for employing effective

stresses and elastic parameters E' and ν' , to obtain deformations in layer A at the time of completion is the consideration of the nonlinearity of the stress-strain relationship. At this stage, the effective stress in the compacted core is generally not equal to zero but has an initial value. This value should be introduced into the analysis before performing the analysis for the next increment of effective stress.

The use of elastic parameters, E' and ν' , to evaluate immediate deformations may be more suitable for the case when volume change due to shear in the soil is not significant. If a saturated soil behaves as a linear elastic material with ideal pore pressure response ($A = \frac{1}{3}$), the use of the elastic parameters, E' and ν' , for evaluating deformations will yield results similar to those obtained with elastic parameters E and ν . This approach has been generally used in the Biot theory. However, if the volume change due to shear is significant, then immediate deformations calculated with E' and ν' may not be the same as those determined with E and ν . In a total stress analysis, zero volume change ($\nu = 0.5$) is usually assumed for saturated soil in undrained loading. In an effective stress analysis, if the volume change due to shear in soil is significant ($A \neq \frac{1}{3}$), undrained pore pressures computed using the Skempton or Henkel expressions, result in a non-zero value of the first invariant of the effective stress tensor and non-zero volume

change. This type of inconsistency has been noted by Hwang et al. (1972).

4.9 The Accuracy of Procedure Used in Effective Stress Analyses

In order to check the accuracy of the present procedure used in an effective stress analysis, a rectangular saturated clay core with incompressible and 'perfectly efficient' side drains (Koppula and Morgenstern, 1972) is studied. The configuration of the problem is shown in Fig. 4.9. The rate of pore pressure dissipation for a similar type of problem has been studied by Koppula and Morgenstern (1972) using the finite difference method. For comparison, it is assumed that there is no friction between the clay core and the side drains in the present analysis. After a uniform load of 2 Kips/ft² is imposed on the surface of clay core, the excess pore pressures at the surface and the interfaces of clay core and side drains are assumed zero at all times. The material properties of the soil skeleton of the clay core are assumed constant and have the following values: Young's modulus, $E' = 500 \text{ Kips/ft}^2$, Poisson's ratio, $\nu' = 0.3$ and the coefficient of permeability, $k = 10^{-2} \text{ ft/month}$. The other necessary parameters are calculated from these basic parameters using the following relationships:

$$m_v = \frac{(1 + \nu')(1 - 2\nu')}{E'(1 - \nu')}$$

$$c_v = \frac{k}{m_v \gamma_w}$$

and

$$E = \frac{(1 - \nu)}{(1 + \nu)} E'$$

where m_v is the one-dimensional compressibility, c_v is the coefficient of consolidation and E is Young's modulus with respect to total stress. For the reasons described in Chapter III, $\nu = 0.49$ is used in the total stress analysis. Since side drains are assumed incompressible in the problem, deformation of the clay core due to two-dimensional pore pressure dissipation occurred only in the vertical direction. Thus in this case, the degree of consolidation settlement should be equal to average degree of pore pressure dissipation. In Fig. 4.10, degrees of consolidation settlement calculated from the present analysis are compared with the average degree of pore pressure dissipation obtained from the finite difference method for different time factors (T). No significant differences in the results can be observed. The degree of consolidation settlement shown in Fig. 4.10 is the ratio of the average surface settlement to the final settlement. The final settlement in this case is $m_v \cdot p \cdot H$. Surface settlements of the portions close to the side drains are always more than those at the center part in the two-dimensional dissipation case. The results of the finite difference coded here is for the case of $H/2w = 0.5$ and λ (impedance factor) $\rightarrow \infty$ (Koppula and Morgenstern, 1972).

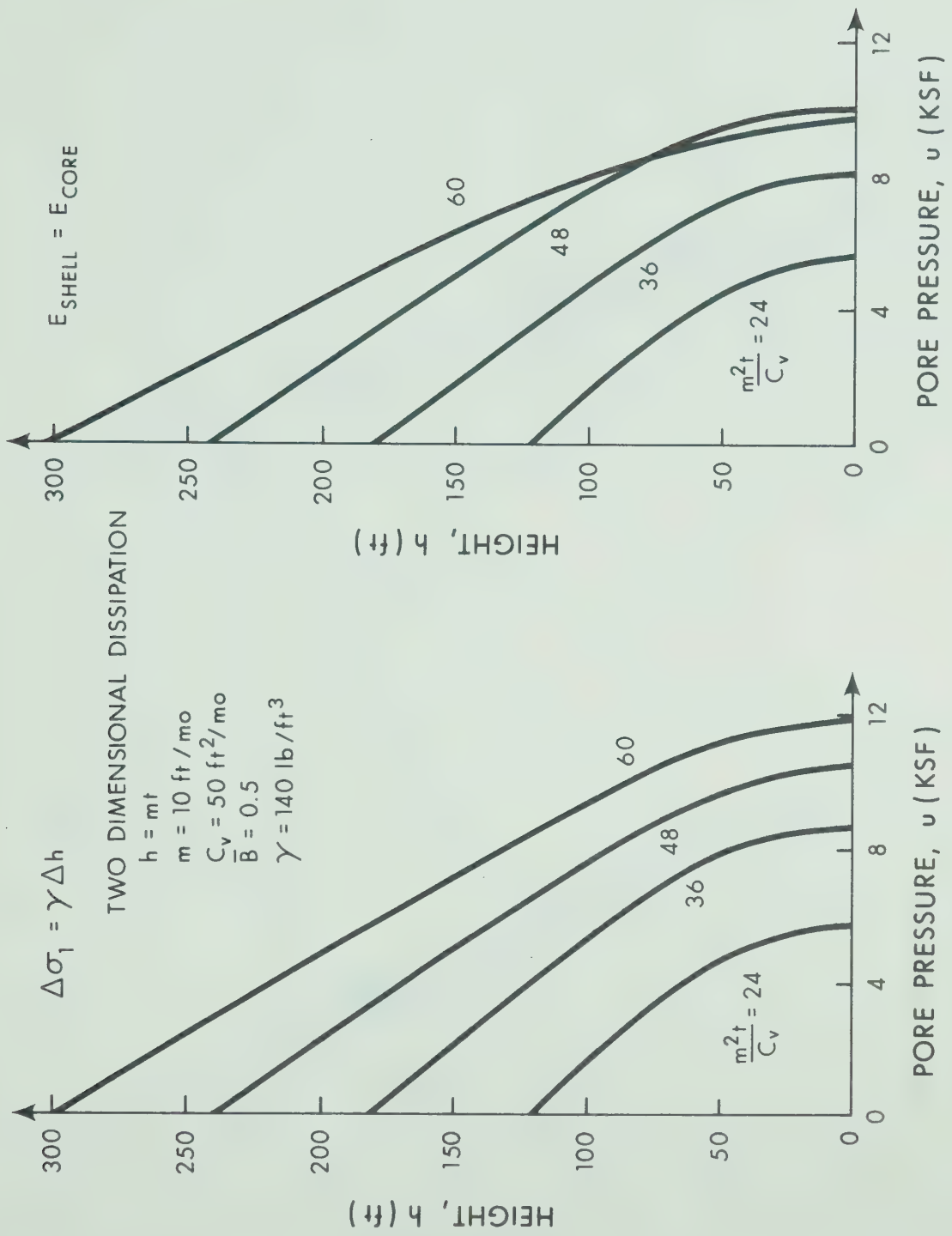


Fig. 4.1 Pore Pressure Set-up in the Center of An Earth Dam During Construction

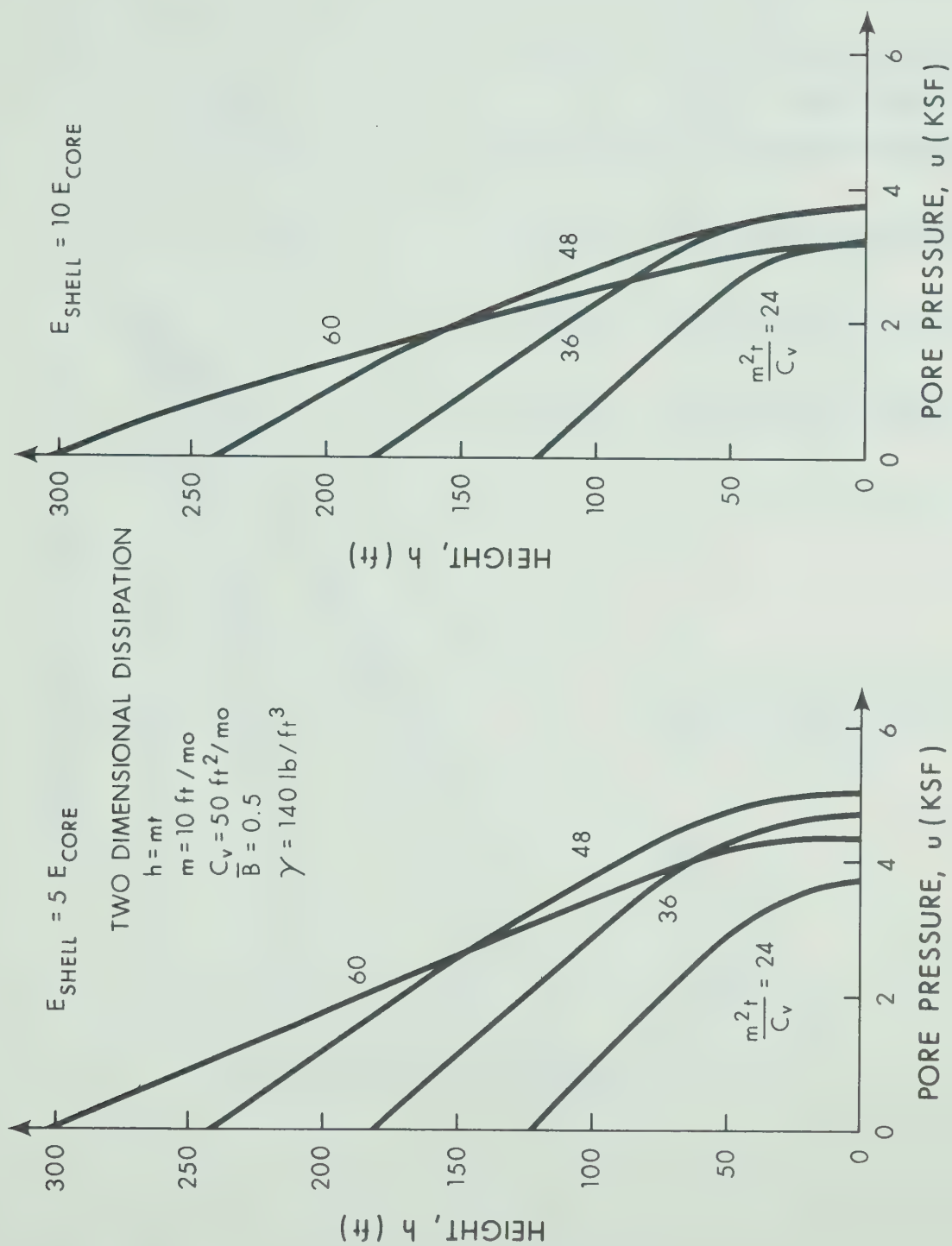


Fig. 4.2 Pore Pressure Set-up in the Center of the Core During Construction ($E_{\text{shell}} = 5E_{\text{core}}$; $E_{\text{shell}} = 10E_{\text{core}}$)

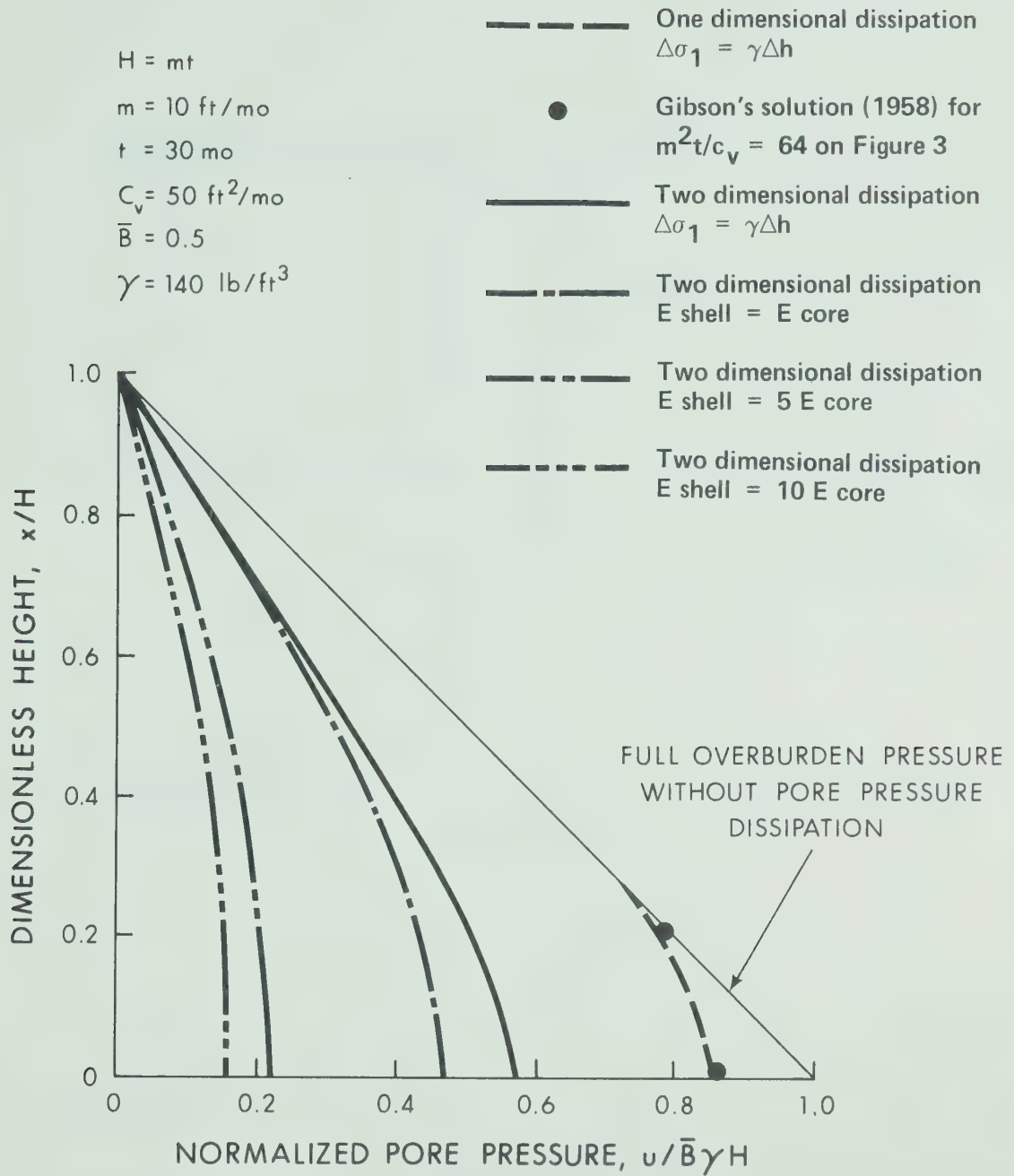
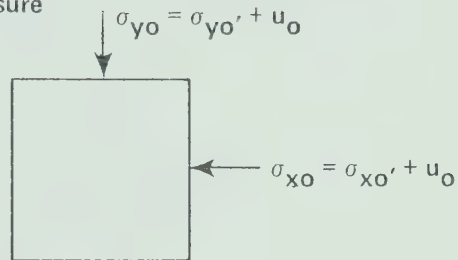
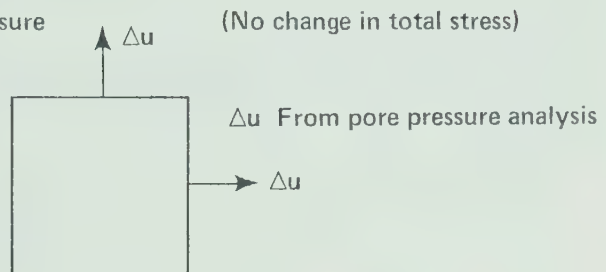


Fig. 4.3 Pore Pressure Profiles in Central Core at the end of Construction for Different Degrees of Load Transfer

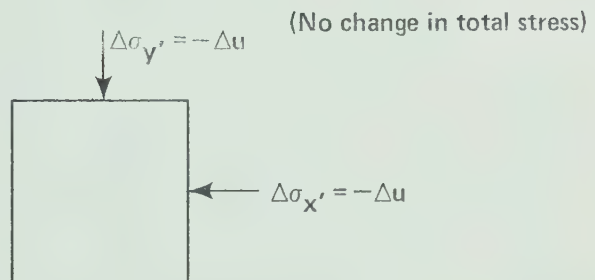
- (1) Before dissipation of pore pressure
at time $t = 0$



- (2) During dissipation of pore pressure
at time $t = t_1$



- (3) Change in effective stress
at time $t = t_1$



- (4) Equivalent nodal forces

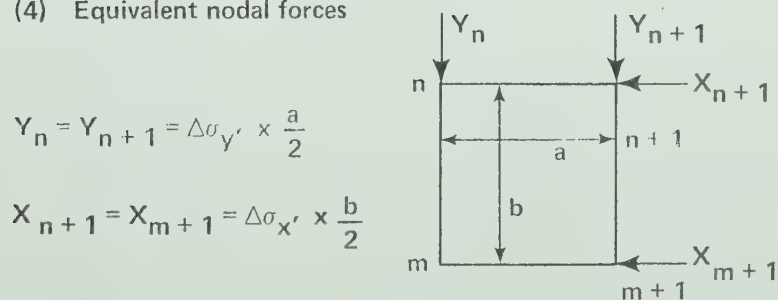


Fig. 4.4 Scheme of Possible Treatment of Total Deformation In Finite Element Analysis

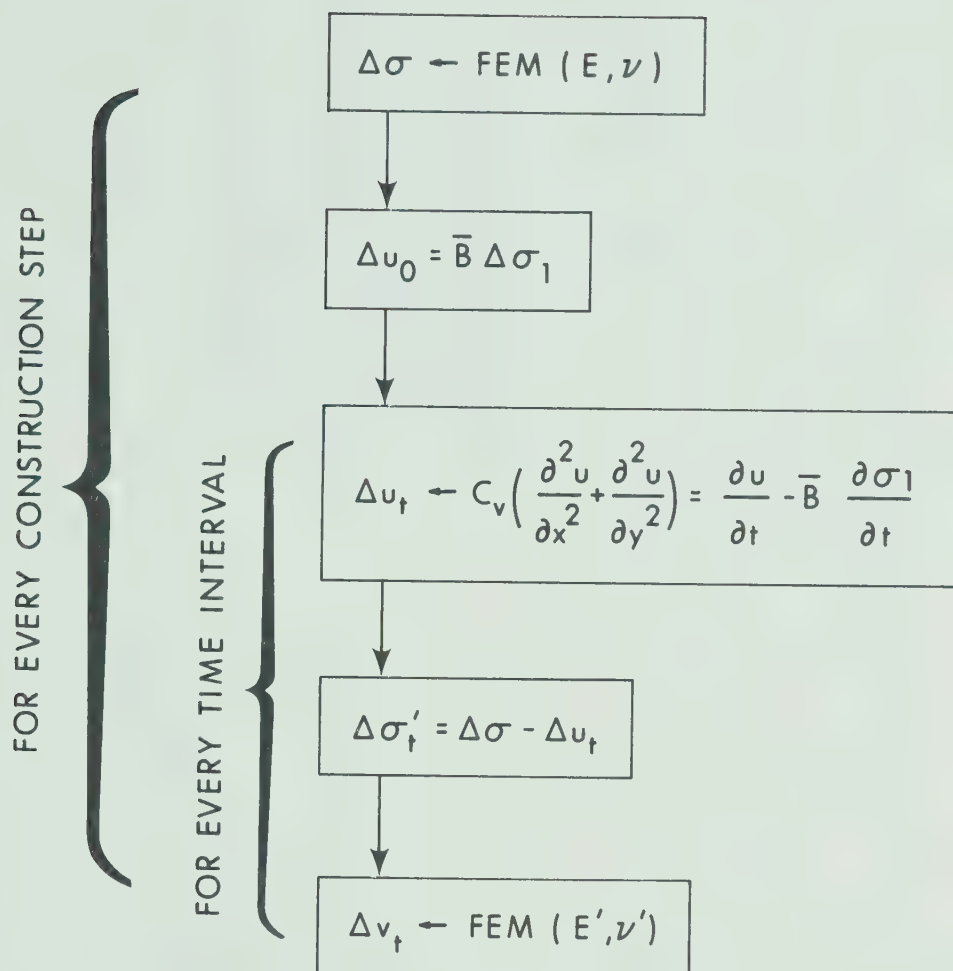


Fig. 4.5 Scheme of Analysis of Consolidation Movements (after Eisenstein, 1974)

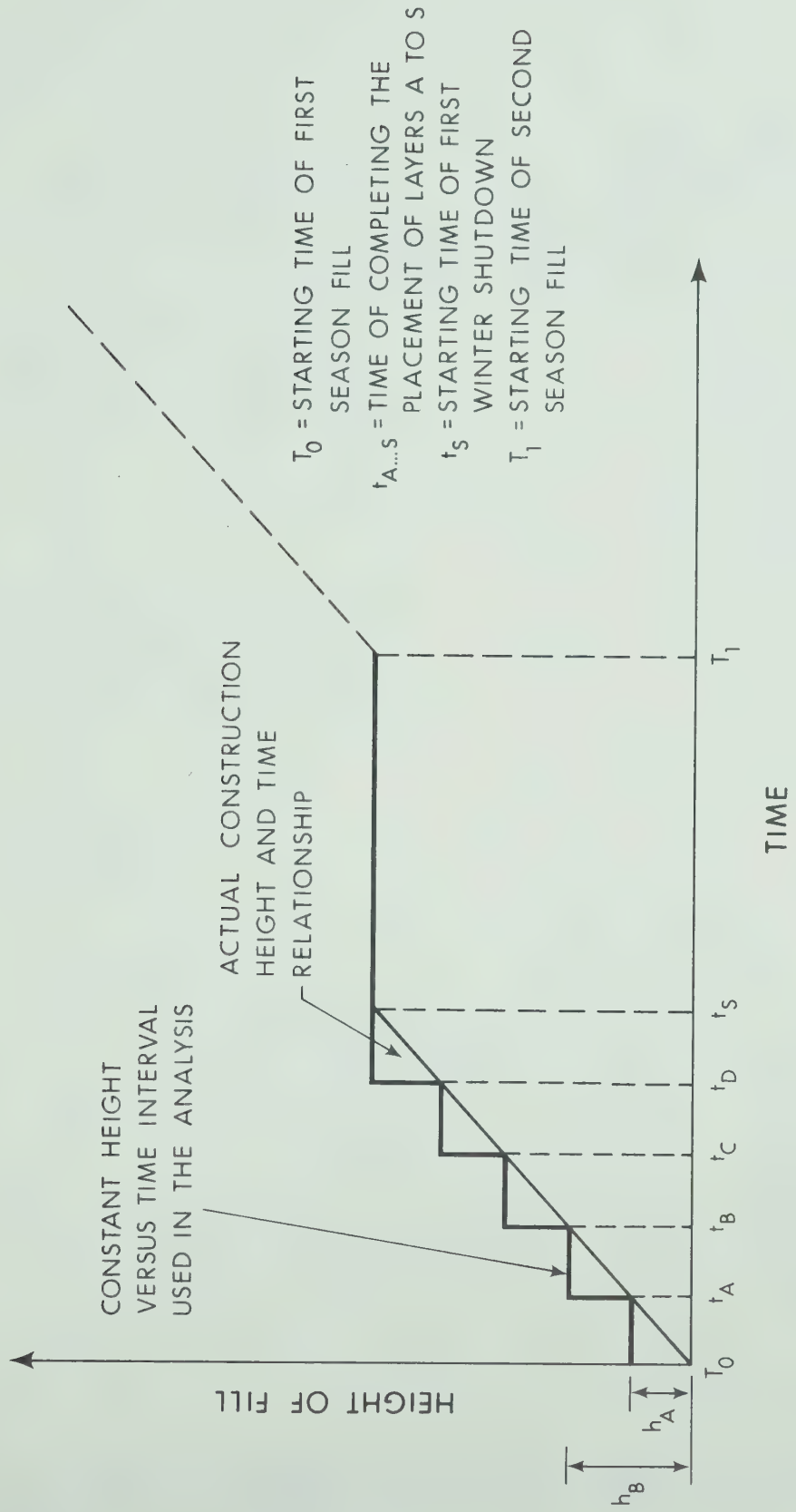


Fig. 4.6 Height Versus Time Relationship Used in the Analysis

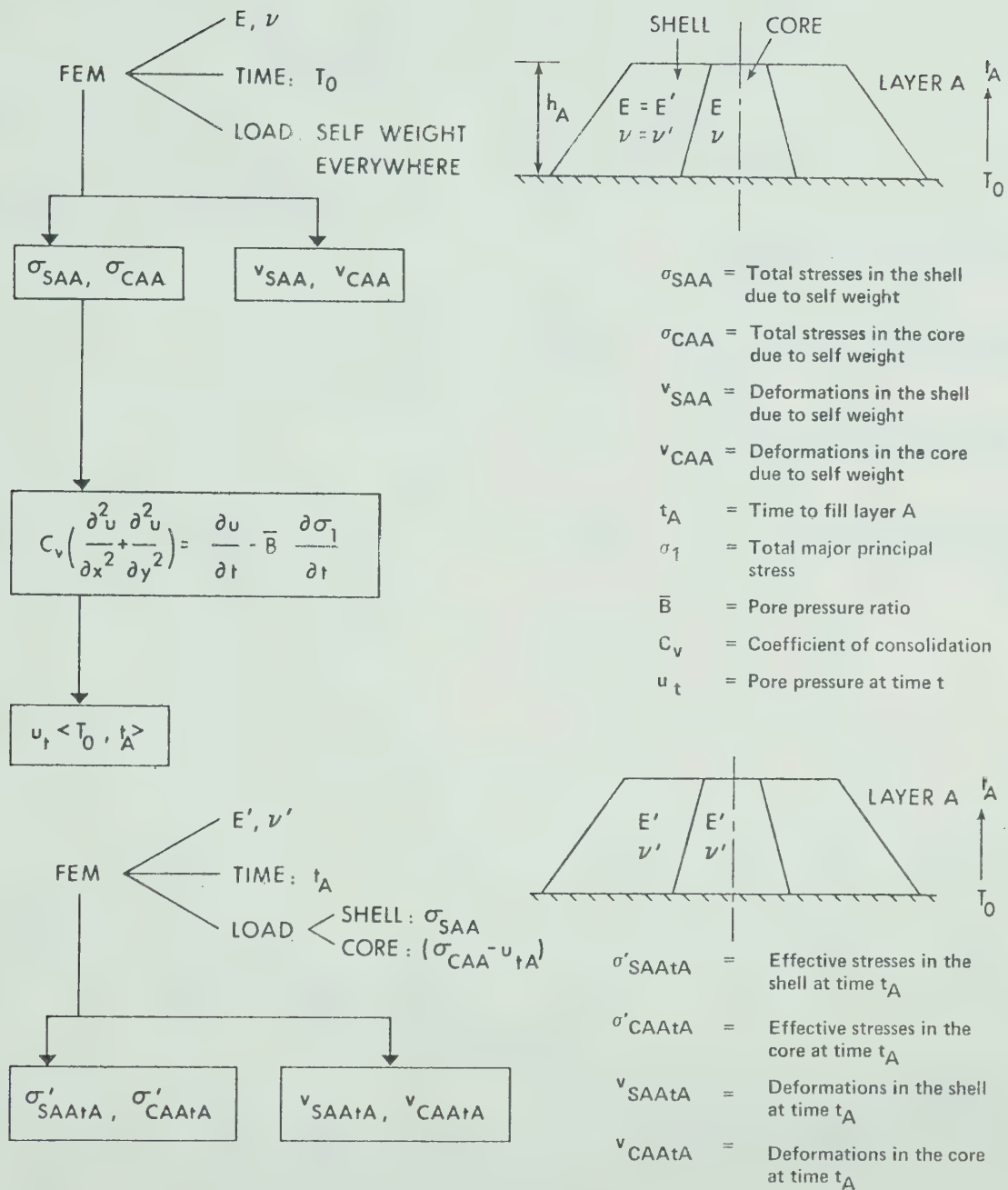
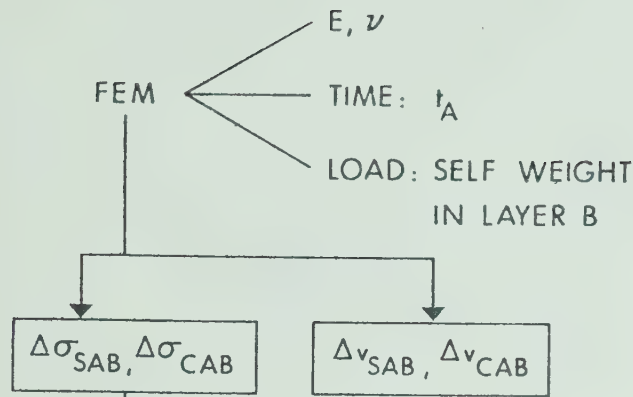
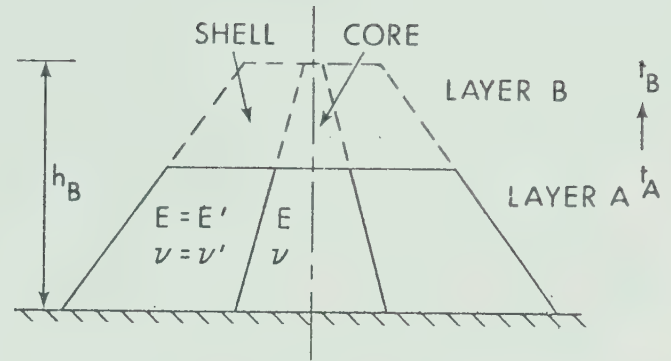
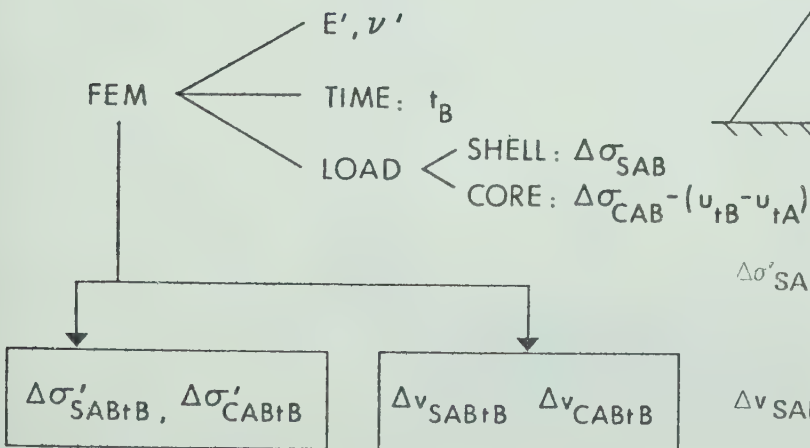


Fig. 4.7 Analysis Procedures for Newly Placed Layer



$$C_v \left(\frac{\partial^2 u}{\partial x^2} + \frac{\partial^2 u}{\partial y^2} \right) = \frac{\partial u}{\partial t} - \bar{B} \frac{\partial \sigma_1}{\partial t}$$

$$u_t < t_A, t_B >$$



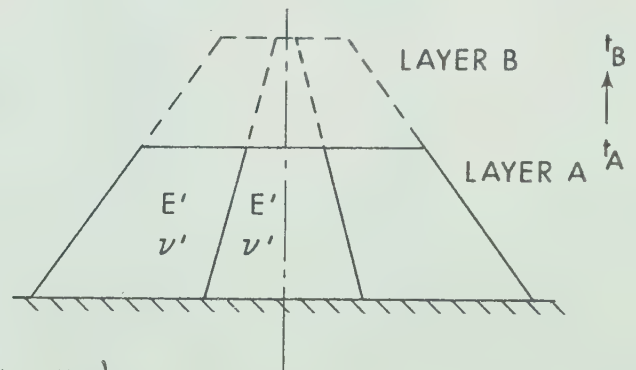
$\Delta\sigma_{SAB}$ = Total stress changes in the shell of layer A due to the weight of layer B

$\Delta\sigma_{CAB}$ = Total stress changes in the core of layer A due to the weight of layer B

Δv_{SAB} = Incremental deformations in the shell of layer A due to the weight of layer B

Δv_{CAB} = Incremental deformations in the core of layer A due to the weight of layer B

t_B = Time to fill layer B



$\Delta\sigma'_{SABtB}, \Delta\sigma'_{CABtB}$ = Effective stress changes in the shell or core of layer A between time t_A and t_B

$\Delta v_{SABtB}, \Delta v_{CABtB}$ = Incremental deformations in the shell or core of layer A between time t_A and t_B

Fig. 4.8 Analysis Procedures for Every Additional Layer

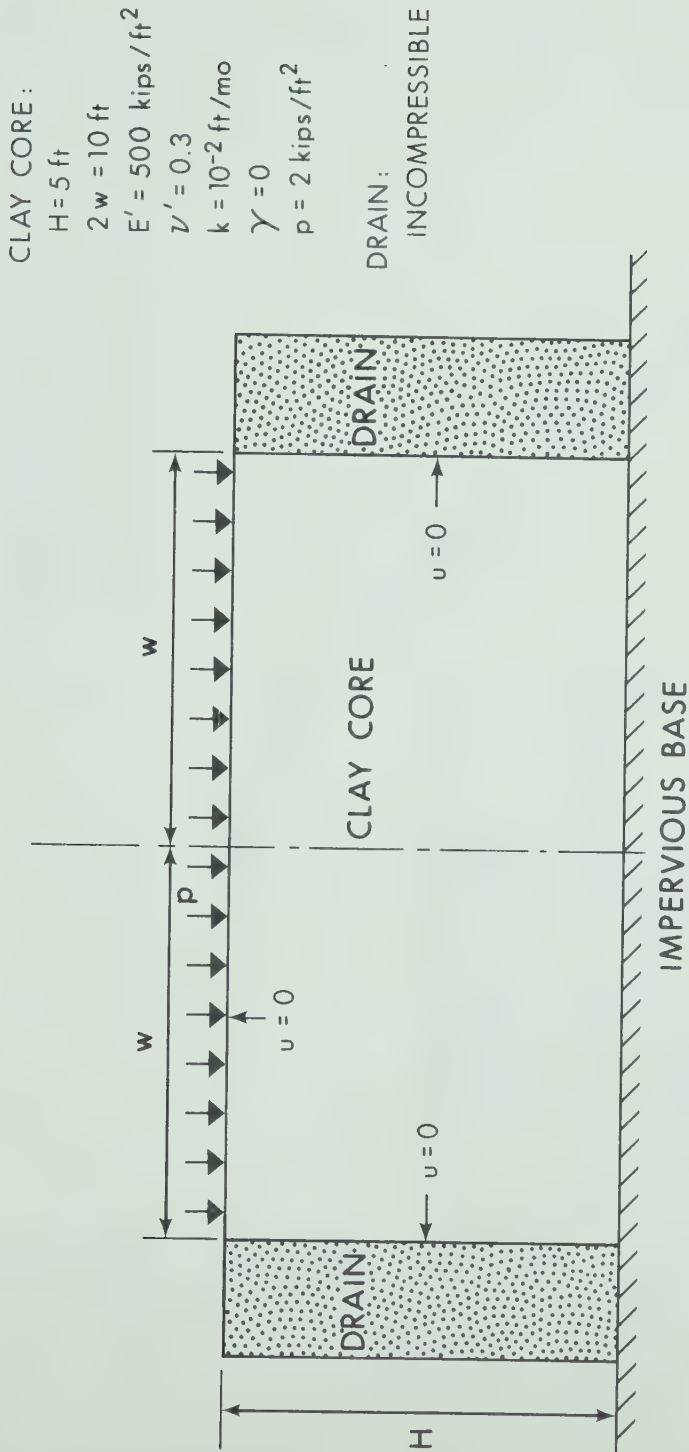


Fig. 4.9 Rectangular Clay Core With Side Drains

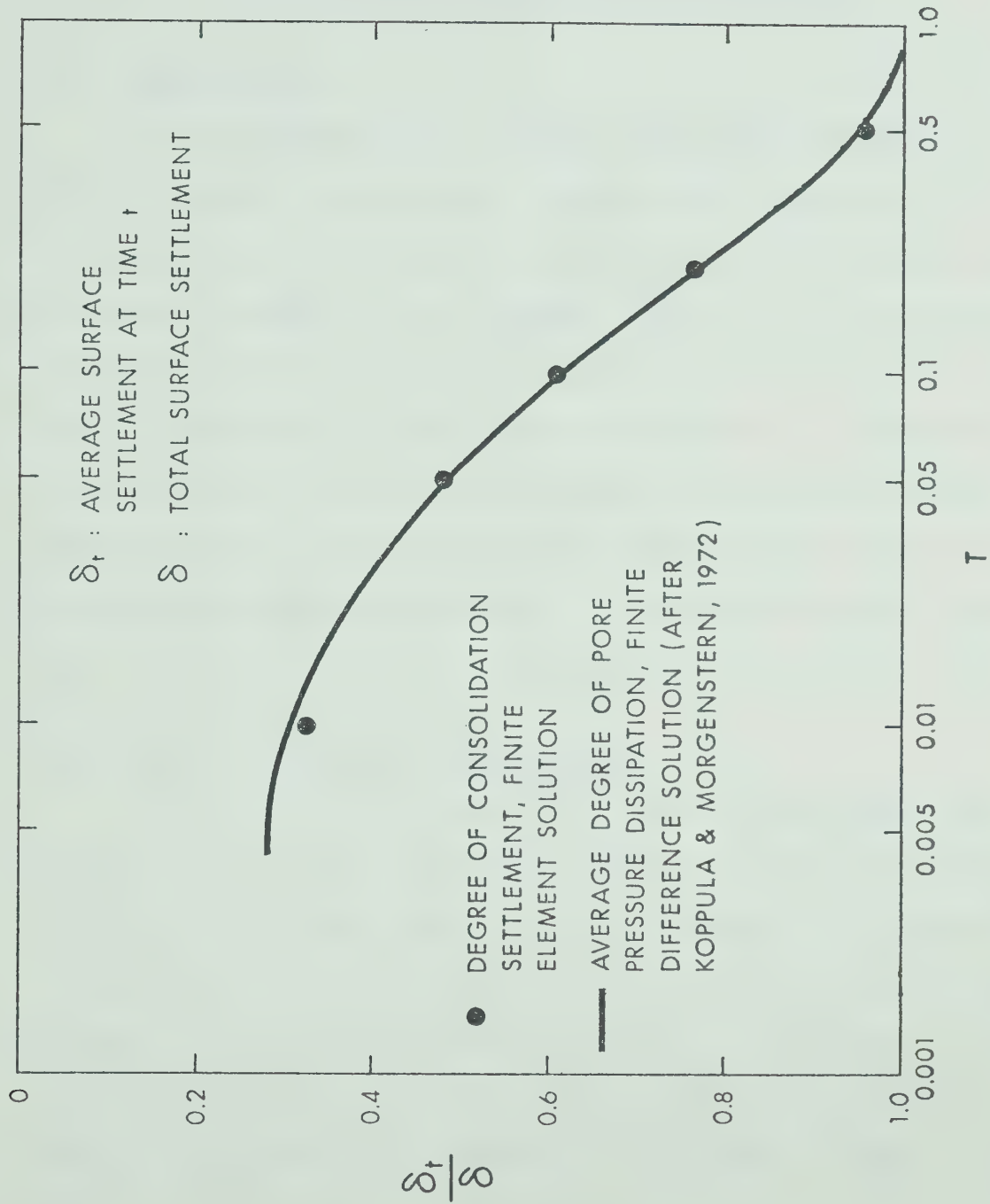


Fig. 4.10 The Rate of Surface Settlement for Rectangular Core With Two-Dimensional Pore Pressure Dissipation

CHAPTER V

ANALYSIS OF DEFORMATIONS IN MICA DAM

5.1 Introduction

The capability of an analytical model to incorporate all the factors which might influence the behaviour of a real structure is limited. Therefore, several assumptions are usually made. If the factors which are not considered are insignificant, the analytical model can predict closely the in-situ behaviour. Thus, the usefulness of any analytical procedure can only be evaluated by studying the behaviour of a real structure. Mica Dam, whose behaviour has been properly monitored during construction, is considered to be a valuable case history and hence it is studied in the present work.

5.2 General Description of the Dam

Mica Dam is situated in a narrow gorge where the Columbia River leaves the Rocky Mountain Trench about 80 miles north of Revelstoke, British Columbia. The location of the dam is shown in Fig. 5.1. The reservoir created by the dam will extend for over 130 miles in the Trench, from Golden to Valemont and will generate 2500 MW of electric power. The general arrangement of the dam is shown in Fig. 5.2.

The dam embankment is 111 ft. wide at the crest and 3100 ft. wide from heel to toe. The crest is 2600 ft. long and has a radius of curvature of 10,000 ft. The greatest height of the structure, from the lowest bedrock surface to the crest, is 800 ft. More details of the dam are listed in Table 5.1. The geometry around the crest zone has been revised from the initial design during construction. In order to avoid possible erosion caused by waves resulting from a large slide or earthquake, the crest was widened from an initial 36 ft. to the present width.

The dam is a zoned earth and rockfill structure with a near-vertical, central impervious core. The core is comprised of glacial till and the shells are mainly sand and gravel. On the outer parts of the shells, compacted and dumped rock was used. The arrangement of the fill is shown in Fig. 5.3. All the till and sand and gravel fills were obtained from upstream borrow areas, namely Wood River Burn, Encampment, Confluence, Little Chief and Dutchman's Creeks. The rockfill, which is mainly granitic gneiss, was obtained from quarrying operations.

The construction started in early 1965. Twin 45 foot diameter diversion tunnels in the left abutment were completed in October 1967. The river was subsequently diverted in November of that year by extending 4 closure dykes across the river, two at each cofferdam. By May, 1968 the cofferdams had been completed and the riverbed dewatered. Dewatering of

the construction area was by tube wells which were phased out when the fill height was beyond any danger of overtopping.

Prior to any excavations in the foundation area, the maximum depth of river overburden is 150 ft. The lowest part of the overburden is dense glacial till with thickness up to 60 ft. This layer was overlain by dense, coarse, granular materials consisting of sand, gravel, cobbles, and boulders containing lenses of heavily over-consolidated silt and clay. Silty fine to medium sand up to 50 ft. deep existed over much of the riverbed at the dam site. In order to eliminate any possibility of a major slumping failure due to liquefaction under an earthquake shock, the silty river overburden sand was excavated under the inner shells and the core was taken to sound rock. A core trench was formed and the foundation for the core was blanket grouted to a depth of 30 ft. In addition to a line of deep holes grouted along the upstream third of the core, two lines located 30 ft. upstream and downstream from this line were also grouted.

Minor fill placement commenced in the upstream shell late in the 1968. Major fill placement was not started until April and May 1969. It occupied four construction seasons roughly from April to November each year, depending on climatic conditions, and was essentially completed by November 1972. Embankment construction progress of each year is shown from Fig. 5.4. to Fig. 5.7. The variation of fill elevation at the dam core with time is shown in Fig. 5.8. More detailed

description of the general aspects of the project are given by Webster (1970) and Meidal and Webster (1973).

5.3 Field Control Data of Placement Materials

Very heavy compaction was specified for the core and shell materials in order to minimize total and therefore differential deformations, to provide increased strength and to decrease the risk of liquefaction. Glacial till was compacted in the main body of the core by 8 passes of 62.5 ton rubber-tired rollers having tire pressures of 120 psi. For granular materials in the inner shells, outer shells and drawdown zone compaction with 4 passes of 10 ton smooth drum vibratory rollers was specified. However, only 2 passes were required for those within 20 ft. of the core. In zone M2 (Fig. 5.3), compaction with 8 passes instead of 4 passes was used for the elevation above 2000 ft. The specified layer thickness after compaction for each zone is shown in Fig. 5.3.

Following the first construction season important changes were made in the composition of the fill. In the shell zones layer height was increased without significant change in the compacted dry density, but the reduction in water content lowered the bulk density somewhat. In the core zones, the water content was reduced by 2% and an appreciable gain in compacted dry density was achieved. The statistics for water content and density of the fills are listed in Table 5.2.

By allowing 10% of the till and 15% of the sand and gravel to lie outside each of the fine and coarse limits, the gradations of the borrow materials met the specified requirements with little or no processing. The statistical gradation envelopes for till and sand and gravel used are shown in Fig. 5.9. It may be noted that both materials are well-graded.

5.4 Instrumentation of the Dam

A comprehensive system of instrumentation has been provided to measure horizontal and vertical movements, earth pressure, pore water pressure and dynamic movements in the dam. The general description of the instruments was given by Webster and Lowe (1971). The numbers of each type of instrument installed up to the end of construction were reported by Meidal and Webster (1973).

In this investigation, data from several vertical and near-vertical movement (MV) gauges were extensively used. Locations of these devices are shown in Fig. 5.10. They consist of telescoping casing and transverse aluminium discs set around and at intervals along the casing. All the gauges were anchored 3 ft. into bedrock, with the exception of MV15 which penetrated 30 ft. into bedrock and MV7 which was seated in the midheight of the core. Some details of installing a typical MV gauge are given in Fig. C.1 of Appendix C. Settlements were read using a latch-cone device or a radiosonde, while lateral movements were measured with

A slope indicator developed by Sinco. Due to very small horizontal movements in the embankment during construction and the limits of instrument accuracy, the horizontal movement data from the MV gauges can only be interpreted in a qualitative manner.

The piezometers were installed at various parts of the dam for monitoring the pore pressures developed during various stages. The number at each part varies with the relative importance of pore pressure in that region. From the distribution numbers reported (CASECO report), it may be noted that most attention has been concentrated on the core and core foundation. Three types of piezometers were used. These were Maihak electric piezometer, Geo-test pneumatic piezometer and USBR embankment type hydraulic piezometer. Regarding the construction pore water pressures in the core, only those recorded by electric and pneumatic piezometer were of major concern, since only these two types of piezometers were equipped with high air entry porous stones. The porous stone used had air entry value of 20 psi and a measuring range of 0 to 30 atmospheres. Other than occasional damage to tubing and electrical leads caused by hauling and rolling equipment, these piezometers function satisfactorily. The performance of various instruments during construction were reported and discussed in CASECO reports on a yearly basis.

5.5 Observed Behaviour During Construction

5.5.1 Effects of Upstream and Down-Stream Water Level

Before the major programs of fill placing started in April 1969, the seepage through the foundation beneath the cofferdams was controlled by the tube wells. These tube wells were used in the upstream and downstream cofferdams and were sunk to earth bedrock or river overburden. Their locations are shown in Fig. 5.3.

After the downstream cofferdam tube wells were abandoned at the end of April, 1969 and subsequently upstream cofferdam tube well operations were discontinued at the beginning of July 1969, the foundation piezometric readings showed a gradual rise in piezometric levels. During the early stages of construction, readings from piezometers at the lower part of the dam were very much influenced by the seepage of upstream and downstream water. Toward the end of the 1969 season, all the piezometers installed in both the till and sand and gravel of the river overburden started reflecting the upstream and downstream free water levels. This situation can be illustrated with some piezometric observations in river overburden as shown in Fig. 5.11. Consequently, it might be assumed that all the shell and river overburden materials below the free water levels were saturated thereafter. As the fill placement continued in subsequent construction seasons all these piezometers

reflected elevations consistent with the upstream and downstream water levels. No excess pore water pressures were built up.

Similar trends were also observed in piezometers in the bedrock. All the piezometers in the bedrock were installed underneath the core and were equally distributed upstream and downstream of the center line deep grout curtain. The elevations in these piezometers closely followed the embankment elevation until mid-August 1969 and then stabilized at an elevation approximating the upstream water level. This condition is illustrated in Fig. 5.12. Pratt et al. (1972) reported that during foundation treatment water testing of drill holes in the rock underlying the core indicated higher permeability in the upper 50 ft. decreasing downward to a depth of about 250 ft. and negligible thereafter. Prior to grouting, permeabilities ranged from greater than 1×10^{-2} cm/sec to less than 1×10^{-7} cm/sec. Joint spacing, commonly less than 2 ft. near the surface, increases with depth. The prevalent joints are parallel to the horizontal strata but other joints dip deeply northwest or southeast. Since the elevations in the piezometers under the core followed so closely the fluctuating river water levels, the efficiency of the line grouting may cause some concern. However, due to the small head difference between upstream and downstream water levels during construction, the efficiency of the grout curtain cannot be judged with

accuracy.

Significant stress relief must have taken place in the bedrock during core trench excavation. About 150' of river overburden material were removed from core contact surface. Heaving resulting from this stress relief was indicated by the movements of the bottom sections of the gauges, MV8 and MV15, which are embedded into the bedrock. From the time the initial elevations of the bottom most casings were established (May 1969) to June 14, 1969 when there was 40 to 50 ft. of fill, MV8 and MV15 had detected bedrock surface heaving of 0.47 and 0.21 ft. respectively. Unfortunately, no intermediate measurements were taken hence, attempts to establish the heaving history were unsuccessful. The question of whether or not there had been a higher heave and the later measurements were only part of the compression or the heave was peaking could not be answered. However, it seems obvious that the heaving was time dependent. Although this phenomenon might be attributed to the fact that rock is not purely elastic but viscoelastic, the increasing water pressure in the foundation in early 1969, as described previously may also be responsible for the heaving behaviour.

5.5.2 Bedrock Settlements

Following the first measurement, readings taken from MV8 and MV15 showed that the bedrock surface under the core started to settle under the rapidly increasing fill weight.

By the time the fill reached its final height settlements of 1.0 and 0.9 ft. were measured in MV8 and MV15 respectively.

No bedrock heaving was detected by other gauges since no major excavations took place in any other part of the foundation. About 0.2 to 0.5 ft. of total bedrock settlement was measured by these gauges during construction.

The relationships between the fill height and bedrock movement measured in the gauges of concern are shown in Fig. C.2 to Fig. C.8 of Appendix C. In the center part of the dam, the bedrock surface settled at a rate of 0.12 to 0.16 ft. per 100 ft. of fill while under the shells, it settled at a rate of 0.04 to 0.08 ft. Because MV5 was anchored 30 ft. into the bedrock, one dimensional compressibility of the upper bedrock can be roughly estimated as in Table C.1 of Appendix C. For the sake of later analyses, the profiles of bedrock movements under section 22 + 50 at various construction stages are plotted and shown in Fig. 5.13.

5.5.3 Pore Pressures in the Dam

Piezometers installed in the dam but outside the core showed no or negligible excess pore water pressures during construction. This condition can be illustrated with piezometric observations in the shells as shown in Fig. 5.11. Within the core, excess pore water pressures were measured in most cases. Especially in the first year (1969) fill, high pore water pressures were observed during construction.

The piezometers installed in the core were located in 10 different sections. The location of these piezometers are shown in Fig. 5.14. Many are in or near sections 22 + 50 and 24 + 50.

Due to the failure of some of the piezometers and low induced pore water pressures at high elevations, only the observations in five selected piezometers in the core will be studied. These are PP21, PE24, PE25 and PE26. The variations of piezometric elevations with time of these five piezometers are shown in Fig. 5.15. From this figure, it may be noted that the measured pore pressures generally increase slightly or remain constant rather than decrease during the first construction shutdown after installation. For PP21 and PP20, this phenomenon might be attributed to the influence of seepage of river water into the lower part of the core. Immediately before the first construction shutdown (1969-1970), the observed elevations in these two piezometers reached the same elevations as upstream and downstream water levels. During the first shutdown season, the piezometric elevations remained at these levels to maintain the equilibrium in pore water pressures with the surrounding shells. For PE24, PE25 and PE26, the reason might be that the time of installation of these piezometers was close to the end of the construction season. Before the equilibrium pore pressure could be established between the surrounding soil and the measuring systems, the construction season had stopped. Consequently,

the pore pressures registered by those piezometers appeared to be lower than what the actual values might be up to this period. The increase in observed piezometric elevations during the first shutdown season appeared to be in the process of reducing these differences and achieving the equilibrium condition. The pore pressures measured by these piezometers after the first construction shutdown might represent the actual pore pressures in the fill. Despite some unexpected behaviour as described previously, the piezometers in the core generally showed 15 to 20% pore pressure dissipation during the subsequent shutdown seasons.

The influences of pore pressure dissipation during shutdown season on subsequent construction pore pressure were discussed by Bishop (1957). The same tendency was observed in Mica Dam. From Fig. 5.16, which is the plot of pore pressure versus overburden pressure, it may be noted that r_u is decreasing in each successive construction season. The value of r_u was defined by Bishop and Morgenstern (1960) as the ratio of pore pressure to overburden pressure in order to differentiate it from \bar{B} , which can only be determined if the actual major principal stress is known. If the fill is relatively undrained during construction, the comparison of these two values will indicate the existence of "arching action" in the fill. This comparison for Mica Dam will be presented in later sections.

5.5.4 Embankment Deformations

Maximum settlement in the embankment ranged from 0.5 to 3.5 ft. Smaller settlements were generally measured by the gauges located in the sand and gravel and close to the abutments. Larger settlements were measured by the gauges installed in the core and near the center of the section of maximum height. For the softer core and stiffer shells, maximum settlements of 3.6 ft. and 2.4 ft. were measured by MV8 and MV10 respectively. Despite some minor irregularities, the measured settlement profiles displayed the typical quasi-parabolic shapes. The settlement data obtained directly from movement gauges usually include the influence of bedrock settlement. The settlement profile without this influence may be derived approximately by following the procedures described in Appendix D. After excluding the influence of bedrock settlements, the maximum settlement values become approximately 2.9 ft. in the core and 2.2 ft. in the shells.

Time dependent deformations which might not be neglected were measured in the core. This behaviour may be illustrated with settlement profiles relative to bedrock at the beginning and at the end of each shutdown season. The plots for MV8 and MV15, which are located in the center of the core, are shown in Fig. 5.17 and Fig. 5.18 respectively. The maximum settlement occurring during each shutdown season

was observed to be in the order of 0.2 to 0.3 ft. At the completion of the dam, a maximum settlement of about 0.6 to 0.8 ft. might be attributed to the consolidation process.

For use in later analyses and the subsequent examination concerning the K_0 stress path condition, the approximate vertical stress and vertical strain relationships in the dam for sand and gravel materials have been studied. Vertical stresses were assumed to be equal to overburden pressures. The incremental strains caused by corresponding incremental stresses were calculated from the settlement data of the movement gauges according to the method described in section 3.2. The vertical stress-strain data thus determined are grouped for three zones, i.e., river overburden, zone M2 and zone M2DI, and presented in Fig. 5.19 to Fig. 5.21. From these figures, it may be noted that quite a consistent behaviour has been measured for each zone. The data fall within a narrow band hence a representative stress-strain curve (best fit curve to the data) can be drawn for the material in each zone. These curves are also shown in the previous figures. The curves for zones M2 and M2DI show slight initial curvature but become approximately a straight line for the latter major portion. The shape of the curve for the river overburden material indicates a lesser incremental strain as the level of stress increases.

5.6 Finite Element Idealization

Two-dimensional analysis has been found useful in the study of deformations in dams. This point has been discussed in Chapter III. In the present study of the behaviour of Mica Dam, two-dimensional analyses were focussed on the transverse section at station 22 + 50. The location of the section is shown in Fig. 5.10. This is the main instrumentation section and close to the maximum height section. The selection of this section is not only convenient for assuming the existence of plane strain conditions but also provides a direct comparison between the analytical results and the field measurements at appropriate locations. A mesh of 729 nodes and 1352 elements was used in the finite element idealization.

The importance of simulating the actual construction process in embankment deformation analysis has been emphasized by Clough and Woodward (1967). Although it is not feasible to simulate a continuous filling in the finite element analysis, it has been reported that the same accuracy can be obtained in the incremental analysis using a certain minimum number of finite layers. Clough and Woodward (1967) adopted 10 lifts as a standard for their analyses. More detailed investigations concerning the required number of layers in the analysis was described by Kulhawy et al. (1969). They used 12 lifts in their subsequent analysis (Kulhawy and Duncan, 1970).

Due to the height of the embankment, the construction of Mica Dam was simulated in 15 lifts. The idealized section is shown in Fig. 5.22. A total of seven materials, which might differ only in stress-strain behaviour or in bulk density, was assumed for all the materials in the dam and the river overburden.

5.7 Analyses Based on Triaxial Test Data

The aim of the analyses was to examine the validity of triaxial test results in predicting deformations using presently available procedures. The results might be used to justify the K_0 stress path approach adopted in this thesis.

5.7.1 Derivation of the Moduli

During the design stage of Mica Dam, different types of triaxial tests, i.e., undrained, consolidated undrained and drained tests, were performed on different materials which were finally used in the dam fill. In order to use these laboratory results for analyses, selections were made to choose those which closely simulated density, water content, gradation and drainage condition which were observed in the field. Results of the selection are summarized in Table 5.3. Consolidated undrained test data was used for the first year core fill because it was thought that such data would be the most representative of the field conditions while pore pressure was excluded in the calculation. Undrained test

results were used for the core fill in the other years since no consolidated undrained triaxial data were available for the material with the same water content. As described in section 5.5.3 no excess pore pressures were measured in the sand and gravel and in river overburden, thus drained test results were used for these materials. The gradation curves of the materials tested are shown in Fig. 5.23. The tests were performed on 6" x 12" samples for all the results presented. The cell pressures ranged up to 350 psi, higher pressures were used in some cases. Details of the tests were described in a CASECO report. The test results were partly reported by Insley and Hillis (1965) and Skermer and Hillis (1970). Since no volume change measurements were made in undrained and CU tests on till samples, the volumetric strain versus axial strain relationships of these tests were approximated by the measurements from drained tests. The stress-strain-volume change curves of the materials considered are shown in Fig. 5.24 to Fig. 5.28.

For confirmation, two analyses with two different methods of describing the nonlinear, stress-dependent stress-strain relationships of the materials were performed. No bedrock movements were introduced in these two analyses, thus the embankment settlements relative to bedrock were used for the comparisons with field measurements. The two analyses are briefly described as follows:

(a) Analysis using hyperbolic stress-strain relationship. The analysis was conducted using the tangent Young's modulus and tangent Poisson's ratio to describe the nonlinear behaviour of the soils as suggested by Kulhawy et al. (1969). The variations of tangent Young's modulus and tangent Poisson's ratio were formulated by assuming the stress-strain relationship of the soils followed a hyperbolic curve. The resulting expressions for these two variables are as follows:

$$E_t = \left[1 - \frac{R_f (1 - \sin\phi)(\sigma_1 - \sigma_3)}{2c \cos\phi + 2\sigma_3 \sin\phi} \right]^2 K_h P_a \left(\frac{\sigma_3}{P_a} \right)^n \quad (5.1)$$

$$v_t = \frac{G_h - F \log (\sigma_3/P_a)}{\left[1 - \frac{d (\sigma_1 - \sigma_3)}{K_h P_a \left(\frac{\sigma_3}{P_a} \right)^n \left[1 - \frac{R_f (\sigma_1 - \sigma_3)(1 - \sin\phi)}{2c \cos\phi + 2\sigma_3 \sin\phi} \right]} \right]^2} \quad (5.2)$$

In the above equations parameters c , ϕ , K_h , n , R_f , G_h , F and d must be determined from a set of triaxial stress-strain-volume change curves having different confining pressures and P_a is atmospheric pressure in the same units as σ_3 and σ_1 . Instead of c and ϕ , parameters c' and ϕ' must be used for drained tests. Procedures for determining these parameters were described by Kulhawy et al. (1969). The values determined for Mica Dam materials are listed in Table 5.4.

For performing this analysis, a subroutine describing the hyperbolic stress-strain relationships of the materials (Appendix E) was incorporated into the main program (Appendix B).

Because of the conveniences provided in separating the volumetric and deviatoric stress effects, bulk modulus, K , and shear modulus, G , were used in the actual calculations. They are related to the tangent Young's modulus, E_t , and tangent Poisson's ratio, ν_t , according to

$$K = \frac{E_t}{3(1 - 2\nu_t)} \quad (5.3)$$

$$G = \frac{E_t}{2(1 + \nu_t)} \quad (5.4)$$

Since an unrealistic high calculated bulk modulus will result when σ_3 and shear stress approaches zero even though the soil is not incompressible, all the previous relationships have been limited to lowest σ_3 value, about 2psi, and the highest ν_t of 0.48. For σ_3 less than 2psi or zero, a similar approach to that suggested by Kulhawy et al. (1969) for the soil failure in tension was used. The bulk modulus was set the same as its previous value, but the shear modulus was reduced to a low value (e.g. bulk modulus/50) rather than zero as suggested.

(b) Analysis using invariant stress-strain relationship. The derivation of the moduli in this analysis consists

of converting the conventional triaxial test data to a form involving the three stress invariants, the axial strain, and the octahedral shear strain. Details of this procedure were described by Krishnayya (1973(a)).

The following expressions were used to calculate the stress invariants and γ_{oct} from the conventional triaxial test data:

$$\sigma_{oct} = (\sigma_1 + 2\sigma_3)/3 \quad (5.5)$$

$$\tau_{oct} = (\sqrt{2}/3) (\sigma_1 - \sigma_3) \quad (5.6)$$

$$J_3 = \sigma_1 (\sigma_3)^2 \quad (5.7)$$

$$\gamma_{oct} = (\sqrt{2}/3) (3\varepsilon_1 - \varepsilon_v) \quad (5.8)$$

With the interpolation procedures, the elastic parameters based on these stress invariants, which were determined from the three known principal stresses in an element, were computed. For two-dimensional plane strain analysis, the intermediate principal stress was calculated from:

$$\sigma_2 = \nu (\sigma_1 + \sigma_3) \quad (5.9)$$

where ν was a trial value of Poisson's ratio.

The shear modulus, G , and Poisson's ratio, ν , were obtained with the following expressions:

$$G = (\Delta \tau_{\text{oct}} / \Delta \epsilon_1) / (\Delta \gamma_{\text{oct}} / \Delta \epsilon_1) \quad (5.10)$$

$$\nu = (3/2\sqrt{2})(\Delta \gamma_{\text{oct}} / \Delta \epsilon_1) - 1 \quad (5.11)$$

The Poisson's ratio was limited to a maximum value of 0.49. Since G and ν were determined, the bulk modulus was further calculated by:

$$K = \frac{2G(1 + \nu)}{3(1 - 2\nu)} \quad (5.12)$$

When one of the principal stresses becomes negative (tensile) it was artificially set to zero in the calculation. The main program listed in Appendix B was developed originally to perform this analysis.

Due to the interpolation procedure adopted in this approach, the triaxial test data supplied must cover the stress range which will exist in the dam. Since no complete test data were available, the lower and upper bound curves having σ_3 of 0 psi and 950 psi respectively were extrapolated using the hyperbolic relationships and the parameters described in a previous subsection (section (a)). All the stress-strain-volume change data were supplied in digital form for the analysis.

5.7.2 Results of the Analyses and Their Implication

The results from the previous two analyses showed similar trends in their predictions. Because insufficient

stress-strain curves at closely spaced values confining pressures the deformations from procedure (b) yielded values slightly larger than those from procedure (a). Despite the slight differences which resulted from the two different procedures for deriving nonlinear moduli, the results of both analyses indicated that the analyses based on triaxial stress data overestimate the measured settlements by about 2.5 to 3.5 times. The comparisons between predicted and measured settlements for several movement gauges are shown in Fig. 5.29 to Fig. 5.31. The analytical results for horizontal movements are shown in Fig. 5.32. Unfortunately no reliable measurements can be used to verify these.

Based on the investigations conducted for different stress paths, Duncan and Chang (1972) indicated that the simple incremental procedures using the conventional triaxial test data result in a reasonably good prediction of strains for unloading-reloading stress paths and for a range of stress paths in the primary loading range. However, the predictions are poor for primary loading under constant or nearly constant stress ratio (σ_3/σ_1) and for certain other types of stress paths. For stress paths with constant or nearly constant stress ratios the strains predicted using modulus values for primary loading are too large and those predicted using modulus values for unloading-reloading are too small.

In view of the results of previous investigations, it seems obvious that deformations in an earth and rockfill dam during construction do not occur under conventional triaxial stress path conditions. The stress path followed is most likely constant or nearly constant stress ratio path, at least for most of the volume of a dam. Regarding the ratio between the width and the height of the fill during construction, it may further be anticipated that the actual stress path in the major part of Mica Dam approximately follows that of the oedometer test (K_0 -stress path). The degree of approximation will be studied in a subsequent section by comparing the deformations predicted based on K_0 -stress path and the measured deformations.

5.8 Analyses Based on Oedometer and Isotropic Compression Test Data

5.8.1 Total Stress Analysis

The analysis was performed to obtain the distribution of total stress within the dam. The influences of pore pressure dissipation on embankment behaviour were not considered in the analysis. The method of deriving nonlinear moduli as described in Chapter II was used. As discussed in that Chapter the Poisson's ratios determined may not vary significantly thus constant values of this parameter were used for each material throughout the analysis. The values used are listed in Table 5.5.

Because of the nonlinear stress-strain behaviour of the soil, corrections are sometimes necessary when the

laboratory data are used to interpret the field measurements and consequently to predict the field performance. The zero stress and strain for the soil in the laboratory and that in the fill must be referred to a comparable condition. The zero stress and strain for all the samples tested in this investigation were referred to the state after compaction: However, due to the installation procedures for each new casing in vertical or near vertical movement gauge as shown in Fig. C.1 of Appendix C, the zero strain for the soil in the fill was referred to a state of having 10 to 15 psi of vertical stress after the compaction. Although this pressure was small compared with maximum vertical stress that would be experienced in the dam, the magnitude of the strain which occurred under this pressure was highly dependent on the water content of the soil (Gould, 1953). From the laboratory results, it was noticed that the vertical strain at this pressure for compacted Mica Till with water content the same as 2nd, 3rd and 4th year core fill was small. The strain for those as in the first year core fill could be as high as 1 to 2%. In order to be comparable, the laboratory stress-strain curves used for the first year core fill in the analyses were corrected by setting the zero strain at a stress level of 10 psi. As discussed in Chapter II, Mica Till samples prepared by kneading compaction in 7 layers with 70 tamps of 150 psi pressure per layer more closely resemble the state of compaction in the field. The average and

corrected stress-strain relationships of the till samples having gradation No. 1 and prepared by the previous compaction method were used in the analyses. These total stress-strain curves are shown in Fig. 5.33.

Since the laboratory studies on stress-strain behaviour of vibratory compacted sand and gravel materials were not included in the present investigation, the approximate vertical stress-strain relationships, which were described in section 5.5.4, have been utilized for the analyses. In the analyses, these relationships were considered as major principal stress and strain relationships obtained from oedometer tests. The curves plotted in the new coordinates are shown in Fig. 5.34. With this interpretation of the former stress-strain data, one may examine indirectly whether or not the stress path in shells and river overburden of Mica Dam follows approximately that of the oedometer tests (K_0 -stress path). If close agreement between observed and predicted deformations are obtained, then it may indicate the existence of close to K_0 -stress path condition. Since no excess pore water pressures were measured in sand and gravel materials, the curves might be used for both total and effective stress analyses. Poisson's ratios for these materials were derived using the following expressions:

$$K_0 = 1 - \sin\phi \quad (\text{Jaky, 1944})$$

and

$$\nu = \frac{K_0}{1 + K_0}$$

where ϕ is the angle of shearing resistance and K_0 is the coefficient of earth pressure at rest. The values of ϕ used are those listed in Table 5.4.

In the analyses, the change in stress-strain behaviour due to wetting was not introduced for the materials under submergence. As described in Chapter I, this mode of deformation was excluded in the present study. Moreover, unlike the cases of reservoir filling and steady seepage, only a very small portion of the dam was submerged during construction.

The influence of bedrock movement was included in the studies and analyses with and without bedrock movements were performed. The incremental movements of bedrock as shown in Fig. 5.13 were introduced in the analyses whenever they were considered.

5.8.2 Analysis of Construction Pore Pressure

Due to the thin core of Mica Dam, two dimensional dissipation was assumed in the analysis. Zero excess pore pressures were assumed at the boundaries between core and shells. This assumption may be justified by Fig. 5.11, which shows the pore pressure measurements in shells at the locations immediately beside the core. The analysis was performed with the finite element program described in Chapter IV. Total stresses obtained in previous total stress analysis were used in the present analysis.

The pore pressure ratios \bar{B} used in the analysis are the values determined in oedometer partial dissipation tests on samples OW-3 and OD-8. These two samples have water contents corresponding to two different average water contents in four years of core fill. The samples are formed with Mica Till having gradation No. 2 (Fig. 2.8). The test results determined on samples having gradation No. 2 were used due to the influence of stone content. The soils having the same gross water content may differ in pore pressure responses due to the difference in stone contents. The stone content may effect the amount of water retained in the fines. The \bar{B} values used in the analysis are listed in Table 5.6. Different \bar{B} values were used for each year's fill for different construction seasons.

The summary of C_v values determined from oedometer partial dissipation tests for Mica Till having high water content has been presented in Table 2.4. The average of these values is about 150 ft.²/month. Although it might be noted that C_v values did vary somewhat with the stress levels, for practical purposes they may be assumed constant. More variation might be expected if some values were determined at stress levels lower than those described. In the present analysis the average value was used for the entire stress range. Since no reliable values were obtained for samples having a lower water content, the same average value was assumed.

For comparison, C_v values derived from several other tests were also reviewed. The ways of derivations are

described briefly as follows:

(a) C_v determined from triaxial dissipation tests:

The details of this procedure are given by Bishop and Henkel (1957). During the design stage of Mica Dam, some triaxial dissipation tests were performed on Mica Till. The samples tested were compacted with the standard Proctor effort and had water contents of optimum and 2% dry of optimum. Several different confining pressures were used in the tests. The results of the tests are shown in Fig. 5.35. From this figure, it can be seen the average value of the coefficient of consolidation is about $10 \times 10^{-3} \text{ cm}^2/\text{sec}$ (or $28 \text{ ft}^2/\text{month}$). One particular feature of these tests was the occurrence of three dimensional strain during the dissipation stage.

(b) C_v determined from laboratory permeability and oedometer compression tests. Some direct permeability tests were performed on Mica Till in the triaxial cell with different confining pressures during design stage. The test results are shown in Fig. 5.36. From this figure, it can be noted that the average coefficient of permeability, k , for the samples with 8.8% water content is about $33 \times 10^{-9} \text{ cm/sec}$.

From the oedometer compression tests performed in this study, the average constrained modulus ($\frac{1}{m_v}$) for Mica Till with water content about 8.8% is about 2000 ksf. As the reciprocal of constrained modulus, one-dimensional compressibility, m_v , for the same material is calculated as $0.5 \times 10^{-3} \text{ Ksf}^{-1}$. As a result, the C_v determined from previous k and m_v

values is about $91 \text{ ft.}^2/\text{month}$.

(c) C_v determined from laboratory permeability and isotropic compression tests. In addition to the oedometer compression tests, isotropic compression tests are always used for determining the compressibility of the soil. The average bulk modulus (K) determined from these tests for Mica Till with water content of about 8.8% is about 1600 Ksf. As the reciprocal of bulk modulus, the volume compressibility for the same material is $0.625 \times 10^{-3} \text{ Ksf}^{-1}$. Using this compressibility value and the value of coefficient of permeability described in previous sub-section (b), the C_v value is calculated as $73 \text{ ft.}^2/\text{month}$.

For easier comparison, the C_v values determined from various methods described in this section are listed in Table 5.7. From this table, it may be noted that, due to the difference in strain conditions of the tests, the value derived from triaxial tests is generally lower than that from the oedometer tests. As discussed previously, the strain condition in the core of Mica Dam might be approximated with no-lateral-strain condition, thus the value determined from oedometer tests was used.

5.8.3 Effective Stress Analysis

The influence of pore pressure dissipation on the deformations of Mica Dam during construction has been studied with the effective stress analysis. Details of the analysis

procedures have been described in Chapter IV. Total stress and pore pressure results obtained from the analyses discussed in sections 5.8.1 and 5.8.2 respectively were utilized in this analysis.

The variation of core fill elevation with time used in the analysis to approximate the actual construction history of the dam core is shown in Fig. 5.37. For clarity, the lift number assigned to the simulated construction sequence of the dam is also shown. In lift No. 5, although there are no change in core fill elevation but there is some additional fill in the shells.

The effective stress-strain curves used for the core materials in the analysis are shown in Fig. 5.38. Two different curves were used for the core fill which had two different average water contents. For the reason mentioned in section 5.8.1, the curves used are the average stress-strain relationships determined in oedometer tests for the till samples having gradation No. 1 and prepared by kneading compaction in 7 layers with 70 tamps of 150 psi pressure per layer. The stress-strain relationships employed for the sand and gravel materials in the analysis were the same as those used in total stress analyses. These stress-strain curves are shown in Fig. 5.34. Constant values of Poisson's ratio were used. The value for each material is listed in Table 5.5. The determination of the values used for core materials has been discussed in section 2.12. For sand and gravel materials,

the same values as those employed in the total stress analysis were used.

5.9 Results of Analyses Based on Oedometer and Isotropic Compression Test Data

5.9.1 Embankment Deformations

The results of calculated settlements from effective stress and total stress analysis together with the observed values at the end of the construction in several movement gauges are shown in Fig. 5.39 to Fig. 5.41. From the results, it may be noted that the effective stress analysis including the realistic boundary conditions has improved the prediction of settlement in the core. The differences between total stress and effective stress analysis results for Mica Dam are about 15 to 20% of settlements observed at the end of construction. The gain in accuracy is usually pronounced for the case where the percentage of deformations due to pore pressure dissipation is high. For the case where deformations due to pore pressure dissipation are less significant, total stress analysis which employs the stress-strain relationship following the stress path condition anticipated in the field may also predict the settlements during construction within the accuracy generally required in practice. In Fig. 5.39, as might be noted, the calculated settlements for MV9 are slightly higher than the observed values. This movement gauge is located in the core but close to the core and shell interface where high shear stress are usually developed. The lower

observed values seem to indicate that the presence of less flexible casing of the gauge has reduced the magnitude of shear deformations in the surrounding soil. As may be expected there are no significant differences between the results of total stress and effective stress analyses in the shells. The calculated settlements are in reasonably good agreement with the observed values. The deviation of calculated settlements from observed values in MV5 as shown in Fig. 5.41 is, in fact, due to the differences in geometry between the plane of analysis and the plane where MV5 is located.

Although no reliable horizontal movement measurements can be used to verify the calculated values in Mica Dam, it is interesting to note that calculated horizontal movements shown in Fig. 5.42 are of the same order of magnitude as those measured in Oroville dam (Kulhawy et. al., 1972). The maximum downstream movement in the center of the downstream shell of Oroville dam was about 0.6 ft. while that calculated for Mica Dam was about 0.5 ft. The height, the location of the sloping core and the configuration of the dam are quite similar for both dams. Moreover, maximum settlements in the core and the shells of these two dams were about the same although somewhat less in Mica Dam. Thus, it was considered that the calculated horizontal movements might not be too far from what might be observed.

5.9.2 The Influences of Bedrock Movements

Some results of major principal stresses calculated from the total stress analysis with and without introducing bedrock movements are presented in Fig. 5.43 and Fig. 5.44. From the results, it may be noted that there is a trend toward reduction of major principal stresses within the core due to the additional differential settlements caused by introducing bedrock movements. These additional differential settlements increase the load transfer effects between core and shells. However, for Mica Dam, the differences in the results of the two analyses were not of practical significance.

As would be anticipated, the embankment settlements calculated from analyses with and without introducing bedrock settlements are not the same. From the illustrations shown in Fig. 5.45, it may be noted that the differences are more for the lower portion of the dam. This situation happened simply due to the incremental construction of the dam. The settlements calculated from analysis with bedrock settlements are usually more than those calculated without bedrock settlements. Without making approximate adjustments as described in Appendix D, the observed settlement data generally include the influence of bedrock settlements. Hence, the proper comparison between observed data and analytical results can only be made if the bedrock settlements are also considered in the analysis.

Due to the increased concern for horizontal movements resulting from foundation settlements (Lee and Shen, 1969) the results of horizontal movements calculated from the analyses with or without introducing bedrock settlements are examined and presented in Fig. 5.46. A different movement mechanism was observed as compared to that in homogeneous dams. Rutledge and Gould (1973) summarized the observations of horizontal movements of concrete-pipe conduits near the base of selected earth dams. Their results indicated that further foundation settlement included the outward movements in the dams. When the bedrock settlements were introduced into the analysis of Mica Dam, the results showed reductions in outward movements. These results appear to indicate that in earth and rockfill dam with a soft sloping core, the bowl shaped settlement profile of the bedrock tends to cause the shell materials to move inward.

5.9.3 Load Transfer in the Dam

Due to the stresses being less sensitive to errors in stress-strain data, the computed stresses are generally believed to represent the field stresses under the same boundary conditions if the movements agree. As was described in the discussion of analysis results (section 5.9.1), reasonably good agreements between observed and calculated settlements were obtained. Thus, it might be interesting to examine the degree of load transfer, which might exist in Mica Dam as the result of differences in compressibility of the materials, from the calculated stresses in the same analysis.

To illustrate the load transfer mechanism, overburden stresses and calculated total major principal stresses on a horizontal plane in the dam are presented in Fig. 5.43. As may be seen, major principal stresses higher and lower than overburden stresses were calculated for the shells close to the core and the core respectively. From Fig. 5.44 which shows the variations of total major principal stresses at the center of the core with height, it may be noted that stresses as low as 50% of overburden stresses were computed for the lower part of the core. The results presented so far were obtained from 2D plane strain analysis. In this analysis, the effects of cross-valley load transfer are usually not considered. The values thus determined may be regarded as the upper bound of actual stresses under 3D condition.

To indicate the magnitude of the possible reduction of σ_1 due to load transfer in the cross valley direction and to study the possibility of a core endangered by hydraulic fracture, results from 3D (Simmons, 1974) and 2D analyses are presented in Fig. 5.47. In the same figure, the hydrostatic pressures which may exist in the dam during the maximum height of the reservoir are also shown. From this figure, it may be noted that if the hydraulic fracture mechanism postulated by Kjaernsli and Torblaa (1968) and shown in Fig. 5.48 is adopted, the stresses in the core below elevation 1950' are in a marginal state. Hydraulic fracture may in fact start to occur when water pressure exceeds the minor principal

stress. The criteria for hydraulic fracture based on σ_3 may also be used. This criteria is more conservative and it may be more suitably used for the design. Here the major principal stresses are examined simply to emphasize the low stress condition which existed in the dam. Low minor principal stresses are simply related to low major principal stresses. However, due to the excellent self-healing property of the till and wide filter zone on the downstream side of Mica Dam, even though the water pressure during maximum reservoir may reach the same magnitude as σ_1 or σ_3 in the lower parts of the core, the fracture or piping is unlikely to happen. Excessive leakage may not be detected.

5.9.4 Construction Pore Pressures

From the comparisons between observed and calculated pore pressures as shown in Fig. 5.49 and Fig. 5.50, it may be noted that the agreement is generally good except for PP21 and PP20 which are about 200 ft. from the plane of analysis. The calculated values, which are presented for comparison, are the results for the projected position of piezometer PP21 on the plane of analysis. Some differences in pore pressures surely could be expected due to different drainage paths resulting from different geometry even if no other factors were involved. However, the main factor for the higher observed values was considered as the result of wetting of lower parts of the core affected by upstream and downstream water.

In Mica Dam, the shells are free draining. Theoretically, for the piezometers located at the same elevation within the core, the one closer to the boundary should have the shorter drainage path and hence the lower excess pore pressure. This point is demonstrated in Fig. 5.49 by the analytical results for PE25 and PE26 which are located close to the boundary and near the center respectively. However, as it may be noted in the same figure the observed data show the opposite trend. The reason for the lower values measured in PE26 may be speculated as being the result of the casing of the movement gauge located near PE26 served as a drainage path.

In Table 5.8, \bar{B} values used in the analysis are compared with observed r_u values. The differences between these two values are clearly shown. As discussed in a previous section, significant load transfer exists in Mica Dam, hence these differences can be expected.

TABLE 5.1

BASIC DATA FOR MICA DAM

	Metric Units	FPS Units
Elevations: Crest	762 m	2,500 ft
Riverbed	563 m	1,850 ft
Lowest bedrock	518 m	1,700 ft
Tailwater	573 m	1,880 ft
Drawdown range	754 to 707 m	2,475 to 2,320 ft
Height above lowest bedrock surface	243 m	800 ft
Height above riverbed	198 m	650 ft
Normal minimum freeboard	8 m	25 ft
Crest length	792 m	2,600 ft
Radius of crest curvature	3,048 m	10,000 ft
Crest width	34 m	111 ft
Heel to toe length	946 m	3,100 ft
Total volume of fill	$33 \times 10^6 \text{ m}^3$	$43 \times 10^6 \text{ yd}^3$
Total volume of core	$3.3 \times 10^6 \text{ m}^3$	$4.3 \times 10^6 \text{ yd}^3$
Slope of upstream face	1 on 2.25	1 on 2.25
Slope of downstream face	1 on 2.00	1 on 2.00

TABLE 5.2
STATISTICS FOR WATER CONTENT AND DENSITY IN MICA DAM

Year	Zone	Dry Density (pcf)	Water Content (%)	Bulk Density (pcf)
1969	M1	131.1	8.8	143.0
	M2	146.1	7.6	158.0
	M2DI	144.4	7.6	156.0
1970	M1	141.5	6.3	150.4
	M2	146.6	3.7	152.0
	M2DI	145.6	4.7	152.4
1971	M1	141.5	6.2	151.0
	M2	146.5	3.6	152.0
	M2DI	145.6	4.7	152.0
1972	Not available			
	1972 materials assumed to be comparable with 1971			

TABLE 5.3

REPRESENTATION OF DAM FILL FROM MATERIAL USED IN TRIAXIAL TEST

Material Type No.	Material Used and Drainage Condition in Triaxial Test	Represented Material in Dam
1	Wood River Burn Sand and Gravel, Gradation 8, Drained Test	First Year Sand and Gravel in Zone M2
2	Fine Medium River Overburden Sand (FM-C), Drained Test	River Overburden
3	Little Chief Fan Sand and Gravel, Gradation 12, Drained Test	First Year Sand and Gravel in Zone M2DI
4	Till at Optimum Water Content, Middle Gradation, Consolidated Undrained Test	First Year Till in Core
5	Wood River Burn Sand and Gravel, Gradation 8, Drained Test	* 2nd, 3rd and 4th Year Sand and Gravel in Zone M2
6	Little Chief Fan Sand and Gravel, Gradation 12, Drained Test	* 2nd, 3rd and 4th Year Sand and Gravel in Zone M2DI
7	Till at Modified Optimum Water Content, Middle Gradation, Undrained Test	2nd, 3rd, and 4th Year Till in Core

* Difference in densities only was assumed as compared to their first year materials

TABLE 5.4

VALUES OF HYPERBOLIC STRESS-STRAIN PARAMETERS USED IN THE ANALYSIS

* Material Type No.	Bulk Density (Ksf)	Cohesion c or c' (Ksf)	Friction Angle ϕ or ϕ' (Degree)	Modulus Number K_h	Modulus Exponent n	Failure Ratio R_f	Poisson's Ratio Parameters	
							G_h	F d
1	0.158	-	39	2180	0.14	0.83	0.51	0.24 4.1
2	0.140	-	37	631	0.41	0.80	0.48	0.18 3.3
3	0.156	-	38	893	0.46	0.81	0.46	0.23 5.7
4	0.143	3.0	28	396	0.75	0.85	0.44	0.17 4.2
5	0.152	-	39	2180	0.14	0.83	0.51	0.24 4.1
6	0.152	-	38	893	0.46	0.81	0.46	0.23 5.7
7	0.151	5.0	31	260	0.54	0.72	0.44	0.17 4.2

*Refer to Table 5.3

TABLE 5.5
POISSON'S RATIOS USED IN TOTAL AND EFFECTIVE STRESS ANALYSES

Material Type [*] No.	Poisson's Ratios Used	
	Total Stress Analysis	Effective Stress Analysis
1	0.28	0.28
2	0.28	0.28
3	0.28	0.28
4	0.40	0.37
5	0.28	0.28
6	0.28	0.28
7	0.35	0.35

^{*} Refer to Table 5.3

TABLE 5.6

 \bar{B} VALUES USED IN THE ANALYSIS

Construction Year Applied	Values for Fill with [*] Higher Water Content	Values for Fill with ⁺ Lower Water Content		
	(1969) Fill	(1970) Fill	(1971) Fill	(1972) Fill
1969	0.52	-	-	-
1970	0.37	0.35	-	-
1971	0.25	0.23	0.35	-
1972	0.16	0.15	0.23	0.35

^{*}Test Data of Sample OW-3⁺Test Data of Sample OD-8

TABLE 5.7

COMPARISON OF C_v VALUES DERIVED FROM VARIOUS TESTS

Procedure	Average C_v Value (ft^2/month)
(1) Determined From Oedometer Dissipation Tests	150
(2) Determined from Triaxial Dissipation Tests	28
(3) Determined from Laboratory Permeability and Oedometer Compression Tests	91
(4) Determined from Laboratory Permeability and Isotropic Compression Tests	73

TABLE 5.8

COMPARISONS BETWEEN r_u and \bar{B}

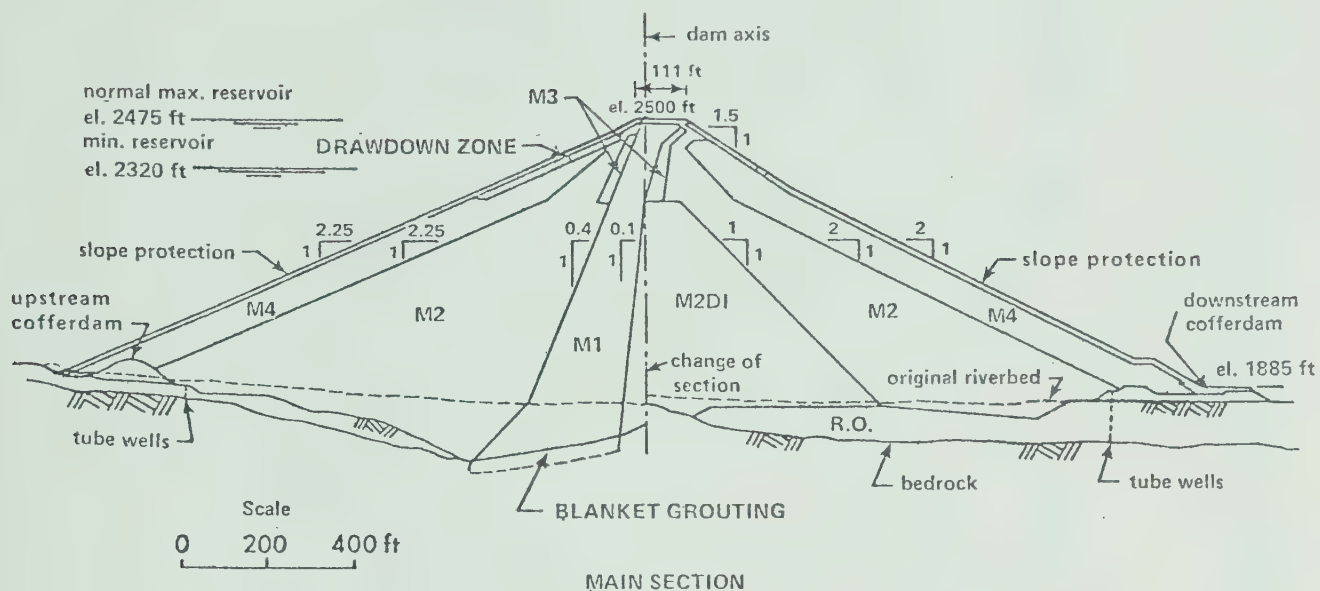
Construction Year Applied	Values for Fill With Higher Water Content				Values for Fill With Lower Water Content			
	\overline{B}	Average r_u			\overline{B}	Average r_u		
		PP21	PP20	PE24		PE25	PE26	
1969	0.52	-	-	-	-	-	-	
1970	0.37	0.23	0.23	0.24	0.35	-	-	
1971	0.25	0.13	0.16	0.10	0.23	0.08	0.07	
1972	0.16	0.33	0.08	0.02	0.15	0.03	0	



Fig. 5.1 Location of Mica Dam
(after CASECO report)



Fig. 5.2 General Arrangement of Mica Dam
(after Meidal and Webster, 1973)



ZONE	DESCRIPTION
M1	Core, glacial till in 25 cm (10") layers
M2	Main shell, sand and gravel in 30 cm (12") layers, changed during construction to 45 cm (18") layers
M2DI	Inner zone of poorer M2 materials
M3	Core support zone, sand and gravel or rock in 15 cm (6") layers
M4	Outer shell, sand and gravel or rock in 60 cm (24") layers
Drawdown Zone	Gravel, cobbles and boulders or rock in 60 cm (24") layers
R.O.	Original River Overburden

Fig. 5.3 Fill Arrangement in Mica Dam

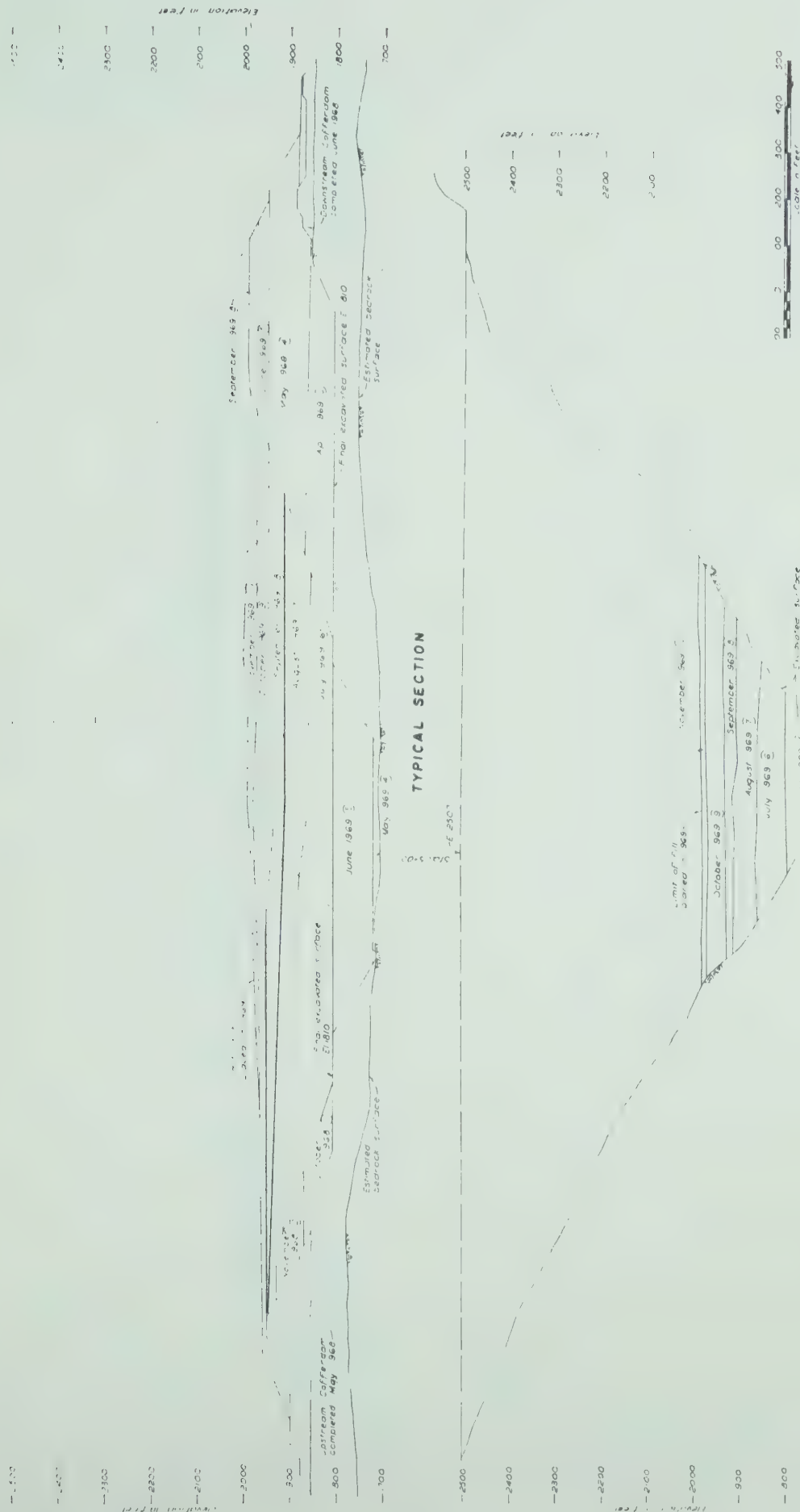


Fig. 5.4 Embankment Construction Progress in 1969, Mica Dam



Fig. 5.5 Embankment Construction Progress in 1970, Mica Dam

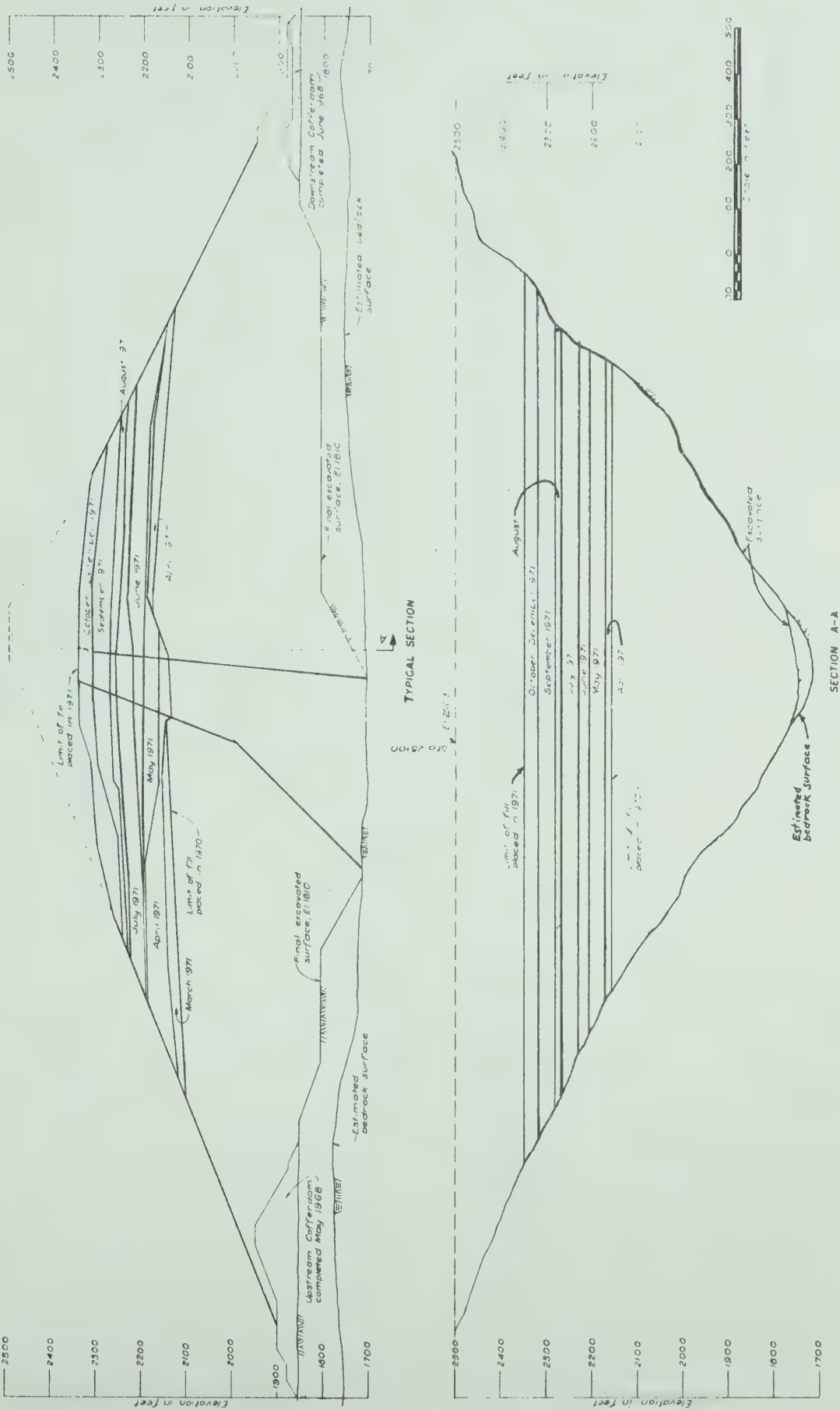


Fig. 5.6 Embankment Construction Progress in 1971, Mica Dam

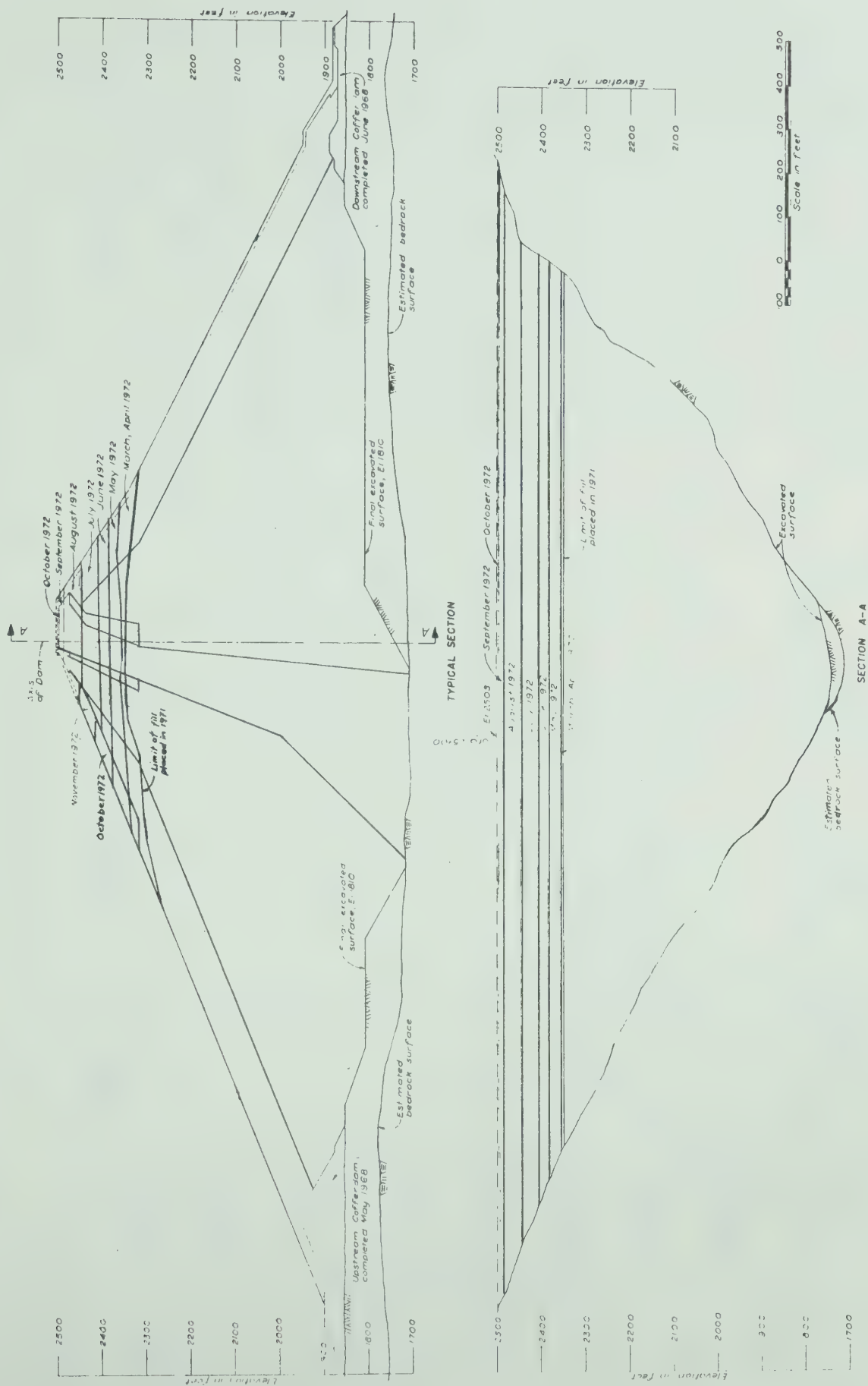


Fig. 5.7 Embankment Construction Progress in 1972, Mica Dam

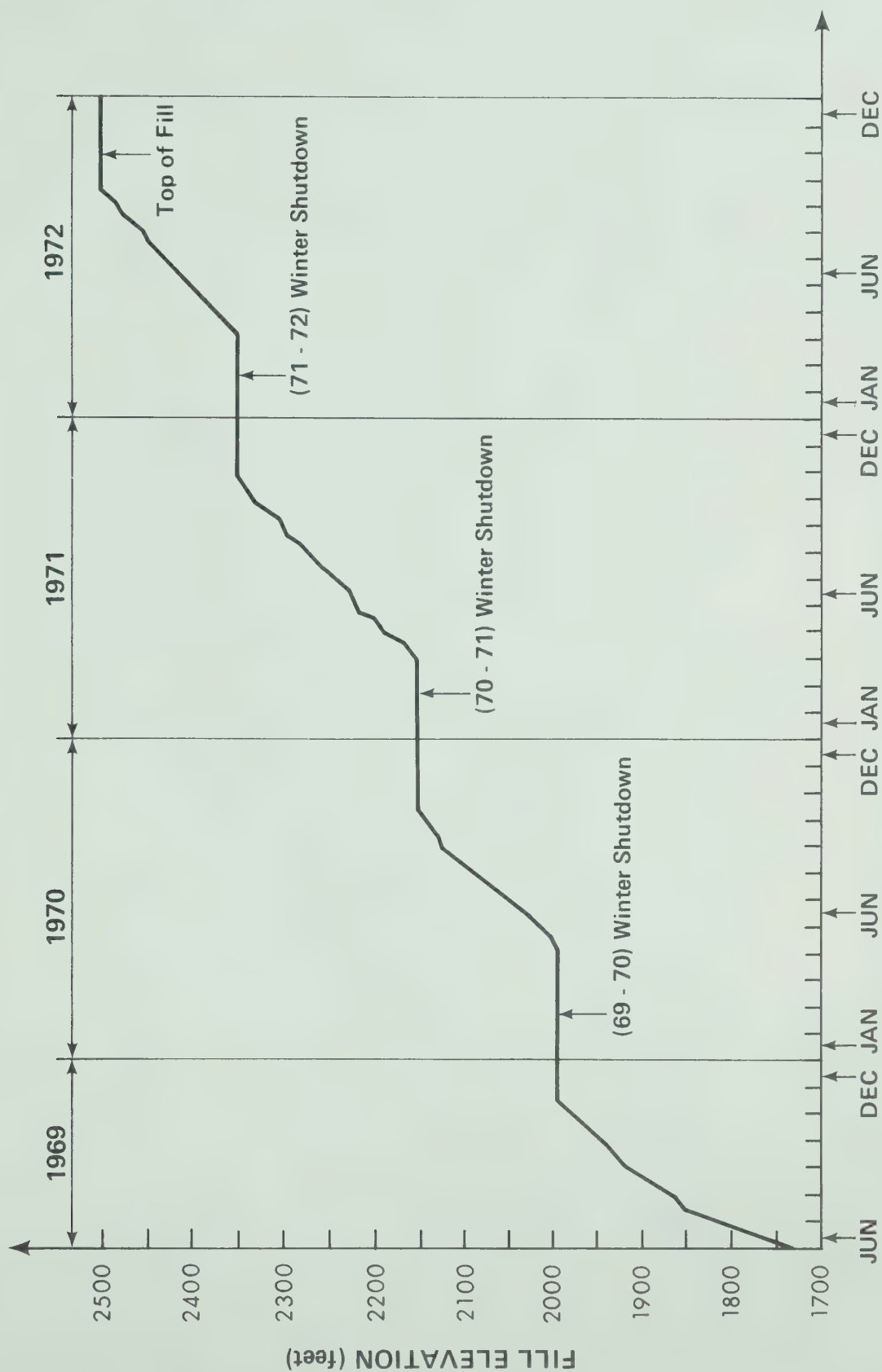


Fig. 5.8 Variation of Fill Elevation at Mica Dam Core With Time

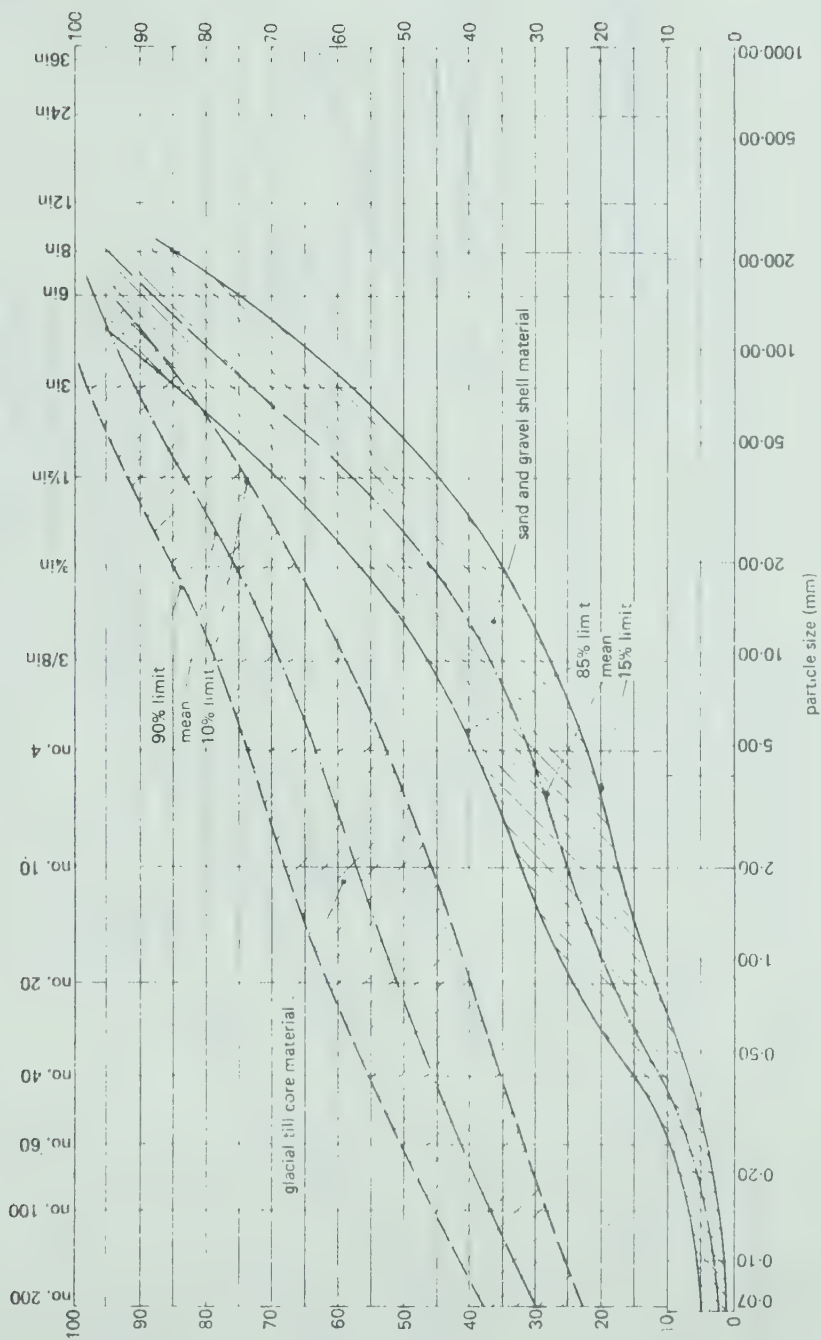
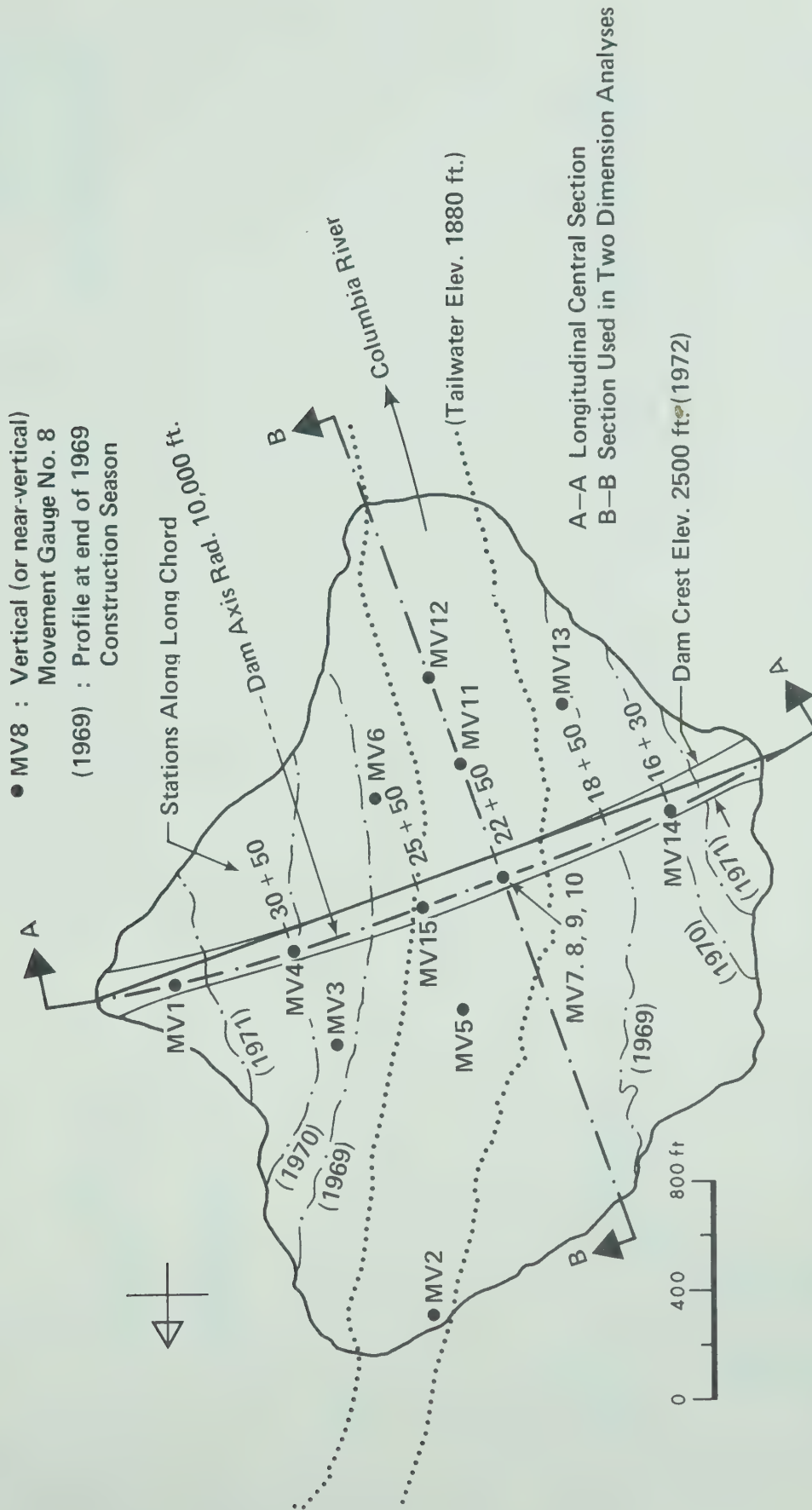


Fig. 5.9 Statistical Gradation Envelopes for Till and Sand and Gravel in Mica Dam (After Meidal and Webster, 1973)



MICA DAM - PLAN VIEW

Fig. 5.10 Location of Vertical and Near-Vertical Movement Gauges

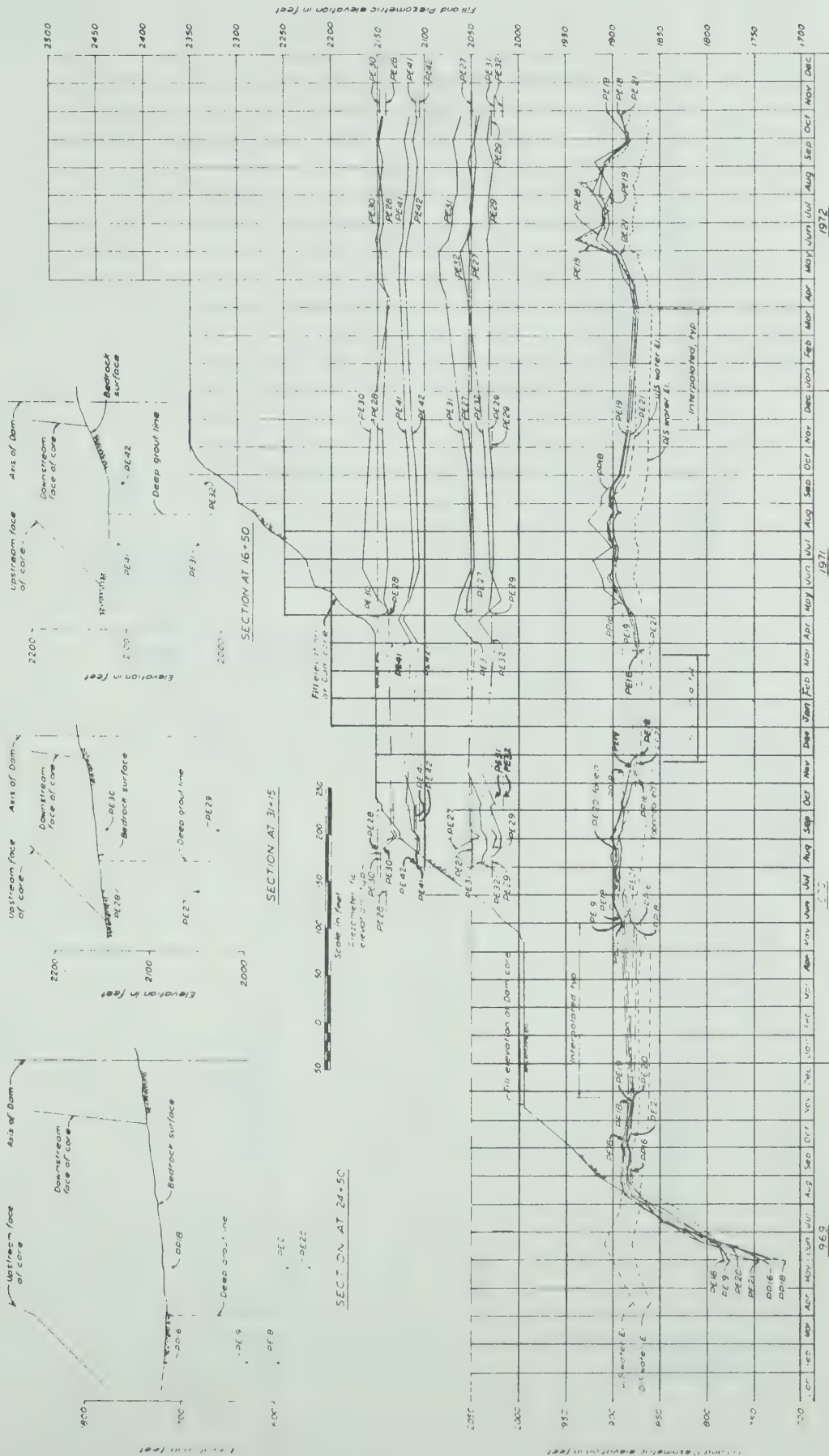


Fig. 5.12 Piezometric Observations in Core Foundation

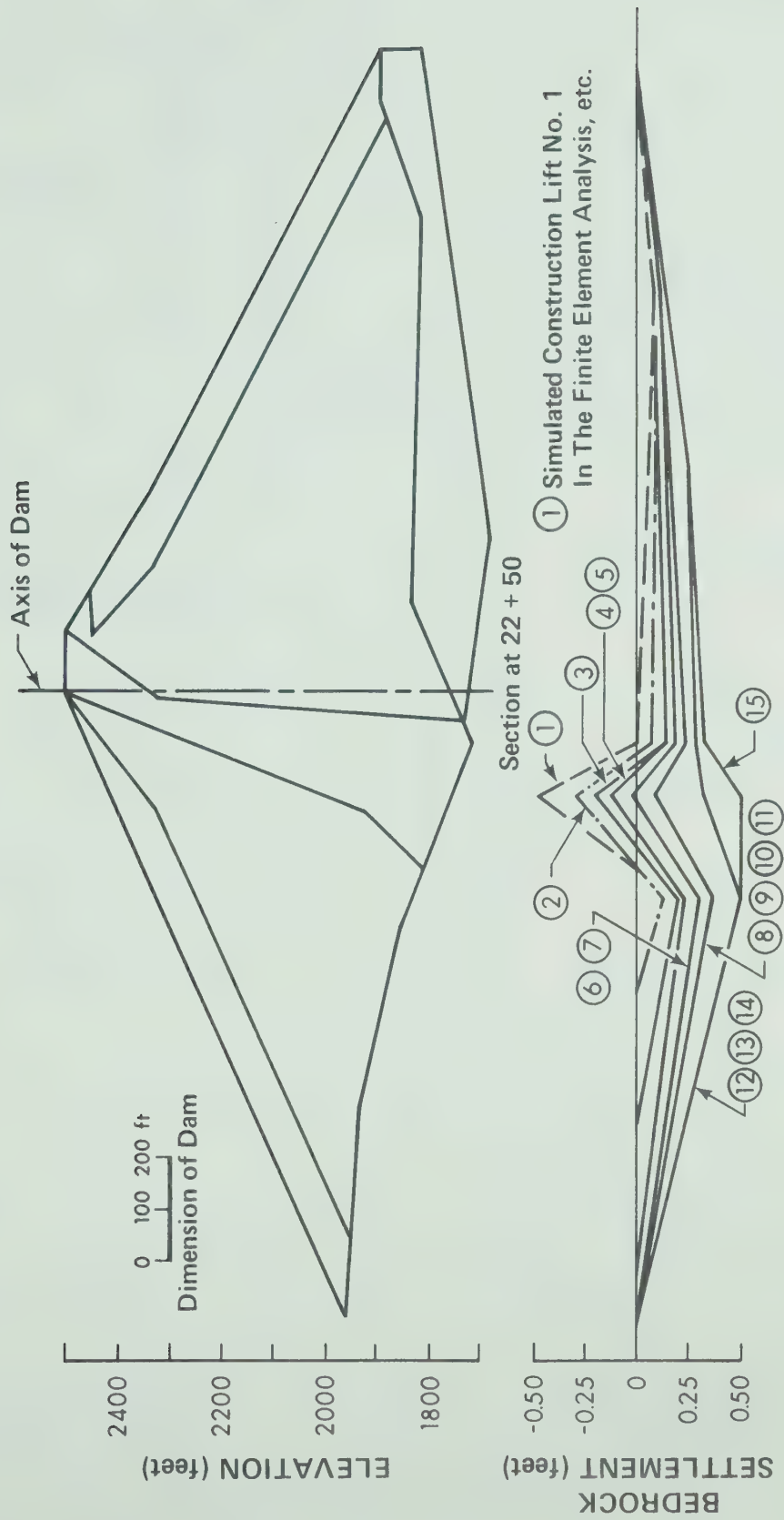
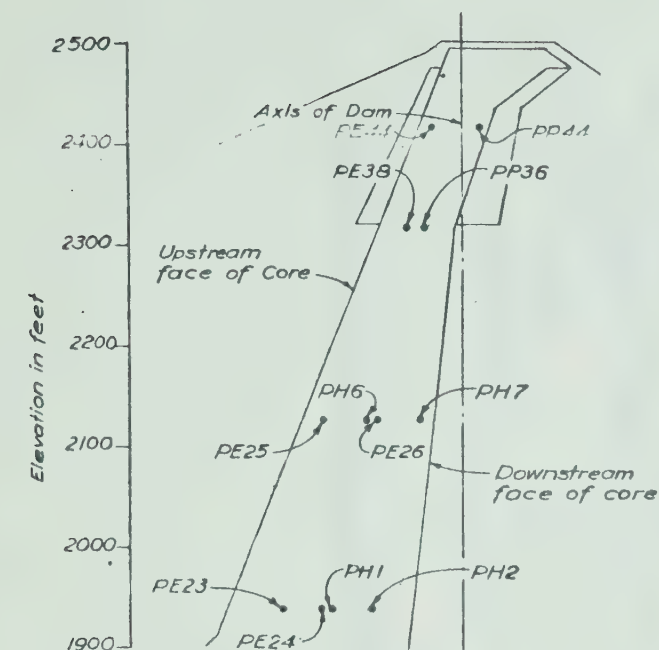
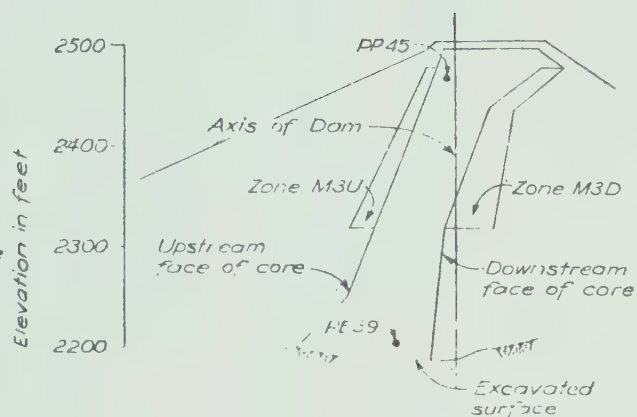


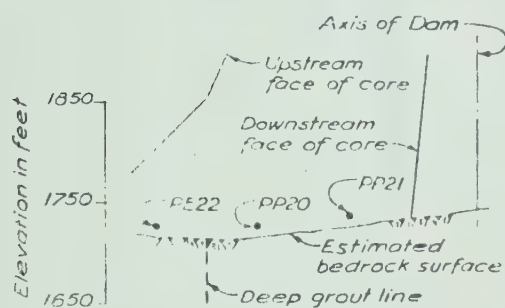
Fig. 5.13 Bedrock Movements as the Boundary Displacements in the Analysis of Mica Dam



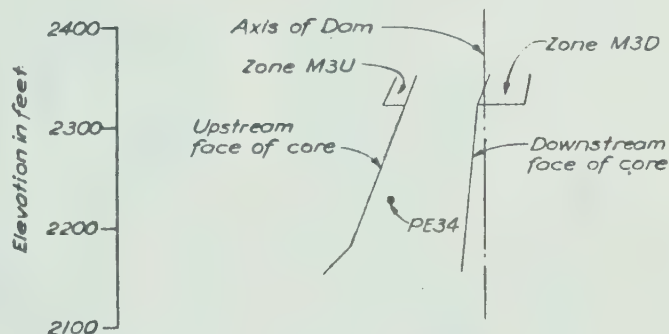
SECTION AT 22+50
PE 44 & PP44 projected from Sta. 22+15



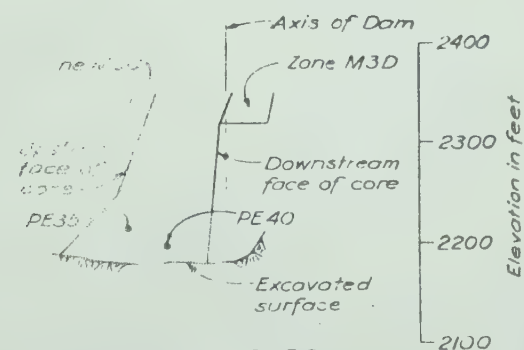
SECTION AT 31+30
PP 45 projected from Sta. 34+35



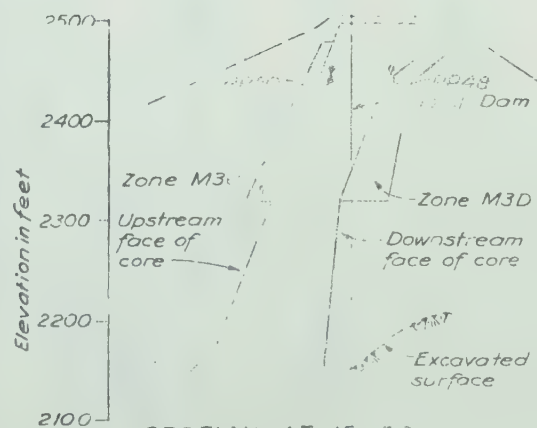
SECTION AT 24+50



SECTION AT 30+50



SECTION AT 16+30
PE35 projected from Sta. 16+50



SECTION AT 15+30
PP48 projected from Sta. 14+00

Fig. 5.14 Locations of Piezometers in the Core of Mica Dam

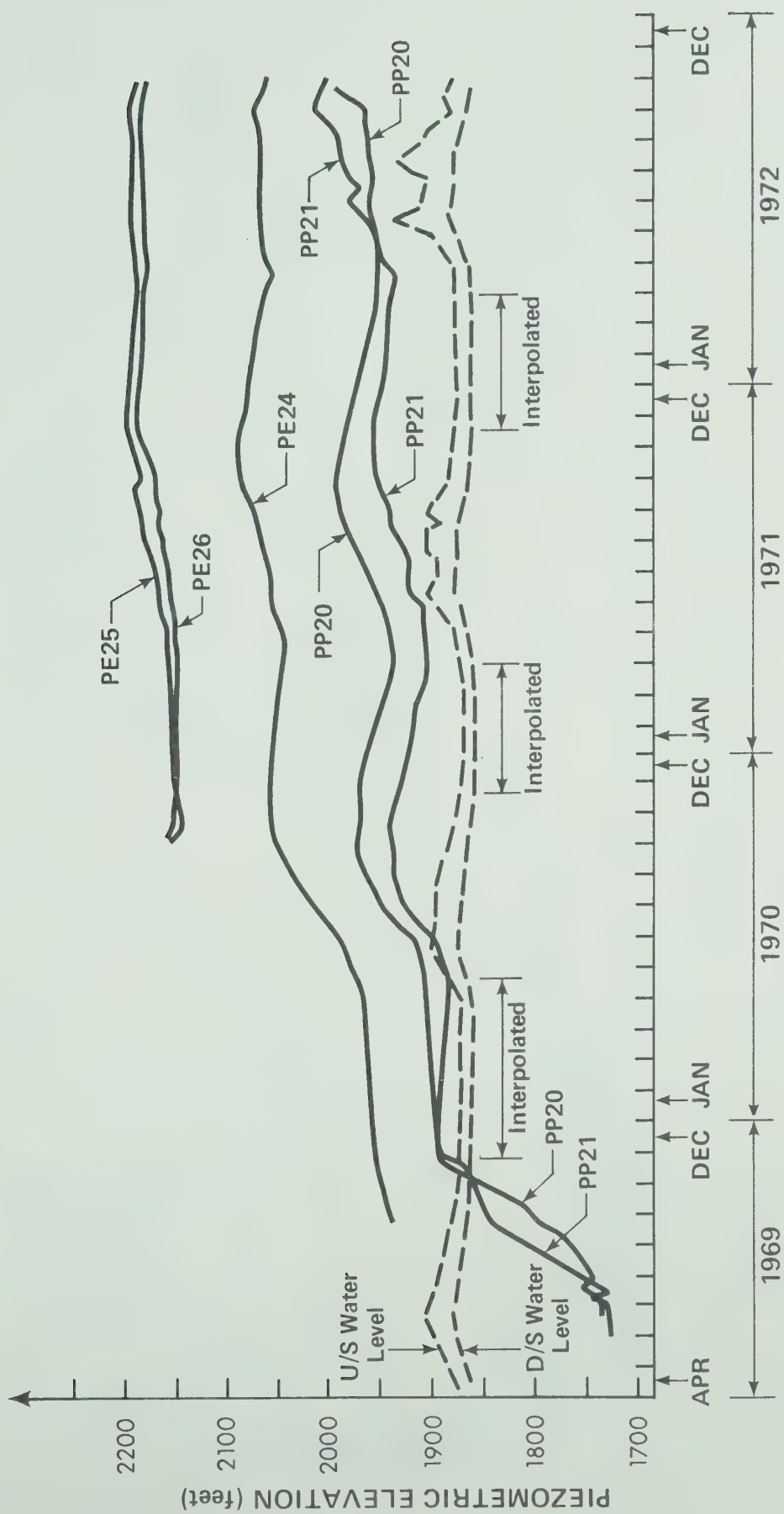


Fig. 5.15 Piezometric Observations in the Core

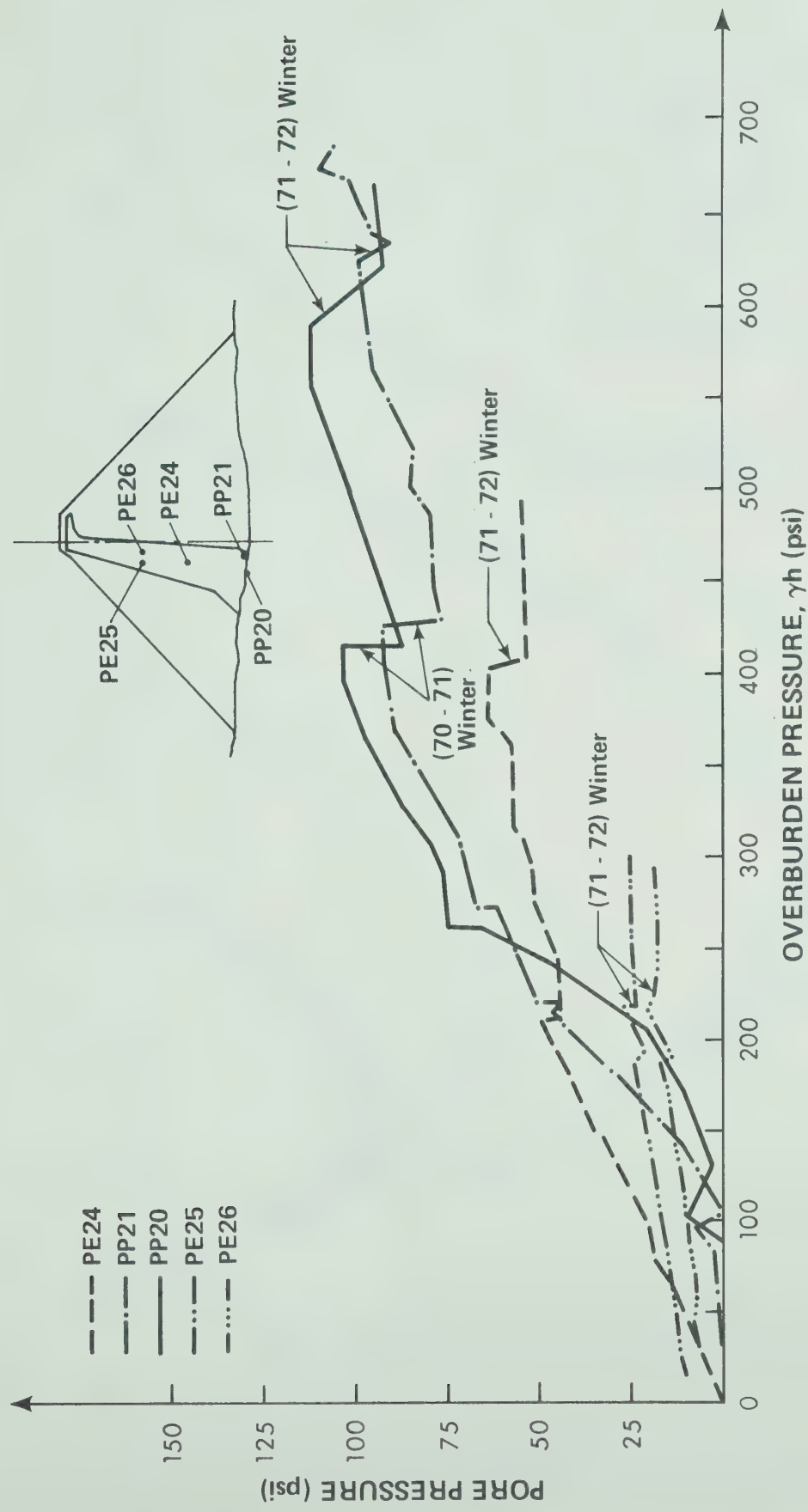


Fig. 5.16 The Variations of Pore Pressure With Overburden Pressure in Mica Dam

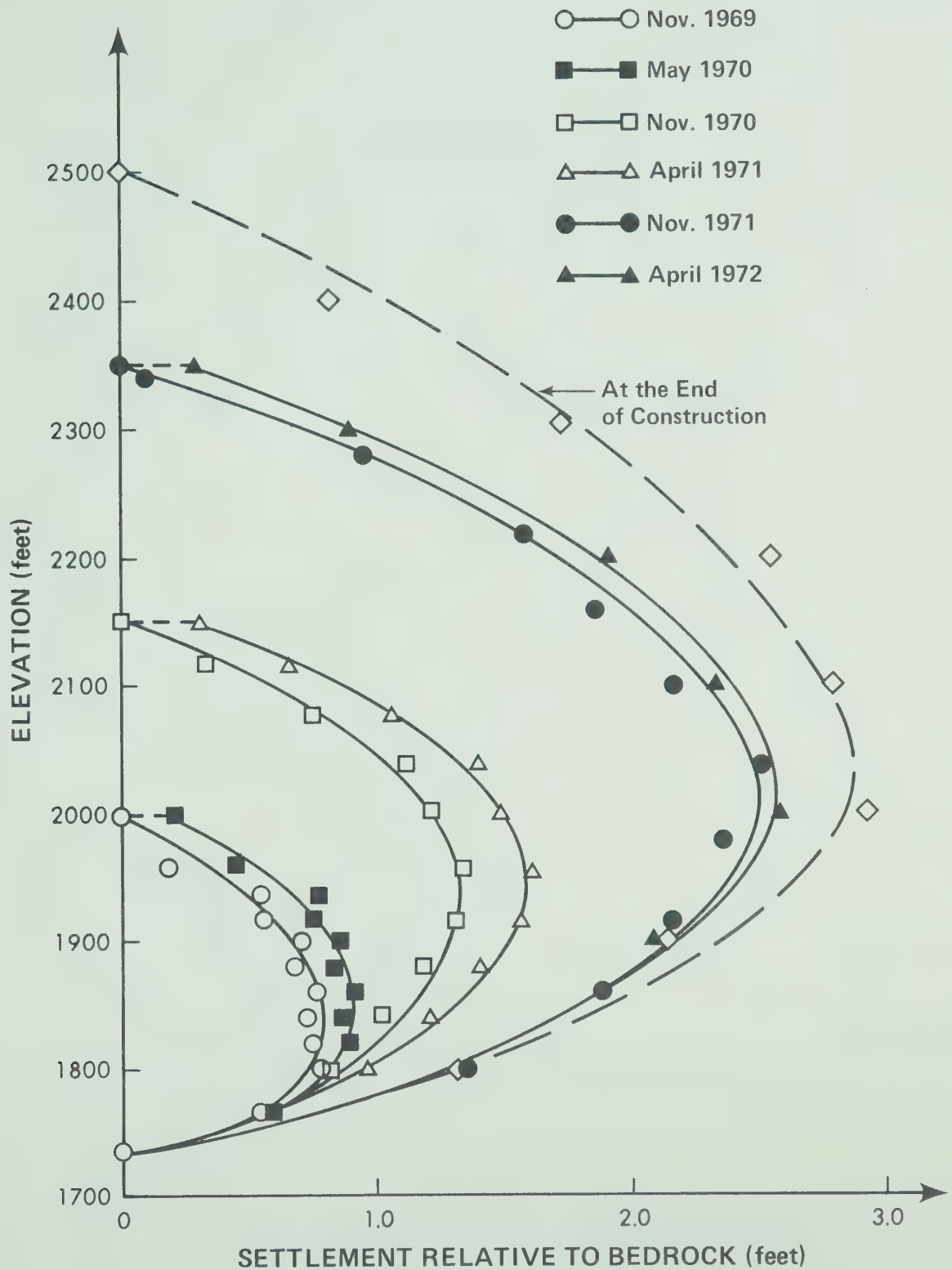


Fig. 5.17 Settlement Profiles Measured in MV8 at the Beginning and the End of Shutdown Seasons

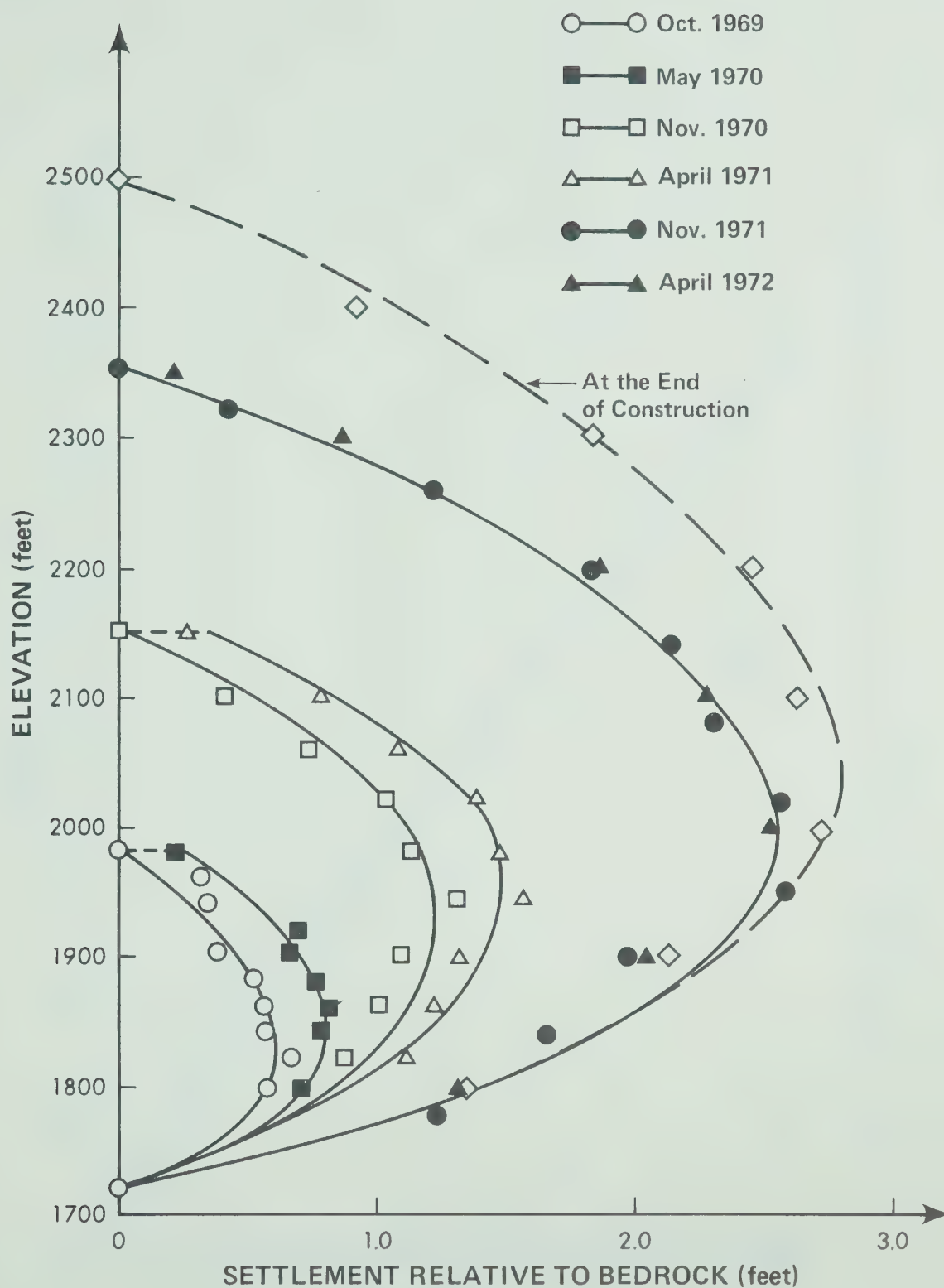


Fig. 5.18 Settlement Profiles Measured in MV15 at the Beginning and the End of Shutdown Seasons

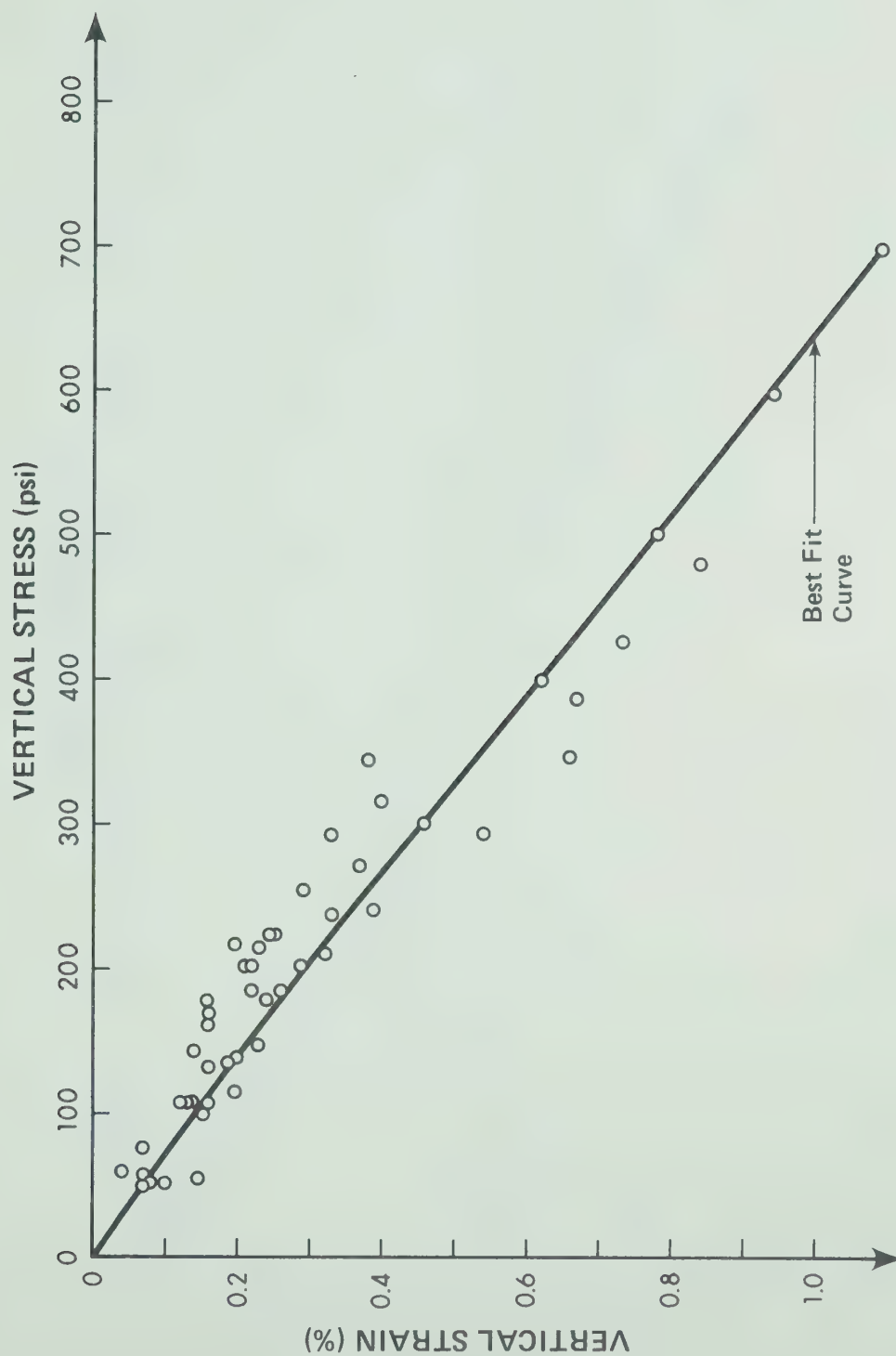


Fig. 5.19 Vertical Stress-strain Relationship for Sand and Gravel in Zone M2

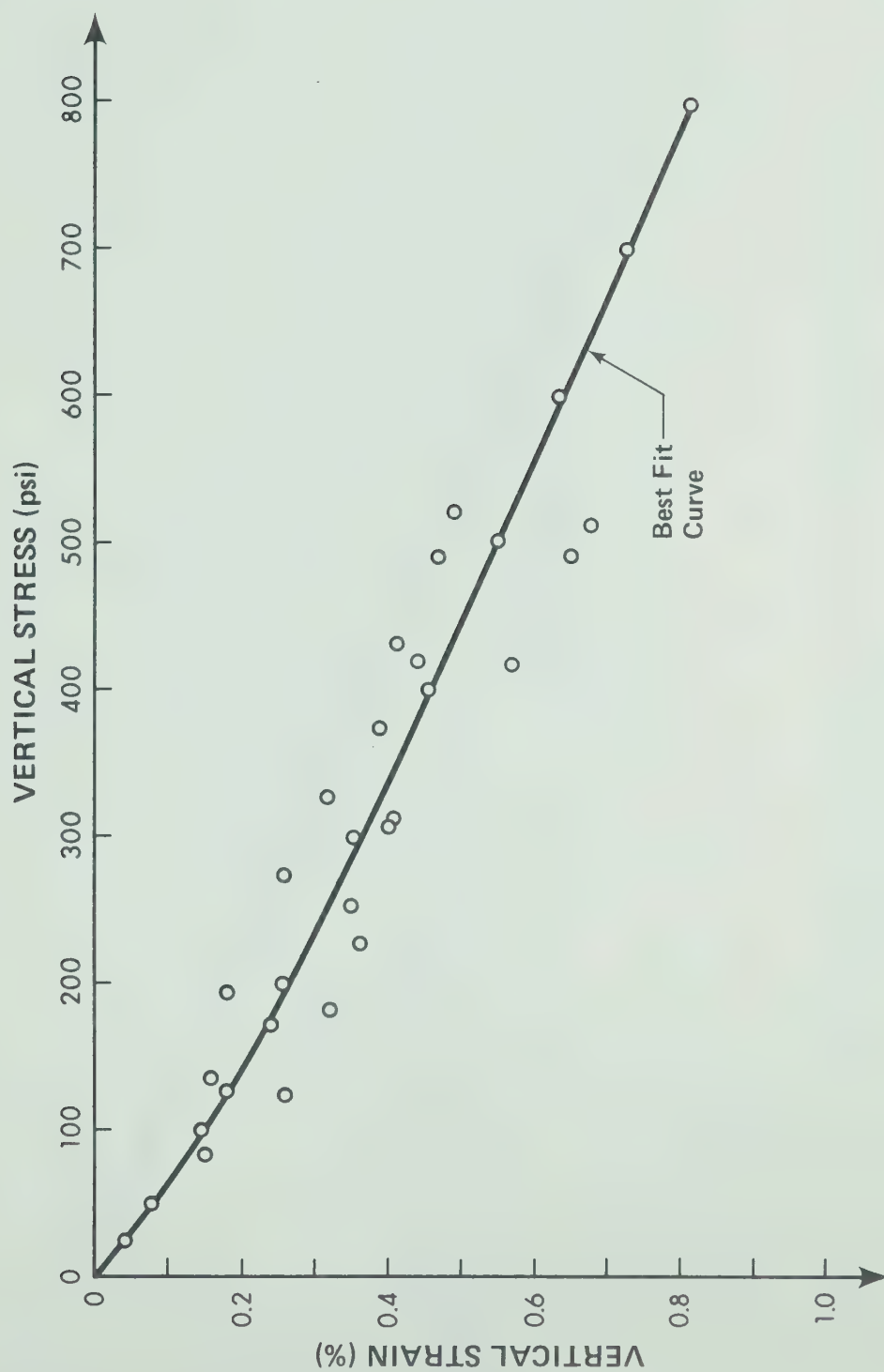


Fig. 5.20 Vertical Stress-strain Relationship for River Overburden Sand

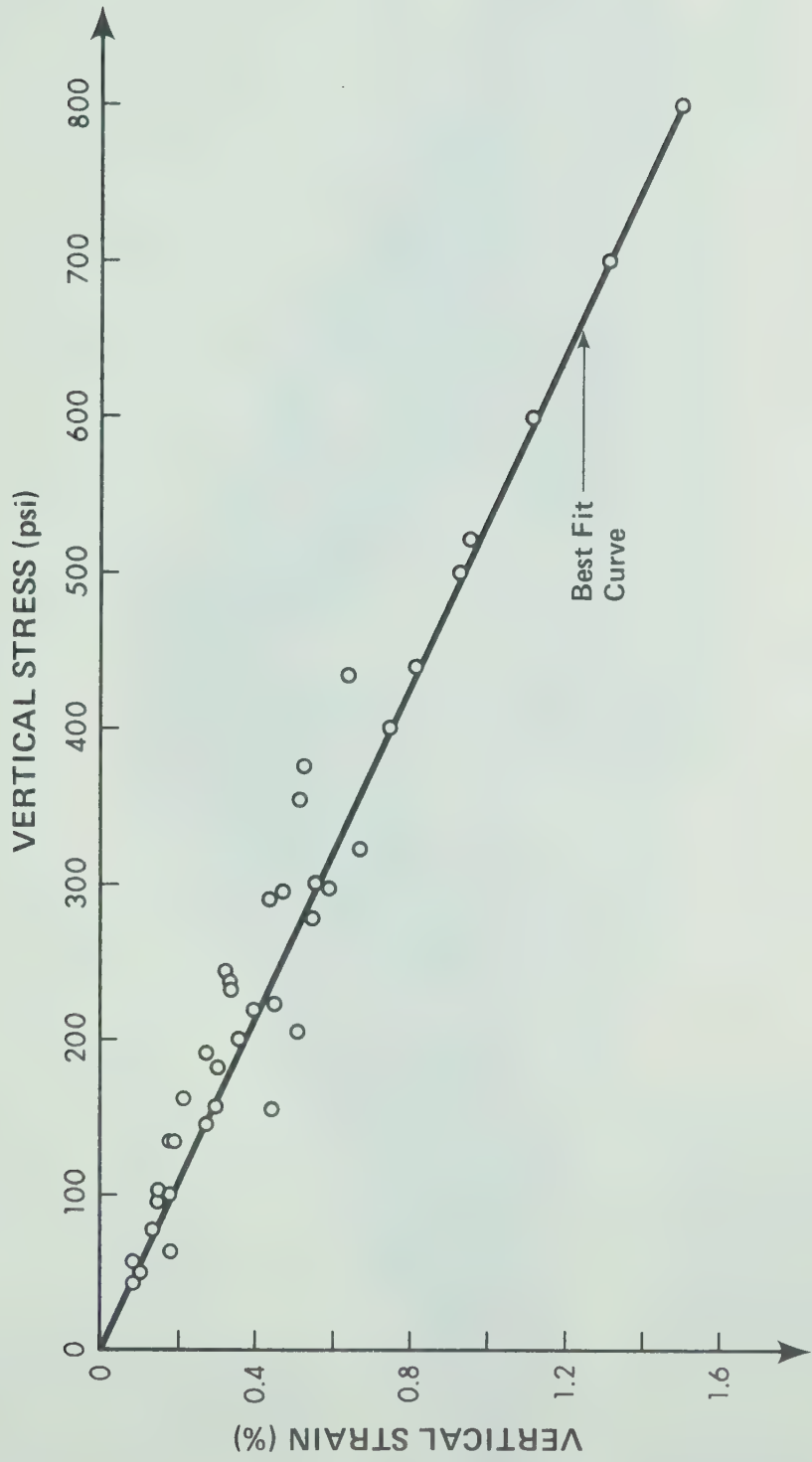


Fig. 5.21 Vertical Stress-strain Relationship for Sand and Gravel in Zone M2DI

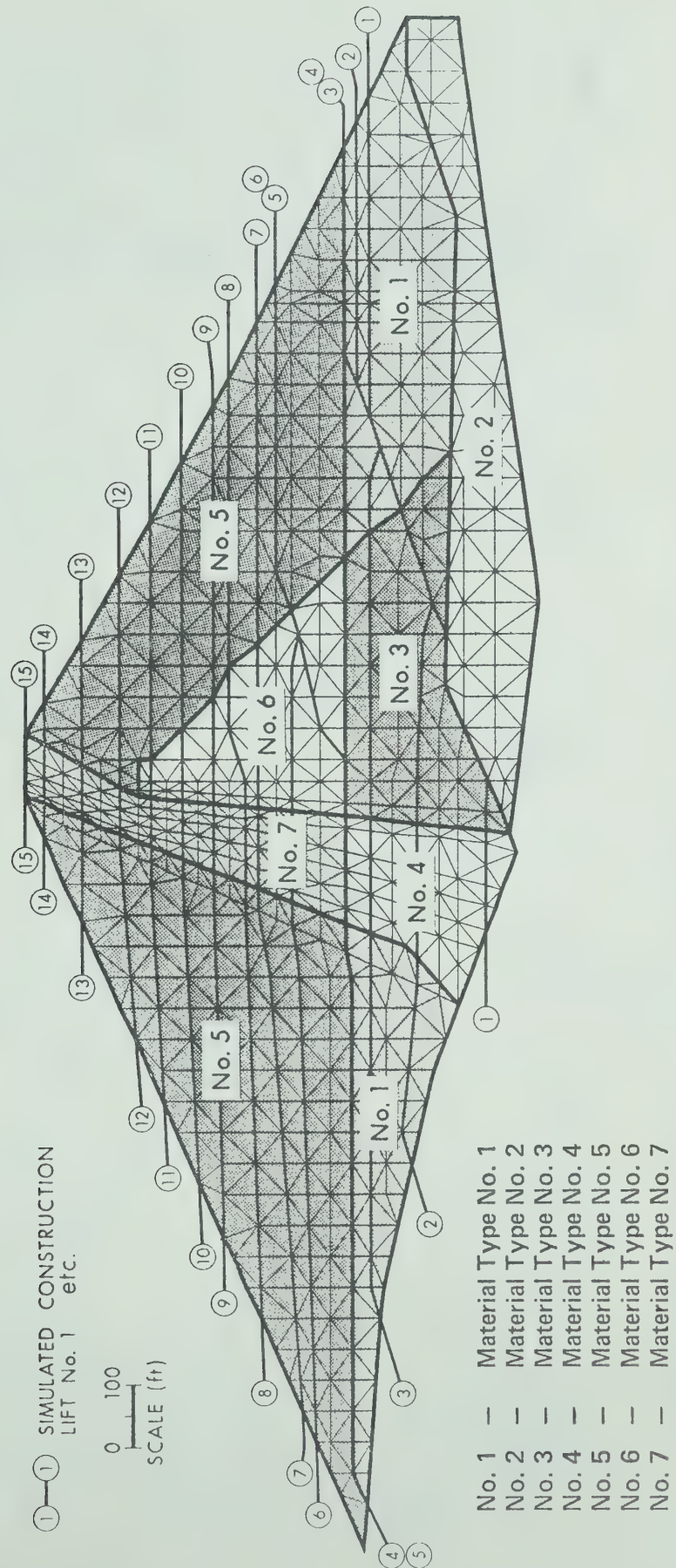


Fig. 5.22 Finite Element Idealization of Mica Dam For 2D Analyses

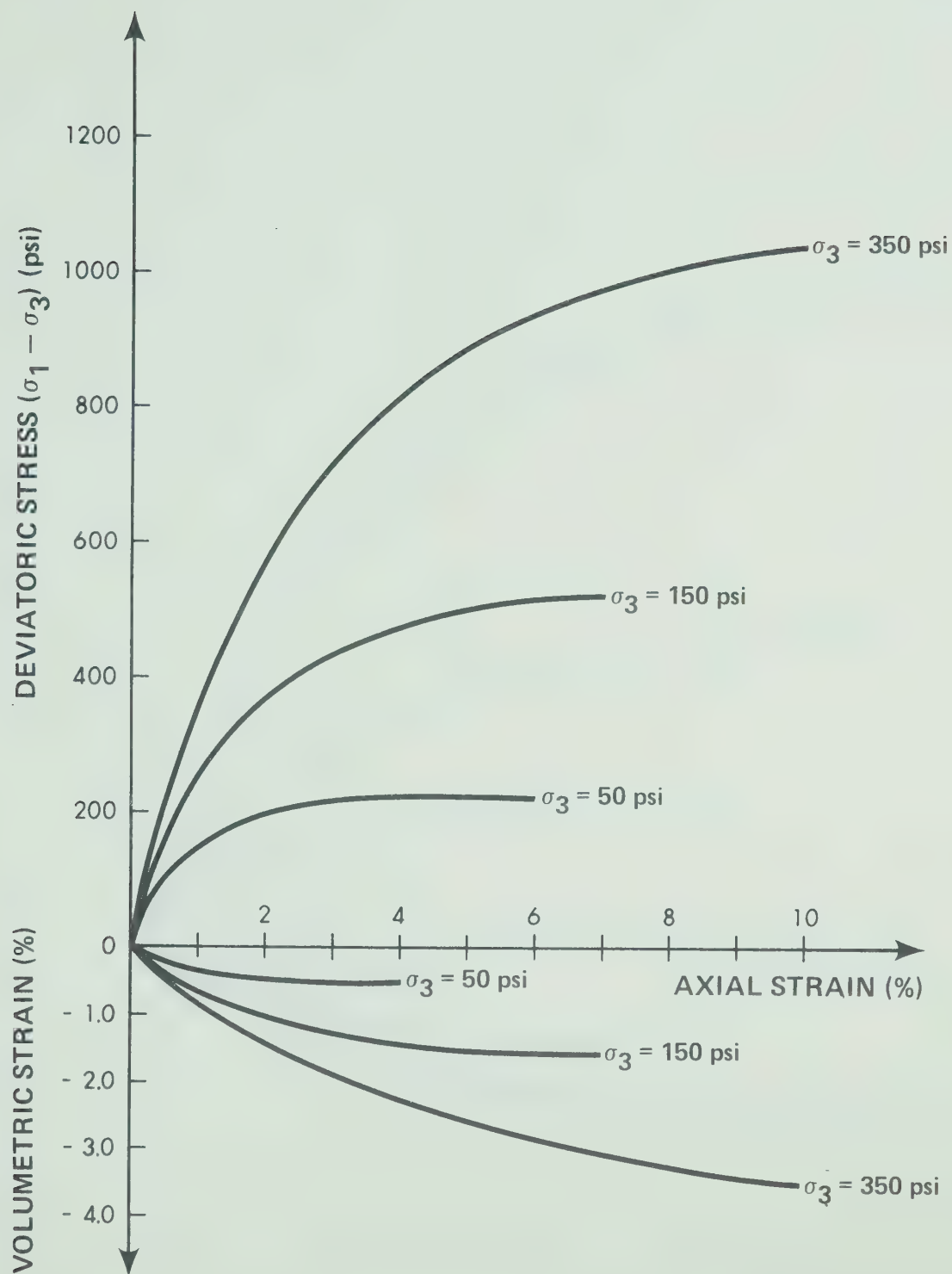


Fig. 5.24 Drained Triaxial Stress-strain Relationships for Sand and Gravel in Zone M2

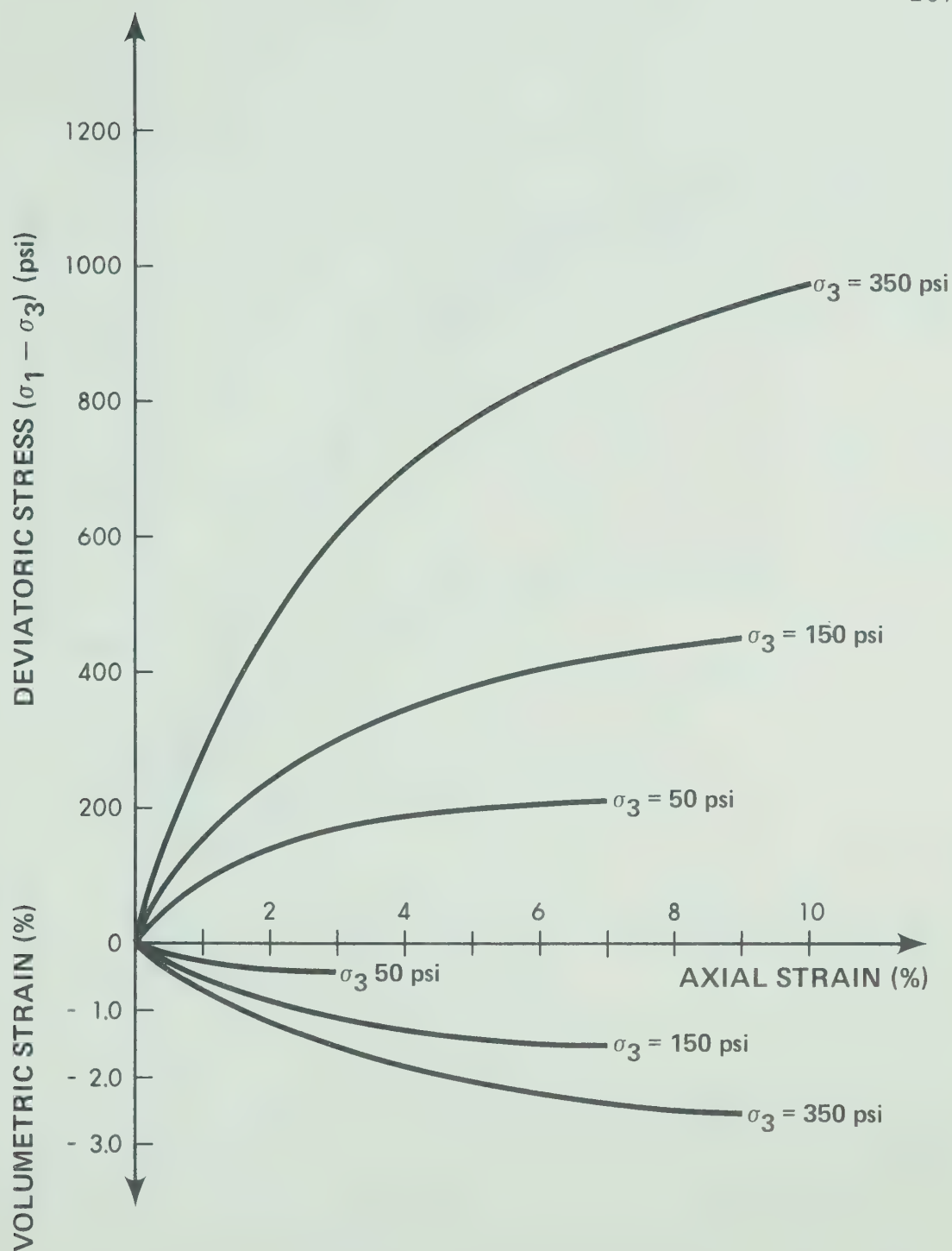


Fig. 5.25 Drained Triaxial Stress-strain Relationships for River Overburden Sand

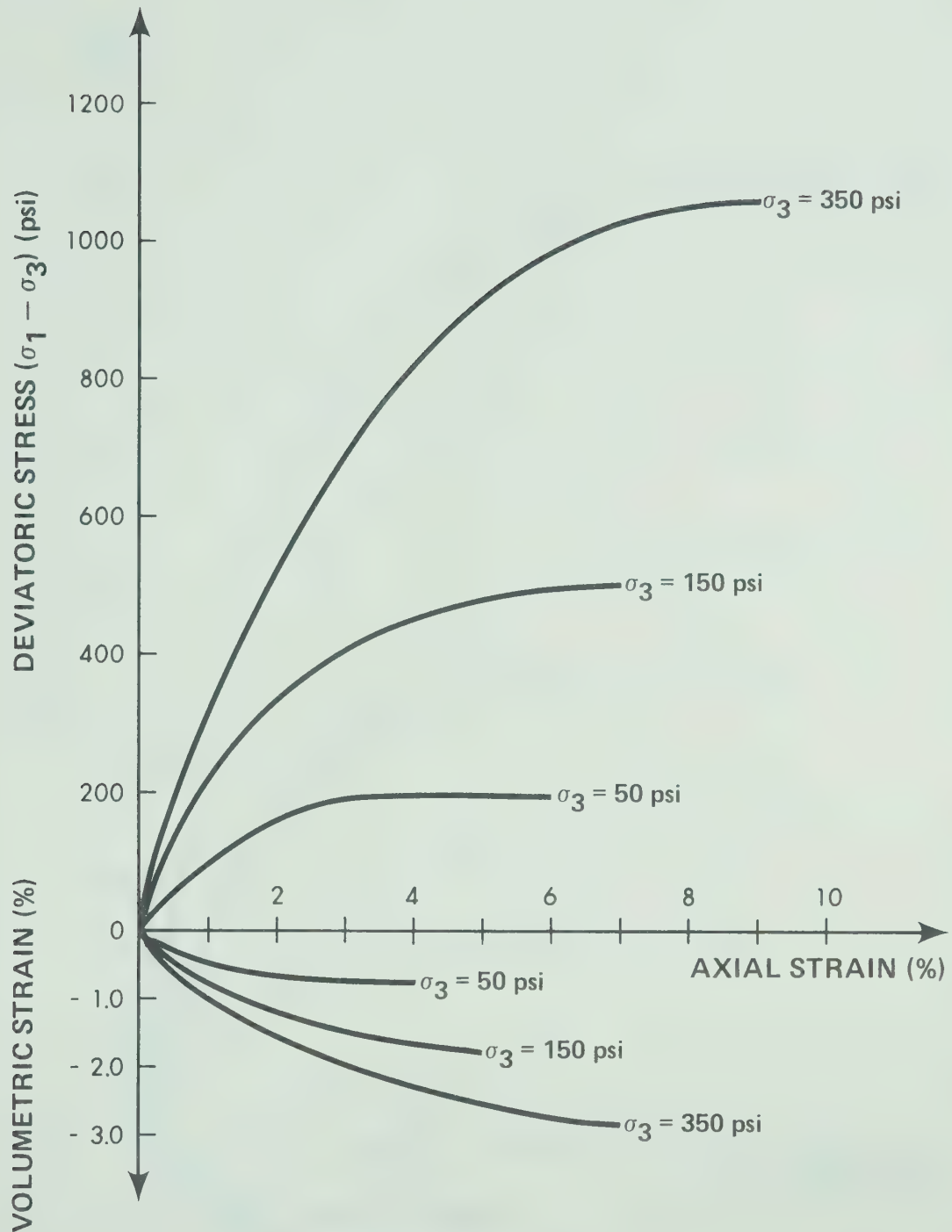


Fig. 5.26 Drained Triaxial Stress-strain Relationships for Sand and Gravel in Zone M2DI

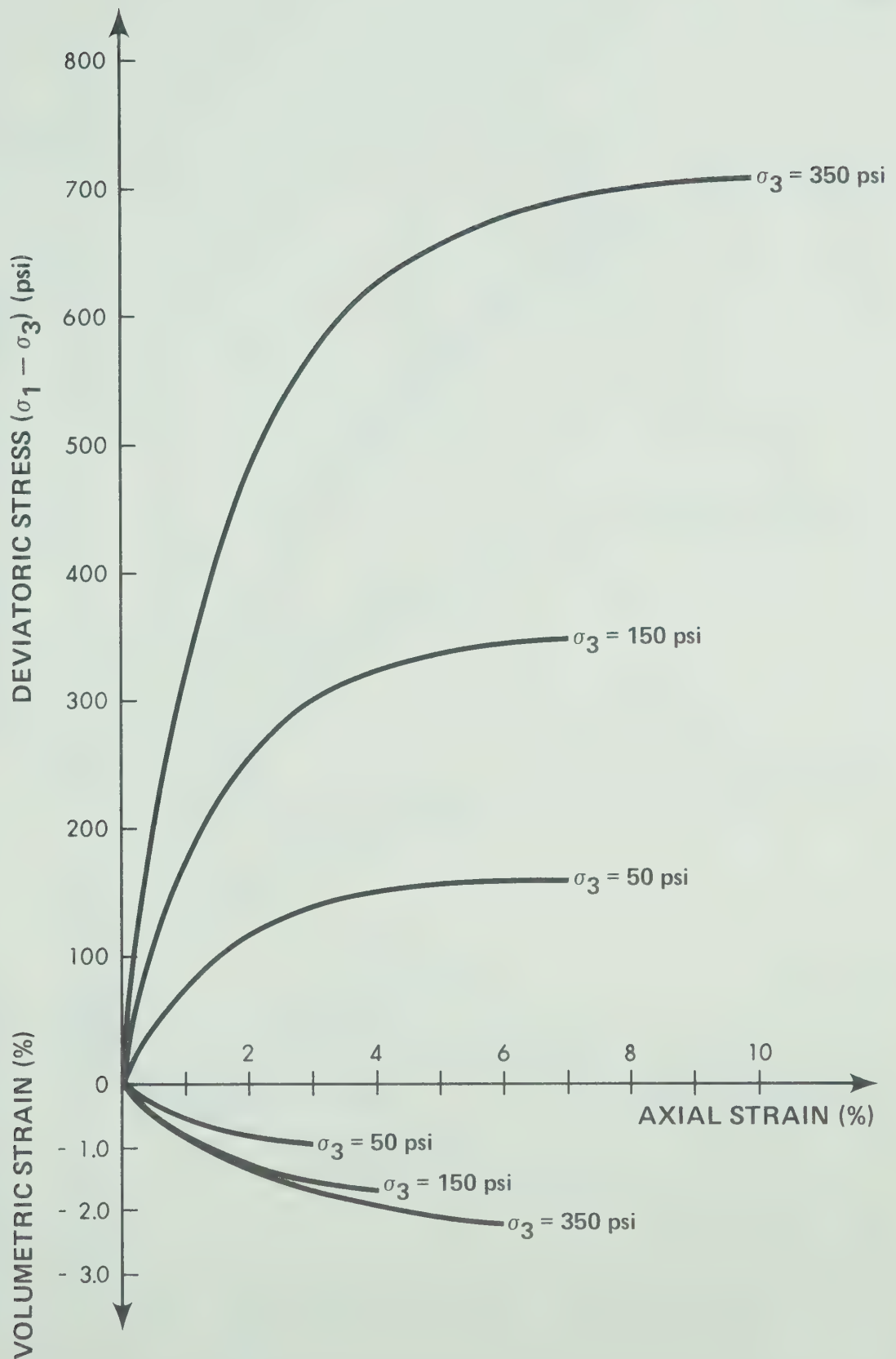


Fig. 5.27 Consolidated Undrained Triaxial Stress-strain Relationships for Mica Till at Optimum Water Content

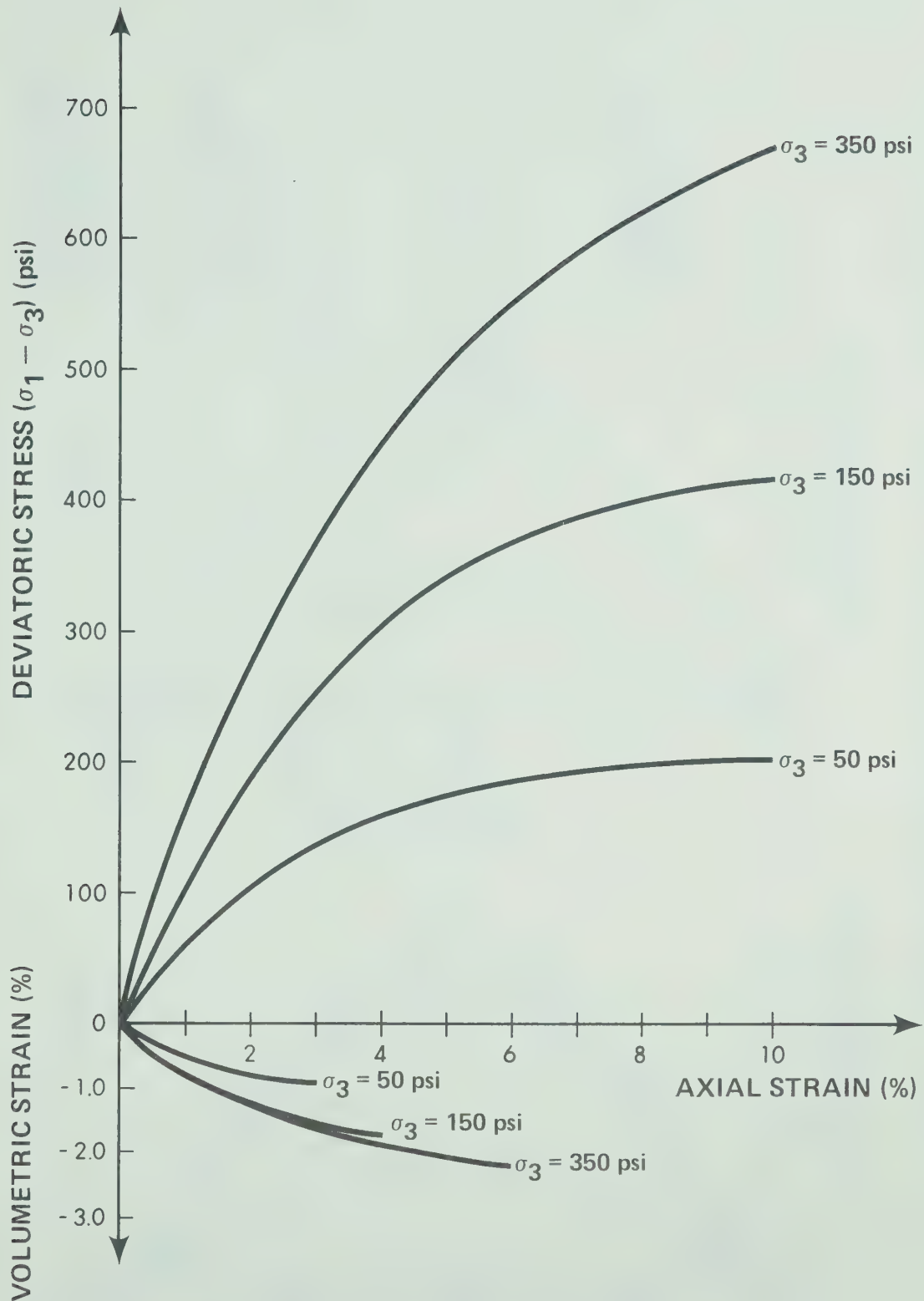


Fig. 5.28 Undrained Triaxial Stress-strain Relationships for Mica Till at Modified Optimum Water Content

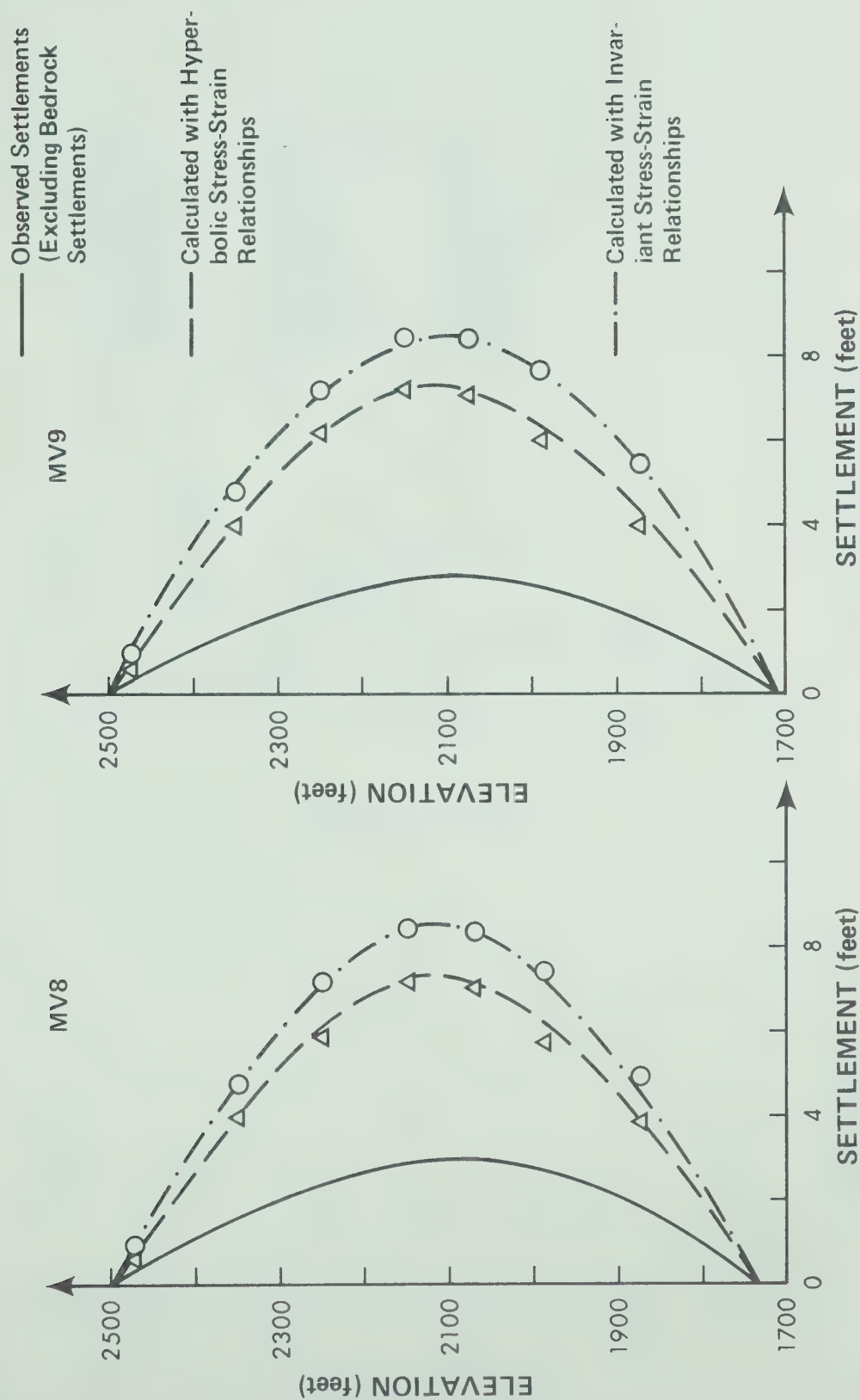


Fig. 5.29 Settlements Calculated with Triaxial Test Data for MV8 and MV9, Mica Dam

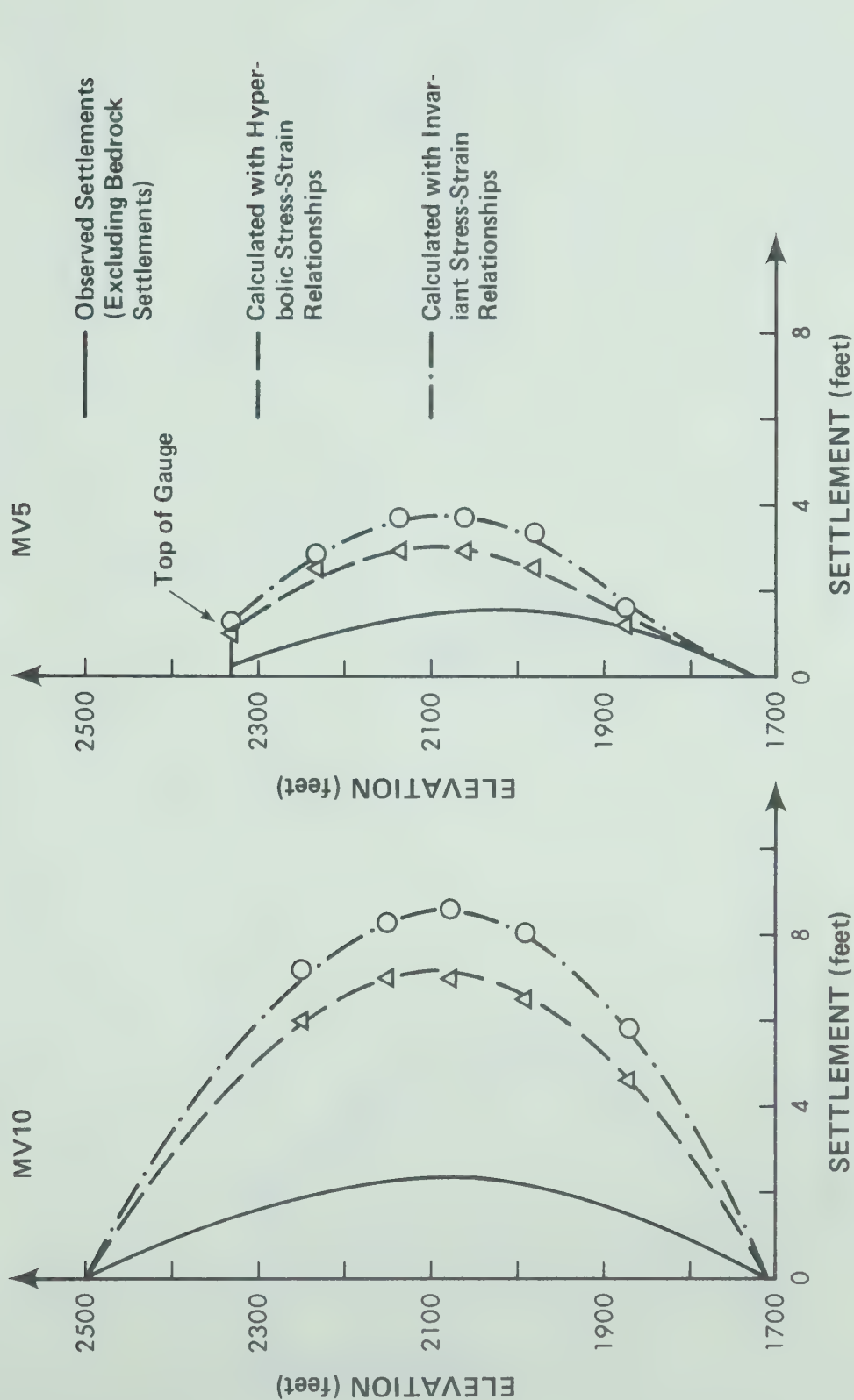


Fig. 5.30 Settlements Calculated with Triaxial Test Data for MV10 and MV5, Mica Dam

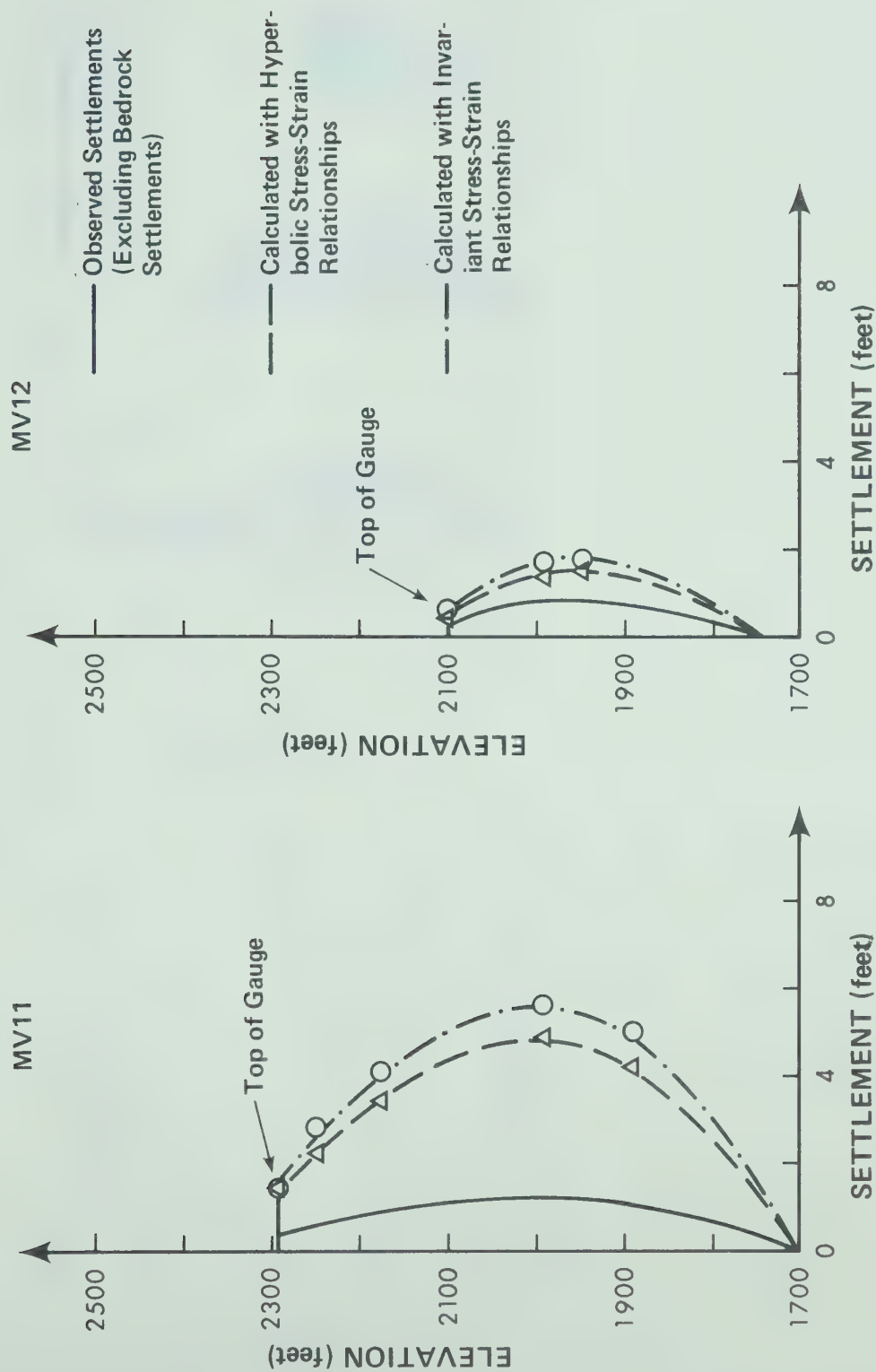


Fig. 5.31 Settlements Calculated with Triaxial Test Data for MV11 and MV12, Mica Dam

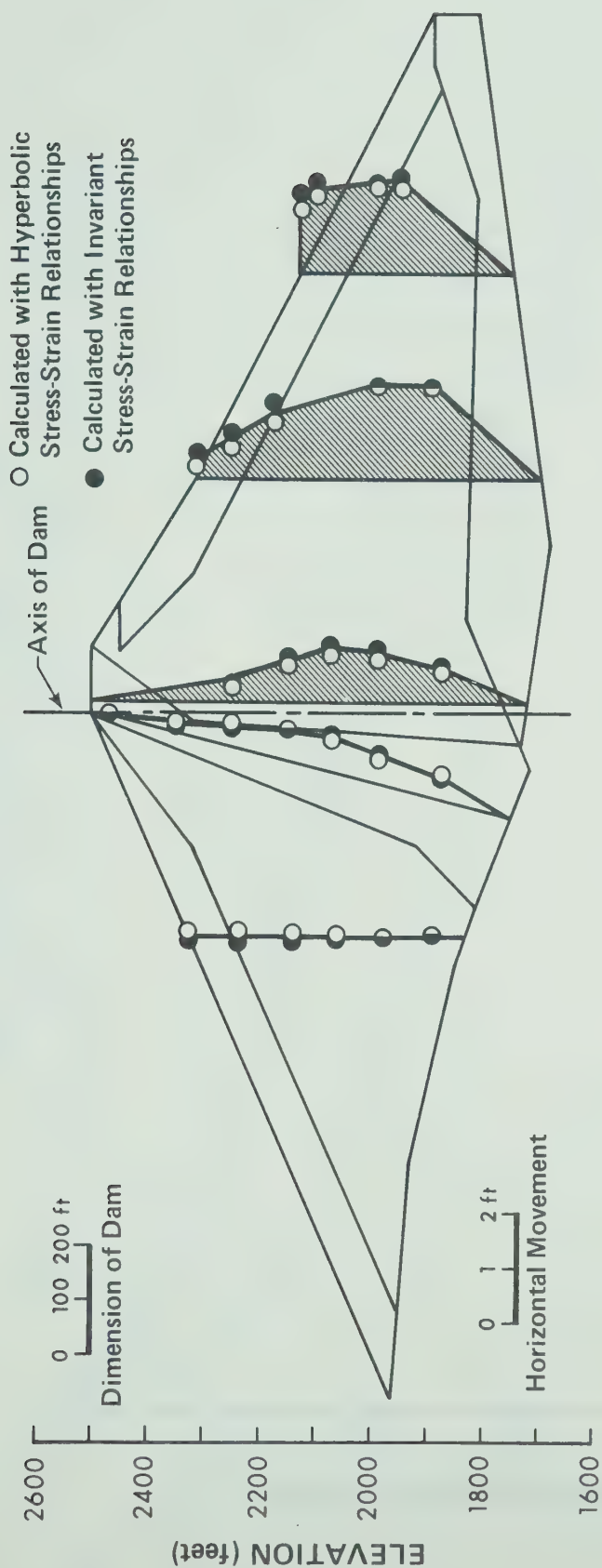


Fig. 5.32 Horizontal Movements Calculated with Triaxial Test Data

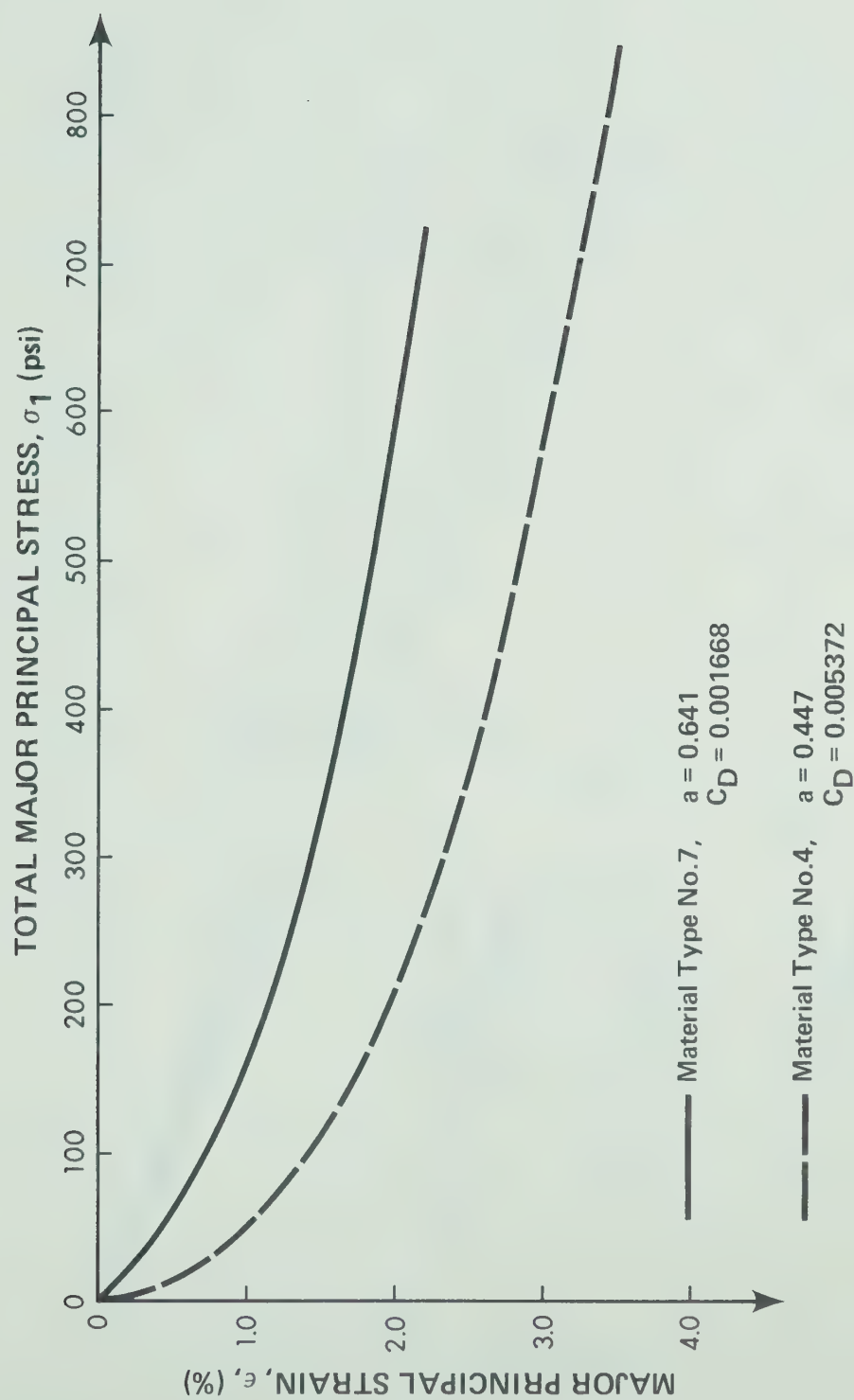


Fig. 5.33 Stress-strain Curves for Core in Total Stress Analysis

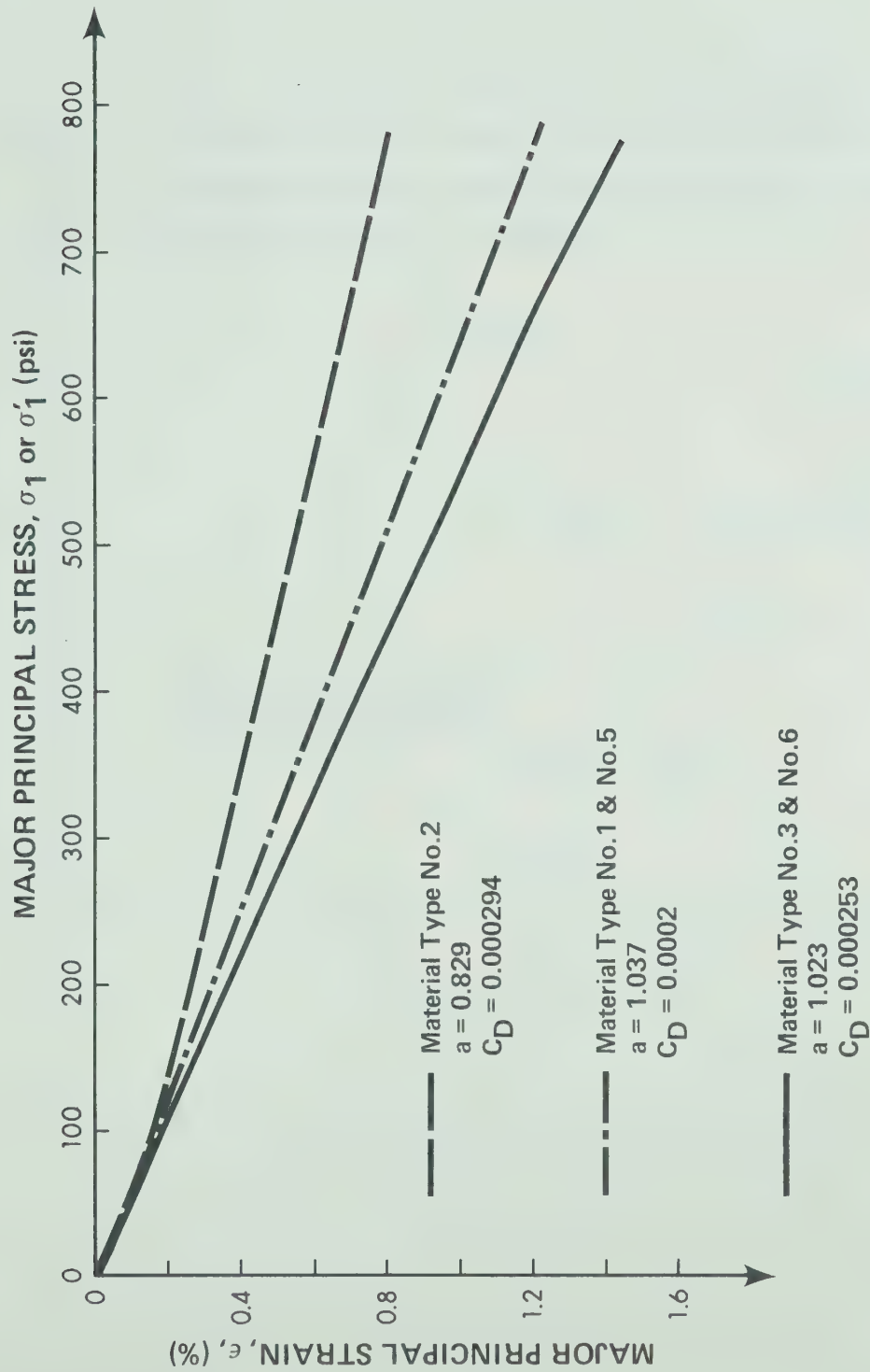


Fig. 5.34 Stress-strain Curves Used in Total and Effective Stress Analysis for Sand and Gravel

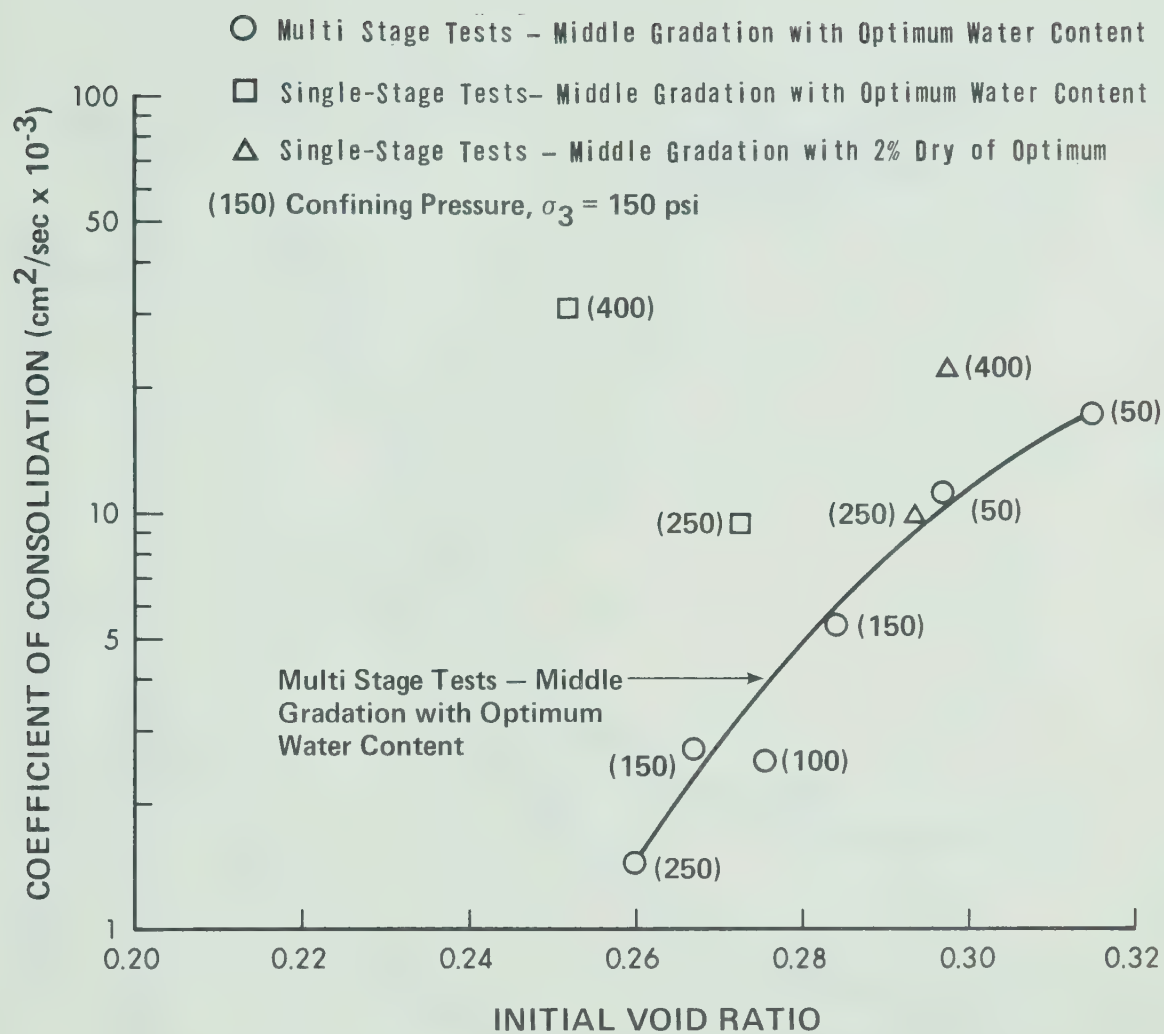


Fig. 5.35 C_v Determined from Triaxial Dissipation Tests for Mica Till (After CASECO Report)

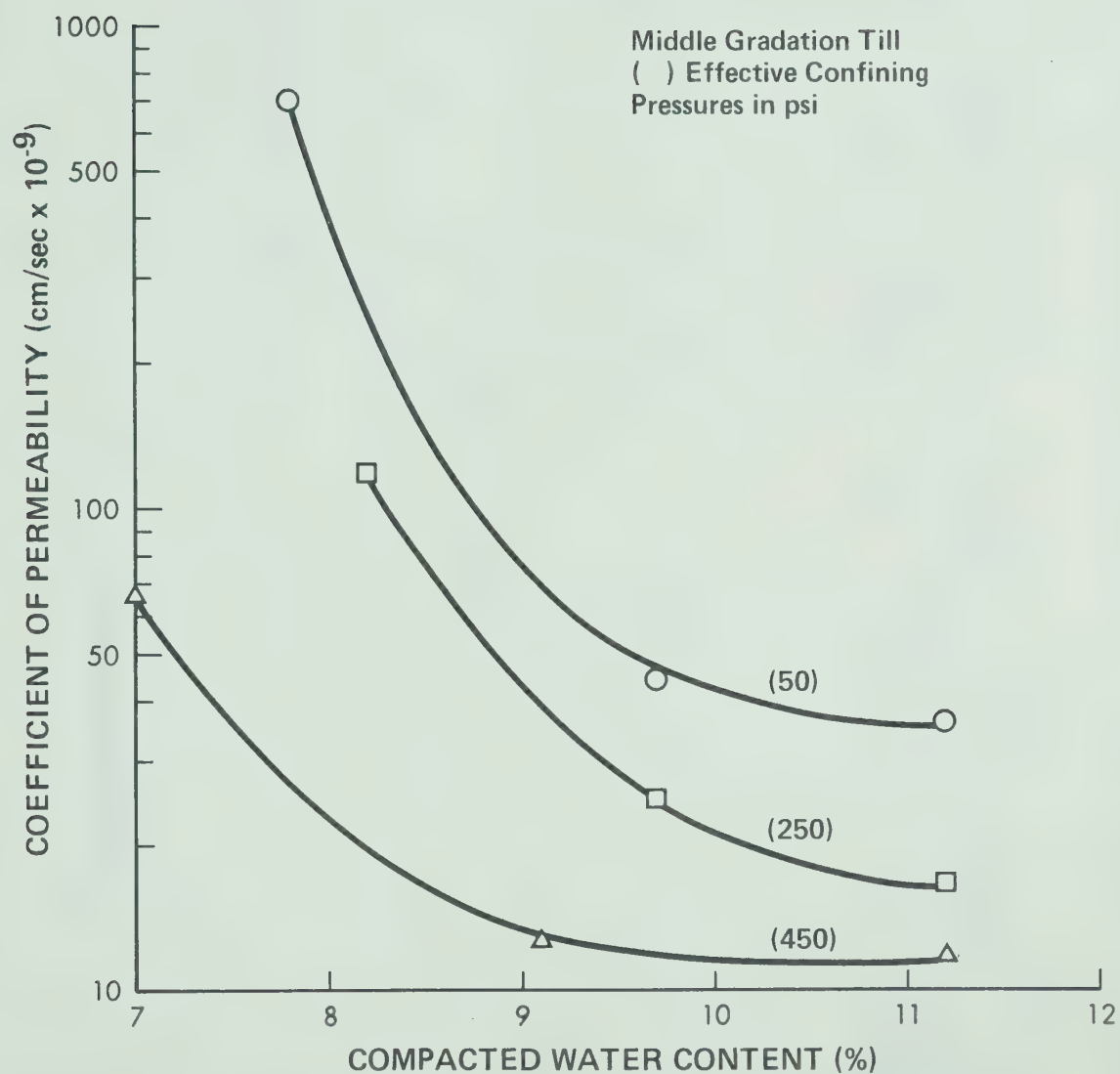


Fig. 5.36 Direct Permeability Test Results for Mica Till (After CASECO Report)

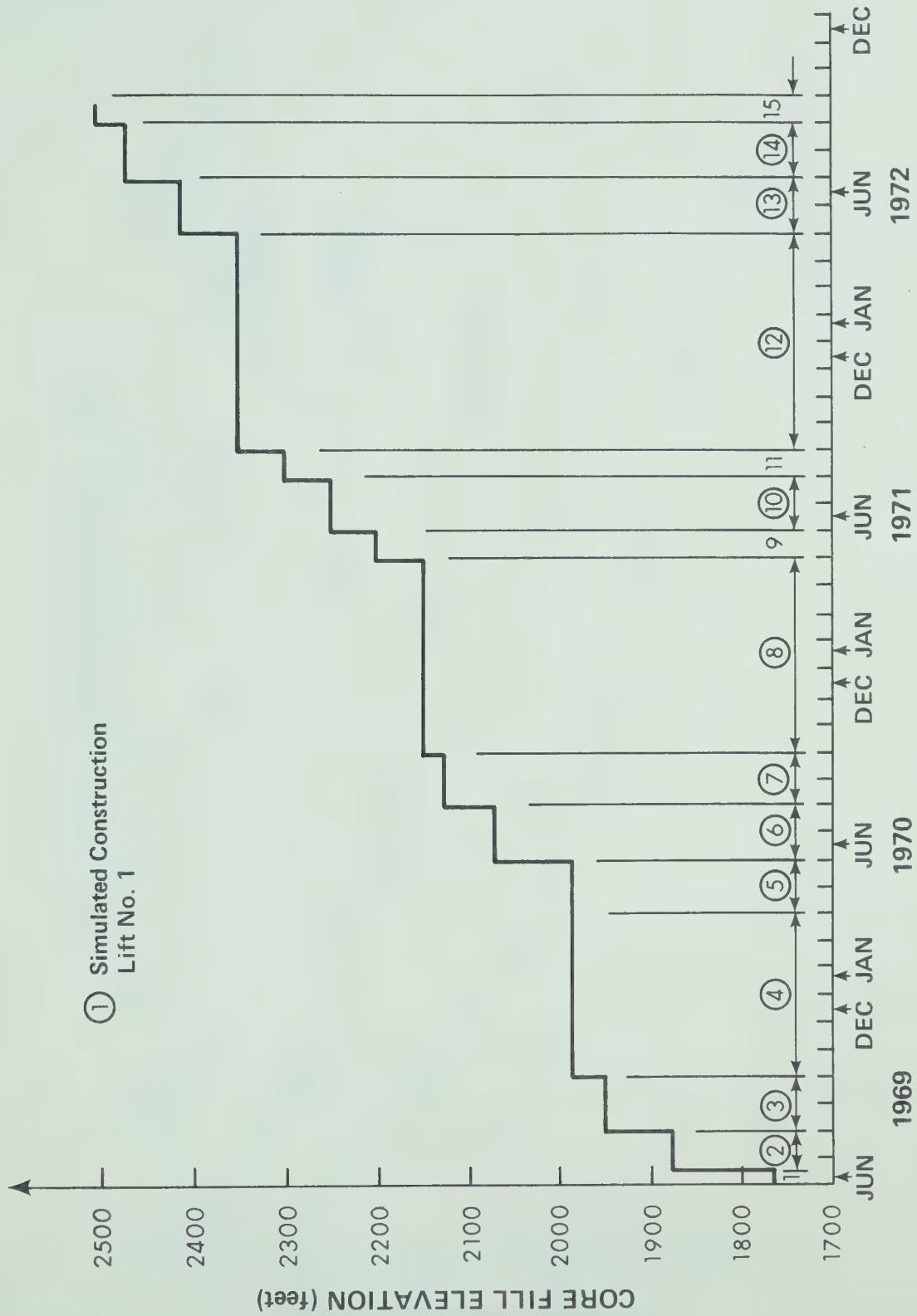


Fig. 5.37 Variation of Core Fill Elevation with Time in the Analysis

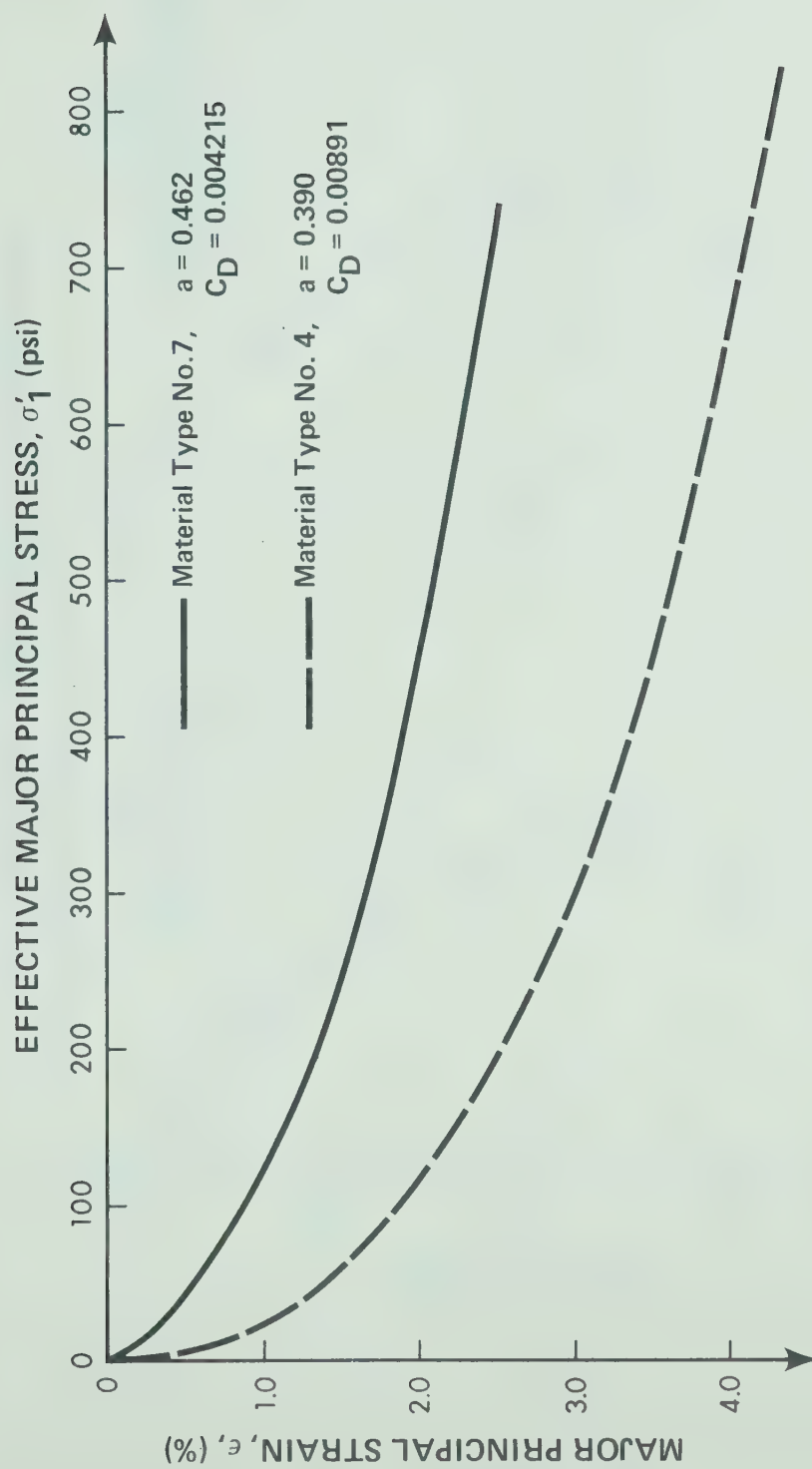


Fig. 5.38 Stress-strain Curves for Core in Effective Stress Analysis

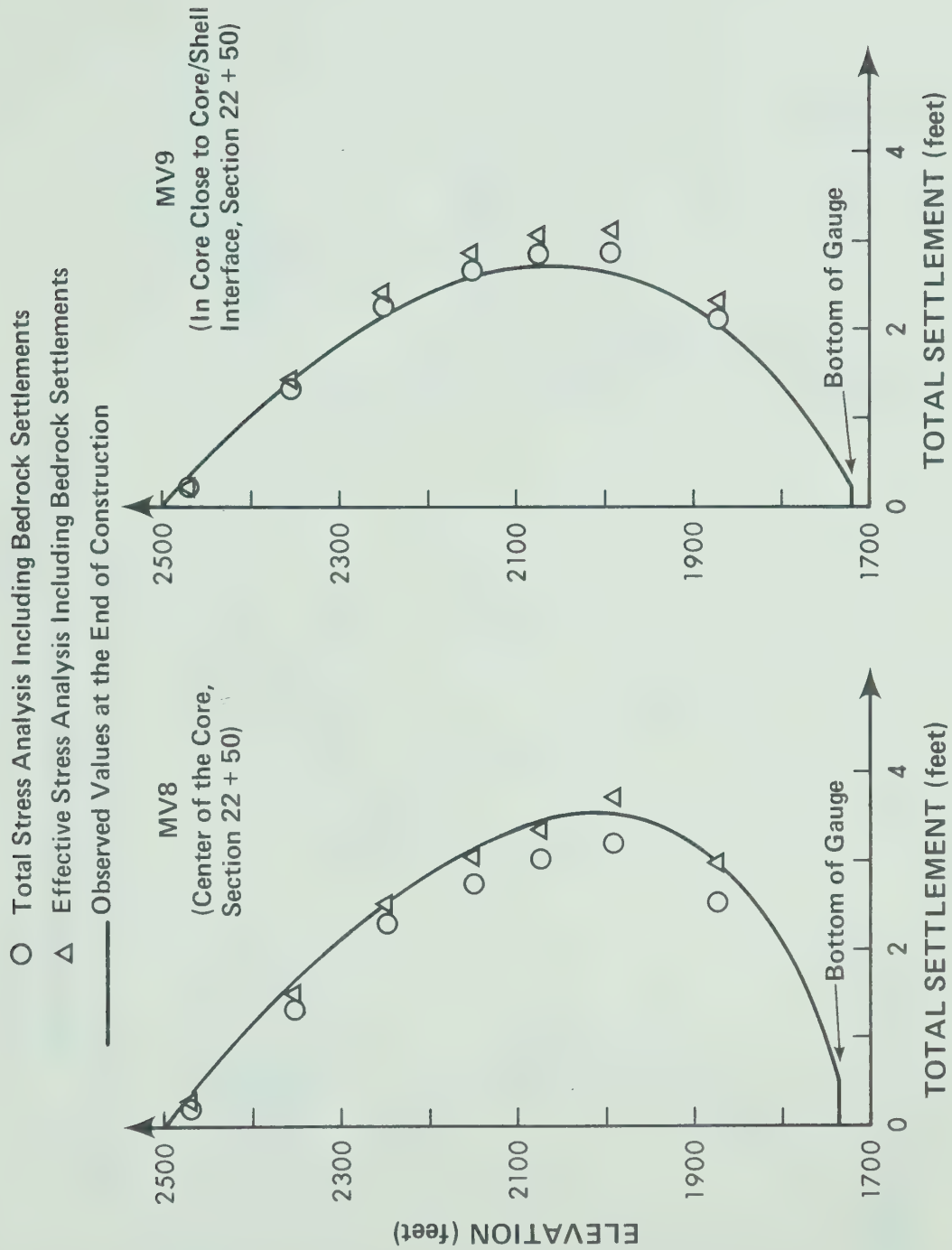


Fig. 5.39 Settlements from Total and Effective Stress Analysis for MV8 and MV9

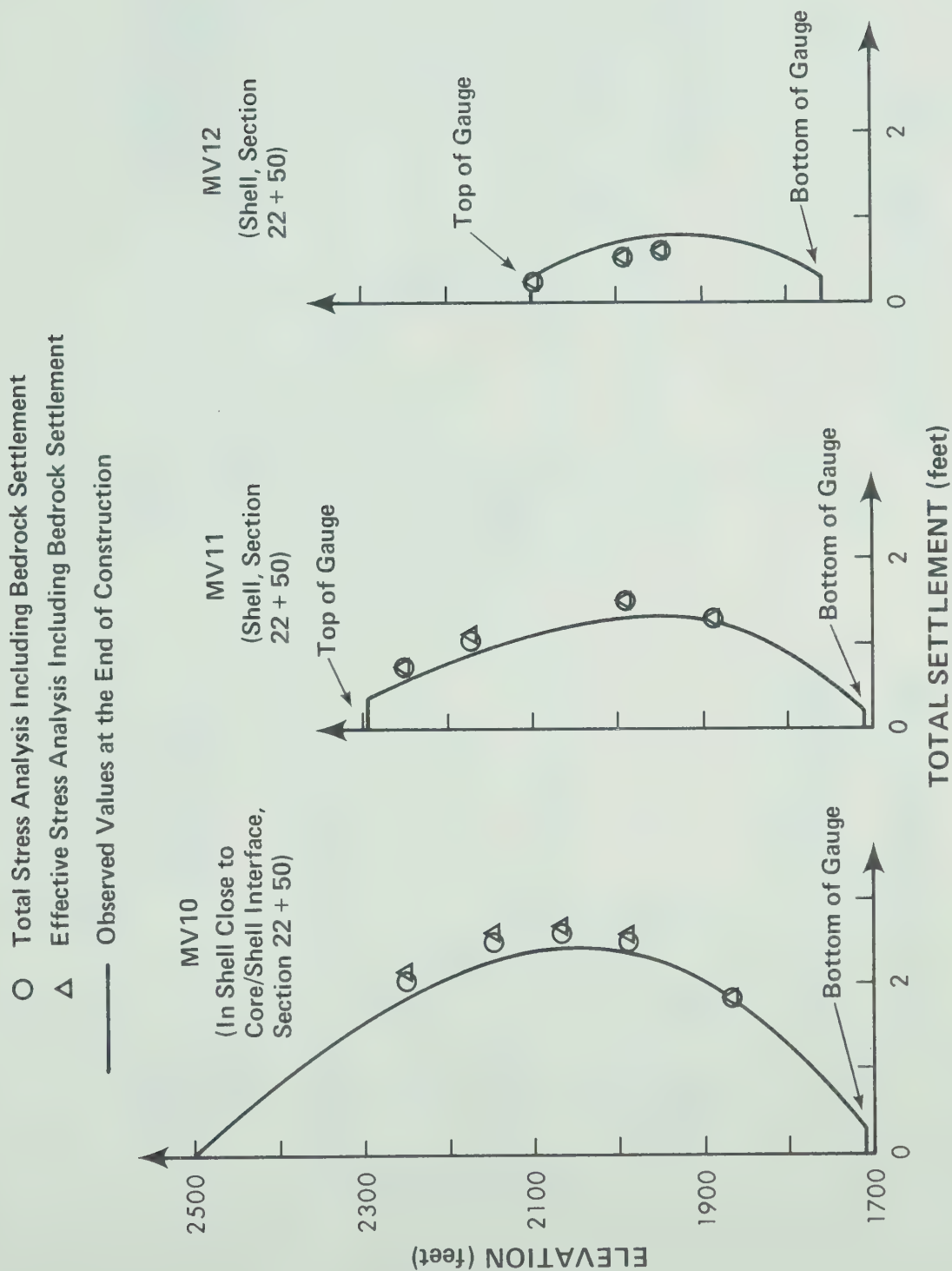


Fig. 5.40 Settlements From Total and Effective Stress Analyses for MV10, MV11 and MV12

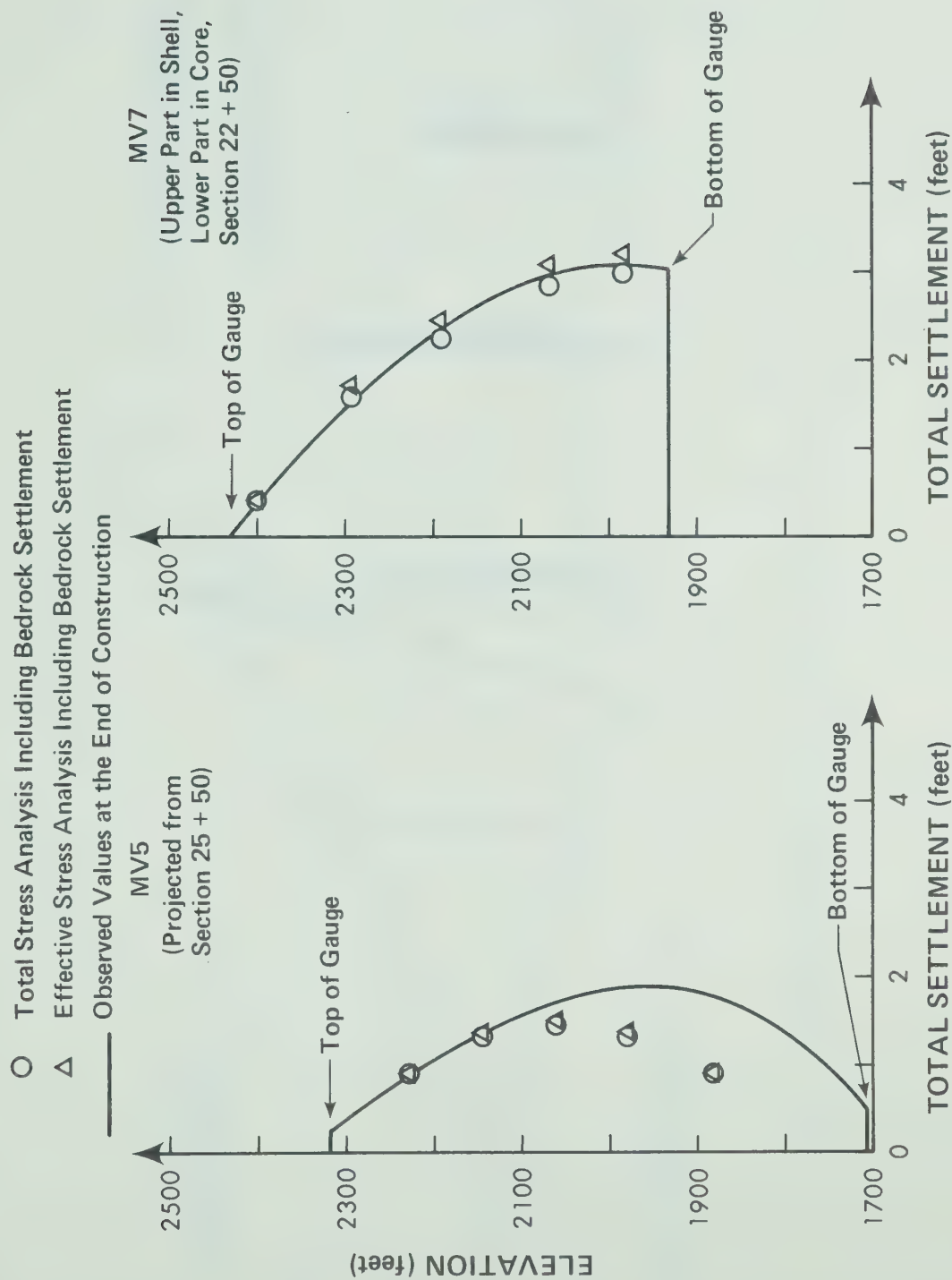


Fig. 5.41 Settlements From Total and Effective Stress Analyses for MV5 and MV7

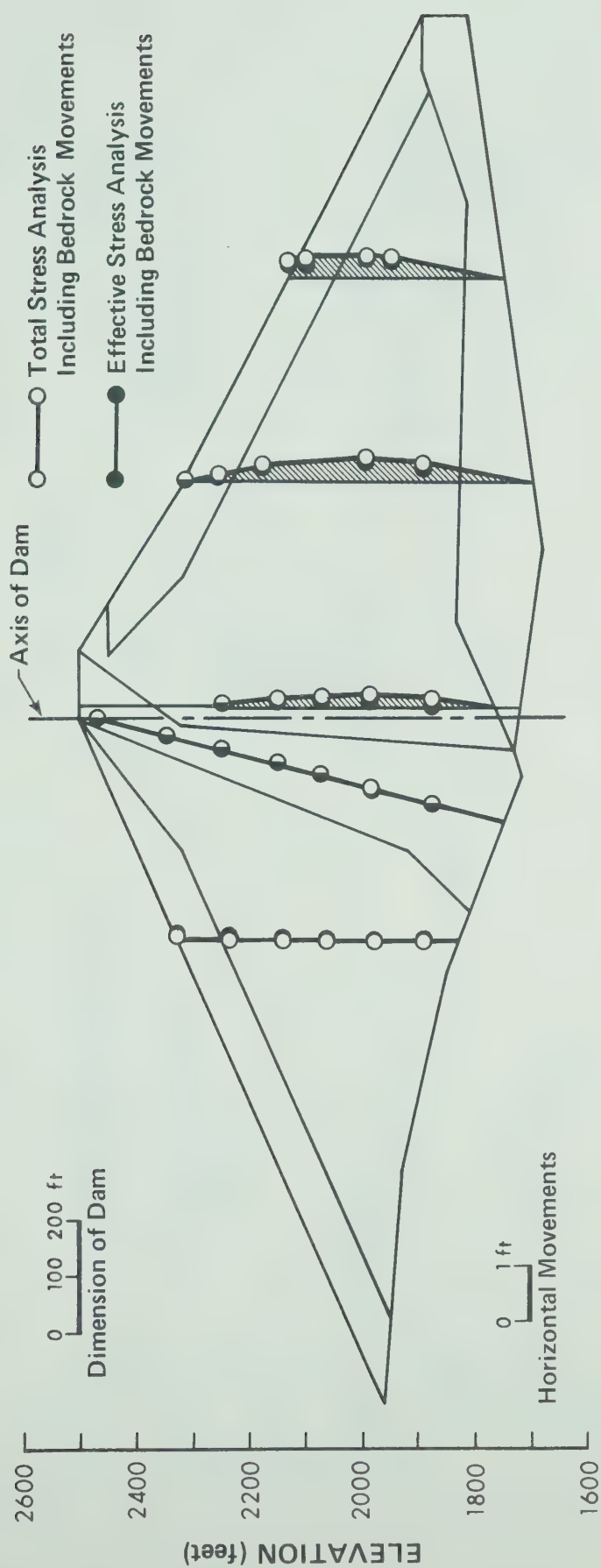


Fig. 5.42 Calculated Horizontal Movements in Mica Dam

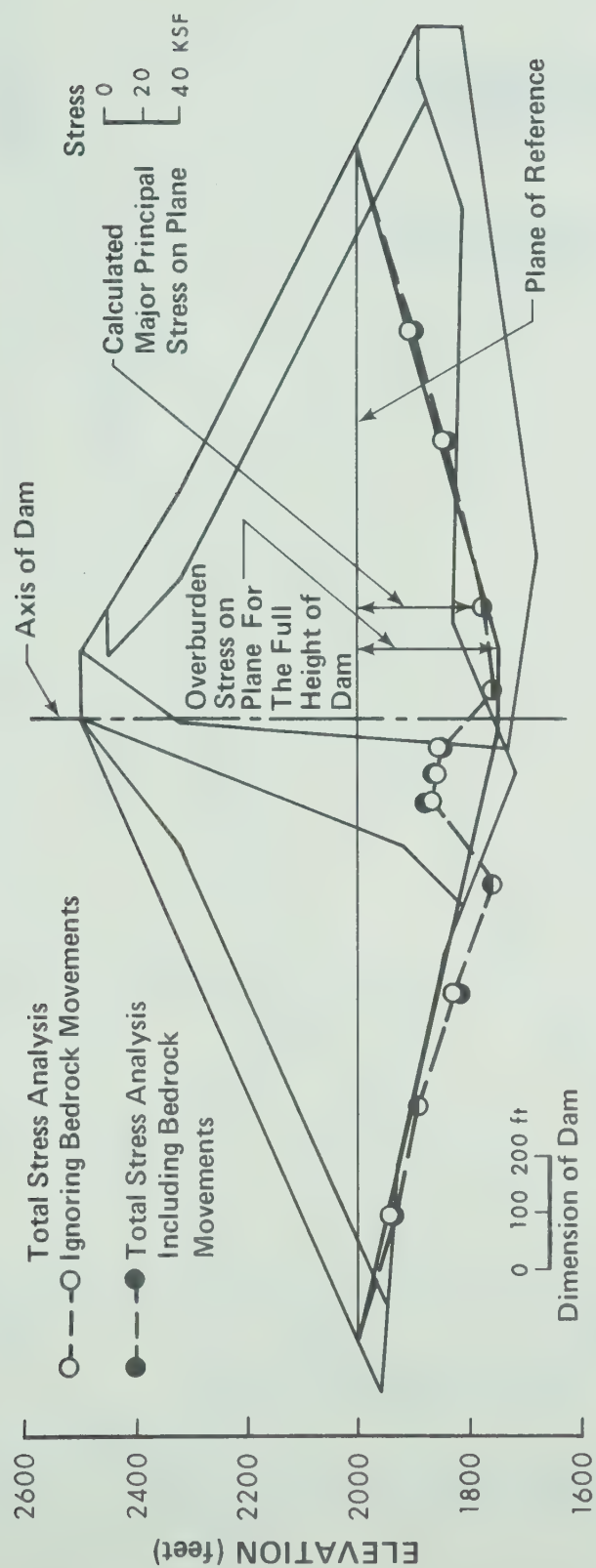


Fig. 5.43 Overburden Stresses and Calculated Major Principal Stresses on a Horizontal Plane in Mica Dam

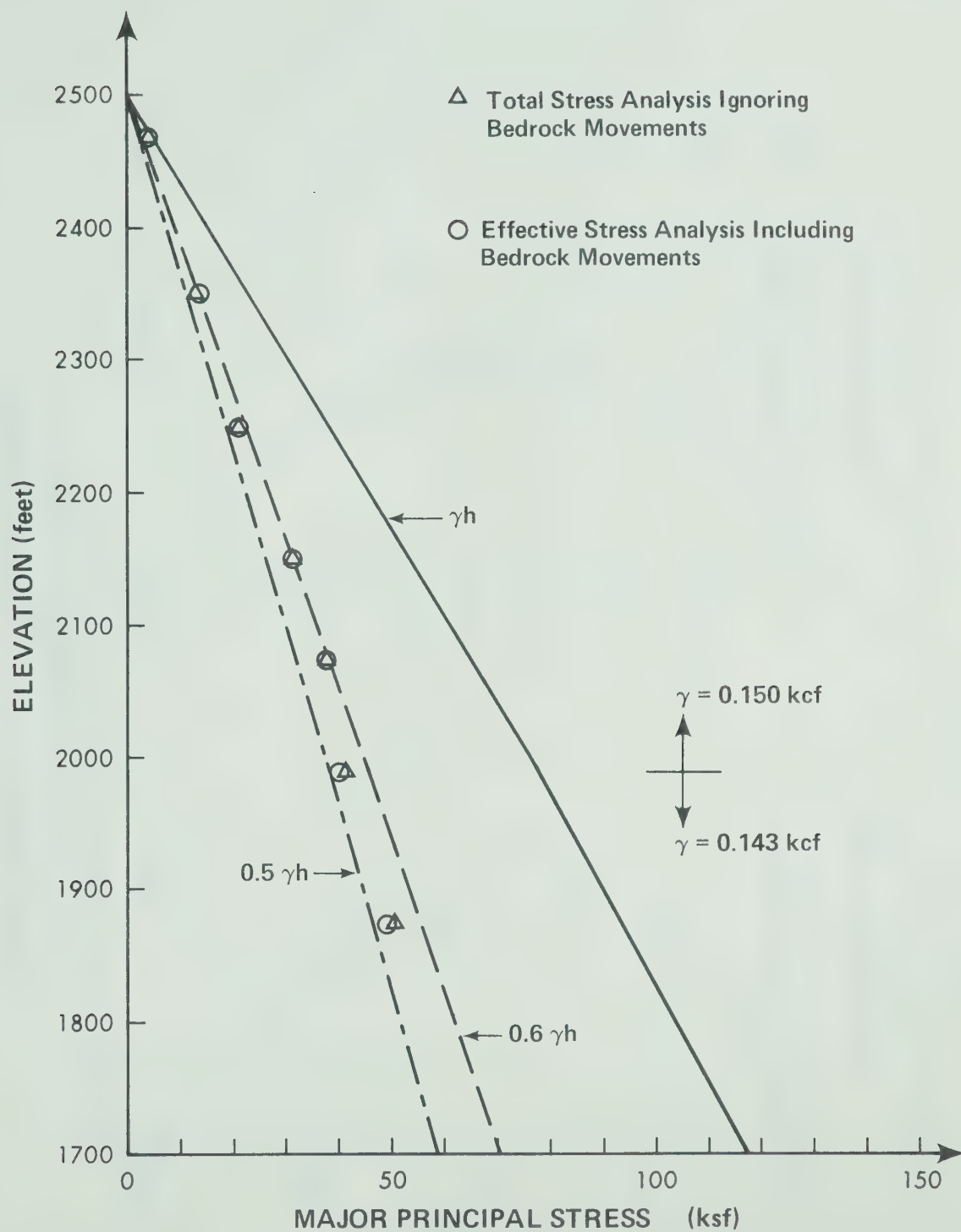


Fig. 5.44 Major Principal Stresses Calculated for the Center of the Core of Mica Dam

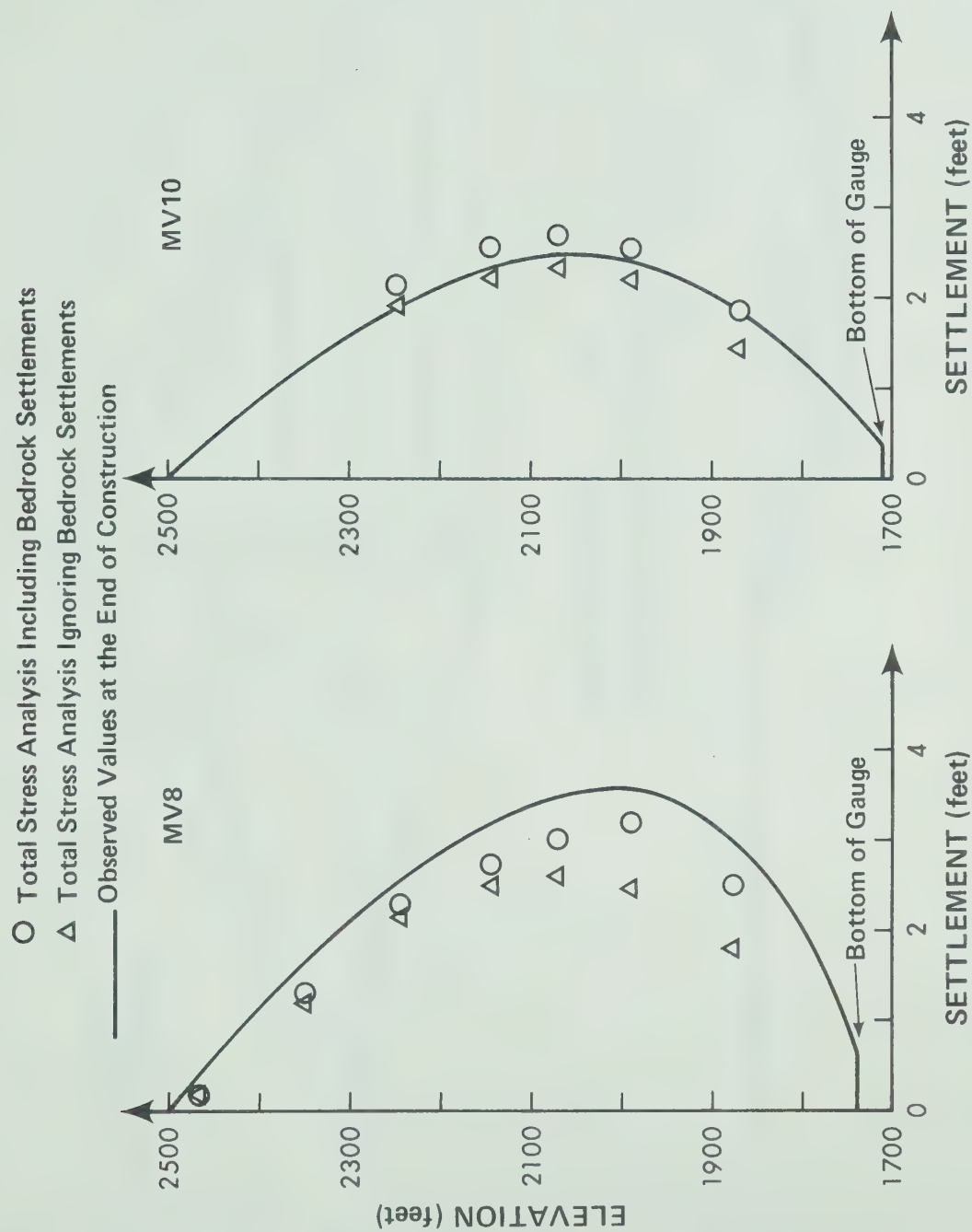


Fig. 5.45 The Influences of Bedrock Settlements on the Calculated Embankment Settlements

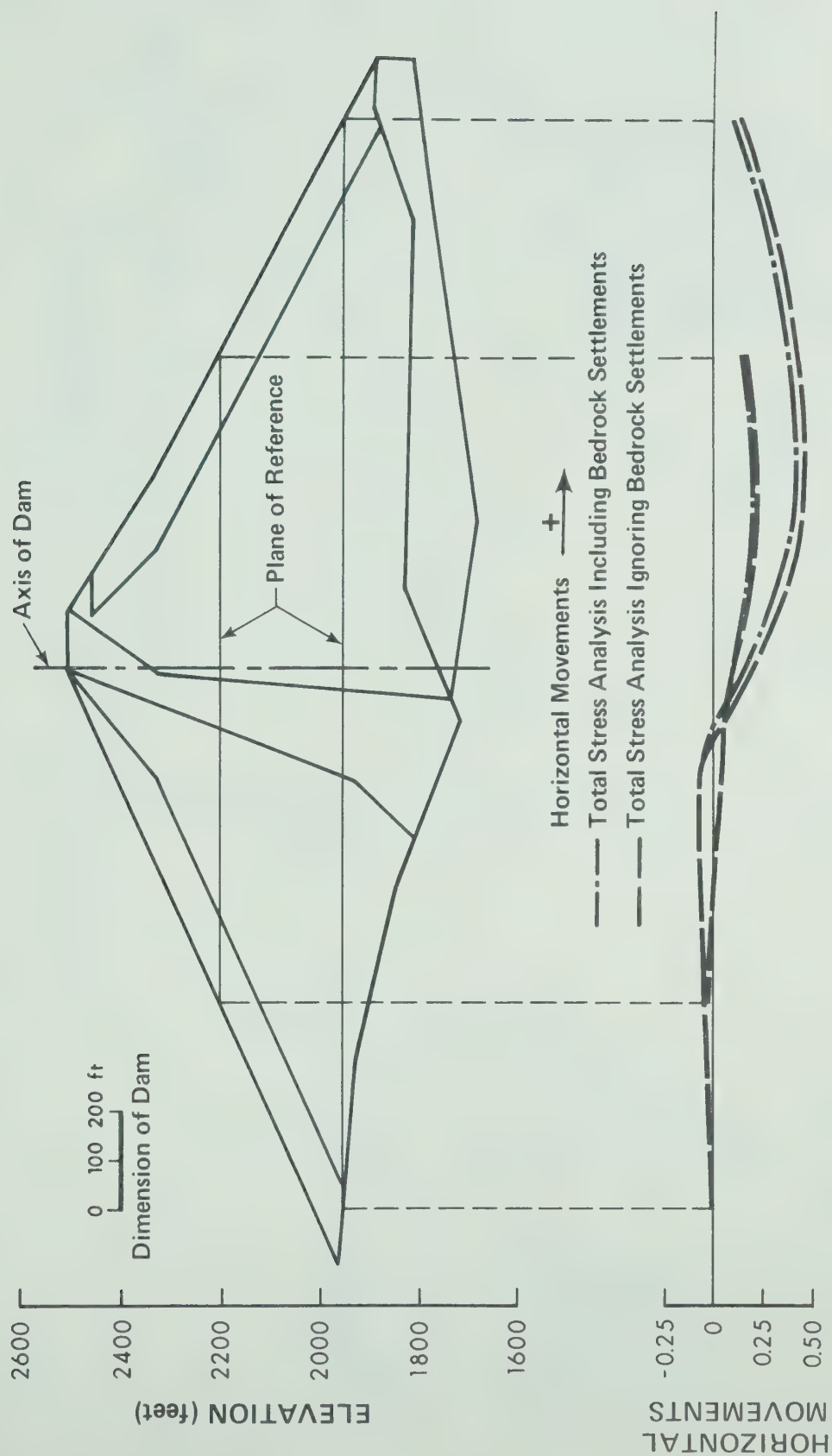


Fig. 5.46 The Influences of Bedrock Settlements on the Calculated Horizontal Movements

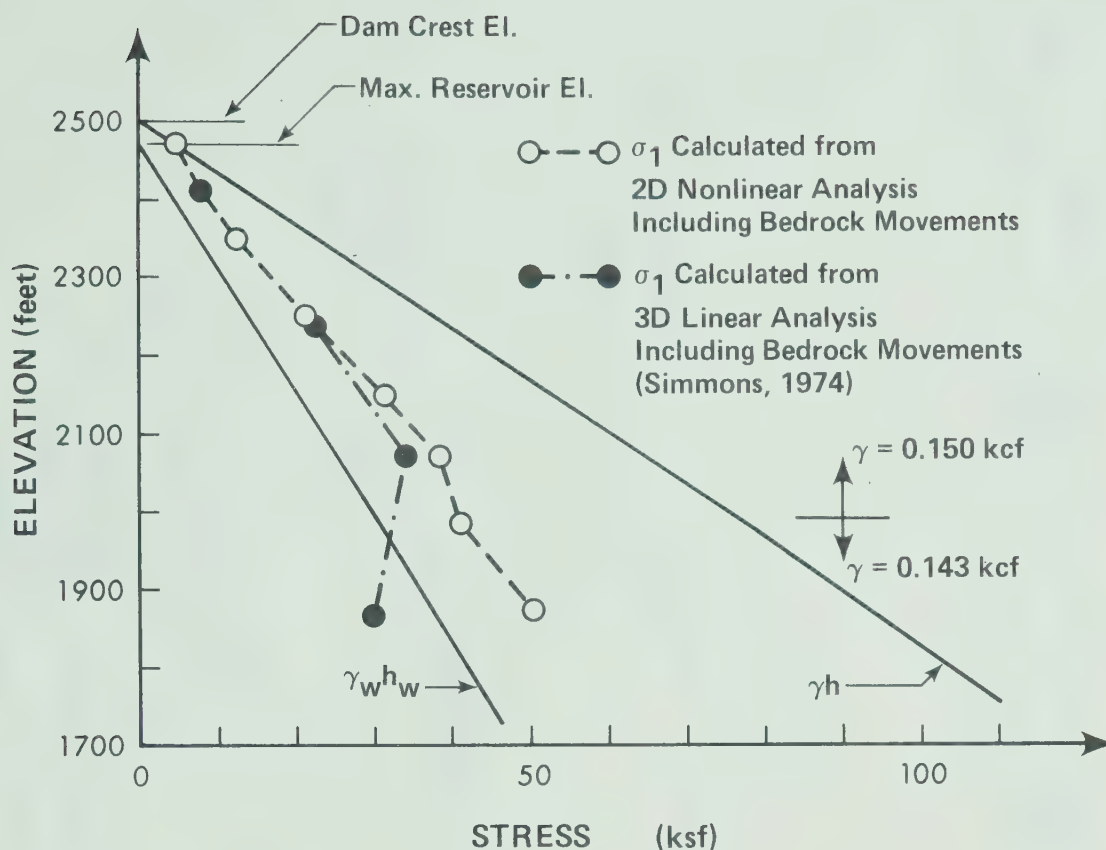


Fig. 5.47 Major Principal Stresses Calculated from 2D and 3D Analyses for the Core

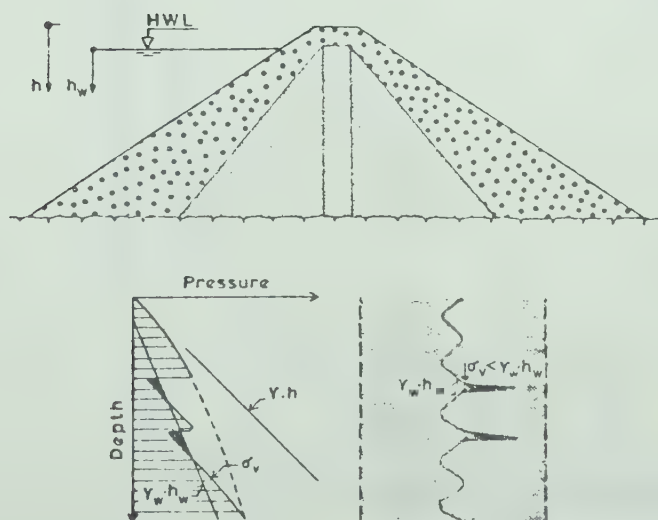


Fig. 5.48 Hydraulic Fracture Mechanism Postulated by Kjaernsli and Torblaa (1968)

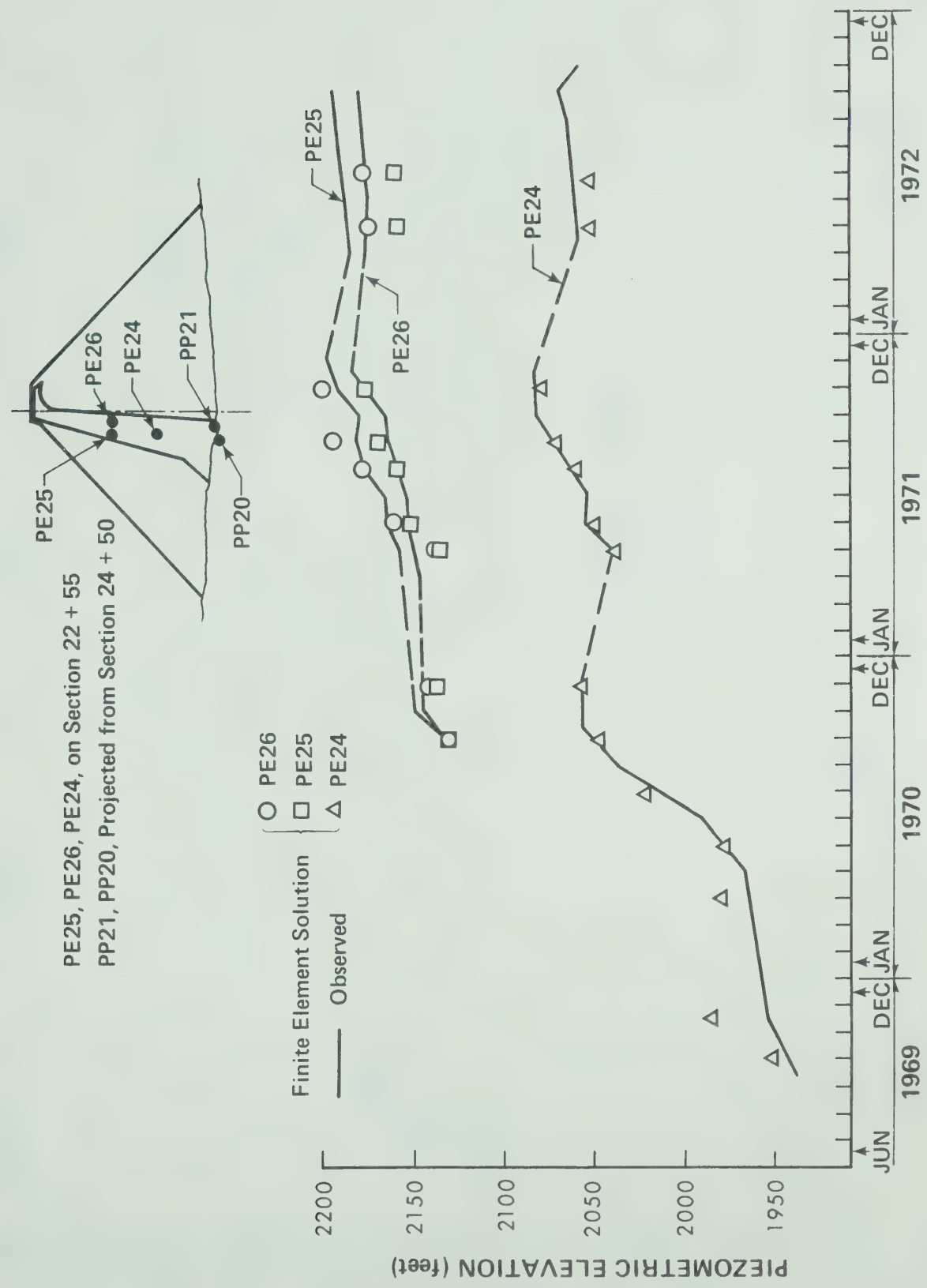


Fig. 5.49 Observed and Calculated Pore Pressure for PE24, PE25 and PE26

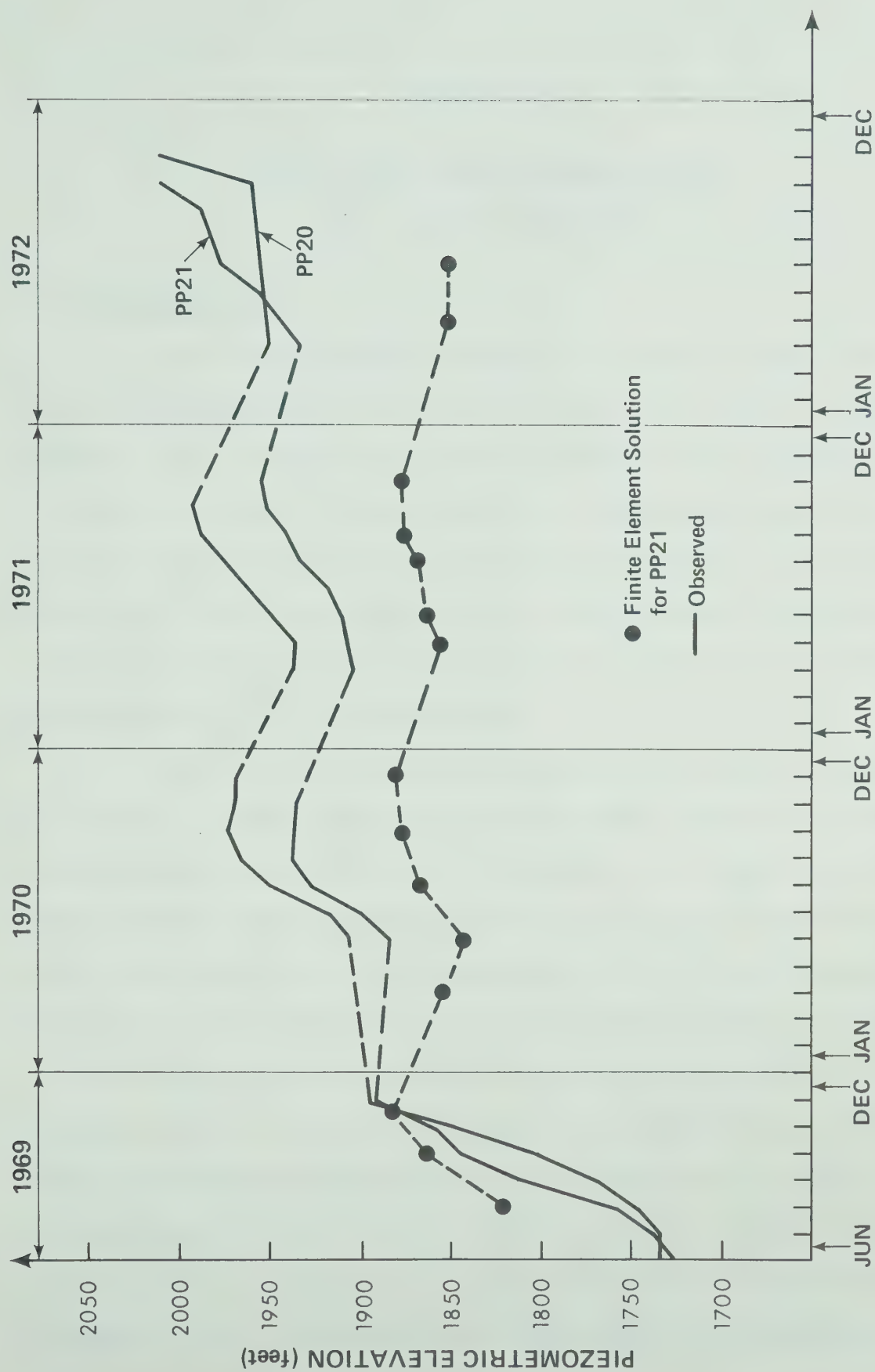


Fig. 5.50 Observed and Calculated Pore Pressures for PP21 and PP20

CHAPTER VI

CONCLUSIONS AND RECOMMENDATIONS FOR FURTHER RESEARCH

6.1 Conclusions

The finite element method is a powerful tool for deformation and stress analysis of earth and rockfill dams. However, the method itself cannot guarantee the accuracy of the prediction. Stress-strain relationships used to describe the soil behaviour are the key element in the entire analysis. The proper simulation of nonhomogeneity, geometry, construction sequence and the boundary conditions of the dam are also of major significance.

The overall deformation pattern in a dam is three-dimensional. Although a three-dimensional analysis to study the deformations in the dam is feasible, the high man-time and computer-time required mitigate against the extensive use of the analysis. Two-dimensional plane strain analyses have been used in the present study since the main purpose of the study was to investigate the important factors influencing the accuracy of analysis of deformation. The results of plane strain analysis can describe the actual deformation behaviour in maximum transverse sections very closely even if the dam is situated in a very steep-walled V-shaped valley. Information of considerable importance

can be obtained from this simpler analysis as the maximum settlements and outward displacements of the dam usually take place in this section.

For clarity, the main conclusions which are related to the deformation analysis of earth and rockfill dams are described in the following sections.

6.1.1 Stress-strain Behaviour of Compacted Soil

From the compression tests performed on Mica Till, it has been shown that stress-strain relationships of a compacted soil are influenced by various factors, namely water content, density (related to compaction method), gradation and maximum grain size. Under the same applied stress, a smaller strain was generally measured on the specimen with a lower water content, higher dry density, and better gradation. For the range of maximum grain size tested in the laboratory, it appears the specimen with the larger maximum grain size has the higher compressibility.

Grain size analyses performed before the test and after the test can be satisfactorily used to study the degree of grain breakage of the soil tested under high pressures. The results for Mica Till have indicated that unusually high pressures cause little grain breakage on the well graded soil composed of hard mineral. Thus, for this type of material, crushing strain would constitute a negligible portion of the total strain occurring under the high pressure

investigated.

6.1.2 Pore Pressure Response and Drainage Characteristic of Compacted Soil

Pore pressure response of compacted soil is mainly influenced by water content and the coarse particle fraction. In the oedometer tests performed on Mica Till, it was found that the specimen with higher water content and higher coarse particle fraction usually had higher pore pressure ratio, \bar{B} .

Pore pressure dissipation tests can be used to determine satisfactorily the coefficient of consolidation, C_v , of compacted soil with water content about optimum. From the oedometer partial dissipation tests performed on Mica Till, it appears that the coarse particle fraction has some effects on the C_v values. Higher C_v values appear to be related to higher coarse particle fraction.

6.1.3 The Simulation of Field Material

It has been indicated that the stress-strain behaviour of compacted soil is influenced by various factors. In order to have a proper prediction of field deformations, test specimens, which are used to obtain stress-strain behaviour of soils, should be prepared using a composition similar to that of the soil in the field. The actual field water content and density, which are the most important compositional factors effecting stress-strain behaviour of soil, are usually

less predictable during the design stage. The test embankment, which is usually made before the construction of the main dam, should be regarded as an important item from which expected water content and density in the main dam may be obtained. For simulating field compaction with a rubber-tired roller, it has been noted that kneading compaction is more appropriate and versatile than other compaction methods.

6.1.4 The Consideration of Stress Path Dependency

The importance of considering stress path dependency of stress-strain behaviour of soil in deformation analyses, has been illustrated. During its primary loading, a major part of an earth dam follows a stress path closer to a constant σ_3/σ_1 stress ratio rather than a conventional triaxial path with σ_3 constant and increasing deviatoric stress. Studies of construction behaviour of Mica Dam has revealed less suitability of conventional triaxial tests for predicting movements in earth dam. Elastic moduli derived from these tests overestimate the observed settlements. In the case of Mica Dam, it has been shown that the stress path followed in the oedometer tests gives reasonably good predictions.

6.1.5 Anisotropy of a Soil and Dam Deformation

Due to the compaction procedure, compacted material in an earth dam is generally anisotropic. The type of

anisotropy which is most likely to occur in a dam is cross-anisotropy. Five elastic parameters are required to describe this type of material. By studying individual effects from three parameters, E_H , ν_{HH} and G_V (section 3.8.4), which are usually not determined on material regarded as isotropic, it is found that the parameter E_H has the most significant effect on the behaviour of a typical embankment. If E_H is less than the value required for isotropic conditions (i.e., $E_V > E_H$), the results calculated from isotropic theory will underestimate the actual maximum settlement. However, for more representative anisotropic properties of soil (refer to limited published data), which E_H and ν_{HH} both deviate from isotropic values, the results calculated with and without considering anisotropy are not greatly different. The difference is about 10% in maximum settlement. For compacted soil with the properties of $E_H/E_V < 1$ and $\nu_{HH}/\nu_{VH} > 1$, the results calculated from isotropy theory underestimate the actual settlements.

6.1.6 Load Transfer in the Zoned Dam

Deformation in the narrow core of an earth and rock-fill dam during construction are not only functions of the weight and the stiffness of the core material but are also influenced by the relative stiffnesses between materials in the core and the shells. Load transfer, which occurs as the result of differences in stiffnesses, hinder the independent

settlement of the core. In most situations, the core is softer than the shells and hence load is transferred from core to shells. As a consequence of this type of load transfer, settlements in the core are always less than those in a homogeneous dam built with core material.

Load transfer can exert a significant influence on the pore pressure set up in the core during construction. For the case where the core is softer than the shells, pore pressures calculated without considering load transfer will overestimate the actual values. The use of the assumption of vertical stresses equal to overburden pressures in pore pressure analyses, is unsuitable for a central core in zoned dam.

With regard to the low stresses which can result in the core and hence create chances for hydraulic fracture, the existence of significant load transfer may be unfavourable. In order to reduce both the total settlement and the occurrence of load transfer, ideally, the dam should be built with core and shell materials having similar compressibilities. However, if the prevention of liquefaction due to earthquake is considered to be the more important aspect in the design, the shell materials are usually heavily compacted and are therefore relatively incompressible. In this case the attempt to have a core as stiff as the shell is difficult to achieve. The prevention of hydraulic fracture should then depend on the self-healing property of the core and a good filter downstream of the core.

6.1.7 Pore Pressure Dissipation and Deformation During Construction

In the central core of the dam, pore pressures are generated and partially dissipated as the dam is being built. Dissipation of pore pressure is especially noticeable during winter shutdowns. When pore pressures are generated, deformations occur more or less under undrained conditions. Additional deformations follow while some pore pressures are dissipated. Thus, deformations in the core during construction are not totally under undrained or drained conditions. In order to calculate deformations of this type, effective stress analysis has been suggested. Effective stress analysis performed in the study of construction behaviour of Mica dam has reasonably determined the additional settlements which cannot be obtained from a total stress analysis.

The present study has a two-fold effect. Firstly, a comprehensive method for analyzing deformations of earth dams has been developed. Then, important features of the mechanics of behaviour of zoned earth and rockfill dams during construction were discussed and explained. The understanding of these features make it possible to examine critically results of not only this but of any similar analysis in the future.

6.2 Recommendations for Further Research

Based on the work presented here, the following further research related to the deformation of earth dams is recommended:

(1) The analysis of deformations of earth dams presented here is limited to the period of construction of dam. It is equally important to study the deformation of earth dams under other critical conditions, such as rapid drawdown, earthquake loading, first filling of reservoir and steady seepage.

(2) An elastic stress-strain model can satisfactorily simulate many aspects of soil behaviour up to failure and has been successful in many published applications. This model, however, cannot describe properly certain characteristics of soil behaviour such as volume change due to shear (including dilatancy) and plastic deformations. It is desirable to develop a stress-strain model which can incorporate these facets of soil behaviour and be affectively used in the deformation analysis of real soil structures.

(3) It is an increasing practice to build an earth dam curving upstream. The relation between curvature and deformations of earth and rockfill has not been thoroughly studied. Research on the actual beneficial effects of curvature to increase axial compression and thus prevent tension crack formation in the core during impounding will be of great practical value.

(4) Stress-strain behaviour of soils subjected to stress paths other than those followed in an oedometer and conventional triaxial tests needs additional study. It is highly desirable to develop means for representing these

stress-strain behaviour with data from more conveniently performed triaxial and oedometer tests.

(5) Reliable field observations on stresses, pore pressures and deformations are of great value in verifying the analytical and testing procedures developed for the deformation analysis of earth dams. The rate of previous success in measuring total stresses is low. Improved methods for installing pressure cells and to obtain reliable total stress measurements are desirable. Reliable total stress measurements are of value in verifying the existence of low vertical stresses in the core due to load transfer and to evaluate the actual stress paths in the dam.

BIBLIOGRAPHY

BIBLIOGRAPHY

- Audibert, J. M. E. (1972), "Prediction and measurement of strain fields in soils" Ph.D. thesis, Duke University.
- Bernell, L. and Nilsson, R. (1957), "Electrical analogy equipment for solving nonstationary two-dimensional flow problems", Proc. 4th Int. Conf. on Soil Mechanics and Foundation Engineering, London, Vol. 2, pp. 291-293.
- Biot, M. A. (1941), "General theory of three-dimensional consolidation", Journal of Applied Physics, Vol. 12, pp. 155-164.
- Bishop, A. W. (1954), "The use of pore-pressure coefficients in practice", Geotechnique, Vol. 4, No. 4, pp. 148-152.
- Bishop, A. W. (1957), "Some factors controlling the pore pressure set-up during the construction of earth dams", Proc. 4th Inter. Conf. Soil Mech. Found. Eng. (London), Vol. 2, pp. 294-300.
- Bishop, A. W. and Henkel, D. J. (1957), "The measurement of soil properties in the triaxial test", Edward Arnold, London
- Bishop, A. W., Alpan, I. Blight, E. E. and Donald, I. B. (1960), "Factors controlling the strength of partly saturated cohesive soils", Proc. ASCE Research Conf. on Shear Strength of Cohesive soils, Boulder, Col., pp. 503-532.
- Bishop, A. W. and Morgenstern, N. R. (1960), "Stability Coefficient for earth slopes", Geotechnique, Vol. 10, pp. 129-150.
- Bishop, A. W., Kennard, M. F. and Vaughan, P. R. (1964), "Developments in the measurement and interpretation of pore pressures in earth dams", Transactions, 8th International Congress on Larger Dams, Edinburgh, Vol. 2, pp. 47-72.
- Blight, G. E. (1973), "Stresses in narrow cores and core trenches of dams", Trans. 11th Int. Cong. on Large Dams, Madrid, Q42-R5, 3, pp. 63-79.
- Brandt, H. (1955), "A study of the speed of sound in porous granular media", Journal of Applied Mechanics, 22, pp. 479-486.

- Brooker, E. W. and Ireland, H. O. (1965), "Earth pressures at rest related to stress history", Canadian Geotechnical Journal, Vol. 2, No. 1, pp. 1-15.
- Bruggeman, J. R., Zanger, C. N. and Brahtz, J. H. A. (1939) "Notes on analytical soil mechanics", Technical Memorandum No. 592, U. S. Bureau of Reclamation, Denver, Colorado, June, 1939.
- CASECO Consultants Limited, Mica Project: Reports on Dam Instrumentation 1969, 1970, 1971, (1972 in preparation), Vancouver, B.C.
- Chang, C. Y. and Duncan, J. M. (1970), "Analysis of soil movements around deep excavation", Journal of the Soil Mechanics and Foundations Division, ASCE, Vol. 96, No. SM5, Septebmer, 1970, pp. 1655-1681.
- Chang, C. Y., Nair, K. and Karwoski, W. J. (1972), "Finite element analysis of excavations in rock", Proc. of Symp. on Applications of the Finite Element Method in Geotechnical Engrg. USAEWES, Vicksburg, Miss., pp. 457-504.
- Clark, J. I. and Robinson, J. L. (1971), "Elastic properties of foundation gravels underlying Husky Tower, Calgary, Alberta "Paper presented to annual meeting A.P.E.G.G.A. May 28, 1971.
- Clough, G. W. and Duncan, J. M. (1971), "Finite element analyses of retaining wall behaviour," Journal of the Soil Mechanics and Foundations Division, ASCE, Vol. 97, No. SM12, p. 1657.
- Clough, R. W. and Woodward, R. J., III (1967), "Analysis of embankment stresses and deformations", Journal of the Soil Mechanics and Foundations Division, ASCE, Vol. 93, No. SM4, July, 1967, pp. 529-549.
- Cole, K. W. and Burland, J. B. (1972), "Observations of retaining wall movements associated with a large excavation", Proc. of the 5th European Conference on Soil Mechanics and Foundation Engineering, Madrid, April, 1972.
- Corotis, R. B., Farzin, M. H. and Krizek, R. J. (1974), "Nonlinear stress-strain formulation for soils", Journal of the Geotechnical Engineering Division, ASCE, Vol. 100, No. GT9, September, 1974, pp. 993-1008.
- Covarrubias, S. W. (1969), "Cracking of earth and rockfill dams", Harvard Soil Mechanics Series, No. 82, April, 1969.

- D'Appolonia, D. J. and Lambe, T. W. (1970), "Method for predicting initial settlement", Journal of the Soil Mechanics and Foundations Division, ASCE, Vol. 96, No. SM2, Proc. paper 7167, March 1970, p. 523.
- Davis, E. H. and Poulos, H. G. (1963), "Triaxial testing and three-dimensional settlement analysis", Proc. 4th Australia - New Zealand Conf. Soil. Mech., University of Adelaide, pp. 233-303.
- Desai, C. S. (1971), "Nonlinear analysis using spline functions", Journal of the Soil Mechanics and Foundations Division, ASCE, Vol. 97, No. SM10, October, 1971, p. 1461.
- Desai, C. S. (1972), "Overview, trends and projections: theory and application of the finite element method in geotechnical engineering", State-of-the Art Report, Proc. of Symp. on Applications of the Finite Element Method in Geotechnical Engrg., USAEWES, Vicksburg, Miss., pp. 3-90.
- Desai, C. S. and Abel, J. F. (1972), Introduction to the finite element method, Van Nostrand Reinhold Company, New York.
- Domaschuk, L. and Wade, N. H. (1969), "A study of bulk and shear moduli of a sand", Journal of the Soil Mechanics and Foundations Division, ASCE, Vol. 95, No. SM2, Proc. paper 6461, March, 1969.
- Drucker, D. C. and Prager, W. (1952), "Soil mechanics and plastic analysis of limit design", Quarterly of Applied Mathematics, Vol. 10, No. 2, pp. 157-165.
- Duncan, J. M. and Chang, C. Y. (1970), "Nonlinear Analysis of stress and strain in soils", Journal of the Soil Mechanics and Foundations Division, ASCE, Vol. 96, No. SM5, pp. 1629-1654.
- Duncan, J. M. (1972), "Finite element analysis of stresses and movements in dams, excavations and slopes", State-of-the-Art Report, Proc. of Symp. on Applications of the Finite Element Method in Geotechnical Engrg., USAEWES, Edited by Desai, C. S., Vicksburg, Miss., pp. 267-326.
- Duncan, J. M. and Chang, C. Y. (1972), Discussion closure of "Non-linear analysis of stress and strain in soils", by Duncan, J. M. and Chang, C. Y., Journal of the Soil Mechanics and Foundations Division, ASCE, Vol. 98, No. SM5, May, 1972, pp. 495-498.

- Dunlop, P., Duncan, J. M., and Seed, H. B. (1968), "Finite element analysis of slopes in soils", Geotechnical Engineering, University of California, Berkeley, Report No. TE-68-3, May, 1968.
- Dunlop, P., and Duncan, J. M. (1970), "Development of failure around excavated slopes", Journal of the Soil Mechanics and Foundations Division, ASCE, Vol. 96, No. SM2, Proc. paper 7162, March, 1970, pp. 471-493.
- El-Sohby, M. A. (1964), "The behaviour of particulate materials under stress", Ph.D. thesis, University of Manchester, Manchester, England.
- El-Sohby, M. A. (1969), "Elastic behaviour of sand", Journal of the Soil Mechanics and Foundations Division, ASCE, Vol. 95, No. SM6, November, 1969.
- Eisenstein, Z., Krishnayya, A.V.G. and Morgenstern, N. R. (1972), "An analysis of cracking at Duncan Dam", ASCE Specialty Conference on Performance of Earth and Earth-Supported Structures, June, 1972, Purdue University, Lafayette, Indiana, Vol. 1, Part 1, pp. 765-777.
- Eisenstein, Z., Krishnayya, A.V.G., and Morgenstern, N. R. (1972a), "An analysis of cracking in earth dams" Proc. of Symp. on Applications of the Finite element method in Geotechnical Engrg., USAEWES, Vicksburg, Miss., pp. 431-455.
- Eisenstein, Z. (1974), "Application of finite element method to analysis of earth dams", State-of-the Art Report, First Brazilian Seminar on Application on Finite Element Method in Soil Mechanics, Universidade Federal do Rio de Janeiro, Sept., 1974.
- Felippa, C. A. (1966), "Refined finite element analysis of linear and non-linear two-dimensional structures", Ph.D. Thesis, University of California, Berkeley, California.
- Fredlund, D. G. (1972), "Manual of volume change test procedures for unsaturated soils", Internal note No. SM12, Dept. of Civil Engineering, Univ. of Alberta, Edmonton, Alberta.
- Fredlund, D. G. (1973) "Volume change behaviour of unsaturated soils", Ph.D. Thesis, The University of Alberta, Edmonton.
- Gibson, R. E. (1958), "The Progress of Consolidation in a clay layer increasing in thickness with time", *Geotechnique*, Vol. 8, pp. 171-182.
- Gibson, R. E. (1974), "The analytical method in soil mechanics", Fourteenth Rankine Lecture, *Geotechnique*, Vol. 24, No. 2, June, 1974, pp. 115-140.

- Girijavallabhan, C. V. and Mehta, K. C. (1969), "Stress-strain relationship from compression tests on nonlinear materials", Proc. of the symposium on application of finite element methods in civil engineering, Vanderbilt, November, 1967, p. 457.
- Goodman, L. E. and Brown, C. B. (1963), "Dead load stresses and the instability of slopes", Journal of the Soil Mechanics and Foundations Division, ASCE, Vol. 89, No. SM3, May, 1963, pp. 103-134.
- Gordon, J. L. and Duguid, D. R. (1970), "Experiences with Cracking at Duncan Dam", Trans. Tenth Congress on Large Dams, Vol. 1, June, 1970, pp. 469-486.
- Gould, J. P. (1953), "The compressibility of rolled fill materials determined from field observations", 3rd International Conference on Soil Mechanics and Foundation Engineering, Zurich, Vol. II, p. 239.
- Henkel, D. J. (1960), "The shear strength of saturated remolded clays", Research Conf. Shear Strength of Cohesive Soils, ASCE, Boulder, pp. 533-554.
- Hilf, J. W. (1948), "Estimating construction pore pressures in rolled earth dams", Proc. 2nd Int. Conf. on Soil Mechanics and Foundation Engineering, Vol. 3, Rotterdam, Netherlands, p. 234.
- Hilf, J. W. (1956), "An investigation of Pore-Water Pressure in compacted cohesive soils", Technical Memorandum No. 654, U.S. Bureau of Reclamation, Denver, Colorado, Oct., 1956.
- Hwang, C. T., Morgenstern, N. R. and Murray, D. W. (1971). "On solutions of plane strain consolidation problems by finite element methods", Can. Geotechnical Journal, Vol. 8, No. 1, pp. 109-118.
- Hwang, C. T., Morgenstern, N. R. and Murray, D. W. (1972), "Application of the finite element method to consolidation problems", Proc. of Symposium on Applications of the finite element method in geotechnical enrg., USAEWES, Vicksburg, Miss., pp. 739-765.
- Insley, A. E. and Hillis, S. F. (1965), "Triaxial shear characteristics of compacted glacial till under unusually high confining pressures", Proc. 6th Int. Conf. on Soil Mechanics and Foundation Engineering, Montreal, Vol. 2, pp. 244-248.

- Jaky, J. (1944), "The coefficient of earth pressure at rest", Journal of the Society of Hungarian Architects and Engineers, pp. 335-358.
- Janbu, N. and Hjeltnes, E. I. (1965), "Principal stress ratios and their influence on the compressibility of soils", Proc. of the 6th Int. Conf. on Soil Mechanics and Foundation Engineering, Montreal, Vol. I, pp. 249-253.
- Kjaernsli, B. and Torblaa, I. (1968), "Leakage through horizontal cracks in the core of Hyttejuvet Dams", Papers on Earth and Rockfill dams in Norway, Publication No. 80, Norwegian Geotechnical Institute, pp. 39-47.
- Ko, H. Y. and Scott, R. F. (1967), "Deformation of sand in hydostatic compression", Journal of the Soil Mechanics and Foundation Division, ASCE, Vol. 93, No. SM3, May, 1967.
- Konder, R. L. (1963), "Hyperbolic stress-strain response: cohesive soils", Journal of the Soil Mechanics and Foundations Division, ASCE, Vol. 89, No. SM1, pp. 115-143.
- Konder, R. L. and Zelasko, J. J. (1963), "Void ratio effects on the hyperbolic stress-strain response of a sand", STP 361 - Laboratory Shear Testing of Soils, ASTM, pp. 250-257.
- Koppula, S. D. (1970), "The consolidation of soil in two dimensions and with moving boundaries", Ph.D. Thesis, The University of Alberta, Edmonton.
- Koppula, S. D. and Morgenstern, N. R. (1972), "Consolidation of clay layer in two dimensions", Journal of the Soil Mechanics and Foundations Divisions, ASCE, Vol. 98, No. SM1, pp. 79-93.
- Krishnayya, A. V. G. (1973a), "Analysis of cracking of Earth Dams", Ph.D. Thesis, University of Alberta, Edmonton, Alberta.
- Krishnayya, A. V. G. (1973b), "Finite element consolidation program for two-dimensional problems (FEC2D)", User's Manual, Soil Mech. No. 22, Dept. of Civil Engineering, University of Alberta, Edmonton, Alberta.
- Kulhawy, F. H., Duncan, J. M. and Seed, H. B. (1969), "Finite element analysis of stresses and movements in embankment during construction", Report No. TE69-4, Office of Research Services, University of California, Berkeley,

- Kulhawy, F. H. and Duncan, J. M. (1970), "Non-linear finite element analysis of stresses and movements in Oroville Dam", Report No. TE70-2, Office of Research Services, University of California, Berkeley.
- Lambe, T. W. (1964), "Methods of Estimating Settlement", Journal of the Soil Mechanics and Foundations Division, ASCE, Vol. 90, No. SM5, Part I, September, 1964, pp. 43-67.
- Lambe, T. W. and Whitman, R. V. (1969), Soil Mechanics, Wiley, New York.
- Lee, K. L. and Seed, H. B. (1967), "Drained strength characteristics of sands", Journal of the Soil Mechanics and Foundations Division, ASCE, Vol. 93, No. SM6, Nov., 1967, pp. 117-141.
- Lee, K. L. and Shen, C. K. (1969), "Horizontal movements related to subsidence", Journal of the Soil Mechanics and Foundations Division, ASCE, Vol. 95, SM1, pp. 139-166.
- Lefebvre, G., Duncan, J. M., and Wilson, E. L. (1973), "Three-dimensional finite element analyses of dams", Journal of the Soil Mechanics and Foundations Division, ASCE, Vol. 99, No. SM7, pp. 495-507.
- Lekhnitskii, S. G. (1963), Theory of Elasticity of an anisotropic elastic body, Translated from Russia by Fern, P., Holden Day, San Francisco.
- Löfquist, B. (1951), "Earth pressure in a thin impervious core", (Question No. 13), Transactions, 4th International Congress on Large Dams, New Delhi, Vol. 1, pp. 99-109.
- Love, A. E. H. (1892), A treatise on the mathematical theory of elasticity, 2 volumes, Cambridge University Press.
- Lowe III, J. (1970), "Recent development in design and construction of earth and rockfill dams", Transaction 10th Congress on Large Dams. Montreal, Vol. 5, Q. 36, pp. 1-60.
- Lowe III, J. (1972), Report, Session II: Earth and Earth-rock dams, ASCE. Speciality Conference on Performance of Earth and Earth Supported Structures, June, 1972, Purdue University, Lafayette, Indiana, Vol. 2, pp. 55-70.
- Matyas, E. L. and Radhakrishna, H. S. (1968), "Volume change characteristics of partially saturated soils", Geotechnique, Vol. 18, No. 4, pp. 432-448.

- Marsal, R. J. and Ramirez de Arellano, L. (1967), "Performance of El Infiernillo Dam, 1963-1966, Journal of Soil Mechanics and Foundations Division, ASCE, Vol. 93, No. SM4, July, 1967, pp. 265-298.
- Marsal, R. J. (1972), "Mechanical properties of rockfill", Casagrande's volume on embankment dam engineering, Edited by Hirschfeld, R. C. and Poulos, S. J., Wiley, New York, pp. 109-200.
- Meidal, P., and Webster, J. L. (1973), "Mica: One of the World's Largest Structures", Water Power, June, 1973, pp. 201-210, and July, 1973, pp. 245-249.
- Morgenstern, N. R. (1968), "Ultimate behaviour of rock structures", Rock Mechanics in Engineering Practice, Edited by Stagg, K. G. and Zienkiewicz, O. C., John Wiley and Sons.
- Morgenstern, N. R. and Tamuly Phukan, A. L. (1969), "Non-linear stress-strain relations for a homogeneous sandstone", Int. J. Rock Mech. and Mining Scis., 6, 127-142.
- Naylor, D. J. and Jones, D. B. (1973), "The prediction of settlement within layered fills", Geotechnique, Vol. 23, No. 4, December, 1973, pp. 589-594.
- Nobari, E. S. and Duncan, J. M. (1972), "Movements in dams due to reservoir filling", Proc. of ASCE Spec. Conf. on Performance of Earth and Earth-Supported Structures, Purdue Univ., Lafayette, Indiana, pp. 797-815.
- Nonveiller, E. and Anagnosti, P. (1961), "Stresses and Deformation in cores of rockfill dams", Proc. Fifth International Conference on Soil Mechanics and Foundation Engineering, Vol. II, Duroid, Paris, pp. 673-680.
- Palmer, J. H. L. and Kenney, T. C. (1971), "Analytical Study of a braced excavation in weak clay", Proc. of the 24th Canadian Geotechnical Conference, Halifax, Nova Scotia, September, 1971.
- Palmerton, J. B. (1972), "Application of three-dimensional finite element analysis", Proc. of Symposium on Applications of the Finite Element Method in Geotechnical Eng., USAEWES, Vicksburg, Miss., pp. 155-214.
- Pariseau, W. G., Voigt, B. and Dahl, H. D. (1970), "Finite element analyses of elastic-plastic problems in the mechanics of geologic media: an overview", Proc., Second Congress of International Soc. of Rock Mechanics, Belgrade.

- Patrick, J. G. (1967) "Post-Construction behaviour of Round Butte Dam", Journal of the Soil Mechanics and Foundations Division, ASCE, Vol. 93, No. SM4, July, 1967, pp. 251-263.
- Penman, A. D. M. and Mitchell, P. B. (1970), "Initial behaviour of Scammonden Dam", Transactions, 10th International Congress on Large Dams, Vol. 1, pp. 723-747.
- Penman, A. D. M., Burland, J. B., and Charles J. A. (1971), "Observed and predicted deformations in a large embankment dam during construction", Proceedings, Institution of Civil Engineers, 49, pp. 1-21.
- Pickering, D. J. (1970), "Anisotropic elastic parameters for soil", Geotechnique, Vol. 20, No. 3, pp. 271-276.
- Pope, R. J. (1967), "Evaluation of Cougar dam embankment performance", Journal of the Soil Mechanics and Foundations Division, ASCE, Vol. 93, SM4, July, 1967, pp. 231-250.
- Pratt, H. K., McMordie, R. C. and Dundas, R. M. (1972), "Foundations and abutments - Bennett and Mica Dams", Journal of the Soil Mechanics and Foundations Division, ASCE, Vol. 98, SM10, October, pp. 1053-1072.
- Reyes, S. F. and Deere, D. U. (1966), "Elastic-Plastic Analysis of Underground openings by the Finite Element Method", Proc. of the First Congress of the International Society of Rock Mechanics, Lisbon, Portugal, September, 1966, Vol. 2, p. 477.
- Roscoe, K. H., Schofield, A. W. and Wroth, C. P. (1958), "On the yielding of soils", Geotechnique, 8, pp. 22-53.
- Roscoe, K. H. and Burland, J. B. (1968), "On the generalized stress-strain behaviour of 'Wet clay'", Engineering Plasticity, Edited by Heyman, J. and Leckie, F. A., Cambridge University Press, pp. 535-609.
- Rowe, P. W. (1962), "The stress-dilatancy relation for static equilibrium of an assembly of particles in contact", Proc. Roy. Soc., A 269, pp. 500-527.
- Rowe, P. W. and Barden L. (1966), "A new consolidation cell", Geotechnique, Vol. XVI, pp. 162-170.
- Rowe, P. W. (1971), "Theoretical meaning and observed values of deformation parameters for soil", Stress-Strain Behaviour of Soils. Edited by R. H. G. Parry, G. T. Foulis & Co. Ltd., Oxfordshire.
- Rutledge, P. C. and Gould, J. P. (1973), "Movements of articulated conduits under earth dams on compressible foundations", In Casagrande's volume on embankment dam engineering, Wiley, New York, pp. 209-237.

- Sandhu, R. S. and Wilson, E. L. (1969), "Finite element analysis of seepage in elastic media", Journal of the Engrg. Mech. Div., ASCE. Vol. 95, pp. 641-652.
- Schiffman, R. L., Chen, A. T. and Jordan, J. C. (1969), "An analysis of consolidation theories", Journal of the Soil Mechanics and Foundations Division, ASCE, Vol. 95, SM1, pp. 285-312.
- Schober, W. (1967), "Behaviour of the Gepatsch Rockfill Dam", Transactions, 9th International Congress on Large Dams, Istanbul, Vol. 3, pp. 677-699.
- Seed, H. B. and Chan, C. K. (1959), "Structure and Strength Characteristics of Compacted Clays", Journal of the Soil Mechanics and Foundations Division, ASCE, Vol. 85, No. SM5, October, 1959.
- Sherard, J. L. Woodward, R. J., Gizienski, S. F. and Clevenger, W. A. (1963), Earth and Earth-rock Dams, Wiley, New York.
- Sherman, W. C. and Clough, G. W. (1968), "Embankment pore pressures during construction", Journal of the Soil Mechanics and Foundations Division, ASCE, Vol. 94, SM2, pp. 527-553.
- Simmons, J. V. (1974), "Three-dimensional analysis of Mica Dam", M. Sc. Thesis, University of Alberta, Edmonton.
- Skempton, A. W. (1954), "The pore pressure coefficients, A and B", Geotechnique, Vol. 4, No. 4, p. 143.
- Skempton, A. W. and Bjerrum, L. (1957), "A contribution to settlement analysis of foundations on clay", Geotechnique, Vol. 7, No. 4, pp. 168-178.
- Skemmer, N. A. and Hillis, S. F. (1970), "Gradation and shear Characteristics of four cohesionless soils", Canadian Geotechnical Journal, Vol. 7, pp. 62-68.
- Skemmer, N. A. (1973), "Finite element analysis of El Infiernillo Dam", Canadian Geotechnical Journal, Vol. 10, No. 2, pp. 129-144.
- Smith, I. M. and Kay, S. (1971), "Stress analysis of contractive or dilative soils", Journal of the Soil Mechanics and Foundation Division, ASCE, Vol. 97, No. SM7, pp. 981-997.
- Squier, L. R. (1967), "A study of deformations in selected rockfill and earth dams", Ph.D. Thesis, University of Illinois, Urbana, Illinois.

- Squier, L. R. (1970), "Load transfer in earth and rockfill dams", Journal of the Soil Mechanics and Foundations Division, ASCE, Vol. 96, No. SM1, January, 1970, pp. 213-233.
- Timenshenko, S. and Goodier, J. N. (1951), Theory of Elasticity, McGraw-Hill, New York.
- Vesic, A. S. and Clough, G. W. (1968), "Behaviour of granular materials under high stresses", Journal of the Soil Mechanics and Foundations Division, ASCE, Vol. 94, SM3, May, 1968, pp. 661-688.
- Ward, W. H., Samuels, S. G. and Butler, M. E. (1959), "Further studies of the properties of London Clay", Geotechnique, Vol. 9, No. 2, pp. 33-58.
- Ward, W. H., Mansland, A. and Samuels, S. G. (1965), "Properties of the London Clay at the Ashford Common Shaft", Geotechnique, Vol. 15, No. 4, pp. 321-344.
- Webster, J. L. (1970), "Mica Dam designed with special attention to control of cracking", Trans. 10th Int. Congr. on Large Dams, Montreal, Q36-R30, 1, pp. 487-510.
- Webster, J. L. and Lowe, W. I. (1971), "Instrumentation for earth and rock-fill dams", Proc. Int. Conf. on Pumped Storage Development, American Water Resources Association, pp. 238-247.
- Wilson, E. L. and Nickell, R. E. (1966), Application of the finite element method to heat conduction analysis", Nuclear Engineering and Design, North-Holland Publishing Co., Amsterdam, Vol. 4, pp. 276-286.
- Wilson, S. D. (1950), "Small soil compaction apparatus duplicates field results closely", Engineering News-Record, November 2, pp. 34-36.
- Wilson, S. D. (1973), "Deformation of earth and rockfill dams", Casagrande's Volume on Embankment Dam Engineering, Edited by Hirschfeld, R. C. and Poulos, S. J., Wiley, New York, pp. 365-418.
- Zegarra, E. J. (1958), Discussion on "Stabilization of materials by compaction", by Turnbull, W. J. and Foster, C. R. ASCE Transaction, Vol. 123, paper No. 2907, pp. 1-26.
- Zienkiewicz, O. C. and Cheung, Y. K. (1967), "The finite element method in structural and continuum mechanics", McGraw-Hill, London.

APPENDICES

APPENDIX A

LABORATORY TEST RESULTS

This appendix presents the results of the tests described in Chapter II. The results of oedometer compression partial dissipation tests are given in Figs. A.1 to A.16. Figs. A.17 to A.19 are oedometer compression drained test results. The subsequent figures are the results of isotropic compression partial dissipation tests. Designation used for each sample here has been listed in Table 2.1. For each partial dissipation test performed the pore water pressure at the base, the total stress and the effective stress versus strain of the sample are presented.

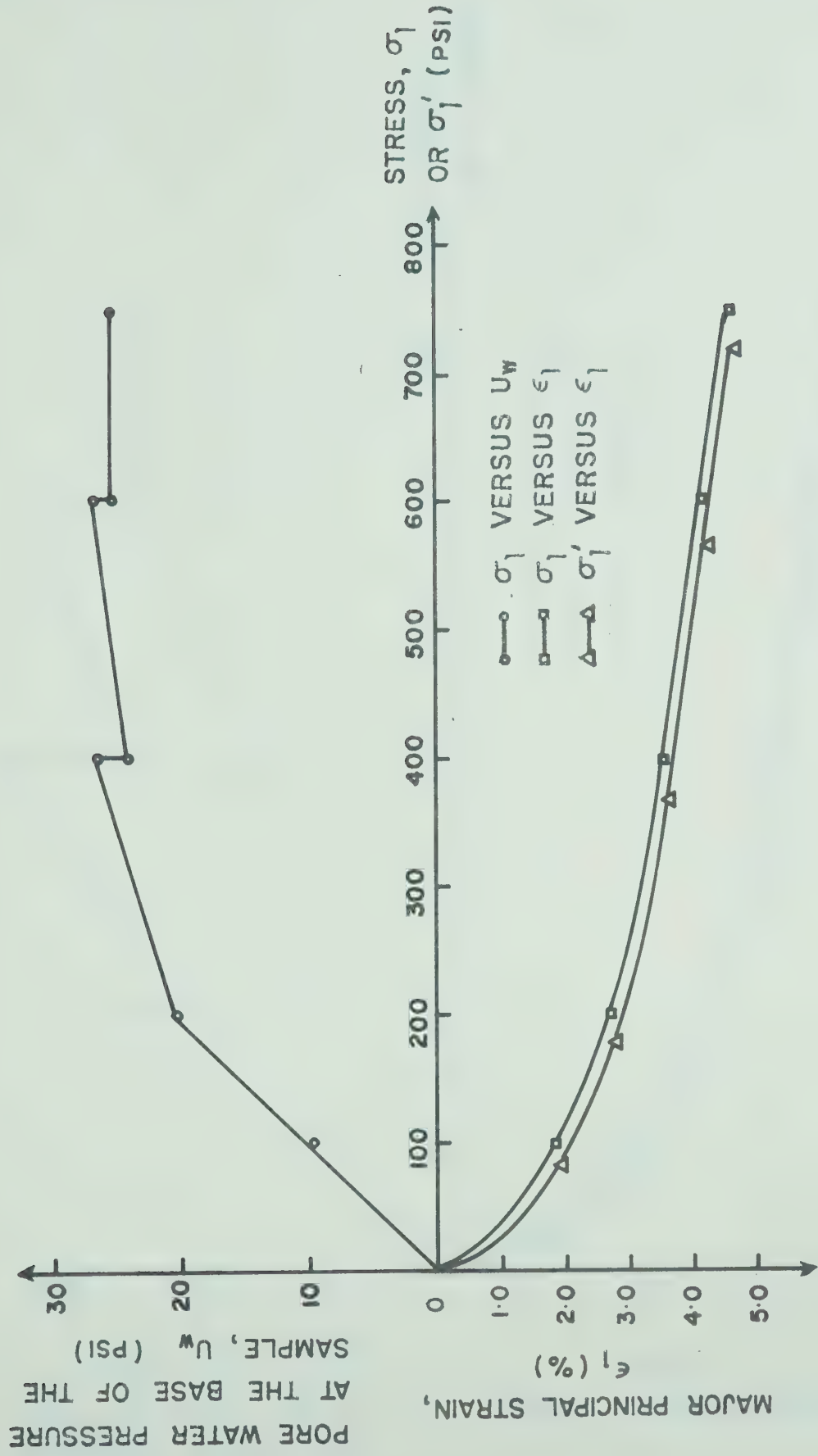


Fig. A.1 Oedometer Compression Partial Dissipation Test (0W-1)

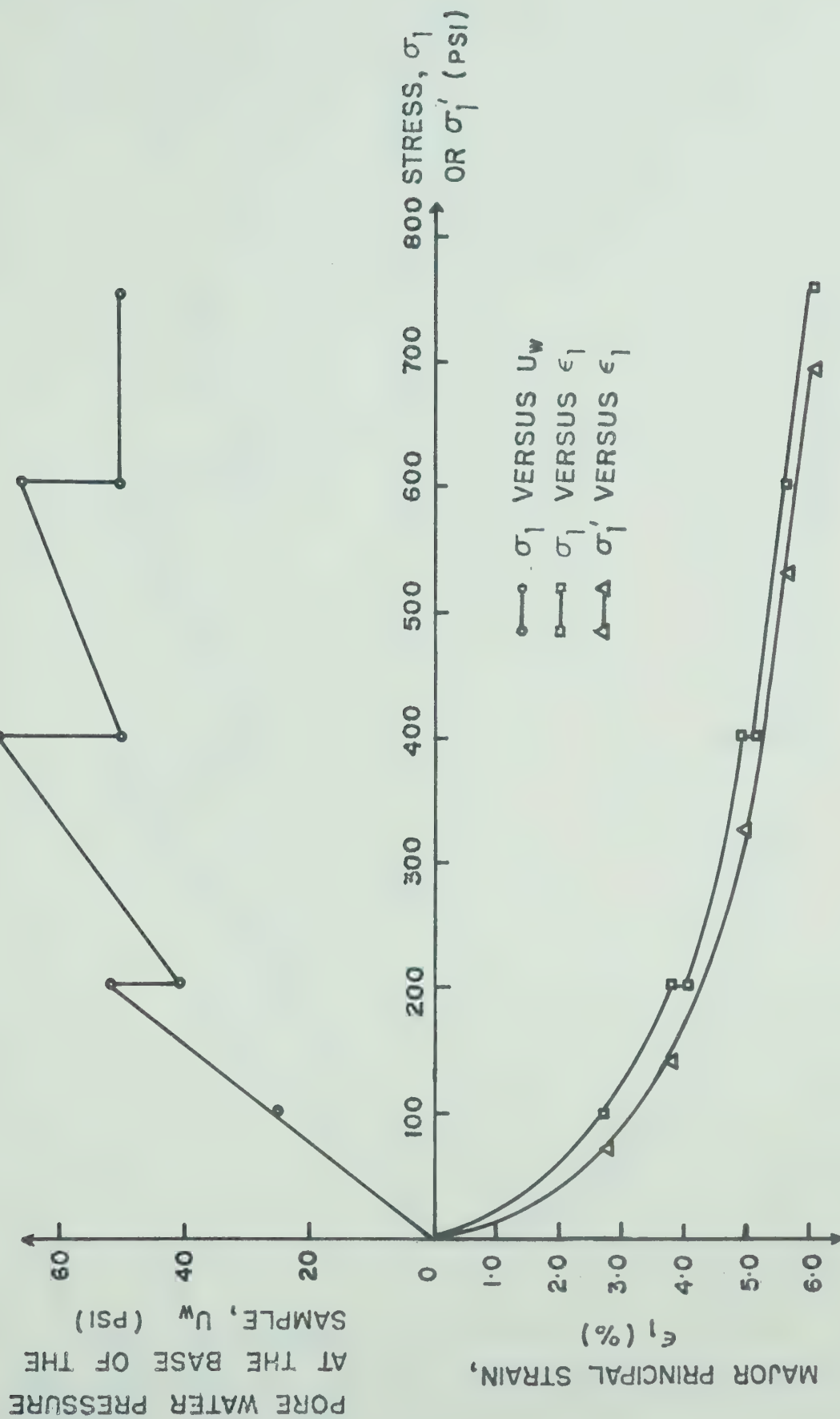


Fig. A.2 Oedometer Compression Partial Dissipation Test (0W-2)

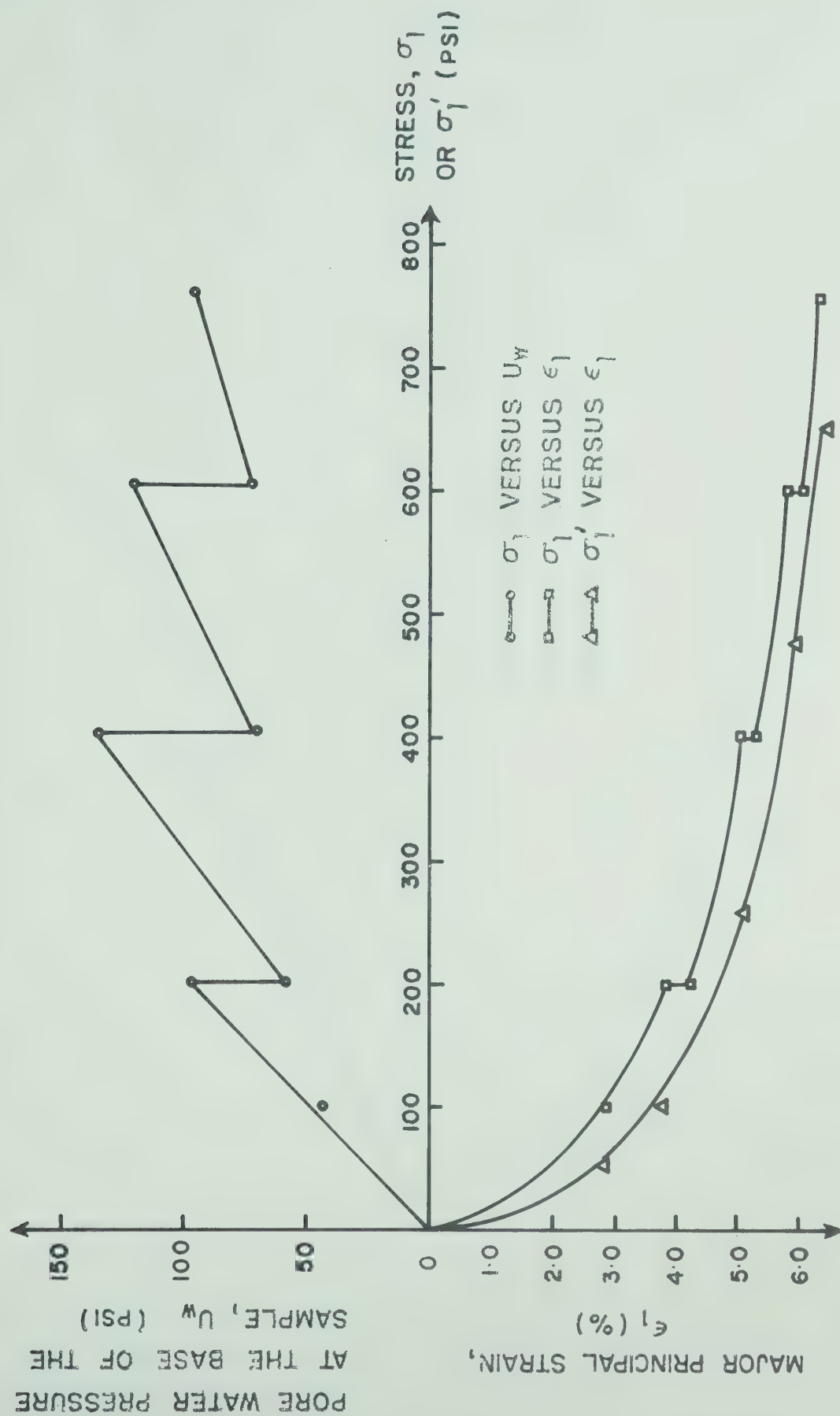


Fig. A.3 Oedometer Compression Partial Dissipation Test (OW-3)

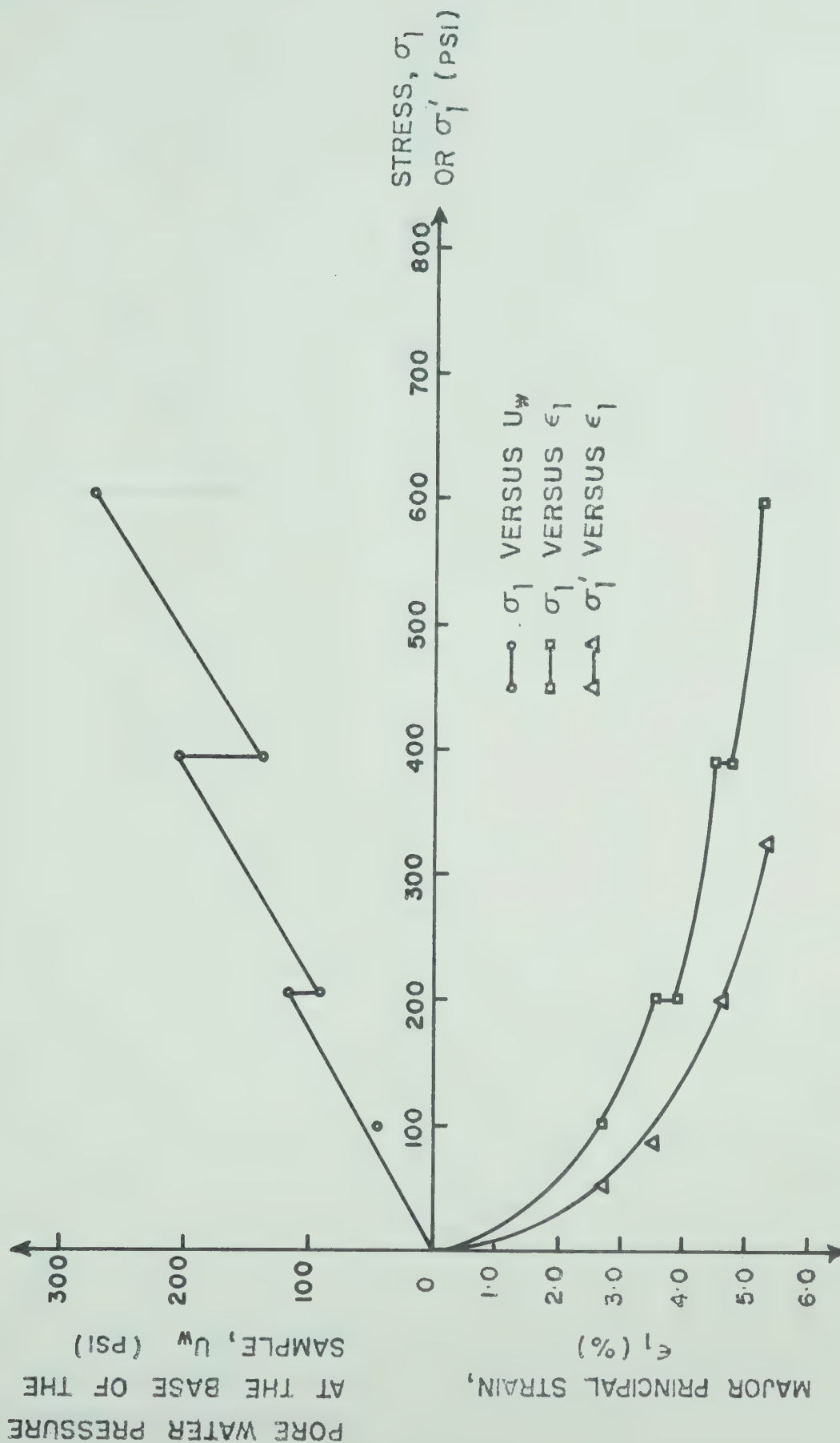


Fig. A.4 Oedometer Compression Partial Dissipation Test (OW-4)

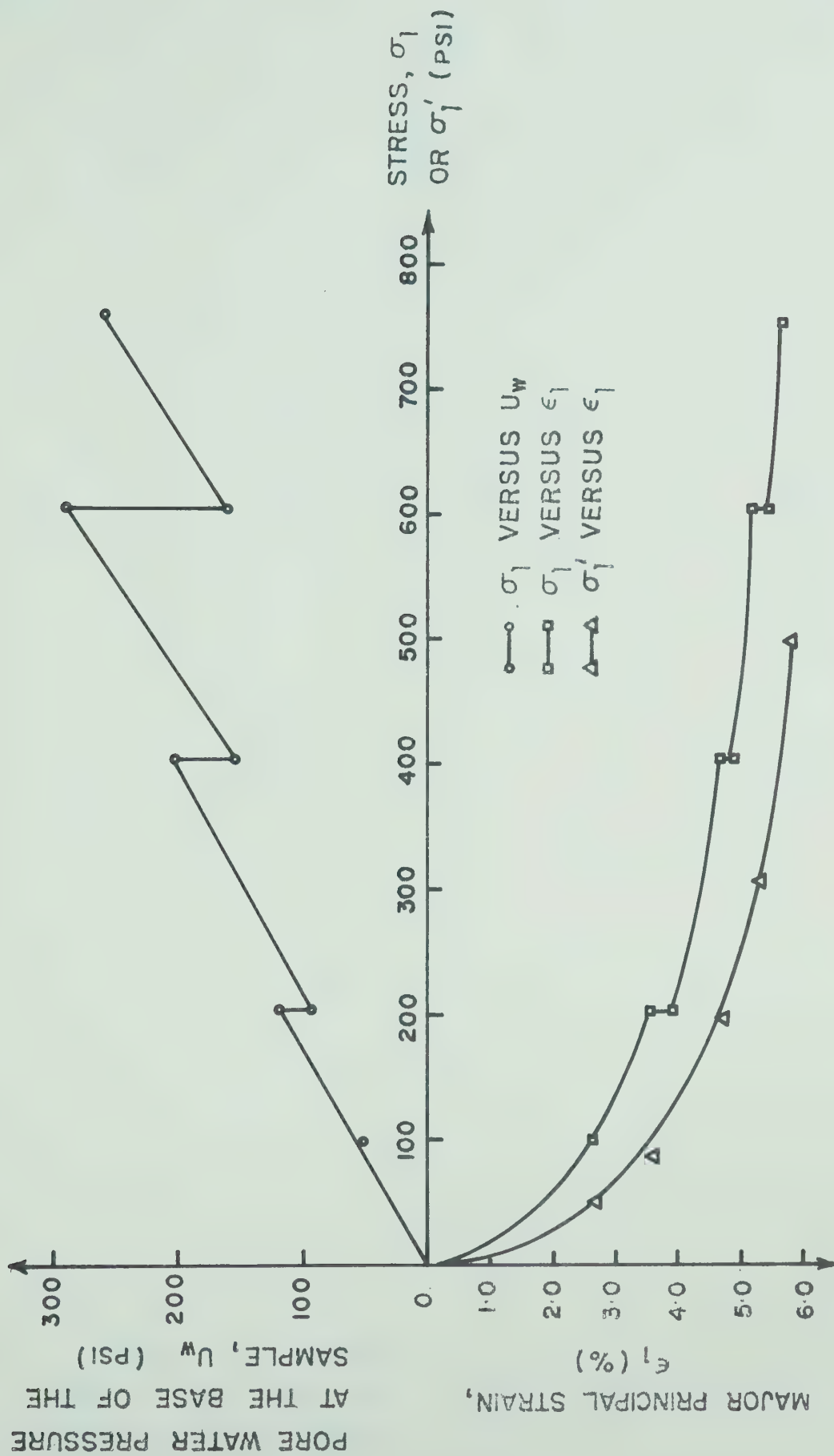


Fig. A.5 Oedometer Compression Partial Dissipation Test (OW-5)

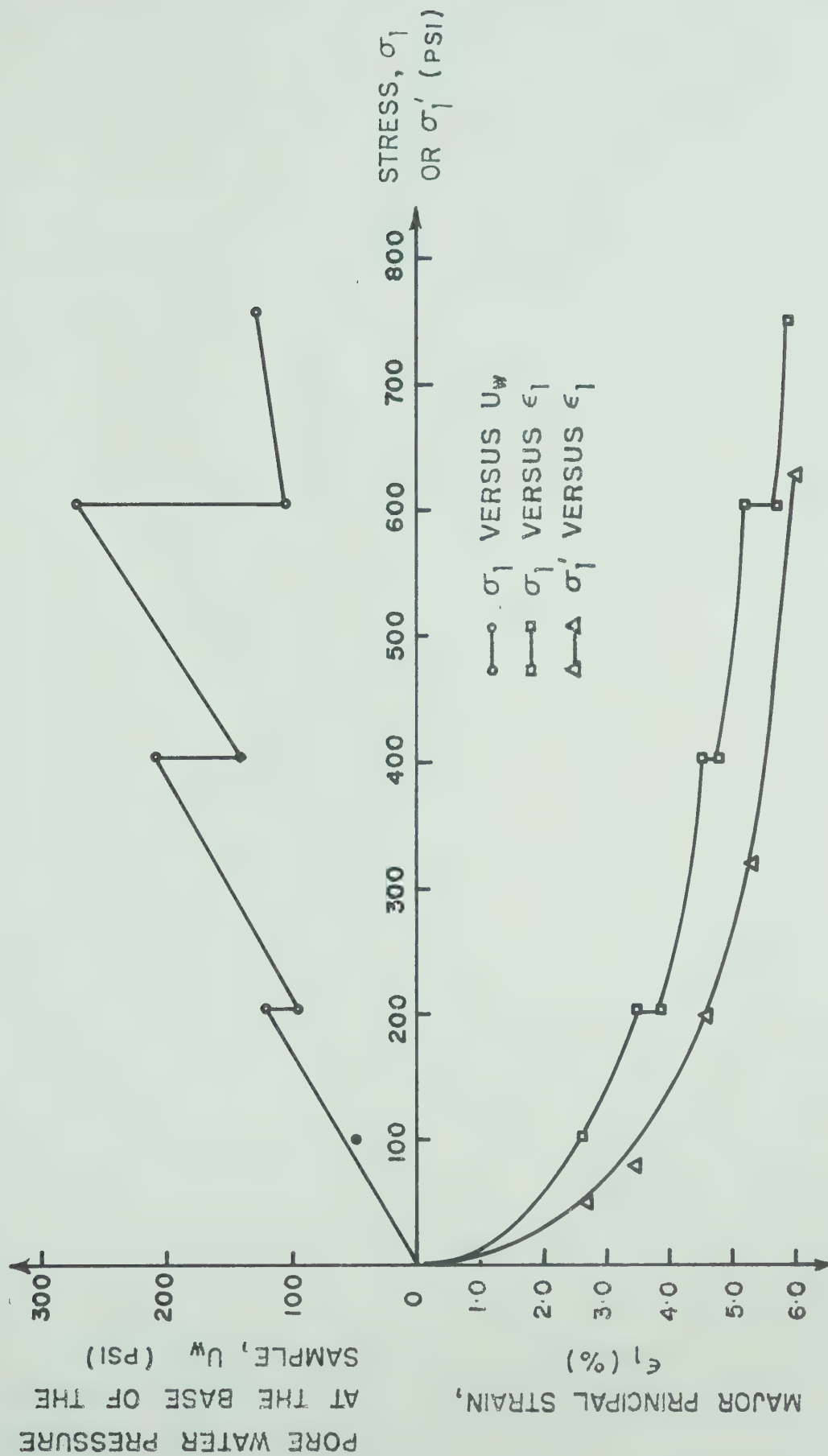


Fig. A.6 Oedometer Compression Partial Dissipation Test (0W-6)

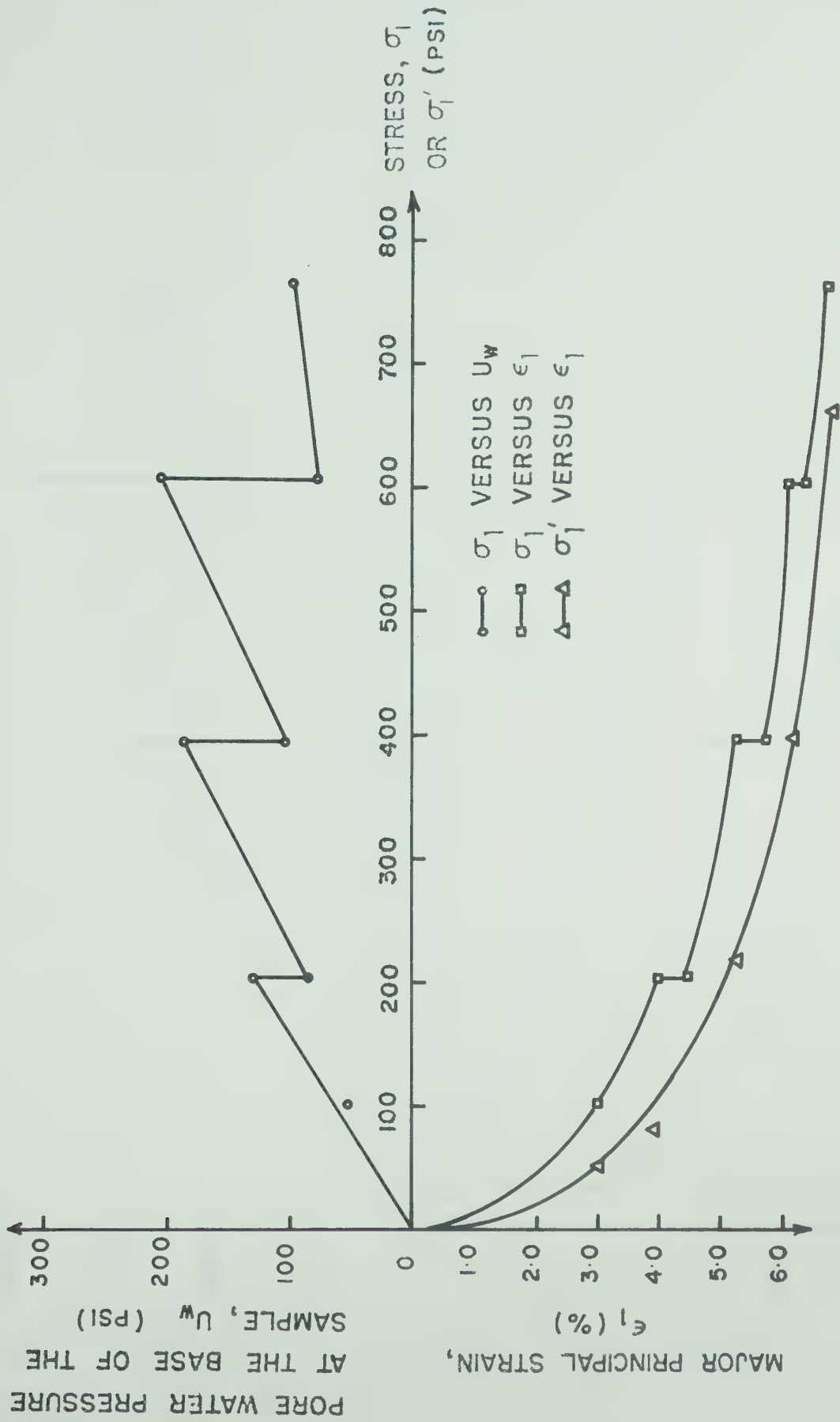


Fig. A.7 Oedometer Compression Partial Dissipation Test (0W-7)

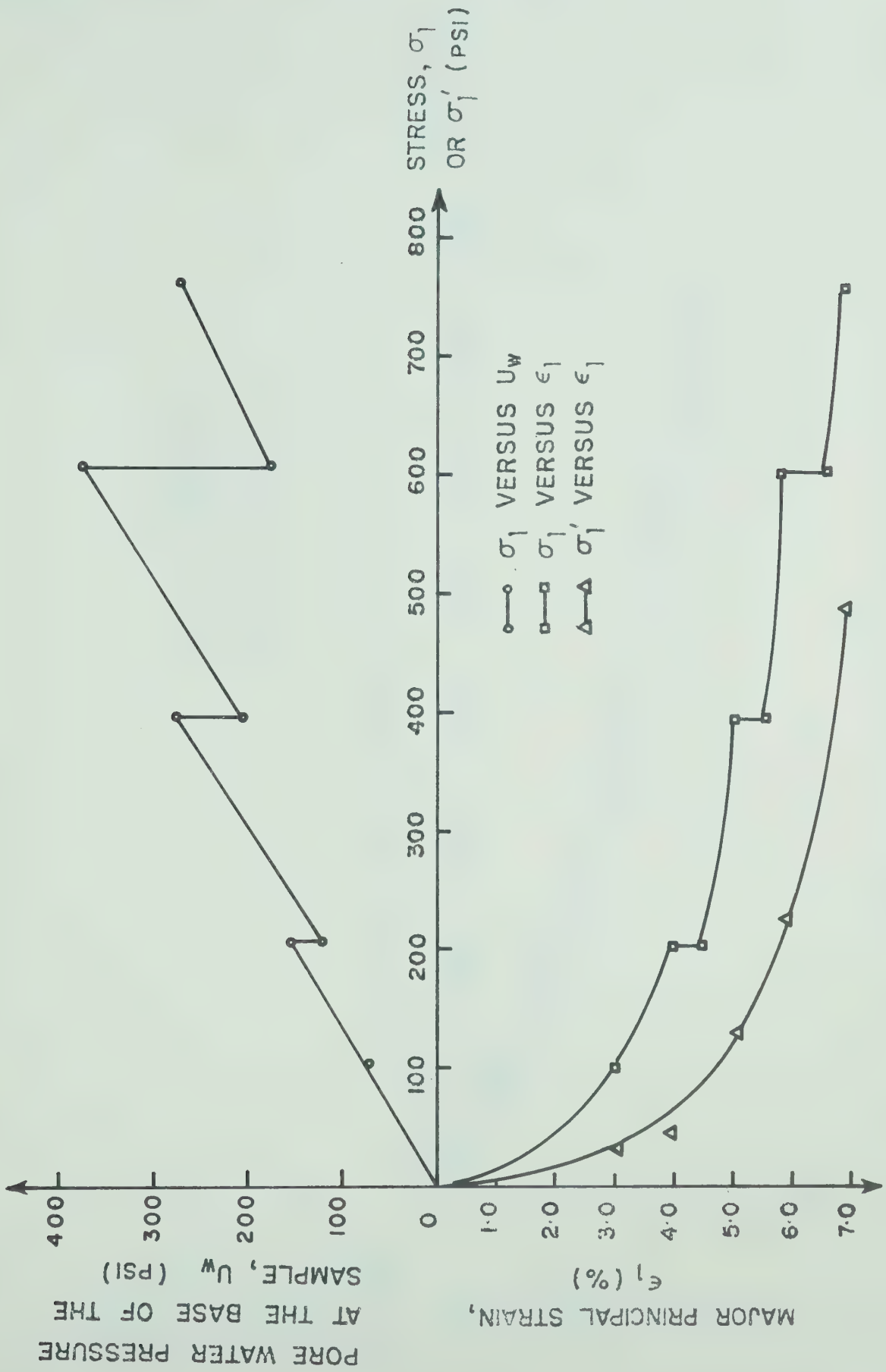


Fig. A.8 Oedometer Compression Partial Dissipation Test (OW-8)

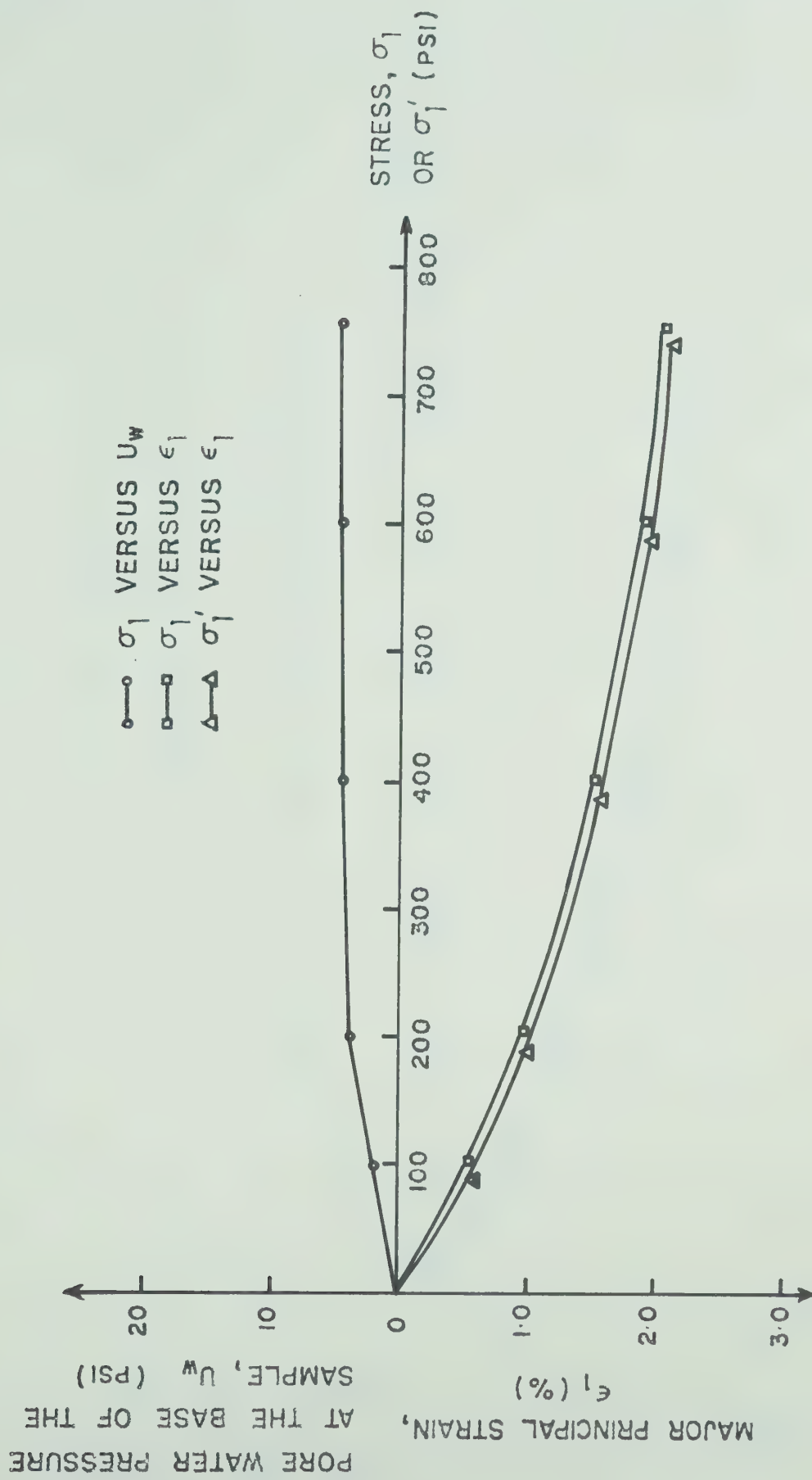


Fig. A.9 Oedometer Compression Partial Dissipation Test (OD-1)

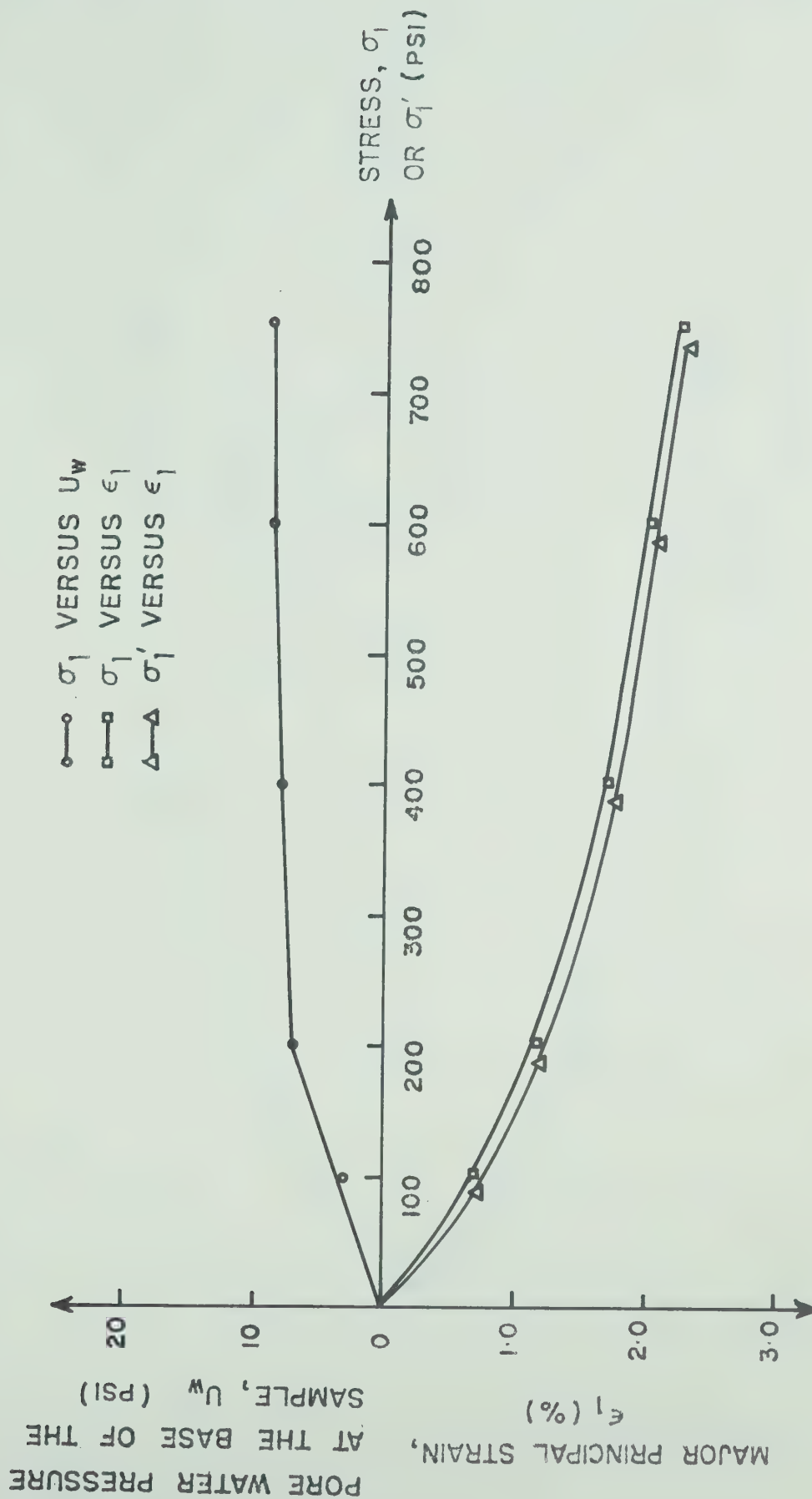


Fig. A.10 Oedometer Compression Partial Dissipation Test (OD-2)

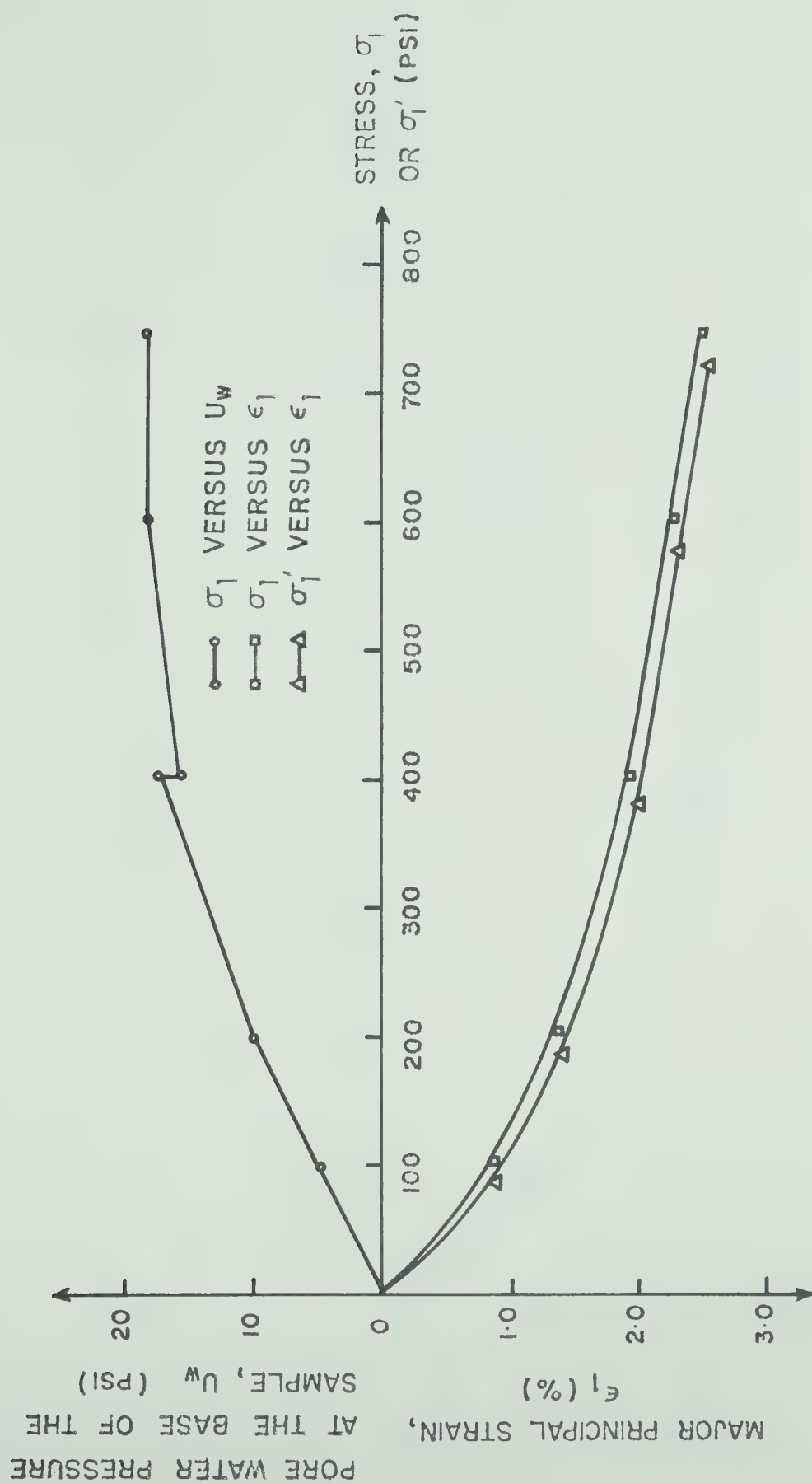


Fig. A.11 Oedometer Compression Partial Dissipation Test (OD-3)

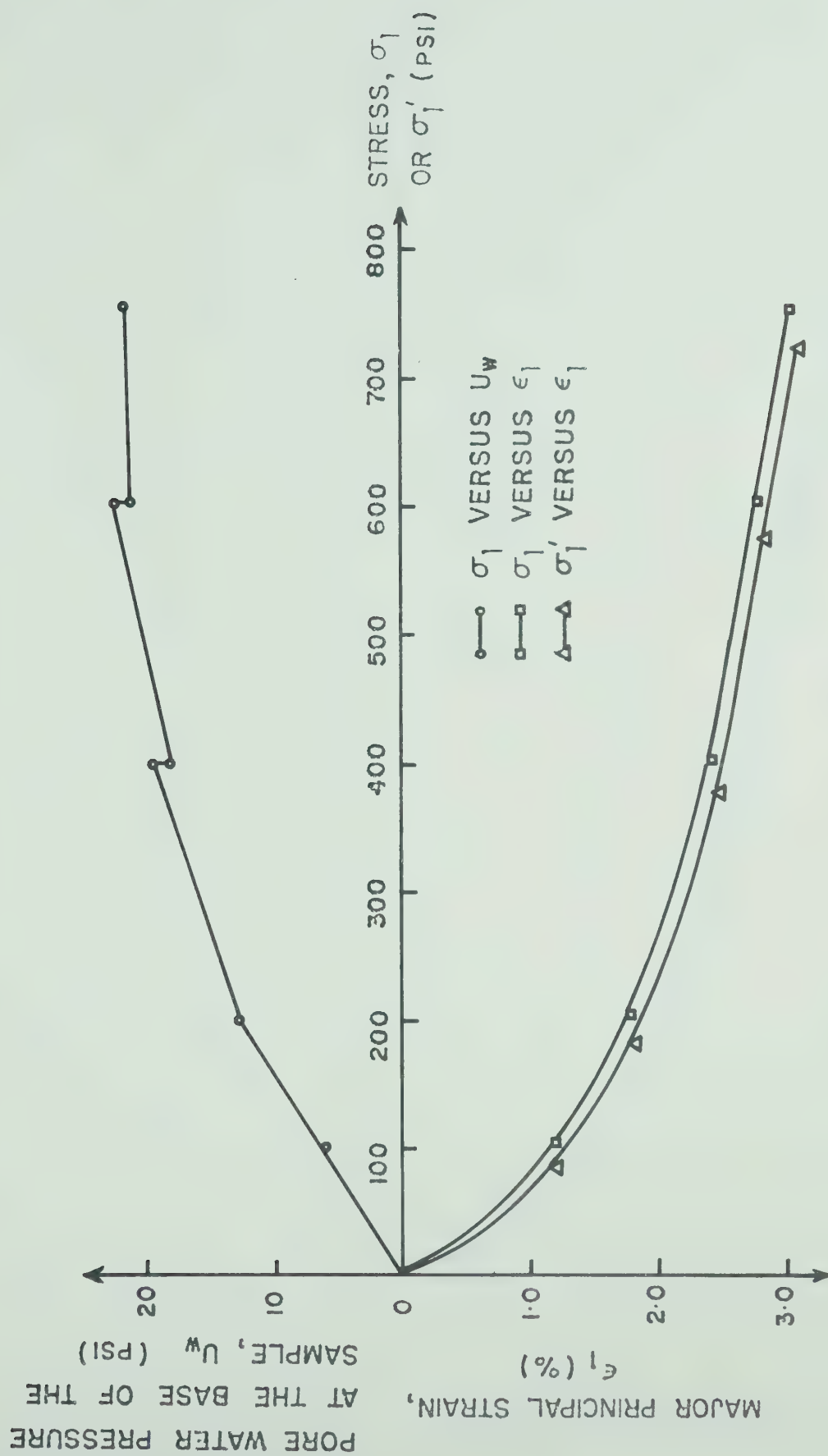


Fig. A.12 Oedometer Compression Partial Dissipation Test (OD-4)

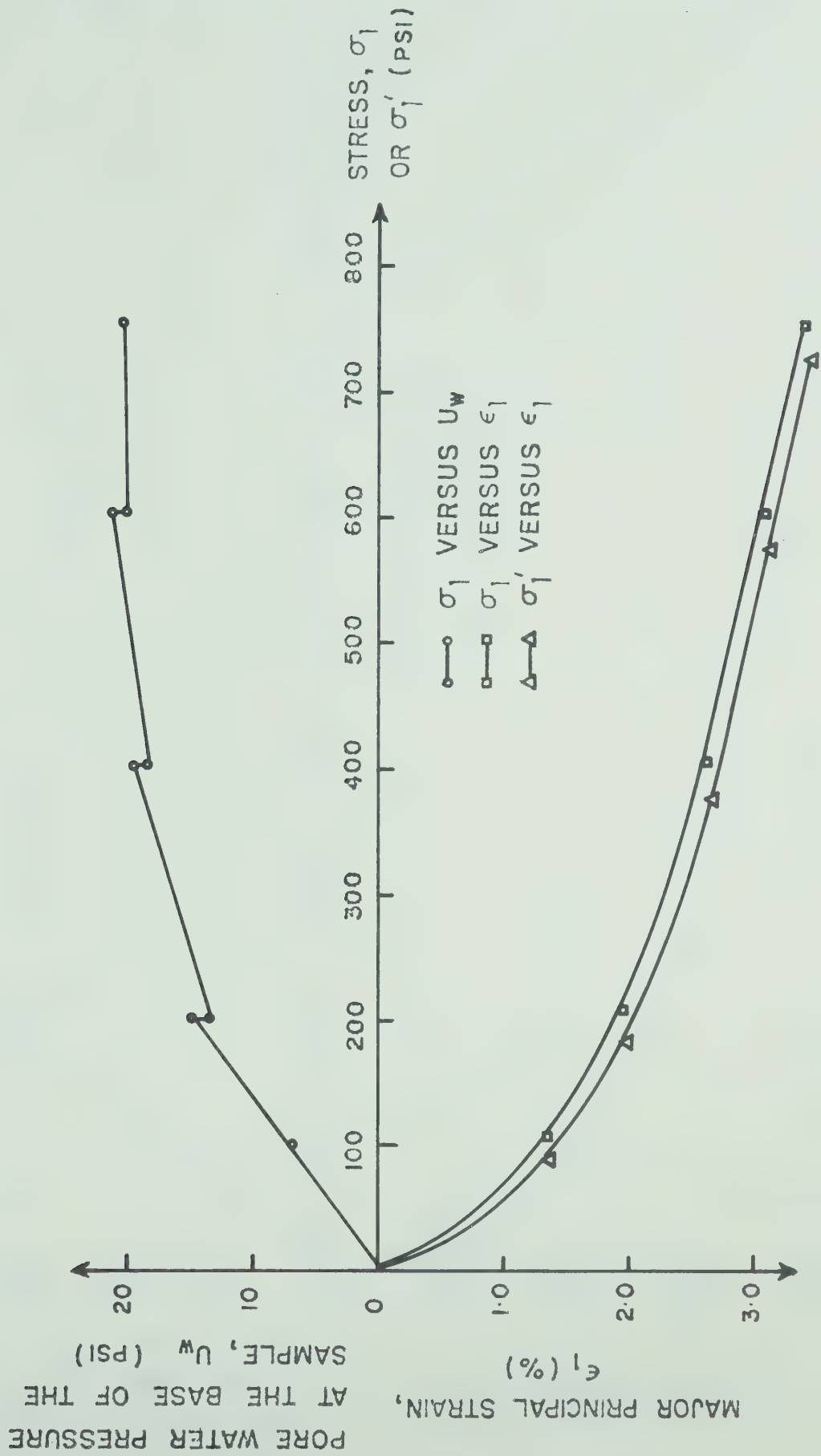


Fig. A.13 Oedometer Compression Partial Dissipation Test (OD-5)

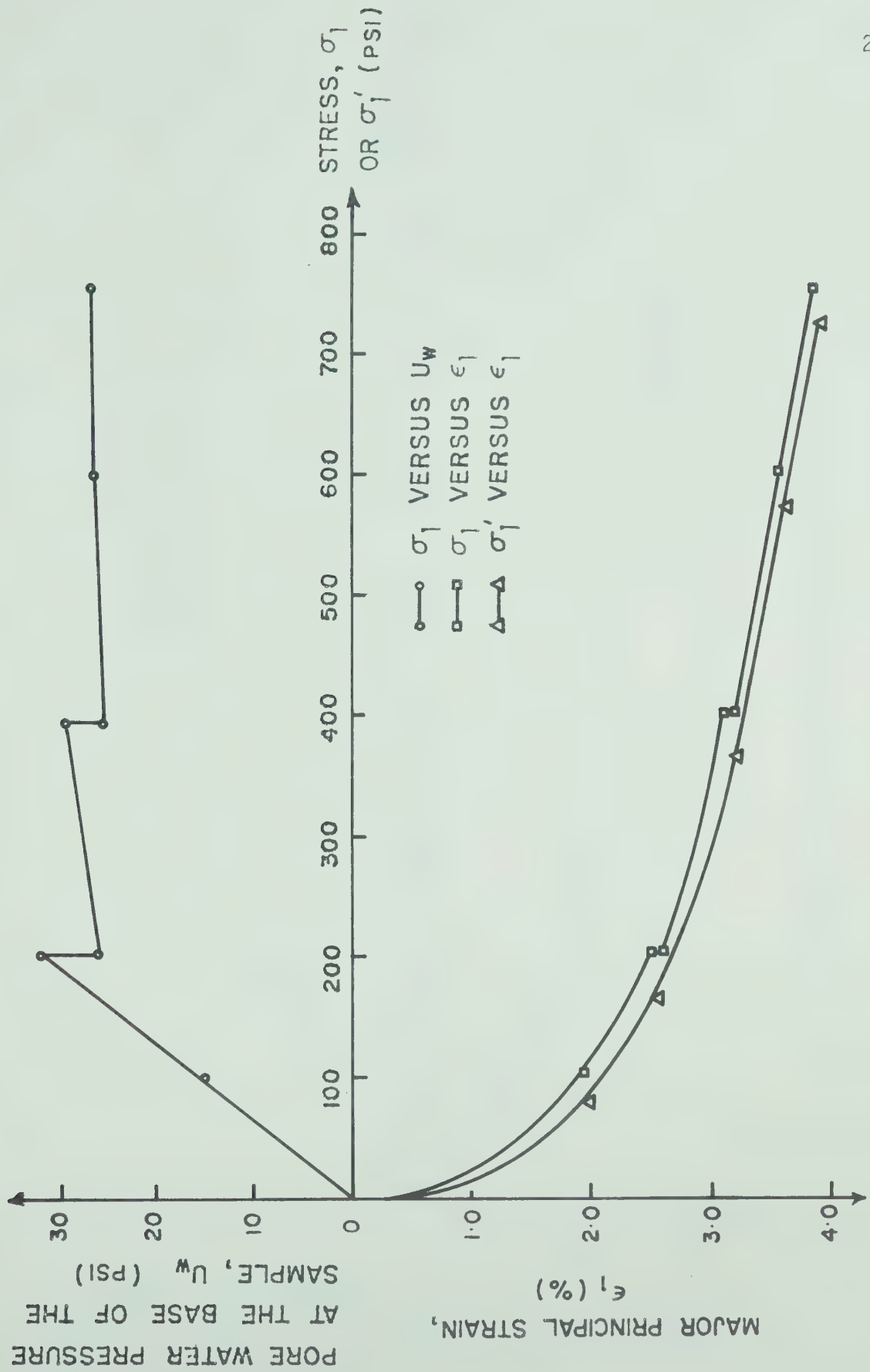


Fig. A.14 Oedometer Compression Partial Dissipation Test (OD-6)

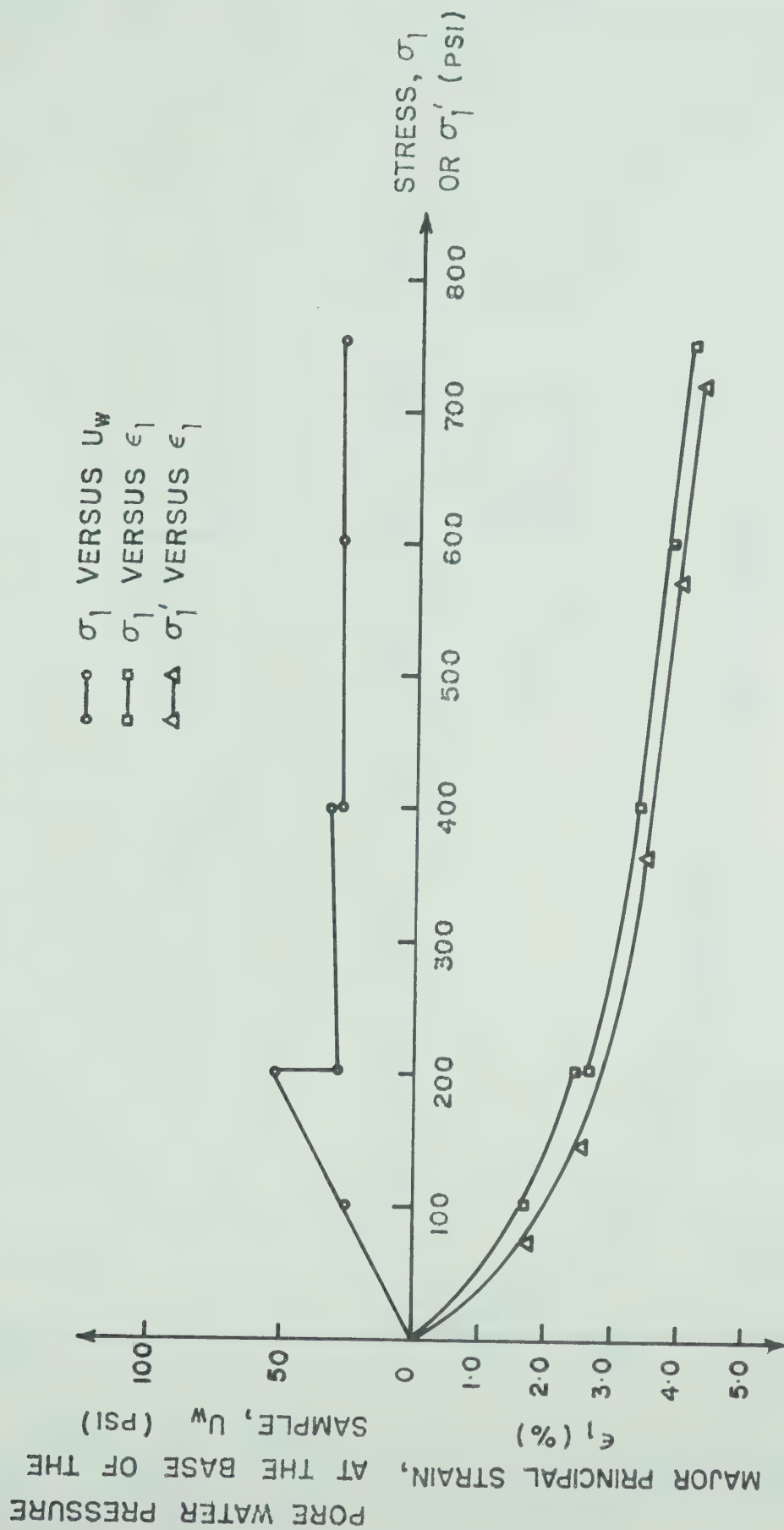


Fig. A.15 Oedometer Compression Partial Dissipation Test (OD-7)

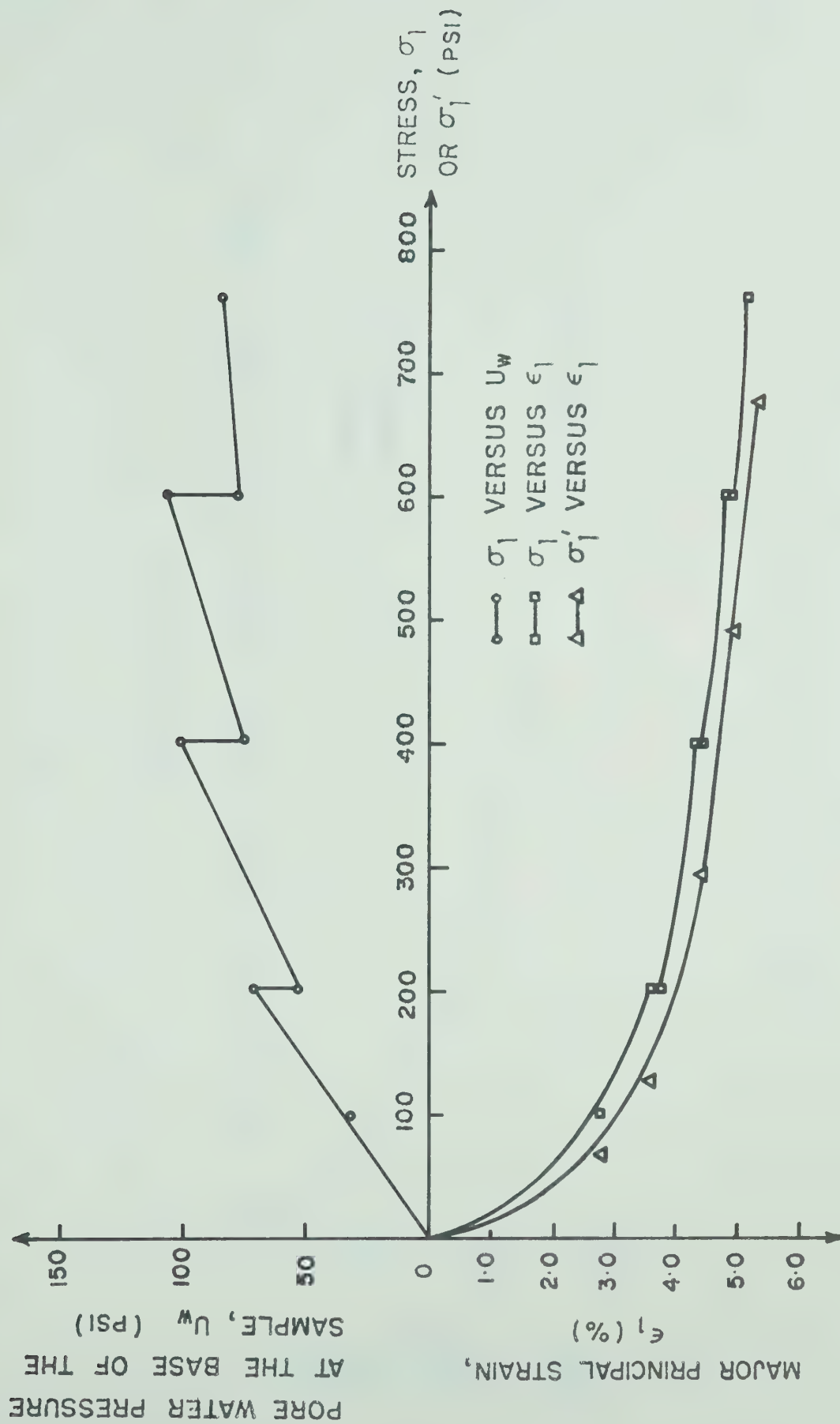


Fig. A.16 Oedometer Compression Partial Dissipation Test (OD-8)

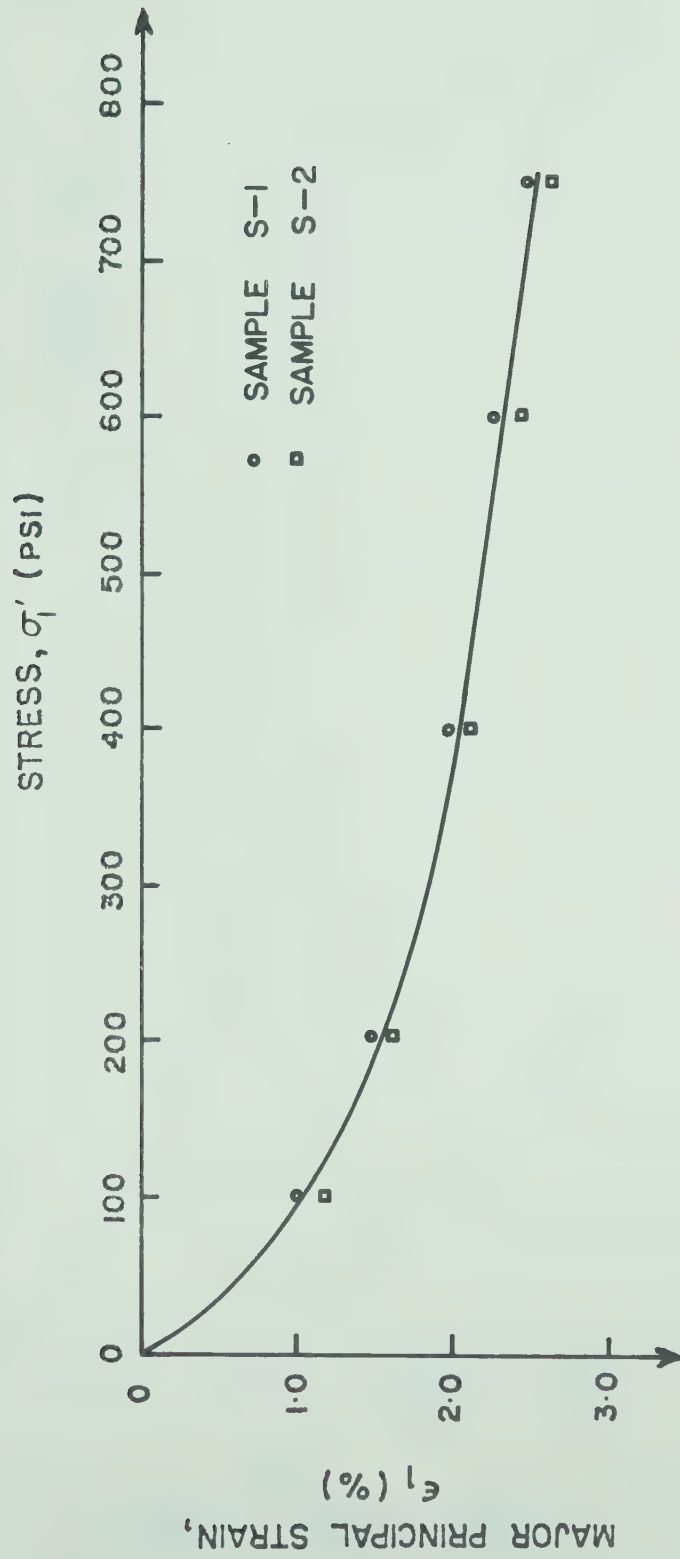


Fig. A.17 Oedometer Compression Drained Tests (S-1 and S-2)

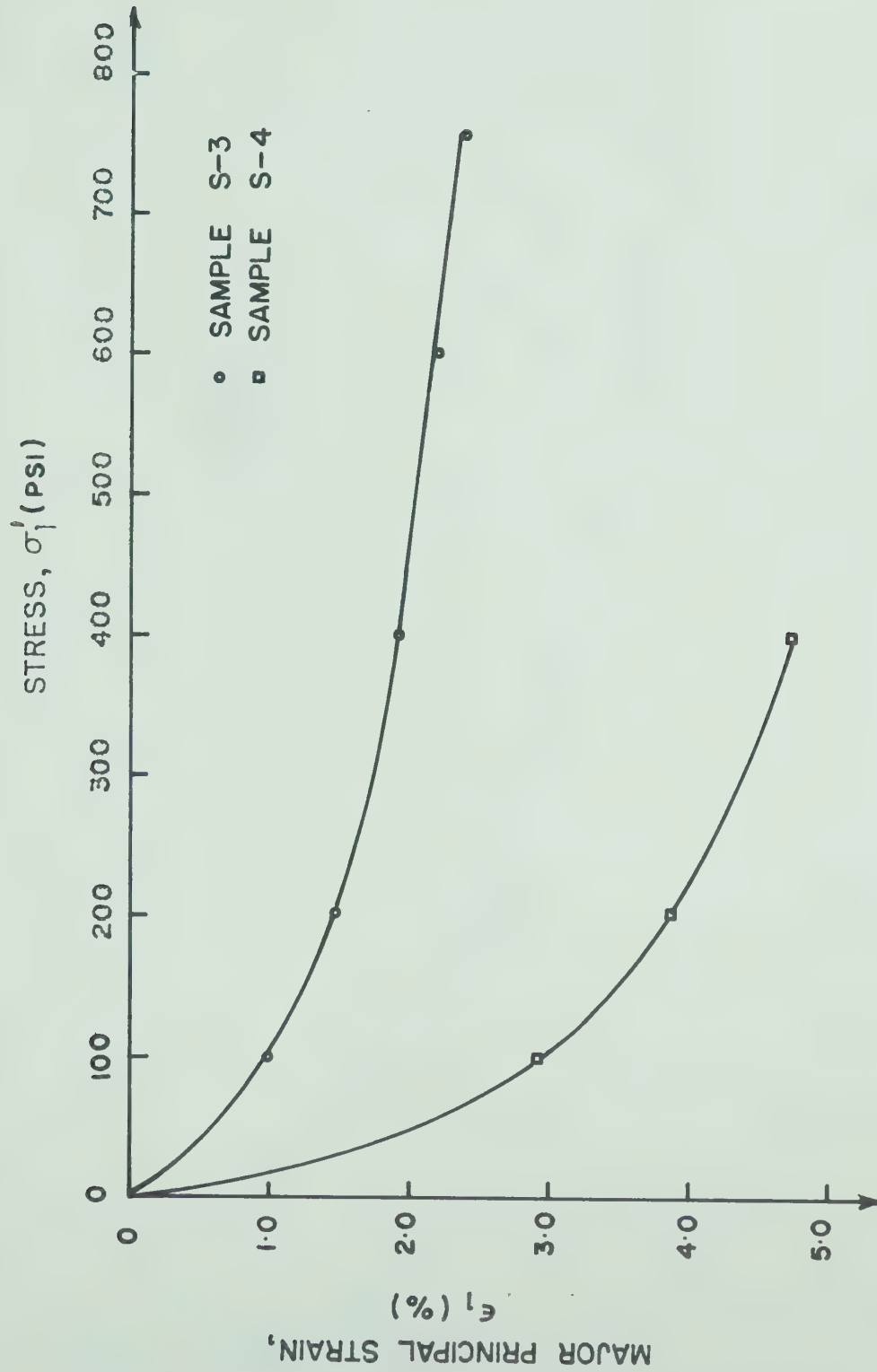


Fig. A.18 Oedometer Compression Drained Tests (S-3 and S-4)

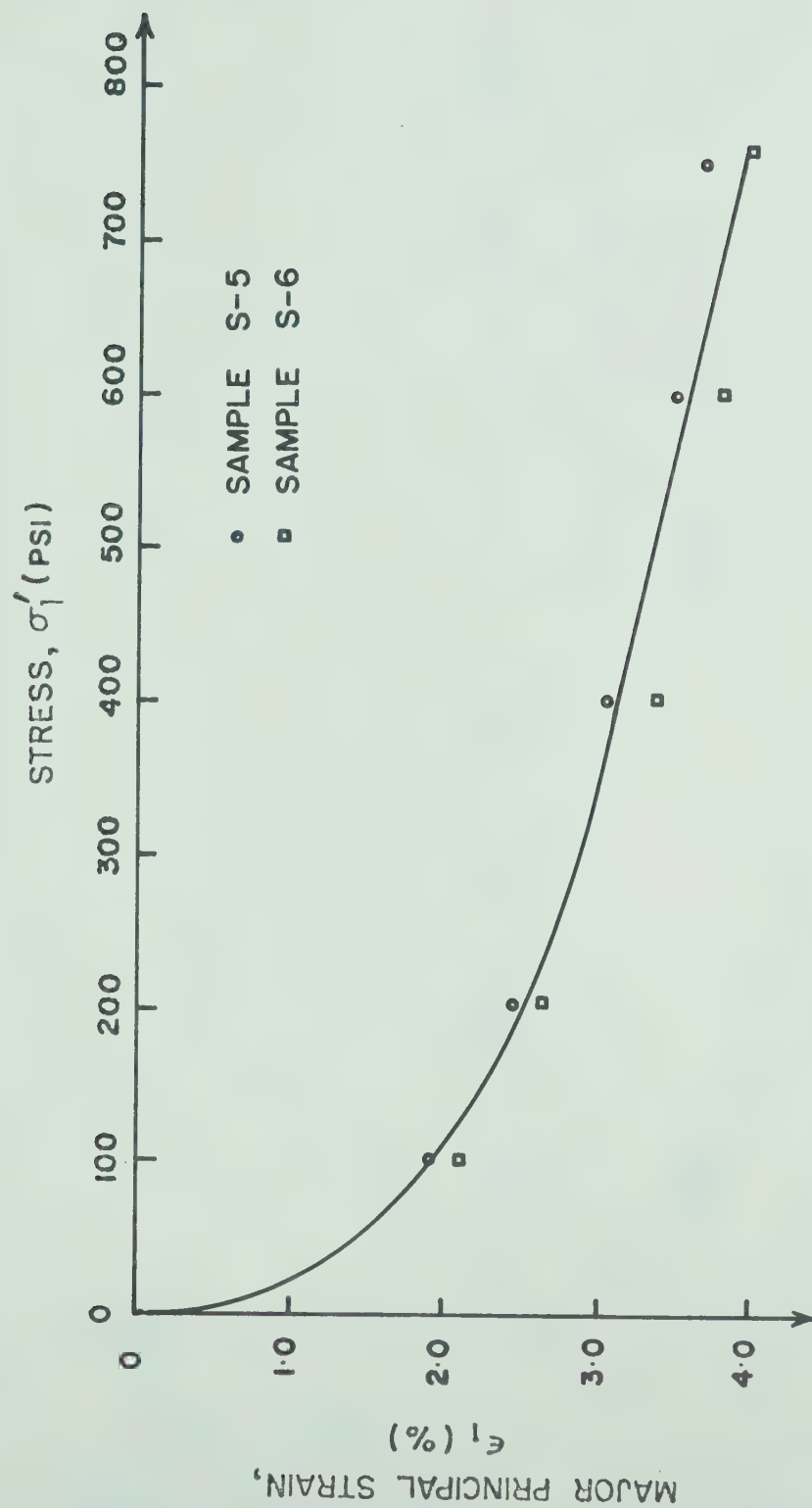


Fig. A.19 Oedometer Compression Drained Tests (S-5 and S-6)

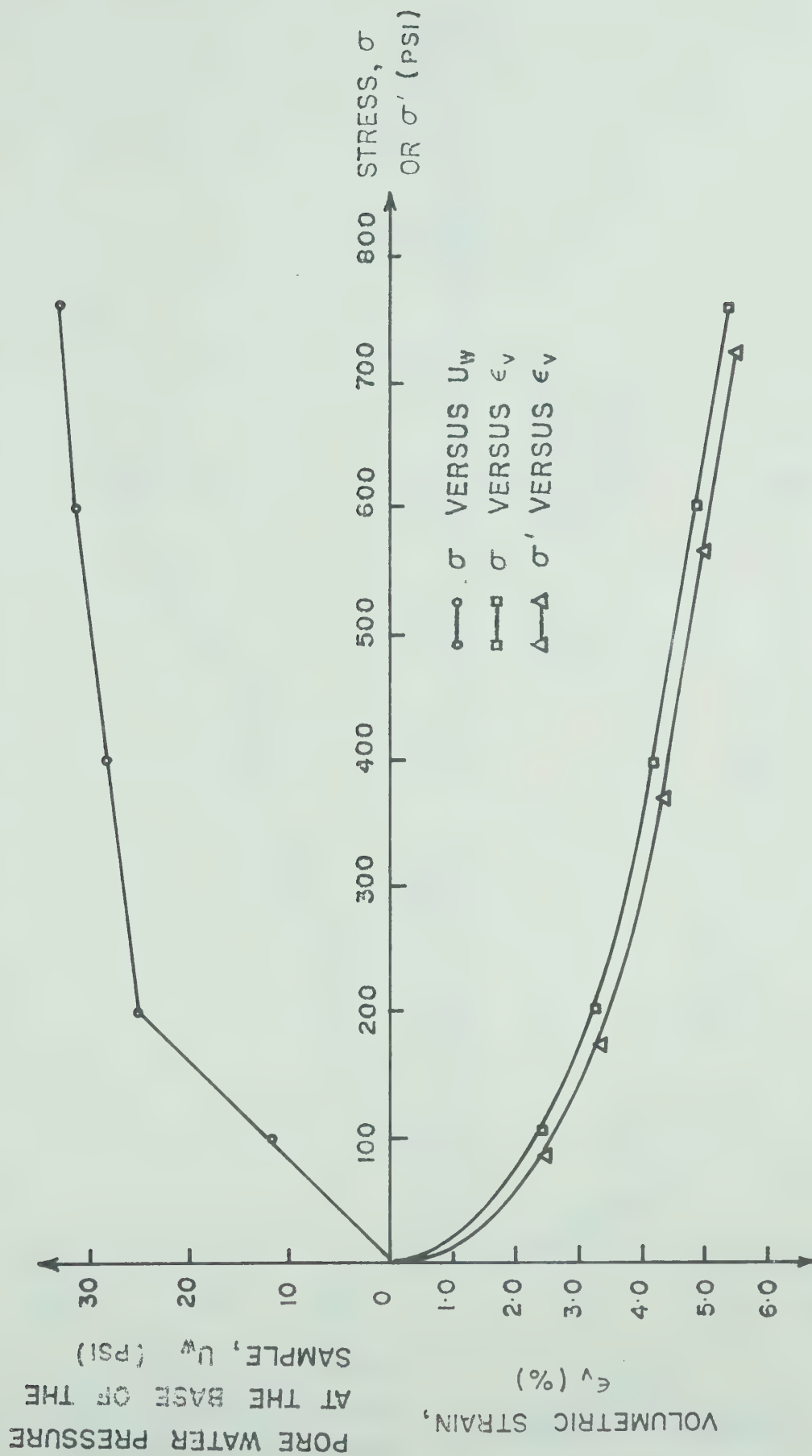


Fig. A.20 Isotropic Compression Partial Dissipation Test (HW-1)

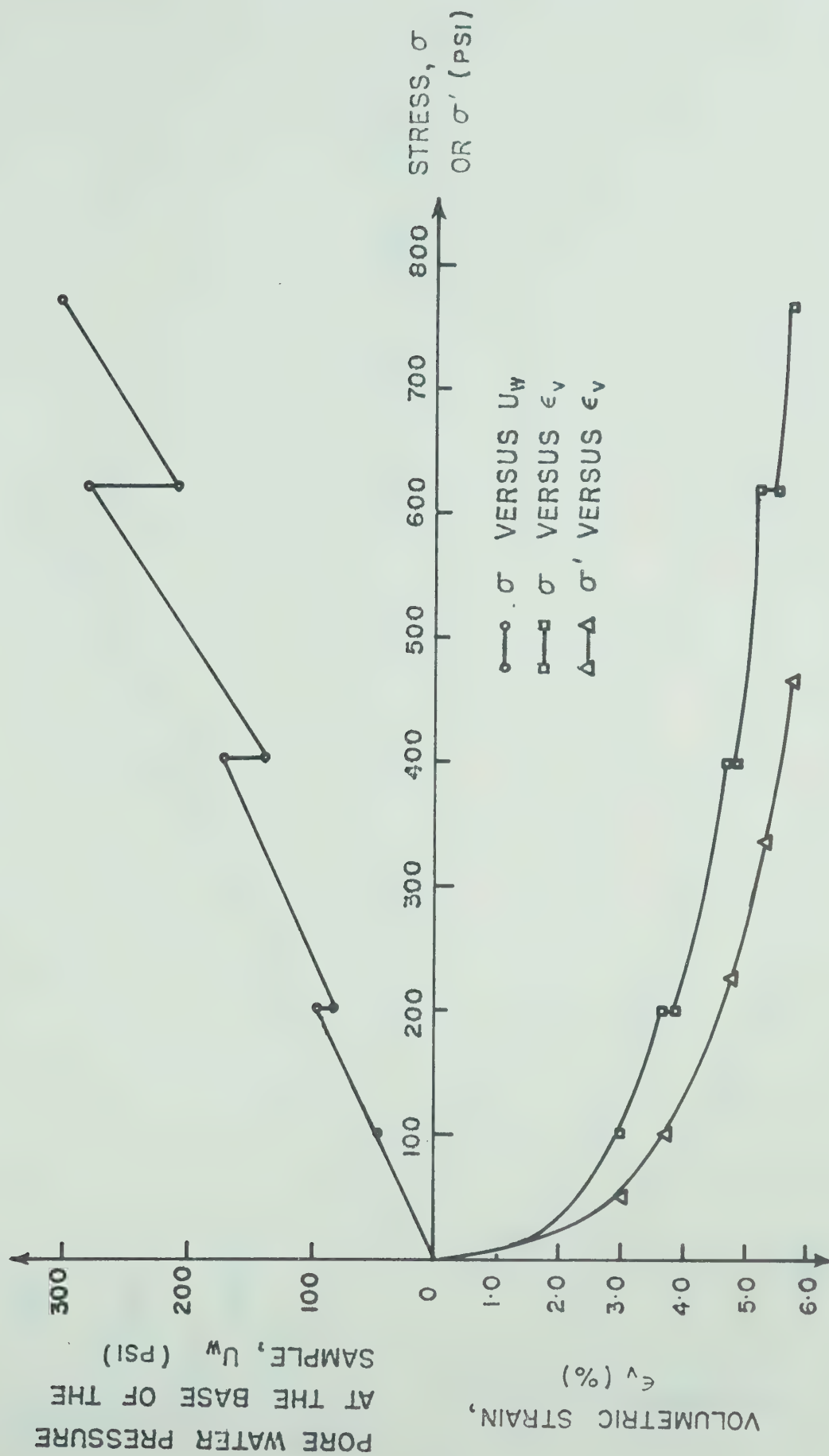


Fig. A.21 Isotropic Compression Partial Dissipation Test (IIW-2)

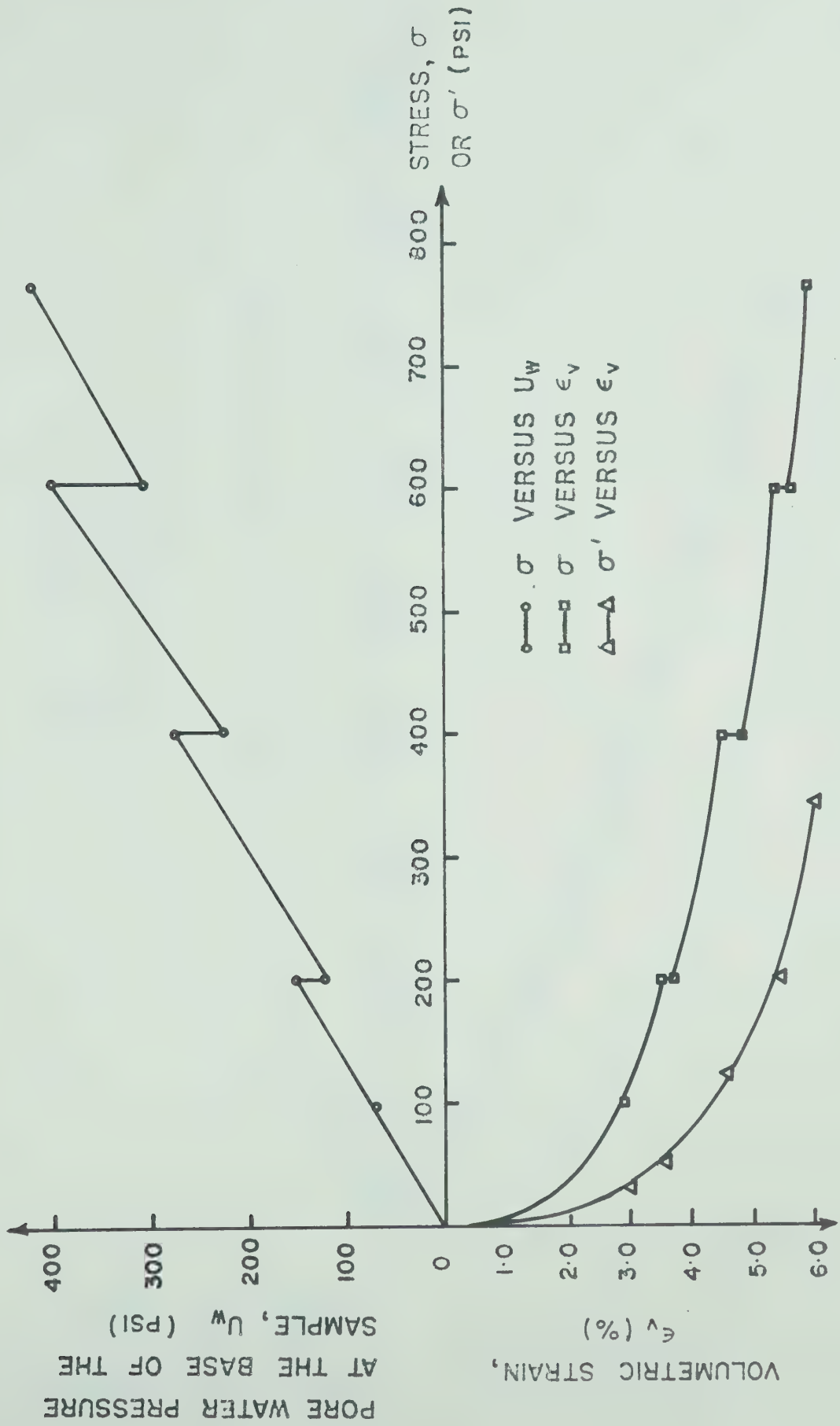


Fig. A.22 Isotropic Compression Partial Dissipation Test (HW-3)

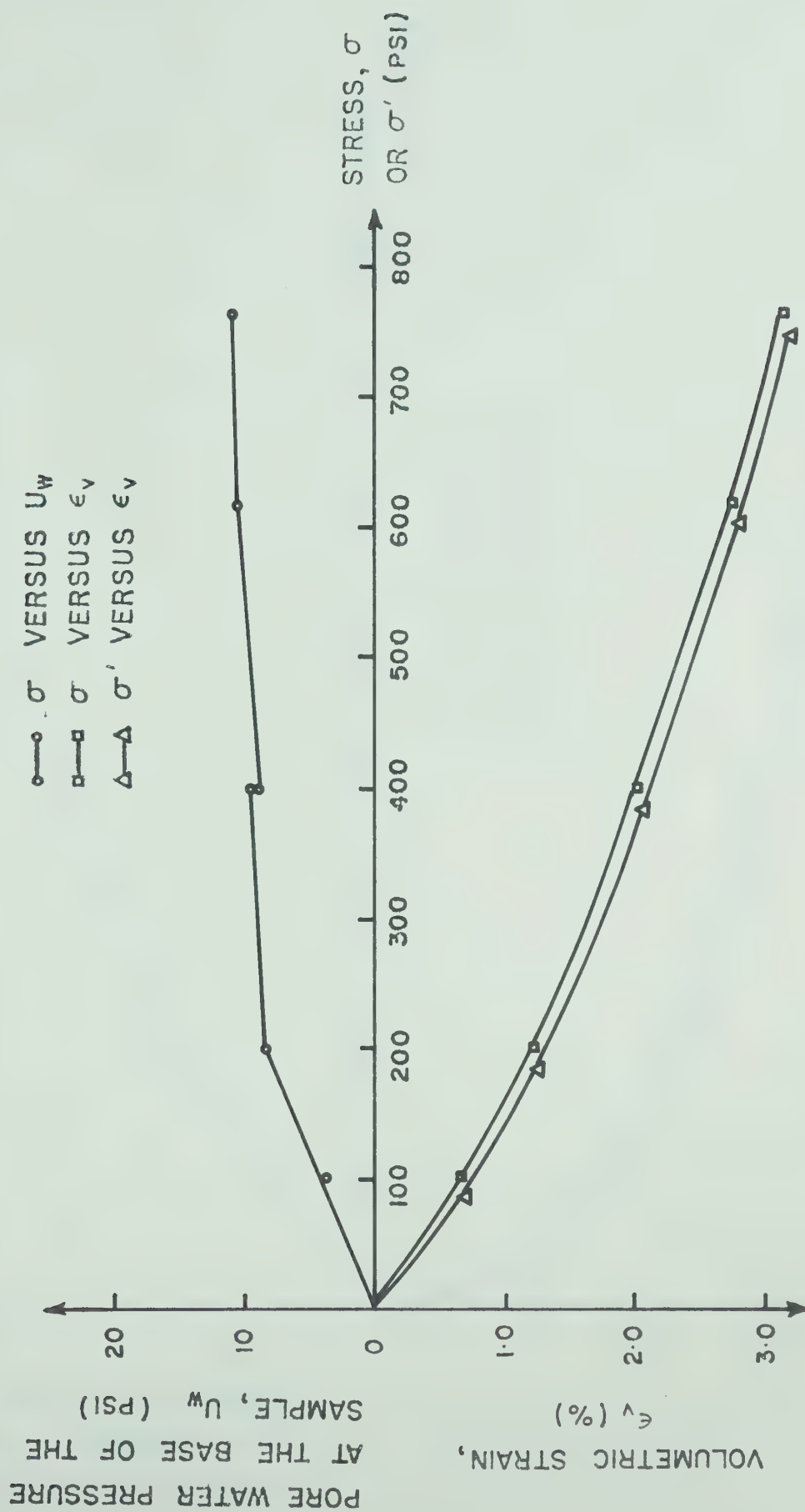


Fig. A.23 Isotropic Compression Partial Dissipation Test (HD-1)

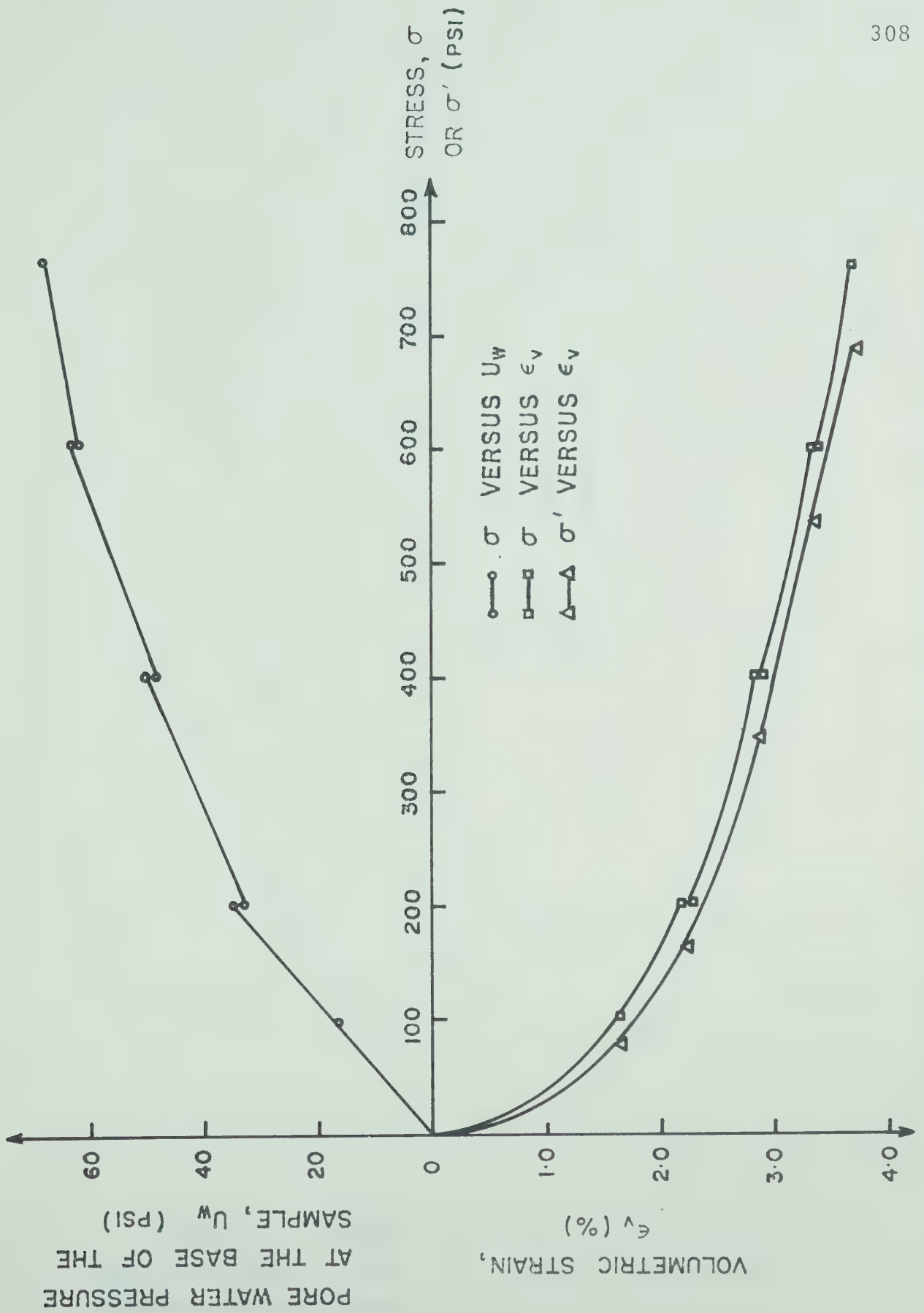


Fig. A.24 Isotropic Compression Partial Dissipation Test (HD-2)

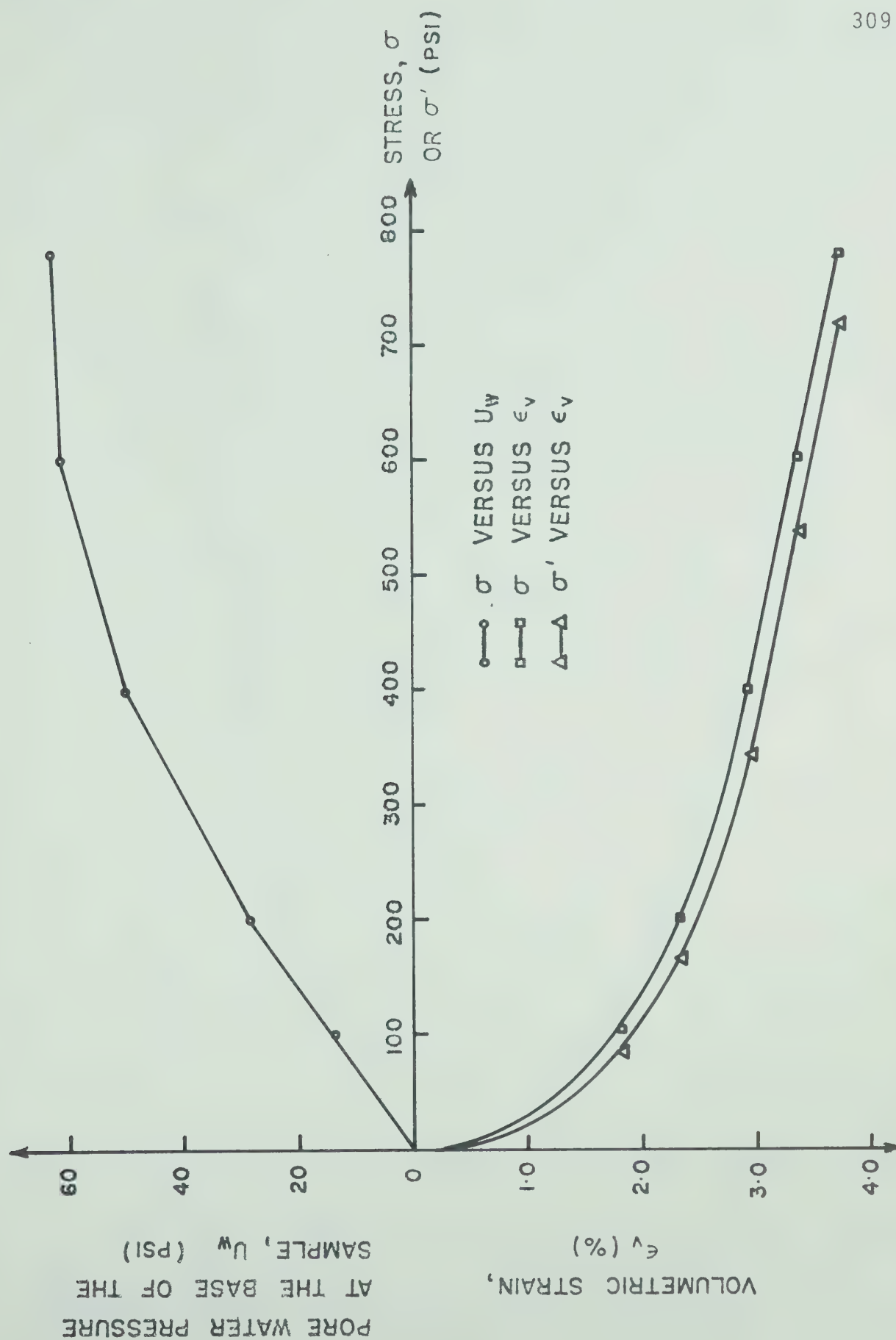


Fig. A.25 Isotropic Compression Partial Dissipation Test (HD-3)

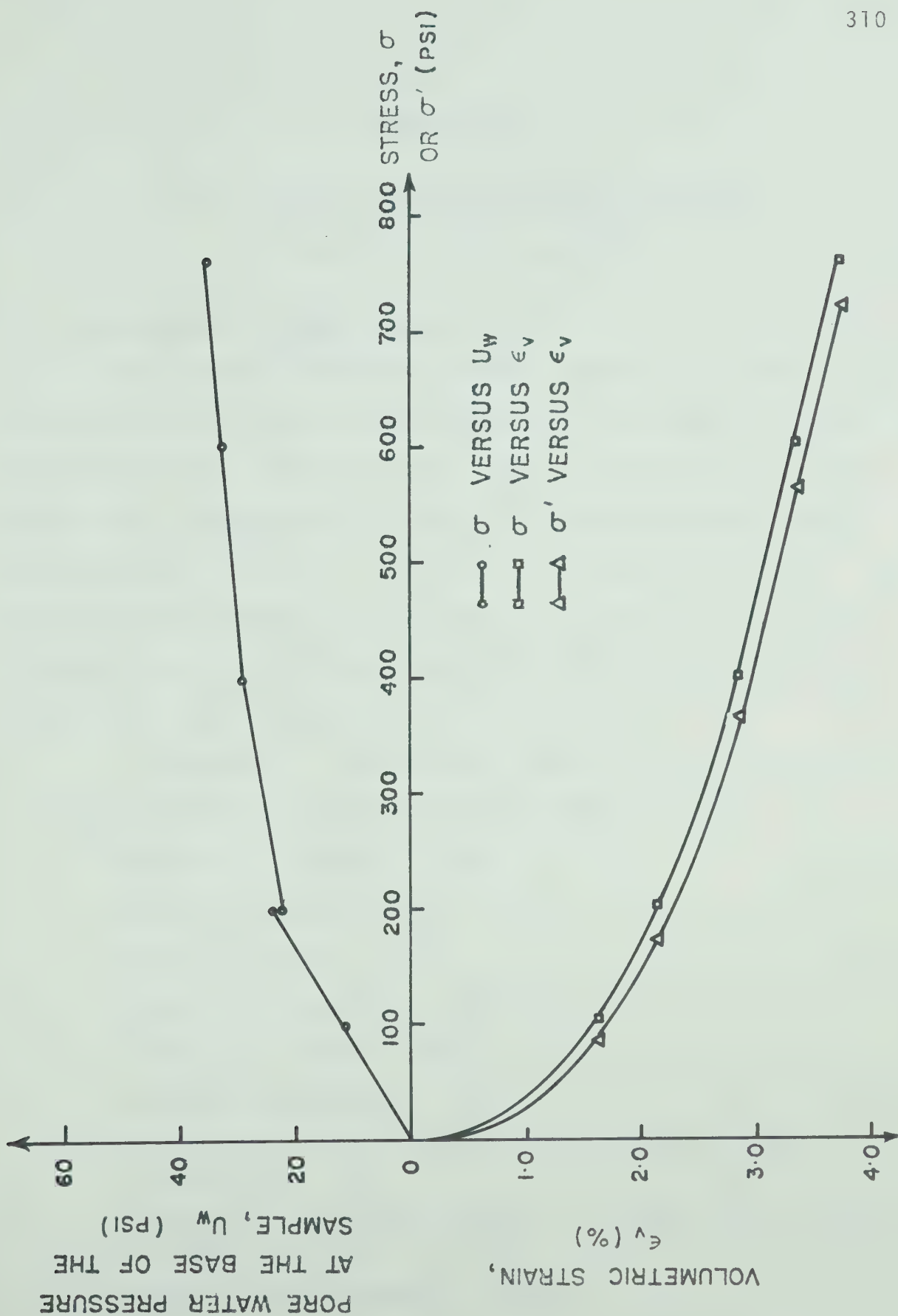


Fig. A.26 Isotropic Compression Partial Dissipation Test (HD-4)

APPENDIX B

FINITE ELEMENT COMPUTER PROGRAM FOR TOTAL OR EFFECTIVE STRESS ANALYSIS

B.1 Description of the Program

The program presented in this appendix is used for two dimensional finite element analysis. The analysis can be performed in terms of either total or effective stresses. The present program was modified from program FENA2D coded by Krishnayya (1973(a)). The facilities added have been described in Chapter III. Fortran IV language was used in programming. The machine adopted was IBM 360/67 computer with a MTS operating system.

The program in the present form can handle a problem less than or equal to the following size:

Number of elements = 1400

Number of read elements = 600

Number of nodes = 750

Number of read nodes = 500

Number of boundary nodes = 60

Number of materials = 8

Number of cell pressures at which triaxial data
is supplied = 10

Number of axial strain points at which triaxial data
is supplied = 20

Number of core elements = 600

If the size of a problem exceeds the previous limits the dimensions have to be increased accordingly. On the other hand if the CPU - virtual Memory Integral charges are to be reduced for small size problem , the dimensions can be decreased.

The program consists of a main and four subroutines called FACTOR, TESTD, RTAPES and DITEST. The function of the main program and each subroutine is briefly described as follows:

MAIN PROGRAM: Most of the operations are performed in this program. It calls other subroutines necessary for the analysis. In the program the element stiffness is formed for all the elements, the equilibrium equations are set up and solved by Gauss-Seidel iterative procedure.

Subroutine FACTOR: This subroutine generates the overburden factors (described in B.2) necessary for elements in nonlinear analysis.

Subroutine TESTD: This subroutine reads the triaxial test data and converts it into the stress-invariant form.

Subroutine RTAPES: This subroutine reads in the pore pressure and total stress data from the tapes. It is called in effective stress analysis.

Subroutine DITEST: This subroutine is used to express the stress-strain relationships of the materials in functional forms. Either DITEST or TESTD will be called in any nonlinear analysis.

B.2 Input Data Procedure

(1) Analysis Control Card (1 Card)(I5)

1-5 NREADD (Equal to zero for total stress analysis; equal to one for effective stress analysis. If NREADD = 1, information for the following (2), (3), (4), (5), (6) and (8) are read in from the tape assigned to I/O unit 3)

(2) Problem Control Cards (2 cards)

If NREADD = 1, the cards for (2) through (6) are omitted.

(a) Card 1 (I8A4)

1-72 HED (Title card for program identification)

(b) Card 2 (I0I5)

1-5 NUMEL (Number of elements in the problem)

6-10 NUREL (Number of read elements)

11-15 NUMNP (Number of nodal points in the problem)

16-20 NURNP (Number of read nodal points)

21-25 NUMBC (Number of boundary points at which displacements are prescribed in the problem)

26-30 NUMAT (Number of material types in the problem)

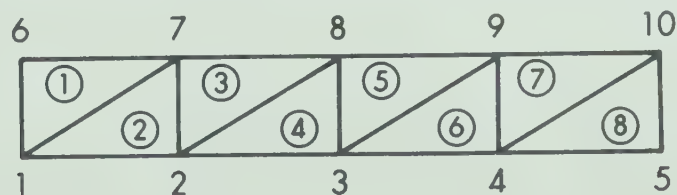
31-35 NANLYS (Equal to zero for linear analysis; equal to one for non-linear analysis)

- 36-40 IANLYS (Equal to zero for plane strains analysis; equal to one for plane stress analysis. Zero is assigned if NREADD equal to one)
- 41-45 IGEN (Equal to zero for non-uniform pattern of generation of element; equal to one for uniform patterns of generation of elements. Refer to (3) for details)
- 46-50 NIAPE (If NTAPE = 1, element data, nodal data, boundary nodal displacements, material types and overburden factors are to be written on the tape assigned to I/O unit 3. Zero is assigned if NREADD equal to one)

(3) Element Cards (Cards = NUREL) (4I5)

- 1-5 NUMER () (Element number for read elements only)
- 6-10 NPIR () (Nodal number for node i of a read element)
- 11-15 NPJR () (Nodal number for node j of a read element)
- 16-20 NPKR () (Nodal number for node K of a read element)

Example for uniform element pattern generation:

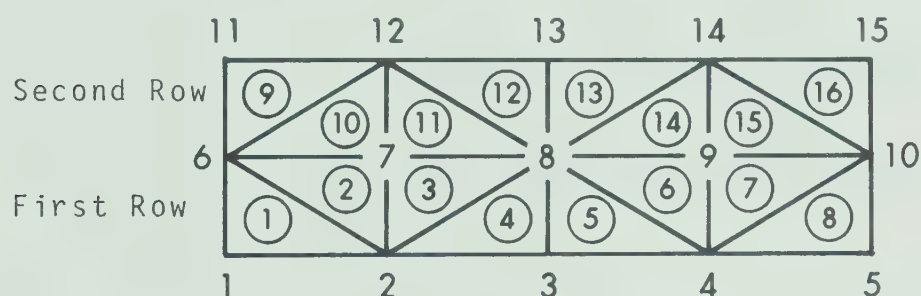


To generate the above mesh pattern it is necessary to supply the information regarding the first (e.g. element 1) and the last (e.g. element 8) elements in a row. The nodes i, j and k for these elements are to be given in the anticlockwise direction as listed below:

<u>Element Number</u>	<u>Node i</u>	<u>Node j</u>	<u>Node k</u>
1	7	6	1
8	10	4	5

NUMEL is 8 and NUREL is 2 for this example.

Example for non-uniform element pattern generation:



To generate the above mesh pattern it is necessary to supply information regarding the first three elements and the last element in the first row and the first and last elements in the second row. This is due to the difference between the orientation of the element 1 and the element 9. For the generation, the following cards should be supplied:

<u>Element Number</u>	<u>Node i</u>	<u>Node j</u>	<u>Node k</u>
1	6	1	2
2	6	2	7
3	8	7	2
8	10	4	5
9	12	11	6
16	14	10	15

- (4) Nodal point cards (Cards = NURNP) (I5, 4F10.0, 2F 12.8)
- | | | | |
|-------|-------|-----|--|
| 1-5 | NPUR | () | (Nodal number of the read nodes only) |
| 6-15 | XORDR | () | (X-coordinate of read nodes only) |
| 16-25 | YORDR | () | (Y-coordinate of read nodes only) |
| 26-35 | XLDR | () | (X-load at read nodes only) |
| 36-45 | YLDR | () | (Y-load at read nodes only) |
| 46-57 | DSXR | () | (Displacement in X-direction given as input only for read nodes) |
| 58-69 | DSYR | () | (Displacement in Y-direction given as input only for read nodes) |

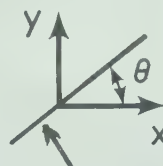
When the intermediate nodes between the two extreme nodes are equally spaced in one coordinate direction with the distance in other coordinate direction being the same, the intermediate nodes are generated with equal distances between them, each distance being equal to the total distance between the extreme nodes read divided by the difference between the nodal numbers. The intermediate nodes are assigned to the proper nodal numbers. The other quantities like displacements, loads, etc. for the intermediate nodes will be the same as those read for the extreme nodes.

- (5) Boundary Point Displacement Cards (Cards = NUMBC)
(2I5, F8.3)
- | | | | |
|-------|-------|-----|--|
| 1-5 | NPB | () | (Nodal number at which the type of boundary displacement is specified) |
| 6-10 | NFIX | () | (Code to indicate the type of boundary displacement conditions prescribed) |
| 11-18 | SLOPE | () | (Slope of the boundary along which a boundary point moves) |

The codes used to define the node of displacement at a given boundary point are listed as follows:

<u>X-direction</u>	<u>Y-direction</u>	<u>Slope Boundary</u>	<u>NFIX()</u>	<u>SLOPE()</u>
Zero or pre-scribed displacement	Zero or pre-scribed displacement		0	0
Zero or pre-scribed displacement			1	0
	Zero or pre-scribed displacement		2	0
		Free to move along a sloping boundary	2	$\tan \theta$

Sloping boundary is as shown:



(6) Material Type Generation Cards

(a) Card 1 (I5)

1-5 MATN (Number of elements to which material number other than 1 is to be assigned. If there is only one material a blank card is required and the cards for following (b) and (c) are omitted)

(b) Card 2 (2I5)

1-5 M (The first element number of a set of elements to which the same material number to be assigned)

6-10 MAT(M) (assigned material number)

(c) Card 3 (2I5)

1-5 M (The last element number of a set of elements to which the same material number to be assigned)

6-10 MAT(M) (Assigned material number. It should be the same number as in (b) card)

Procedures (b) and (c) are to be repeated for each set of elements. The sum of elements in all sets should equal to MATN.

(7) Material Properties Cards (Cards = NUMAT) (5F10.0)

1-10 ROREAD () (Density of the material)

11-20 EBREAD () (Bulk modulus read for each material type; normally assigned in a linear analysis)

21-30 ESREAD () (Shear modulus read for each material type; normally assigned in a linear analysis)

31-40 ACOEF () (Shear strength parameters associated with cohesion given by $2C \cos\phi / (1 - \sin\phi)$; needed if shear failure has to be considered)

41-50 BCOEF () (Shear strength parameters associated with σ_3 given by $2\sigma_3 \sin\phi / (1 - \sin\phi)$; needed if shear failure has to be considered)

(8) Overburden Factor Cards

If NREADD = 1, the cards for (8) are omitted.

(a) Card 1 (I5)

1-5 NOBSET (Code to identify whether the generation of overburden factors is required in the problem; if the analysis is linear NOBSET = 0 and the following (b), (c), (d) and (e) are omitted)

(b) Card 2 (I5)

1-5 NSTLPP (Number of steps considered in the generation of overburden factors; normally equal to the number of steps for the analysis)

(c) Card 3 (I5)

1-5 NSKIPF (If generation of overburden factors is not needed for a particular step
NSKIPF = 0 and (d) and (e) are omitted)

(d) Card 4 (3I5)

1-5 MJ1 (The first element number in the step considered)

6-10 NUMELF (The last element number in the step considered)

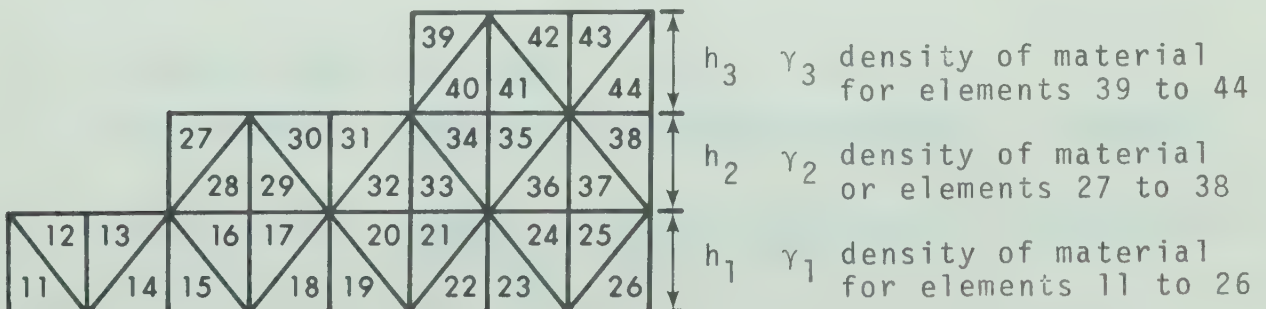
11-15 NGROUP (Number of sets of elements for which the overburden factor is to be generated in the step considered)

(e) Cards = NGROUP (2I5)

1-5 NEL1 (The first element number of a set of elements to which the overburden factor to be assigned)

6-10 NEL2 (The last element number of a set of elements to which the overburden factor to be assigned)

Procedures (c) to (e) are to be repeated for each step. The following example provides an explanation for (c) to (e).



When a non-linear analysis has to be performed for gravity loaded structures the initial moduli are computed for each element considering the overburden pressure at the mid height of the element. In the sketch shown above there are 34 elements in a particular step. The overburden factor for the element 26 can be defined as:

$$\text{OBFAC}(26) = (\gamma_1 h_1/2 + \gamma_2 h_2 + \gamma_3 h_3)/(\gamma_1 h_1/2)$$

OBFAC(M) = 1.0 is automatically set in the program and hence need not be considered in the generation. In the present example elements 11 to 14, 27 to 32 and 39 to 44 will have an overburden factor equal to unity. For this example the cards to be supplied are as follows:

NSKIPF = 1

<u>MJ1</u>	<u>NUMELF</u>	<u>NGROUP</u>
11	44	2
<u>NEL1</u>	<u>NEL2</u>	
15	26	
33	38	

(9) Triaxial Test Data Control Card (1 card) (2I5, F 10.0)

1-5	NCELP	(Number of confining pressures at which triaxial test data is supplied as input)
6-10	NSTRN	(Number of axial strain points at which the triaxial data is supplied)

11-20 CONFAC (Conversion factor used to convert the triaxial test results to the units in which analysis is performed)

If the analysis is linear or non-linear without using digital representation of triaxial stress-strain data a blank card for (9) has to be substituted and (10), (11) and (12) are to be omitted.

(10) Cell Pressure Card (1 card) (10F 5.0)

If the test results are to be supplied say at 0, 5, 10, 30 and 40 psi cell pressure values, the input is as follows:

1-5	0.0
6-10	5.0
11-15	10.0
16-20	30.0
21-25	40.0

(11) Axial Strain and Deviatoric Stress Cards (Cards = NSTRN)
(11F 5.0)

Each card will have the axial strain punched in the first five columns and the deviatoric stresses corresponding to the various cell pressures (given in (10)) at that particular axial strain are punched in the subsequent columns.

(12) Axial Strain and Volumetric Strain Cards (Cards = NSTRN)
(11F 5.0)

Each card will have the axial strain punched in the first five columns and the volumetric strain corresponding to

the various cell pressures (given in (10)) at that particular axial strain are punched in the subsequent columns. Volume expansion has to be neglected while giving the volumetric strain input.

Procedures (10) to (12) are to be repeated for each material type.

(13) Stress-Strain Parameter Cards

If NCELP > 0 or NANLYS = 0, the cards for (13) are omitted.

(a) Card 1 (F 10.0)

1-10 AP (Atmospheric pressure expressed in the same unit as stresses)

(b) Cards = NUMAT (3F 10.0)

1-10 CDR () (Parameter C_D for power function stress-strain relationship. Refer to Chapter II).

11-20 AR () (Parameter a for power function stress-strain relationship. Refer to Chapter II)

21-30 XUR () (Poisson's ratio of the material)

(14) Option for "No Tension" Analysis (1 card) (I5)

1-5 KOPT (Equal to zero when "no tension" analysis if not needed and equal to one when it is needed)

(15) Option for Analyzing Each Step Once or Twice (1 card)(I5)

1-5 ITOPT (Equal to zero for analysis once and equal to one for analysis twice. If the analysis is linear ITOPT = 0)

(16) Number of Steps and Options for Consideration of Shear Failure (1 card) (2I5)

1-5 NSTEP (For a single step analysis NSTEP = 1)

6-10 NTENS (If shear failure is to be considered NTENS = 1, otherwise NTENS = 0)

(17) Core Element Cards

If NREADD = 0, the cards for (17) are omitted.

(a) Card 1 (I5)

1-5 NECORE (Number of elements in the core)

(b) Cards = NECORE/19 (19I4)

NELC () (The core element numbers corresponding to the overall mesh)

(18) Current Step Control Card (1 card) (6I5, 2F 10.0, 3I5)

1-5 NUMELS (Number of elements in the step considered)

6-10 NUMNPS (Number of nodal points in the step considered)

11-15 NUMBCS (Number of boundary points at which displacements are specified in the step considered)

16-20 NCPIN (Cycle interval for the point of the force unbalanced)

21-25 NOPIN (Cycle interval for the point of displacements and stresses)

26-30 NCYCM (Maximum number of iterations permitted in one step)

31-40 TOLER (Convergence limit for unbalanced forces)

41-50 XFAC (Over-relaxation factor: between 1.8 and 1.95)

51-55 LNUM (Current step number)

- 56-60 NCONSL (If NREADD = 1, NCONSL is set equal to one)
- 61-65 NWTAPE (If NWTAPE > 0 the results of the current step are written on the tape assigned to I/O unit 3)

(19) Write on Tape Card (1 card)

If NWTAPE = 0 the card for (19) is omitted

- 1-5 NFWRD (Number of tape files to be skipped forward for writing the results of current step on a tape on I/O unit 3)
- 6-10 NBWRD (Number of tape files to be skipped backward for locating total stress data to be used in next step. If NREADD = 0, NBWRD is set equal to zero)

(20) Nodal Loads Control Card (1 card) (I5)

- 1-5 NLOAD (Number of nodes at which the loads are specified in the step considered. If NLOAD = 0, the cards for (21) are omitted)

(21) Nodal Load Cards (Cards = NLOAD) (I5, 2F 10.0)

- 1-5 N (Nodal number)
- 6-15 YLOAD (N) (Y-Load specified for a node in the step considered)
- 16-25 XLOAD (N) (X-Load specified for a node in the step considered)

(22) Nodal Displacements Control Card (1 card) (I5)

- 1-5 NBOUN (Number of nodes at which the boundary displacements are specified in the step considered)

(23) Nodal Displacements Cards (Cards = NBOUN) (I5, 2F 10.0)

1-5 M (Nodal number)

6-15 DSY (M) (Displacement in y-direction specified for a node in the step considered)

16-25 DSX (M) (Displacement in x-direction specified for a node in the step considered)

(24) Read Tape Cards (2 Cards)

If NCONSL = 0, the cards for (24) are omitted.

(a) Card 1 (2I5)

1-5 NCODE (If NCODE > 0, pore pressures in the core for current step are read from a tape on I/O unit 2)

6-10 NFPPR (Number of tape files to be skipped for locating the pore pressure data needed in the next step)

(b) Card 2 (I5)

1-5 NFTST (Number of tape files to be skipped for locating total stress data used in the current step)

Procedures (18) to (24) are to be repeated for each step.

B.3 Listing of Program

A listing of the program is given as follows:


```

C
C
C TWO DIMENSIONAL FINITE ELEMENT PROGRAM WITH CONSTANT STRAIN TRIANGULAR
C ELEMENTS OF 6 DEGREES OF FREEDOM FOR EACH ELEMENT.
C
C
C ORIGINAL PROGRAM DEVELOPED BY E.L.WILSON (UNIVERSITY OF CALIFORNIA,1962)
C PROGRAM MODIFIED BY Z.EISENSTEIN (UNIVERSITY OF ALBERTA,1969) AND
C A.V.G. KRISHNAYYA (UNIVERSITY OF ALBERTA, 1970) AND
C T. C. LAW (UNIVERSITY OF ALBERTA, 1972)
C
C MAIN PROGRAM
C
C
C DIMENSION AND COMMON STATEMENTS
C
C DIMENSION HEAD(18),NP(750,10),SXX(750,9),NUMER(600),
1SXY(750,9),SYX(750,9),SYY(750,9),NAP(750),NPNUR(500),XORDR(500),
2YORDR(500),XLDR(500),YLDR(500),DSXR(500),DSYR(500),TAD(750),
3TAL(750),GAMV(1400),
4NPIR(600),NPJR(600),NPKR(600),LM(3),A(6,6),B(6,6),S(6,6),THETA(50)
COMMON/AREA1/ AJ(1400),BJ(1400),AK(1400),BK(1400)
COMMON/AREA2/ XORD(750),YORD(750),NPI(1400),NPJ(1400),NPK(1400),
1NPNUM(750),NUME(1400),NUMNP,NUMEL,NUMBC,NANLYS,JM,NSTEP
COMMON/AREA3/
1 ST(20,8),SL(20,8),SD(20,10,8),VS(20,10,8),NUMAT,
2NCELP,CONFAC,NSTRN
COMMON/AREA4/ XLOAD(750),YLOAD(750),DSX(750),DSY(750),DSXQ(750),
1DSYQ(750),XN(750),YN(750),RPS(750),DSXQT(750),DSYQT(750),
2XLOAD1(750),YLOAD1(750),XLOAD2(750),YLOAD2(750),SLOPE(60),NPB(60),
3NFI(60),PIN(750),P3N(750),KOUN(750),XYN(750)
COMMON/AREA5/EBULK(1400),ESHEAR(1400),PA(1400),MAT(1400),RD(1400),
1XV(1400),YV(1400),XYV(1400),EPXV(1400),EPYV(1400),XMAX(1400),
2EMAX(1400),EMIN(1400),XVT(1400),YVT(1400),XYVT(1400),EPXVT(1400),
3EPYVT(1400),NELC(600),UEL(1400),DBFAC(1400),SIGM1,BULKM,SHEARM
4,SIGM2,SIGM3,XMIN(1400),XVT1(1400),YVT1(1400),XYVT1(1400)
COMMON/AREA6/NK,ITOFT,NITER,JEJ,AP,CDR(8),AR(8),XUR(8),
1CD(1400),AA(1400),XU(1400)
DIMENSION ROREAD(8),EBREAD(8),ESREAD(8),ACOE(8),BCOE(8)
C
C READ PROBLEM CONTROL CARDS
C
C READ(5,6) NREADD
IF (NREADD.GT.0) GO TO 608

```



```

      READ(5,100)HEAD
      WRITE(6,99)
      WRITE(6,100)HEAD
      READ(5,1)NUMEL,NUREL,NUMNP,NURNP,NUMBC,NUMAT,NANLYS,IANLYS,IGEN
1,NTAPE
      WRITE(6,101)NUMEL
      WRITE(6,825)NUREL
      WRITE(6,102)NUMNP
      WRITE(6,824)NURNP
      WRITE(6,103)NUMBC
      WRITE(6,2000) NUMAT
C
C
C  READ ELEMENT DATA
C
C
      READ(5,9)(NUMER(N),NPIR(N),NPJR(N),NPKR(N),N=1,NUREL)
C
C
C  READ NCDAL DATA
C
C
      READ (5, 3)
1      (NPNUR(M),XORDR(M),YORDR(M),XLDR(M),YLDR(M),
2DSXR(M),DSYR(M),M=1,NURNP)
C
C  GENERATION OF NOT READ ELEMENTS
C
      DO 161 N=1,NUREL
      M=N+1
      IF(M-NUREL) 162,162,163
162 I=NUMER(M)-NUMER(N)
      IF(I-1)163,163,164
164 L=NUMER(N)
      NPA=NPIR(N)
      NPC=NPKR(N)
      K=0
      KO=2*K
      KE=1
      IO=I+1
      IF(IGEN.EQ.0) GO TO 3000
      DO 3166 JO=1,IO
      J=JO-1
      LJ=L+J
      NUME(LJ)=NUMER(N)+J
      IF(2-KE) 3168,3168,3167
3167 NPI(LJ)=NPA+KO
      NPJ(LJ)=NPA-1+KO
      NPK(LJ)=NPC+KO
      GO TO 3174
3168 NPI(LJ)=NPA+KO
      NPJ(LJ)=NPC+KO
      NPK(LJ)=NPC+1+KO
      K=K+1
      KO=K
      KE=0
3174 KE=KE+1
3166 CONTINUE
      GO TO 161
3000 DO 166 JO=1,IO

```



```

      J=JO-1
      LJ=L+J
      NUME(LJ)=NUMER(N)+J
      IF(2-KE) 169,168,167
167  NPI(LJ)=NPA+KO
      NPJ(LJ)=NPA-1+KO
      NPK(LJ)=NPC+KO
      GO TO 174
168  NPI(LJ)=NPA+KO
      NPJ(LJ)=NPC+KO
      NPK(LJ)=NPC+1+KO
      GO TO 174
169  IF(3-KE) 172,171,166
171  NPI(LJ)=NPA+KO
      NPJ(LJ)=NPC+1+KO
      NPK(LJ)=NPC+2+KO
      GO TO 174
172  NPI(LJ)=NPA+KO
      NPJ(LJ)=NPC+2+KO
      NPK(LJ)=NPA+1+KO
      K=K+1
      KO=2*K
      KE=0
174  KE=KE+1
166  CONTINUE
      GO TO 161
163  L=NUMER(N)
      NUME(L)=NUMER(N)
      NPI(L)=NPIR(N)
      NPJ(L)=NPJR(N)
      NPK(L)=NPKR(N)
161  CONTINUE
C
C
C      GENERATION OF NOT READ NODAL POINTS
C
      DO 151 M=1,NURNP
      N=M+1
      IF(N-NURNP) 152,152,186
152  I=NPNUM(N)-NPNUM(M)
      GO TO 154
186  I=0
154  L=NPNUM(M)
      IO=I+1
      DO 156 JO=1,IO
      J=JO-1
      LJ=L+J
      NPNUM(LJ)=NPNUM(M)+J
      IF(I=0) 188,188,189
188  XORD(LJ)=XORDR(M)
      YORD(LJ)=YORDR(M)
      GO TO 191
189  XORD(LJ)=XORDR(M)+((XORDR(N)-XORDR(M))/I)*J
      YORD(LJ)=YORDR(M)+((YORDR(N)-YORDR(M))/I)*J
191  IF(J=0) 158,158,159
159  IF(J=1) 157,153,156
158  XLOAD(LJ)=XLDR(M)
      YLOAD(LJ)=YLDR(M)
      DSX(LJ)=DSXR(M)
      DSY(LJ)=DSYR(M)

```



```

      GO TO 156
153  XLOAD(LJ)=XLDR(N)
      YLOAD(LJ)=YLDR(N)
      DSX(LJ)=DSXR(N)
      DSY(LJ)=DSYR(N)
      GO TO 156
157  XLOAD(LJ)=0
      YLOAD(LJ)=0
      DSX(LJ)=0
      DSY(LJ)=0
156  CONTINUE
151  CONTINUE
608  IF (NREADD.GT.0) CALL RTAPES(1)
C
C      INITIALIZE TOTAL DISPLACEMENTS AND STRESSES AND STRAINS
606  DO 10 J=1,NUMNP
      DSXQ(J)=0.0
      DSYQ(J)=0.0
10   CONTINUE
      DO 11 J=1,NUMEL
      XV(J)=0.
      YV(J)=0.
      XYV(J)=0.
      EPXV(J)=0.
      EPYV(J)=0.
11   CONTINUE
      WRITE(6,111)
      WRITE(6,109) (NPNUM(M),XORD(M),YORD(M),XLOAD(M),YLOAD(M),
1DSX(M),DSY(M),M=1,NUMNP)
      IF (NREADD.GT.0) GO TO 466
C
C
C      READ BOUNDARY CONDITIONS.
C
C
      READ(5,4)(NPB(L),NFI X(L),SLOPE(L),          L=1,NUMBC)
C
C
466  WRITE(6,112)
      WRITE(6,4)(NPB(L),NFI X(L),SLOPE(L),          L=1,NUMBC)
C
C
      IF (NREADD.GT.0) GO TO 56
C  ASSIGN PROPER MATERIAL NUMBER IF NECESSARY
      DO 854 I=1,NUMEL
854  MAT(I)=1
      READ(5,6) MATN
      IF(MATN.EQ.0) GO TO 56
      NMAT=0
5000 IF (NMAT.EQ.MATN) GO TO 56
      READ (5,20) M,MAT(M)
      MM=M
      READ (5,20) M,MAT(M)
      NMAT=NMAT+(M-MM)+1
      LL=MM+1
5002 IF (M-LL) 5000,5000,5003
5003 MAT(LL)=MAT(M)
      LL=LL+1
      GO TO 5002
C
C  ACOEF=2.*COS(PHI)/(1.-SIN(PHI)),BCOEF=2.*SIN(PHI)/(1-SIN(PHI))

```



```

C
C
C  READ MATERIAL PROPERTIES.
C
C
56  DO 850 I=1,NUMAT
      READ(5,2010) ROREAD(I),EBREAD(I),ESREAD(I),ACDEF(I),BCDEF(I)
      WRITE(6,2020)ROREAD(I),EBREAD(I),ESREAD(I),ACDEF(I),BCDEF(I)
850  CONTINUE
      DO 57 N=1,NUMEL
          I=MAT(N)
          RO(N)=ROREAD(I)
          EBULK(N)=EBREAD(I)
          ESHEAR(N)=ESREAD(I)
          IF (NREADD.EQ.0) OBFAC(N)=1.0
57  CONTINUE
C
C
C  READ OVERBURDEN FACTOR
C
      IF (NREADD.GT.0) GO TO 48
      READ (5,6) NOBSET
      IF (NOBSET.EQ.0) GO TO 48
      CALL FACTOR
C
C
C  READ TRIAXIAL TEST DATA CONTROL CARD.
C
C
48  READ(5,2021) NCELP,NSTRN,CONFAC
      IF(NCELPEQ.0) GO TO 44
C
      CALL TESTD
C
C  INTERPOLATE INITIAL MODULI FOR ALL ELEMENTS
C
C
      DO 600 M=1,NUMEL
          IF(RO(M).LE.0.0) GO TO 600
          I=NPI(M)
          J=NPJ(M)
          K=NPK(M)
          Y1=ABS(YORD(I)-YORD(J))
          Y2=ABS(YORD(J)-YORD(K))
          Y3=ABS(YORD(K)-YORD(I))
          DEPTH=0.0
          IF(Y1.GT.DEPH) DEPTH=Y1
          IF(Y2.GT.DEPH) DEPTH=Y2
          IF(Y3.GT.DEPH) DEPTH=Y3
          DEPTH=DEPTH/2.
          NCOUNT=0
          N=MAT(M)
          OBP=DEPTH*RO(M)*OBFAC(M)
          AVGSIG=OBP*0.5
18  NCCUNT=NCOUNT+1
          SIGM1=OBP
          SIGM2=AVGSIG
          SIGM3=AVGSIG
          SIGOCT=(SIGM1+SIGM2+SIGM3)/3.
          SIGIN=SIGM1*SIGM2*SIGM3

```



```

CONF5=SIGIN/(SIGOCT**2)
DIVOCT=SQRT((SIGM1-SIGM2)**2+(SIGM2-SIGM3)**2+(SIGM3-SIGM1)**2)
DIVOCT=DIVOCT/3.
DO 720 J=1,NCELP
JLS=J
IF( CONF5-SL(J,N)) 721,720,720
720 CONTINUE
721 CONTINUE
DO 790 K=1,NSTRN
JS1=K
IF(DIVOCT-SD(K,JLS-1,N)) 791,790,790
790 CONTINUE
791 CONTINUE
DO 50 K=1,NSTRN
JS2=K
IF(DIVOCT-SD(K,JLS,N)) 51,50,50
50 CONTINUE
51 CONTINUE
PR1=1.061*(VS(JS1,JLS-1,N)-VS(JS1-1,JLS-1,N))/(ST(JS1,N)-ST(JS1-1,
1N))-1.0
IF(PR1.GT.0.49) PR1=0.49
PR2=1.061*(VS(JS2,JLS ,N)-VS(JS2-1,JLS ,N))/(ST(JS2,N)-ST(JS2-1,
1N))-1.0
IF(PR2.GT.0.49) PR2=0.49
PR3=PR1+((PR2-PR1)*(CONF5-SL(JLS-1,N))/(SL(JLS,N)-SL(JLS-1,N)))
IF(PR3.GT.0.49 ) PR3=0.49
CONST=PR3/(1.-PR3)
HPR=OBP*CONST
HPR=(HPR+AVGSIG)/2.
CSTRS=ABS(HPR-AVGSIG)
IF(NCCOUNT.GE.21) GO TO 52
IF(ABS(HPR-AVGSIG).LT.0.01) GO TO 52
AVGSIG=HPR
GO TO 18
52 CONTINUE
DIF1=SD(JS1,JLS-1,N)-SD(JS1-1,JLS-1,N)
ETP1=DIF1/(ST(JS1,N)-ST(JS1-1,N))
GTP1=ETP1/(0.9428*(1.+PR1))
DIF2=SD(JS2,JLS,N)-SD(JS2-1,JLS,N)
ETP2=DIF2/(ST(JS2,N)-ST(JS2-1,N))
GTP2=ETP2/(0.9428*(1.+PR2))
GTP=GTP1+ (GTP2-GTP1)*(CONF5 -SL(JLS-1,N))/(SL(JLS,N)-SL(JLS-1,N))
GTP=100.*GTP
EBULK(M)=GTP*2.*(1.+PR3)/(3.*(1.-2.*PR3))
ESHEAR(M)=GTP
600 CONTINUE
IF(NCELP.NE.0) GO TO 46
44 IF(NANLYS.EQ.0) GO TO 46
CALL D1TEST(1)
46 WRITE(6,110)
IF (NREADD.EQ.0) GO TO 60
DO 61 N=1,NUMEL
61 RO(N)=0.0
C
C
C PRINT ELEMENT DATA
C
C
60 WRITE(6,2055)(NUME(N),NPI(N),NPJ(N),NPK(N),EBULK(N),RO(N),ESHEAR(N
1), MAT(N), N=1,NUMEL)

```



```

      IF (NTAPE.GT.0) WRITE (3) NUMEL,NUMNP,NUMBC,NUMAT,NANLYS
      IF (NTAPE.GT.0) WRITE (3) (XORD(N),YORD(N),XLOAD(N),YLOAD(N),
1DSX(N),DSY(N),N=1,NUMNP)
      IF (NTAPE.GT.0) WRITE(3) (NUME(N),NPI(N),NPJ(N),NPK(N),EBULK(N),
1RO(N),ESHEAR(N),MAT(N),OBFAC(N),N=1,NUMEL)
      IF (NTAPE.GT.0) WRITE(3) (NPB(N),NFIX(N),SLOPE(N),N=1,NUMBC)
      IF (NTAPE.GT.0) ENDFILE 3
C
C
C  READ PARTICULARS ABOUT CURRENT STEP.
C
C
      READ(5,6) KOPT
      READ(5,6) ITOPT
      READ(5,20) NSTEP,NTENS
      IF (NREADD.EQ.0) GO TO 3200
      DO 3273 N=1,NUMNP
      XLOAD1(N)=0.0
      YLOAD1(N)=0.0
      XLOAD2(N)=0.0
      YLOAD2(N)=0.0
3273  CONTINUE
      IANLYS=0
C  READ THE NUMBER OF ELEMENTS IN THE CORE FOR THE GIVEN STAGE OF CONSTRUCTION
      READ (5,6) NECORE
C  READ THE CORE ELEMENT NUMBERS CORRESPONDING TO THE OVER ALL MESH
      READ (5,3250) (NELC(I),I=1,NECCRE)
3250  FORMAT (19I4)
3200  DO 500 JM = 1,NSTEP
      READ(5,13)NUMELS,NUMNPS,NUMBCS,NCPIN,NOPIN,NCYCM,TOLER,XFAC,LNUM,
1NCONSL,NWTAPE
      IF (NWTAPE.GT.0) READ (5,20) NFWRD,NEWRD
      NUMEL=NUMELS
      NUMNP=NUMNPS
      NUMBC=NUMBCS
      DO 761 N=1,NUMNP
      TAD(N)=0.0
      TAL(N)=0.0
761  CONTINUE
C
C
C  READ BOUNDARY LOADS FOR CURRENT STEP
C
C
      READ(5,6) NLOAD
      IF(NLOAD.EQ.0) GO TO 4050
      DO 4051 I=1,NLOAD
      READ(5,602) N,YLOAD(N),XLOAD(N)
      IF(YLOAD(N).NE.0.0) TAL(N)=2.0
      IF(XLOAD(N).NE.0.0) TAL(N)=1.0
4051  CONTINUE
C
C
C  READ BOUNDARY DISPLACEMENTS FOR CURRENT STEP
C
C
4050  READ(5,6) NBOUN
      IF(NBOUN.EQ.0) GO TO 41
      DO 601 N=1,NBOUN
      READ(5,602) M,DSY(M),DSX(M)

```



```

        IF(DSY(M).NE.0.0) TAD(M)=2.0
        IF(DSX(M).NE.0.0) TAD(M)=1.0
601  CONTINUE
41   WRITE (6,101) NUMEL
      WRITE(6,102)NUMNP
      WRITE(6,103)NUMBC
      WRITE(6,104)NCPIN
      WRITE(6,105)NOPIN
      WRITE(6,106)NCYCM
      WRITE(6,107)TOLER
      WRITE(6,108)XFAC
      WRITE(6,117)LNUM
      NITER=0
      IF (NCONSL.GT.0) CALL RTAPES(2)

C
C   INITIALIZATION
C
160  NCYCLE=0
      NITER=NITER+1
      NUMPT=NCPIN
      NUMOPT=NOPIN
      DO 175 L=1,NUMNP
      DO 170 M=1,9
        SXX(L,M)=0.0
        SXY(L,M)=0.0
        SYX(L,M)=0.0
        SYY(L,M)=0.0
170  NP(L,M)=0
        NP(L,10)=0
175  NP(L,1)=L

C
C   MODIFICATION OF LOADS AND ELEMENT DIMENSIONS
C
      NERROR=0
      DO 180 N=1,NUMEL
        I=NPI(N)
        J=NPJ(N)
        K=NPK(N)
        AJ(N)=XORD(J)-XORD(I)
        AK(N)=XORD(K)-XORD(I)
        BJ(N)=YORD(J)-YORD(I)
        BK(N)=YORD(K)-YORD(I)
176  AREA=(AJ(N)*BK(N)-BJ(N)*AK(N))/2.
        IF(AREA) 701,701,177
177  CONTINUE
        DL=AREA*RC(N)/3.
        YLOAD (I)=YLOAD(I)-DL
        YLOAD (J)=YLOAD(J)-DL
        YLOAD (K)=YLOAD(K)-DL
        IF (NCCNSL.EQ.0) GO TO 3260
        IF(ITOPT.GT.0.AND.NITER.EQ.2) GO TO 62
        XVT(N)=-XVT(N)-UEL(N)
        YVT(N)=-YVT(N)-UEL(N)
        XYVT(N)=-XYVT(N)
        XVT1(N)=XVT(N)
        YVT1(N)=YVT(N)
        XYVT1(N)=XYVT(N)
62  IF(ITOPT.GT.0.AND.NITER.EQ.1) GO TO 63
        XVT(N)=XVT1(N)
        YVT(N)=YVT1(N)

```



```

      XYVT(N)=XYVT1(N)
63  XLOAD2(I)=XVT(N)*(BK(N)-BJ(N))/2.+XYVT(N)*(AJ(N)-AK(N))/2.+XLOAD2(
1 I)
      XLOAD2(J)=-XVT(N)*BK(N)/2.+XYVT(N)*AK(N)/2.+XLOAD2(J)
      XLOAD2(K)=XVT(N)*BJ(N)/2.-XYVT(N)*AJ(N)/2.+XLOAD2(K)
      YLOAD2(I)=YVT(N)*(AJ(N)-AK(N))/2.+XYVT(N)*(BK(N)-BJ(N))/2.+YLOAD2(
1 I)
      YLOAD2(J)=YVT(N)*AK(N)/2.-XYVT(N)*BK(N)/2.+YLOAD2(J)
      YLOAD2(K)=-YVT(N)*AJ(N)/2.+XYVT(N)*BJ(N)/2.+YLOAD2(K)
3260 IF (AREA.GT.0.0) GO TO 180
701  WRITE(6,711)N
      NERROR=NERROR+1
180  CONTINUE
      IF (NCONSL.EQ.0) GO TO 3271
      DO 3270 N=1,NUMNP
      XLOAD(N)=XLOAD(N)+XLOAD2(N)-XLOAD1(N)
      YLOAD(N)=YLOAD(N)+YLOAD2(N)-YLOAD1(N)
      IF (ITOPT.GT.0.AND.NITER.EQ.1) GO TO 64
      XLOAD1(N)=XLOAD2(N)
      YLOAD1(N)=YLOAD2(N)
64  XLOAD2(N)=0.0
      YLOAD2(N)=0.0
3270 CONTINUE
3271 CONTINUE
      IF (NERROR.GT.0) GO TO 925
C
C   FORMATION OF STIFFNESS ARRAY
C
      DO 200 N=1,NUMEL
      AREA=(AJ(N)*BK(N)-AK(N)*BJ(N))*0.5
      COMM=0.25/AREA
      A(1,1)=BJ(N)-BK(N)
      A(1,2)=0.0
      A(1,3)=BK(N)
      A(1,5)=-BJ(N)
      A(1,6)=0.0
      A(2,1)=0.0
      A(2,2)=AK(N)-AJ(N)
      A(2,3)=0.0
      A(2,4)=-AK(N)
      A(2,5)=0.0
      A(2,6)=AJ(N)
      A(3,1)=AK(N)-AJ(N)
      A(3,2)=BJ(N)-BK(N)
      A(3,3)=-AK(N)
      A(3,4)=BK(N)
      A(3,5)=AJ(N)
      A(3,6)=-BJ(N)
      IF (IANLYS.EQ.0) COM1=EBULK(N)+ESHEAR(N)*(4./3.)
      IF (IANLYS.EQ.0) COM2=EBULK(N)-ESHEAR(N)*(2./3.)
      IF (IANLYS.GT.0) COM1=4.*ESHEAR(N)*(EBULK(N)+ESHEAR(N)/3.)/(EBULK(N)
1)+(4./3.)*ESHEAR(N))
      IF (IANLYS.GT.0) COM2=2.*ESHEAR(N)*(EBULK(N)-(2./3.)*ESHEAR(N))/(EB
1ULK(N)+(4./3.)*ESHEAR(N))
      B(1,1)=COMM*COM1
      B(1,2)=COMM*COM2
      B(1,3)=0.0
      B(2,1)=COMM*COM2
      B(2,2)=COMM*COM1
      B(2,3)=0.0

```



```

      B(3,1)=0.0
      B(3,2)=0.0
      B(3,3)=COMM*ESHEAR(N)
C
      DO 182 J=1,6
      DO 182 I=1,3
      S(I,J)=0.0
      DO 182 K=1,3
182  S(I,J)=S(I,J)+B(I,K)*A(K,J)
      DO 183 J=1,6
      DO 183 I=1,3
183  B(J,I)=S(I,J)
      DO 184 J=1,6
      DO 184 I=1,6
      S(I,J)=0.0
      DO 184 K=1,3
184  S(I,J)=S(I,J)+B(I,K)*A(K,J)
C
      LM(1)=NPI(N)
      LM(2)=NPJ(N)
      LM(3)=NPK(N)
      DO 200 L=1,3
      DO 200 M=1,3
      LX=LM(L)
      MX=0
185  MX=MX+1
      IF(NP(LX,MX)-LM(M)) 190,195,190
190  IF(NP(LX,MX)) 185,195,185
195  NP(LX,MX)=LM(M)
      IF(MX-10) 196,702,702
196  SXX(LX,MX)=SXX(LX,MX)+S(2*L-1,2*M-1)
      SXY(LX,MX)=SXY(LX,MX)+S(2*L-1,2*M)
      SYX(LX,MX)=SYX(LX,MX)+S(2*L,2*M-1)
200  SYX(LX,MX)=SYX(LX,MX)+S(2*L,2*M)
C
C   COUNT OF ADJACENT NODAL POINTS
C
      DO 206 M=1,NUMNP
      MX=1
205  MX=MX+1
      IF (NP(M,MX)) 206,206,205
206  NAP(M)=MX-1
C
C   INVERSION OF NODAL POINT STIFFNESS
C
      DO 210 M=1,NUMNP
      COMM=SXX(M,1)*SYY(M,1)-SXY(M,1)*SYX(M,1)
      TEMP=SYY(M,1)/COMM
      SYY(M,1)=SXX(M,1)/COMM
      SXX(M,1)=TEMP
      SXY(M,1)=-SXY(M,1)/COMM
      SYX(M,1)=-SYX(M,1)/COMM
210  CONTINUE
C
C   MODIFICATION OF BOUNDARY FLEXIBILITIES
C
      DO 240 L=1,NUMBC
      M=NPB(L)
      NP(M,1)=0
      IF(NFIX(L)-1) 225,220,215

```



```

215 C=(SXX(M,1)*SLOPE(L)-SXY(M,1))/(SYX(M,1)*SLOPE(L)-SYY(M,1))
    R=1.-C*SLOPE(L)
    SXX(M,1)=(SXX(M,1)-C*SYX(M,1))/R
    SXY(M,1)=(SXY(M,1)-C*SYY(M,1))/R
    SYX(M,1)=SXX(M,1)*SLOPE(L)
    SYY(M,1)=SXY(M,1)*SLOPE(L)
    GO TO 240
220 SYY(M,1)=SYY(M,1)-SYX(M,1)*SXY(M,1)/SXX(M,1)
    GO TO 230
225 SYY(M,1)=0.0
230 SXX(M,1)=0.0
235 SXY(M,1)=0.0
    SYX(M,1)=0.0
240 CONTINUE
C
C   ITERATION OF NODAL POINT DISPLACEMENTS
C
    KOUNT=0
243 WRITE(6,119)
    KOUNT=KOUNT+1
244 SUM=0.0
    DO 290 M=1,NUMNP
        NUM=NAF(M)
        IF (SXX(M,1)+SYY(M,1)) 275,290,275
275 FRX=XLOAD(M)
        FRY=YLOAD(M)
        DO 280 L=2,NUM
            N=NP(M,L)
            FRX=FRX-SXX(M,L)*DSX(N)-SXY(M,L)*DSY(N)
280 FRY=FRY-SYX(M,L)*DSX(N)-SYY(M,L)*DSY(N)
            DX=SXX(M,1)*FRX+SXY(M,1)*FRY-DSX(M)
            DY=SYX(M,1)*FRX+SYY(M,1)*FRY-DSY(M)
            IF(SXX(M,1).EQ.0.0.AND.SXY(M,1).EQ.0.0) DX=0.0
            DSX(M)=DSX(M)+XFAC*DX
            DSY(M)=DSY(M)+XFAC*DY
            IF(NP(M,1)) 285,290,285
285 SUM=SUM+ABS(DX/SXX(M,1))+ABS(DY/SYY(M,1))
290 CONTINUE
C
C   CYCLE COUNT AND PRINT CHECK
C
    NCYCLE=NCYCLE+1
    IF (NCYCLE-NUMPT) 305,300,300
300 NUMPT=NUMPT+NCPIN
    WRITE(6,120)NCYCLE,SUM
305 IF (SUM-TOLER) 400,400,310
310 IF(NCYCM-NCYCLE) 400,400,315
315 IF (NCYCLE-NUMOPT) 244,320,320
320 NUMOPT=NUMCPT+NOPIN
C
C   PRINT OF DISPLACEMENTS AND STRESSES
C
400 CONTINUE
    IF (SUM-TOLER) 440,440,430
430 IF (NCYCM-NCYCLE) 440,440,243
440 WRITE(6,975)SUM,TOLER
    IF (SUM.EQ.0.0) GO TO 1851
975 FORMAT(5H0SUM=1E15.6,6HTCLER=1E15.6)
    DO 421 N=1,NUMEL
        I=NPI(N)

```



```

J=NPJ(N)
K=NPK(N)
EPX=(BJ(N)-BK(N))*DSX(I)+BK(N)*DSX(J)-BJ(N)*DSX(K)
EPY=(AK(N)-AJ(N))*DSY(I)-AK(N)*DSY(J)+AJ(N)*DSY(K)
GAM=(AK(N)-AJ(N))*DSX(I)-AK(N)*DSX(J)+AJ(N)*DSX(K)
1 +(BJ(N)-BK(N))*DSY(I)+BK(N)*DSY(J)-BJ(N)*DSY(K)
CCMM=1./(AJ(N)*BK(N)-AK(N)*BJ(N))
IF(IANLYS.EQ.0) COM1=EBULK(N)+ESHEAR(N)*(4./3.)
IF(IANLYS.EQ.0) COM2=EBULK(N)-ESHEAR(N)*(2./3.)
IF(IANLYS.GT.0) COM1=4.*ESHEAR(N)*(EBULK(N)+ESHEAR(N)/3.)/(EBULK(N)
1)+(4./3.)*ESHEAR(N))
IF(IANLYS.GT.0) COM2=2.*ESHEAR(N)*(EBULK(N)-(2./3.)*ESHEAR(N))/(EB
1ULK(N)+(4./3.)*ESHEAR(N))
COM3=ESHEAR(N)
X=COMM*(COM1*EPX+COM2*EPY)
Y=COMM*(COM2*EPX+COM1*EPY)
XY=CCMM*COM3*GAM
XV(N)=XV(N)+X
YV(N)=YV(N)+Y
XYV(N)=XYV(N)+XY
EPXV(N)=EPXV(N)+(EPX*100.)/(AJ(N)*BK(N)-AK(N)*BJ(N))
EPYV(N)=EPYV(N)+(EPY*100.)/(AJ(N)*BK(N)-AK(N)*BJ(N))
GAMV(N)=GAMV(N)+GAM*100.*CCMM
C=(XV(N)+YV(N))/2.0
R=SQRT(((YV(N)-XV(N))/2.0)**2+XYV(N)**2)
XMAX(N)=C+R
XMIN(N)=C-R
PA(N)=0.5*57.29578*ATAN(2.*XYV(N)/(YV(N)-XV(N)))
IF(2.*XV(N)-XMAX(N)-XMIN(N))405,420,420
405 IF(PA(N)) 410,420,415
410 PA(N)=PA(N)+90.0
GO TO 420
415 PA(N)=PA(N)-90.0
420 ANG=PA(N)*11./630.
CC=COS(ANG)**2
SS=SIN(ANG)**2
SC=COS(ANG)*SIN(ANG)
EMAX(N)=EPXV(N)*CC+EPYV(N)*SS-SC*GAMV(N)
EMIN(N)=EPXV(N)*SS+EPYV(N)*CC+SC*GAMV(N)
IF(ITOPT.EQ.0) GO TO 421
IF(NITER.EQ.2) GO TO 421
XV(N)=XV(N)-X
YV(N)=YV(N)-Y
XYV(N)=XYV(N)-XY
EPXV(N)=EPXV(N)-(EPX*100.)/(AJ(N)*BK(N)-AK(N)*BJ(N))
EPYV(N)=EPYV(N)-(EPY*100.)/(AJ(N)*BK(N)-AK(N)*BJ(N))
GAMV(N)=GAMV(N)-GAM*100.*CCMM
421 CONTINUE
C
C
C FIND THE MAXIMUM AND MINIMUM PRINCIPAL STRESSES
SIG1=0.0
SIG2=0.0
M1=0
M2=0
DO 630 M=1,NUMEL
IF(XMAX(M).LT.SIG1) GO TO 631
SIG1=XMAX(M)
M1=M
631 IF(XMIN(M).GT.SIG2) GO TO 630

```



```

      SIG2=XMIN(M)
      M2=M
630  CONTINUE
      WRITE(6,117) JM
      WRITE (6,633) (SIG1,M1,SIG2,M2)
C
1851 DO 650 J=1,NUMNP
      IF(ITOPT.EQ.1.AND.NITER.EQ.1) GO TO 770
      XLOAD(J)=0.0
      YLOAD(J)=0.0
      XORD(J)=XORD(J)+DSX(J)
      YORD(J)=YCRD(J)+DSY(J)
      DSXQ(J)=DSX(J)+DSXQ(J)
      DSYQ(J)=DSY(J)+DSYQ(J)
      DSX(J)=0.0
      DSY(J)=0.0
      GO TO 650
770  DSXQ(J)=DSX(J)+DSXQ(J)
      DSYQ(J)=DSY(J)+DSYQ(J)
      IF (ITOPT.EQ.1.AND.NITER.EQ.1) GO TO 30
      WRITE (6,122) NFNUM(J),DSXQ(J),DSYQ(J)
30   DSXQ(J)=DSXQ(J)-DSX(J)
      DSYQ(J)=DSYQ(J)-DSY(J)
      IF(TAD(J).EQ.1.0) DSY(J)=0.0
      IF(TAD(J).EQ.2.0) DSX(J)=0.0
      IF(TAD(J).NE.0.0) GO TO 5001
      DSX(J)=0.0
      DSY(J)=0.0
5001 IF(TAL(J).EQ.1.0) YLOAD(J)=0.0
      IF(TAL(J).EQ.2.0) XLOAD(J)=0.0
      IF(TAL(J).NE.0.0) GO TO 650
      XLOAD(J)=0.0
      YLOAD(J)=0.0
650  CONTINUE
      IF (ITOPT.EQ.1.AND.NITER.EQ.1) GO TO 8002
      DO 6006 JJ=1,NUMNP
      KOUN(JJ)=0
      XN(JJ)=0.0
      YN(JJ)=0.0
      XYN(JJ)=0.0
6006 CONTINUE
      DO 6007 N=1,NUMEL
      DO 6007 II=1,3
      IF (II.EQ.1) JJ=NPI(N)
      IF (II.EQ.2) JJ=NPJ(N)
      IF (II.EQ.3) JJ=NPK(N)
      KOUN(JJ)=KOUN(JJ)+1
      XN(JJ)=XN(JJ)+XV(N)
      YN(JJ)=YN(JJ)+YV(N)
      XYN(JJ)=XYN(JJ)+XYV(N)
6007 CONTINUE
      DO 6008 JJ=1,NUMNP
      RK=KOUN(JJ)
      XN(JJ)=XN(JJ)/RK
      YN(JJ)=YN(JJ)/RK
      XYN(JJ)=XYN(JJ)/RK
      C=(XN(JJ)+YN(JJ))/2.
      R=SQRT (((YN(JJ)-XN(JJ))/2.)**2+XYN(JJ)**2)
      P3N(JJ)=C+R
      P1N(JJ)=C-R

```



```

      RPS(JJ)=P3N(JJ)/P1N(JJ)
6008 CONTINUE
8002 IF (KOPT.EQ.0) GO TO 664
      IF( ITOPT.GT.0.AND.NITER.EQ.1.AND.KOPT.GT.0) GO TO 664
      IF(KOUNT.GT.1) GO TO 681
      WRITE(6,121)
      WRITE(6,122)(NPNUM(M),DSXQ(M),DSYQ(M),M=1,NUMNP)
      WRITE(6,123)
      WRITE(6,124) (NUME(N),XV(N),YV(N),XYV(N),XMAX(N),XMIN(N),PA(N),
1EPXV(N),EPYV(N),EMAX(N),EMIN(N),N=1,NUMEL)
681  IF(NSTEP.EQ.1) GO TO 925
      IF(JM.EQ.NSTEP) GO TO 925
      IF(SIG1.LE.0.005) GO TO 664
C   TENSILE STRESS REMOVED
      DO 660 M=1,NUMEL
      IF(XMAX(M).LE.0.0) GO TO 660
      ANG=PA(M)*11./630.
      I=NPI(M)
      J=NPJ(M)
      K=NPK(M)
      AJ(M)=XORD(J)-XORD(I)
      AK(M)=XORD(K)-XORD(I)
      BJ(M)=YORD(J)-YORD(I)
      BK(M)=YORD(K)-YORD(I)
      AJ1=AJ(M)*COS(ANG)+BJ(M)*SIN(ANG)
      BJ1=-AJ(M)*SIN(ANG)+BJ(M)*COS(ANG)
      AK1=AK(M)*COS(ANG)+BK(M)*SIN(ANG)
      BK1=-AK(M)*SIN(ANG)+BK(M)*COS(ANG)
      R1I=XMAX(M)*(BK1-BJ1)/2.
      R1I=-R1I
      R1J=-XMAX(M)*BK1/2.
      R1J=-R1J
      R1K=XMAX(M)*BJ1/2.
      R1K=-R1K
      XMAX(M)=0.0
      XV(M)=XMIN(M)*(SIN(ANG)**2)
      YV(M)=XMIN(M)*(COS(ANG)**2)
      XYV(M)=XMIN(M)*SIN(ANG)*COS(ANG)
      IF(XMIN(M).LE.0.0) GO TO 661
      R2I=XMIN(M)*(AJ1-AK1)/2.
      R2I=-R2I
      R2J=XMIN(M)*AK1/2.
      R2J=-R2J
      R2K=-XMIN(M)*AJ1/2.
      R2K=-R2K
      XMIN(M)=0.0
      XV(M)=0.0
      YV(M)=0.0
      XYV(M)=0.0
      XLOAD(I)=COS(ANG)*R1I+XLOAD(I)-SIN(ANG)*R2I
      XLOAD(J)=COS(ANG)*R1J+XLOAD(J)-SIN(ANG)*R2J
      XLOAD(K)=COS(ANG)*R1K+XLOAD(K)-SIN(ANG)*R2K
      YLOAD(I)=SIN(ANG)*R1I+YLOAD(I)+COS(ANG)*R2I
      YLOAD(J)=SIN(ANG)*R1J+YLOAD(J)+COS(ANG)*R2J
      YLOAD(K)=SIN(ANG)*R1K+YLOAD(K)+COS(ANG)*R2K
      GO TO 660
661  XLOAD(I)=COS(ANG)*R1I+XLOAD(I)
      XLOAD(J)=COS(ANG)*R1J+XLOAD(J)
      XLOAD(K)=COS(ANG)*R1K+XLOAD(K)
      YLOAD(I)=SIN(ANG)*R1I+YLOAD(I)

```



```

        YLOAD(J)=SIN(ANG)*R1J+YLCAC(J)
        YLOAD(K)=SIN(ANG)*R1K+YLOAD(K)
660    CONTINUE
        WRITE(6,6)KOUNT
        GO TO 243
664    IF(ITOPT.GT.0.AND.NITER.EQ.1) GO TO 764
        WRITE (6,121)
        WRITE(6,122)(NPNUM(M),DSXQ(M),DSYQ(M),M=1,NUMNP)
        WRITE (6,123)
        WRITE (6,124) (NUME(I),XV(I),YV(I),XYV(I),XMAX(I),XMIN(I),PA(I),
1    EPXV(I),EPYV(I),EMAX(I),EMIN(I),I=1,NUMEL)
        WRITE (6,3051)
        WRITE(6,3050) (XN(I),YN(I),XYN(I),P1N(I),P3N(I),RPS(I),I=1,NUMNP)
3050    FORMAT(2X,6E12.5)
        IF (NWTAPE.GT.0) CALL SKIP (NFWRD,0,3)
        IF (NWTAPE.GT.0) WRITE (3) LNUM,NUMNP,NUMEL
        IF(NWTAPE.GT.0) WRITE (3)(NPNUM(I),DSXQ(I),DSYQ(I),I=1,NUMNP)
        IF (NWTAPE.GT.0) WRITE (3) (NUME(I),XV(I),YV(I),XYV(I),XMAX(I),
1    XMIN(I),PA(I),EPXV(I),EPYV(I),EMAX(I),EMIN(I),I=1,NUMEL)
        IF (NWTAPE.GT.0) WRITE (3) (XN(I),YN(I),XYN(I),P1N(I),P3N(I),
1    RPS(I),I=1,NUMNP)
        IF (NWTAPE.GT.0) ENDFILE 3
        IF (NWTAPE.GT.0) CALL SKIP (NBWRD,0,3)
C
C
C    INTERPOLATE MODULI FOR THE NEXT STEP OR FOR REPETITION OF SAME STEP
C
C
764    DO 501 JJ=1,NUMEL
        NCOUN=0
        IF(ITOPT.EQ.0) RO(JJ)=0.0
        IF(NITER.EQ.2) RC(JJ)=0.0
        IF (NANLYS.EQ.0) GO TO 501
        IF(KOPT.GT.0.AND.ITOPT.EQ.1.AND.NITER.EQ.1.AND.XMAX(JJ).GE.0.0) GO
1    TO 501
        AVGSIG=ABS(XMAX(JJ))
        IF(XMAX(JJ).GE.0.0)AVGSIG=0.001
        DIVS=ABS(XMIN(JJ))-AVGSIG
        DIVS=ABS(DIVS)
        N=MAT(JJ)
        DIVSF=ACOE(N)+BCOE(N)*ABS(XMAX(JJ))
        IF(XMAX(JJ).GE.0.0) DIVSF=ACOE(N)
        SIGM1=ABS(XMIN(JJ))
        SIGM2=(AVGSIG+SIGM1)/2.
        SIGM3=AVGSIG
        IF(IANLYS.GT.0) SIGM2=0.0
        IF(NCELP.EQ.0) GO TO 852
950    NCOUN=NCOUN+1
        SIGOCT=(SIGM1+SIGM2+SIGM3)/3.
        SIGIN=SIGM1*SIGM2*SIGM3
        CONF5=SIGIN/(SIGOCT**2)
        DIVOCT=SQRT((SIGM1-SIGM2)**2+(SIGM2-SIGM3)**2+(SIGM3-SIGM1)**2)
        DIVOCT=DIVOCT/3.
        DO 26 J=1,NCELP
            JLS=J
            IF( CONF5-SL(J,N)) 27,26,26
26    CONTINUE
27    CONTINUE
        DO 28 K=1,NSTRN
            JS1=K

```



```

      IF(DIVOC T-SD(K,JLS-1,N)) 29,28,28
28  CONTINUE
29  CONTINUE
      DO 751 K=1,NSTRN
      JS2=K
      IF(DIVOC T-SD(K,JLS,N)) 752,751,751
751  CONTINUE
752  CCNTINUE
      PR1=1.061*(VS(JS1,JLS-1,N)-VS(JS1-1,JLS-1,N))/(ST(JS1,N)-ST(JS1-1,
1N))-1.0
      IF(PR1.GT.0.49) PR1=0.49
      PR2=1.061*(VS(JS2,JLS ,N)-VS(JS2-1,JLS ,N))/(ST(JS2,N)-ST(JS2-1,
1N))-1.0
      IF(PR2.GT.0.49) PR2=0.49
      PR3=PR1+((PR2-PR1)*(CONF S-SL(JLS-1,N))/(9L(JLS,N)-SL(JLS-1,N)))
      IF(PR3.GT.0.49 ) PR3=0.49
      DIF1=SD(JS1,JLS-1,N)-SD(JS1-1,JLS-1,N)
      ETP1=DIF1/(ST(JS1,N)-ST(JS1-1,N))
      GTP1=ETP1/(0.9428*(1.+PR1))
      DIF2=SD(JS2,JLS,N)-SD(JS2-1,JLS,N)
      ETP2=DIF2/(ST(JS2,N)-ST(JS2-1,N))
      GTP2=ETP2/(0.9428*(1.+PR2))
      GTP=GTP1+ (GTP2-GTP1)*(CONF S -SL(JLS-1,N))/(SL(JLS,N)-SL(JLS-1,N))
      GTP=100.*GTP
      BULKM =GTP*2.*(1.+PR3)/(3.*(1.-2.*PR3))
      SHEARM=GTP
      IF(IANLYS.GT.0) GO TO 852
      SIGMM2=PR3*(SIGM1+SIGM3)
      SIGMM2=(SIGMM2+SIGM2)/2.
      STRS=ABS(SIGMM2-SIGM2)
      IF(NCDUN.GE.11) GO TO 851
      IF(ABS(SIGMM2-SIGM2).LT.0.01) GO TO 851
      SIGM2=SIGMM2
      GO TO 950
851  CONTINUE
852  IF (NCELP.GT.0) GO TO 8000
      NK=N
      JEJ=JJ
      CALL D1TEST(2)
8000 IF(NITER.EQ.1)TEBULK=BULKM
      IF(NITER.EQ.2)EBULK(JJ)=BULKM
      IF(ITOPT.GT.0.AND.NITER.EQ.1)EBULK(JJ)=(EBULK(JJ)+TEBULK)/2.
      IF(ITOPT.EQ.0.AND.NITER.EQ.1)EBULK(JJ)=TEBULK
      IF(NITER.EQ.1)TSHEAR=SHEARM
      IF(NITER.EQ.1.AND.CIVS.GE.DIVSF.AND.NTENS.GT.0) TSHEAR=EBULK(JJ)/5
10.
      IF(NITER.EQ.2)ESHEAR(JJ)=SHEARM
      IF(NITER.EQ.2.AND.CIVS.GE.DIVSF.AND.NTENS.GT.0) ESHEAR(JJ)=EBULK(J
1J)/50.
      IF(ITOPT.GT.0.AND.NITER.EQ.1)ESHEAR(JJ)=(ESHEAR(JJ)+TSHEAR)/2.
      IF(ITOPT.EQ.0.AND.NITER.EQ.1)ESHEAR(JJ)=TSHEAR
      IF(ESHEAR(JJ).GT.(1.45*EBULK(JJ)))ESHEAR(JJ)=1.45*EBULK(JJ)
      IF(ESHEAR(JJ).LT.(EBULK(JJ)/50.))ESHEAR(JJ)=EBULK(JJ)/50.
501  CONTINUE
      IF (ITOPT.EQ.1.AND.NITER.EQ.1) GO TO 31
      WRITE(6,110)
      WRITE(6,2055)(NUME(N),NPI(N),NPJ(N),NPK(N),EBULK(N),RO(N),ESHEAR(N
1), MAT(N), N=1,NUMEL)
31  IF(ITOPT.EQ.0) GO TO 500
      IF(NITER.EQ.1) GO TO 160

```



```

500  CONTINUE
C
      GO TO 925
C
C      PRINT OF ERRORS IN INPUT DATA
C
702  WRITE(6,712)LX
C
C      FORMAT STATEMENTS
C
      1  FORMAT(10I5)
      2  FORMAT(1I5,3I4,4E12.4,1F8.4)
      3  FORMAT(1I5,4F10.0,2F12.8)
      4  FORMAT (2I5,1F6.3)
      5  FORMAT (3E15.8)
      6  FORMAT(1I5)
      7  FORMAT(I4,6F8.0)
      8  FORMAT(2I4,2F8.0)
      9  FORMAT(4I5)
     13  FORMAT(6I5,2F10.0,3I5)
     20  FORMAT (2I5)
     21  FORMAT(7F5.0)
     23  FORMAT (1X,'LATSTRESS',6X, 6F8.3/)
     24  FORMAT (1X,'STRAIN',3X,1F6.2, 6F8.3/)
    40  FORMAT(12F6.0)
     99  FORMAT (1H1)
    100  FORMAT(19A4)
    101  FORMAT (30HNUMBER OF ELEMENTS           =1I4/)
    102  FORMAT (30H NUMBER OF NOCAL POINTS       =1I4/)
    103  FORMAT (30H NUMBER OF BOUNDARY PCINTS     =1I4/)
    104  FORMAT (30H CYCLE PRINT INTERVAL         =1I4/)
    105  FORMAT (30H OLTPUT INTERVAL OF RESULTS   =1I4/)
    106  FORMAT (30H CYCLE LIMIT                   =1I4/)
    107  FORMAT (30H TOLERANCE LIMIT               =1E12.4/)
    108  FORMAT (30H OVER RELAXATION FACTOR        =1F6.3)
    117  FORMAT (30H LIFT NUMBER                   =1I4/)
    109  FORMAT (1I8,4F12.6,2F12.8)
    110  FORMAT (74H1EL.  I   J   K           EBULK   DENSITY   ESHEAR
      1MAT NO.           )
    111  FORMAT(80H1           NP           X-ORD   Y-ORD   X-LOAD   Y-LOAD
      1   X-DISP   Y-DISP   )
    112  FORMAT(20H BOUNDARY CONDITIONS)
    119  FORMAT(34H0           CYCLE   FORCE UNBALANCE)
    120  FORMAT (1I12,1E20.6)
    121  FORMAT(42H0NCDAL POINT X-DISPLACEMENT Y-DISPLACEMENT)
    122  FORMAT (1I12,2E15.6)
    123  FORMAT(5H1ELNO 4X,8HX-STRESS 4X,8HY-STRESS 3X,9HXY-STRESS 2X,10HMA
      1X-STRESS 2X,10HMIN-STRESS 2X,9H0IRECTICN 3X,8HX-STRAIN 3X,8HY-STRA
      2IN 1X,10HMAX-STRAIN 1X,10HMIN-STRAIN)
    124  FORMAT(1I5,5E12.5,5E11.4)
    125  FORMAT(2I5,3E12.5)
    126  FORMAT(1I4,2E12.5)
    602  FORMAT(1I5,2F10.0)
    633  FORMAT ('0',
      1'MAX. PRINCIPAL STRESS=',F10.5,'AND OCCURS IN ELEM.',I6//
      2'MIN. PRINCIPAL STRESS=',F10.5,'AND OCCURS IN ELEM.',I6//)
    711  FORMAT(32H0ZERO OR NEGATIVE AREA, EL.NC. =1I4)
    712  FORMAT(33H0OVER 8 N.P. ADJACENT TO N.P. NO.1I4)

```



```

670  FORMAT(/,4I5,6F12.6)
753  FORMAT(2I5,F10.0)
823  FORMAT('1','NODE      X-STRESS      Y-STRESS      XY-STRESS      MAX.STRS
1      MIN.STRS      (P3/P1) '//)
824  FORMAT (30H NUMBER OF READ NODAL PCINTS =1I4/)
825  FORMAT (30H NUMBER OF READ ELEMENTS      =1I4/)
1010 FORMAT(I5,6F5.0)
1020 FORMAT(I5,4F15.6)
1030 FORMAT(3I5)
2000 FORMAT('0','NUMBER OF THE MATERIAL=' ,I5/)
2010 FORMAT(5F10.0)
2020 FORMAT('0',10X,'DENSITY=' ,F15.6//,10X,'BULK MODULUS=' ,F15.6//,10X,
1'SHEAR MODULUS=' ,F15.6//,10X,'ACOEFF=' ,F15.6//,10X,'BCOEFF=' ,F15.6)
2021 FORMAT(2I5,F10.0)
2051 FORMAT(1CF5.0)
2052 FORMAT(11F5.0)
2053 FORMAT('0',10X,'STRESS-STRAIN RELATIONSHIPS FOR MATERIAL=' ,I5//)
2055 FORMAT(I5,3I4,3E12.4,I5)
6005 FORMAT (I4,6E15.5)
8001 FORMAT ('1',' CALCULATED OVERBURDEN FACTOR' ,//)
3051 FORMAT (13H1NODE-XSTRESS 2X,12HNODE-YSTRESS 2X,13HNODE-XYSTRESS 2X
1,14HNODE-MAXSTRESS 2X,14HNODE-MINSTRESS 2X,16HNODE-STRESSRATIO)

C
C
C 925  STOP
C

END
SUBROUTINE FACTOR
COMMON/AREA1/ AJ(1400),BJ(1400),AK(1400),BK(1400)
COMMON/AREA2/ XORD(750),YORD(750),NPI(1400),NPJ(1400),NPK(1400),
1NPNUM(750),NUME(1400),NUMNP,NUMEL,NUMBC,NANLYS,JM,NSTEP
COMMON/AREA5/EBULK(1400),ESHEAR(1400),PA(1400),MAT(1400),RO(1400),
1XV(1400),YV(1400),XYV(1400),EPXV(1400),EPYV(1400),XMAX(1400),
2EMAX(1400),EMIN(1400),XVT(1400),YVT(1400),XYVT(1400),EPXVT(1400),
3EPYVT(1400),NELC(600),UEL(1400),OBFAC(1400),SIGM1,BULKM,SHEARM
4,SIGM2,SIGM3,XMIN(1400),XVT1(1400),YVT1(1400),XYVT1(1400)
READ (5,6) NSTEPF
DO 300 N=1,NSTEPF
READ (5,6) NSKIPF
IF (NSKIPF.EQ.0) GO TO 300
READ (5,7) MJ1,NUMELF,NGROUP
DO 300 NJ=1,NGROUP
READ (5,7) NEL1,NEL2
DO 300 M=NEL1,NEL2
II=NPI(M)
JJ=NPJ(M)
KK=NPK(M)
XCENT=(XORD(II)+XORD(JJ)+XCRD(KK))/3.
YCENT=(YORD(II)+YORD(JJ)+YCRD(KK))/3.
SAREA=0.0
ARC=0.0
DO 500 MJ=MJ1,NUMELF
I=NPI(MJ)
J=NPJ(MJ)
K=NPK(MJ)
IF (XORD(I).EQ.XCENT) GO TO 400
IF (XORD(J).EQ.XCENT) GO TO 400
IF (XORD(K).EQ.XCENT) GO TO 400
IF (XCENT.GT.XORD(I).AND.XCENT.LT.XORD(J)) GO TO 400
IF (XCENT.GT.XORD(J).AND.XCENT.LT.XORD(K)) GO TO 400

```



```

      IF (XCENT.GT.XORD(K).AND.XCENT.LT.XORD(I)) GO TO 400
      GO TO 500
400  YMID=(YORD(I)+YORD(J)+YCRD(K))/3.
      IF (YCENT.GT.YMID) GO TO 500
      AJ(MJ)=XCRD(J)-XCRD(I)
      AK(MJ)=XORD(K)-XORD(I)
      BJ(MJ)=YORD(J)-YCRD(I)
      BK(MJ)=YCRD(K)-YORD(I)
      AREA=(AJ(MJ)*BK(MJ)-AK(MJ)*BJ(MJ))*0.5
      SAREA=SAREA+AREA
      ARO=ARO+AREA*RO(MJ)
      YMAX=YCENT
      IF (YORD(I).GT.YMAX) YMAX=YORD(I)
      IF (YORD(J).GT.YMAX) YMAX=YORD(J)
      IF (YORD(K).GT.YMAX) YMAX=YORD(K)
500  CONTINUE
      YCON=YCENT
      IF (YORD(II).GT.YCCN) YCCN=YORD(II)
      IF (YORD(JJ).GT.YCCN) YCCN=YORD(JJ)
      IF (YORD(KK).GT.YCCN) YCCN=YORD(KK)
      OBFAC(M)=((YMAX-YCENT)*ARO/SAREA)/((YCON-YCENT)*RO(M))
300  CONTINUE
      6 FORMAT (15)
      7 FORMAT (315)
      8 FORMAT (15,F10.4)
      RETURN
      END
      SUBROUTINE TESTD
C
C
C
C  CCNVERSION OF TRIAXIAL TEST DATA FROM CONVENTICNAL FORM TO STRESS
C  INVARIANT FORM AND  INTERPOLATICN
C
C
C
      DIMENSION SL(20, 8),SD(20,10, 8),VS(20,10, 8),SIGINV(20,10, 8),
1  VSTN(20,10, 8)
      COMMCN/AREA3/
      1ST(20, 8),SIGINT(20, 8),TOCTD(20,10, 8),GOCT(20,10, 8),NUMAT,
2  NCELP,CONFAC,NSTRN
C
C
C
C  READ CELL PRESSURE DATA FOR GIVEN MATERIALS
C
C
      DO 10 N=1,NUMAT
      READ(5,1010) (SL(J,N),J=1,NCELP)
      DO 15 J=1,NCELP
      SL(J,N)=SL(J,N)*CCNFAC
      SIGINT(J,N)=SL(J,N)
15  CONTINUE
C
C
C  READ DEVIATORIC STRESS DATA FOR GIVEN MATERIALS
C
C
      DO 20 K=1,NSTRN
      READ(5,1020) ST(K,N),(SD(K,J,N),J=1,NCELP)

```



```

DO 25 J=1,NCELP
SD(K,J,N)=SD(K,J,N)*CONFAC
25 CONTINUE
20 CONTINUE
WRITE (6,1030) N
WRITE(6,1040) (SL(J,N),J=1,NCELP)
C
C
C READ VOLUMETRIC STRAIN DATA FOR GIVEN MATERIALS
C
C
DO 30 K=1,NSTRN
READ (5,1020) ST(K,N),(VS(K,J,N),J=1,NCELP)
WRITE(6,1050) ST(K,N),(VS(K,J,N),J=1,NCELP)
30 CONTINUE
DO 35 K=1,NSTRN
WRITE(6,1050) ST(K,N),(SD(K,J,N),J=1,NCELP)
35 CONTINUE
10 CONTINUE
DO 40 N=1,NUMAT
DO 45 J=1,NCELP
DO 50 K=1,NSTRN
PROD= (SL(J,N)**2)*(SD(K,J,N)+SL(J,N))
SIGOCT=SL(J,N)+(SD(K,J,N))/3.
IF(J.EQ.1.AND.K.EQ.1) GO TO 51
SIGINV(K,J,N)=PROD/(SIGOCT**2)
51 IF(J.EQ.1.AND.K.EQ.1) SIGINV(K,J,N)=0.0
50 CONTINUE
45 CONTINUE
DO 70 I=1,NCELP
DO 55 K=1,NSTRN
DO 60 J=1,NCELP
JLS=J
IF(SIGINT(I,N)-SIGINV(K,J,N))61,60,60
60 CONTINUE
61 CONTINUE
TOCTD(K,I,N)=SD(K,JLS-1,N)+(SD(K,JLS,N)-SD(K,JLS-1,N))*(SIGINT(I,N)
1)-SIGINV(K,JLS-1,N))/(SIGINV(K,JLS,N)-SIGINV(K,JLS-1,N))
TOCTD(K,I,N)=TOCTD(K,I,N)*0.4714
VSTN(K,I,N)=VS(K,JLS-1,N)+(VS(K,JLS,N)-VS(K,JLS-1,N))*(SIGINT(I,N)
1-SIGINV(K,JLS-1,N))/(SIGINV(K,JLS,N)-SIGINV(K,JLS-1,N))
GOCT(K,I,N)=0.4714*(3.*ST(K,N)-VSTN(K,I,N))
55 CONTINUE
70 CONTINUE
40 CONTINUE
1000 FORMAT(3I5,F10.0)
1010 FORMAT(10F5.0)
1020 FORMAT(11F5.0)
1030 FORMAT('0','DATA IN CONVENTIONAL FORM FOR MATERIAL NO.',I5/)
1031 FORMAT('0','DATA IN STRESS INVARIANT FORM FOR MATERIAL NO.',I5/)
1040 FORMAT(1X,'LATSTRESS',6X,10F8.3/)
1041 FORMAT(1X,'J3/(SIGOCT)**2',1X,10F8.3/)
1050 FORMAT(1X,'STRAIN',3X,F6.2,10F8.3/)
1060 FORMAT(I5)
1070 FORMAT(3F10.0)
1071 FORMAT(3F8.3,4F12.4)
RETURN
C
END
SUBROUTINE RTAPES (NC)

```



```

COMMON/AREA2/ XORD(750),YORD(750),NPI(1400),NPJ(1400),NPK(1400),
1 NPNUM(750),NUME(1400),NUMNP,NUMEL,NUMBC,NANLYS,JM,NSTEP
COMMON/AREA3/
1      ST(20,8),SL(20,8),SD(20,10,8),VS(20,10,8),NUMAT,
2 NCELP,CONFAC,NSTRN
COMMON/AREA4/ XLOAD(750),YLOAD(750),DSX(750),DSY(750),DSXQ(750),
1 DSXQ(750),XN(750),YN(750),RPS(750),DSXQT(750),DSYQT(750),
2 XLOAD1(750),YLOAD1(750),XLOAD2(750),YLOAD2(750),SLOPE(60),NPB(60),
3 NFIX(60),PIN(750),P3N(750),KDUN(750),XYN(750)
COMMON/AREA5/EBULK(1400),ESHEAR(1400),PA(1400),MAT(1400),RO(1400),
1 XV(1400),YV(1400),XYV(1400),EPXV(1400),EPYV(1400),XMAX(1400),
2 EMAX(1400),EMIN(1400),XVT(1400),YVT(1400),XYVT(1400),EPXVT(1400),
3 EPYVT(1400),NELC(600),UEL(1400),DBFAC(1400),SIGM1,BULKM,SHEARM
4 ,SIGM2,SIGM3,XMIN(1400),XVT1(1400),YVT1(1400),XYVT1(1400)
DIMENSION UELC(1400),U(800)

C
C
C
      IF (NC.EQ.2) GO TO 70
      READ (3) NUMEL,NUMNP,NUMBC,NUMAT,NANLYS
      READ (3) (XORD(N),YORD(N),XLOAD(N),YLOAD(N),DSX(N),DSY(N),
1 N=1,NUMNP)
      READ (3) (NUME(N),NPI(N),NPJ(N),NPK(N),EBULK(N),RO(N),ESHEAR(N),
1 MAT(N),DBFAC(N),N=1,NUMEL)
      READ (3) (NPB(N),NFIX(N),SLOPE(N),N=1,NUMBC)
      DO 150 I=1,NUMNP
150 NPNUM(I)=I
      GO TO 100
      70 READ (5,1050) NCCODE,NFPPR
      READ (5,1000) NFTST
      DO 160 I=1,NUMEL
160 UEL(I)=0.0
      IF (NCCODE.EQ.0) GO TO 30
      READ (2,1000) NUMCP
      READ (2,1017) (U(N),N=1,NUMCP)
      READ (2,2015) ISTEP,NT,NUMCN,NCOUNT
      WRITE (6,2015) ISTEP,NT,NUMCN,NCOUNT
      READ (2,1017) (UEL(N),N=1,NUMCN)
      WRITE (6,1017) (UEL(N),N=1,NUMCN)
      CALL SKIP (NFPPR,0,2)
      DO 20 M=1,NUMCN
      I=NELC(M)
      UEL(I)=UEL(M)
20 CONTINUE
30 CALL SKIP (NFTST,0,3)
      READ (3) LNUM,NUMNP,NUMEL
      READ (3) (NPNUM(I),DSXQT(I),DSYQT(I),I=1,NUMNP)
      READ (3) (NUME(I),XVT(I),YVT(I),XYVT(I),XMAX(I),XMIN(I),PA(I),
1 EPXVT(I),EPYVT(I),EMAX(I),EMIN(I),I=1,NUMEL)
      READ (3) (XN(I),YN(I),XYN(I),PIN(I),P3N(I),RPS(I),I=1,NUMNP)
100 RETURN
1000 FORMAT (I5)
1017 FORMAT (8F10.3)
1050 FORMAT (2I5)
2015 FORMAT (4I5)
END
SUBROUTINE D1TEST(N1D)
COMMON/AREA2/ XORD(750),YORD(750),NPI(1400),NPJ(1400),NPK(1400),
1 NPNUM(750),NUME(1400),NUMNP,NUMEL,NUMBC,NANLYS,JM,NSTEP
COMMON/AREA3/

```



```

1      ST(20,8),SL(20,8),SD(20,10,8),VS(20,10,8),NUMAT,
2NCELP,CONFAC,NSTRN
COMMON/AREA5/EBULK(1400),ESHEAR(1400),PA(1400),MAT(1400),RO(1400),
1XV(1400),YV(1400),XYV(1400),EPXV(1400),EPYV(1400),XMAX(1400),
2EMAX(1400),EMIN(1400),XVT(1400),YVT(1400),XYVT(1400),EPXVT(1400),
3EPYVT(1400),NELC(600),UEL(1400),DBFAC(1400),SIGM1,BULKM,SHEARM
4,SIGM2,SIGM3,XMIN(1400),XVT1(1400),YVT1(1400),XYVT1(1400)
COMMON/AREA6/NK,ITOPT,NITER,JEJ,AP,CDR(8),AR(8),XUR(8),
1CD(1400),AA(1400),XU(1400)
IF (N1D.EQ.2) GO TO 5
READ (5,301) AP
301 FORMAT (F10.0)
DO 302 I=1,NUMAT
302 READ (5,303) CDR(I),AR(I),XUR(I)
303 FORMAT (3F10.0)
DO 6001 M=1,NUMEL
I=MAT(M)
CD(M)=CDR(I)
AA(M)=AR(I)
6001 XU(M)=XUR(I)
DO 6000 M=1,NUMEL
IF (RO(M).LE.0.0) GO TO 6000
I=NPI(M)
J=NPJ(M)
K=NPK(M)
Y1=ABS(YORD(I)-YORD(J))
Y2=ABS(YORD(J)-YORD(K))
Y3=ABS(YORD(K)-YORD(I))
DEPTH=0.0
IF (Y1.GT.DEPTH) DEPTH=Y1
IF (Y2.GT.DEPTH) DEPTH=Y2
IF (Y3.GT.DEPTH) DEPTH=Y3
DEPTH=DEPTH/2.
OBP=DEPTH*RO(M)*DBFAC(M)
SXU=(1.0-2.0*XU(M))*(1.0+XU(M))/(1.0-XU(M))
ET=(SXU*OBP*(AP)**AA(M))/(CD(M)*AA(M)*OBP**AA(M))
EBULK(M)=ET/(3.*(1.-2.*XU(M)))
ESHEAR(M)=ET/(2.*(1.+XU(M)))
6000 CONTINUE
GO TO 6
5 SXU=(1.0-2.0*XU(JEJ))*(1.0+XU(JEJ))/(1.0-XU(JEJ))
ET=(SXU*SIGM1*(AP)**AA(JEJ))/(CD(JEJ)*AA(JEJ)*SIGM1
1**AA(JEJ))
BULKM =ET/(3.*(1.-2.*XU(JEJ)))
SHEARM =ET/(2.*(1.+XU(JEJ)))
6 RETURN
END

```


APPENDIX C

DETAILS OF MV GAUGE INSTALLATION AND FIELD BEDROCK MOVEMENT DATA

In Fig. C.1 of this appendix the installation details of a typical MV gauge in Mica Dam are shown. Each new section of casing, which is about 5 feet long on average, is installed by excavating a pit of 8 to 10 feet deep in the compacted fill. After the installation, finer backfill material is placed and compacted with hand-guided compactor. Elevation of the bottom of each casing section is measured as installed. This elevation is the original elevation of each measuring point along the gauge. The change in elevation of the bottom of casing is referred to as the settlement of dam fill. It can be noted from the field observation data that top two or three sections of casings generally do not display any change in elevation at the current fill height even though certain magnitude of overburden pressure exists.

The bedrock movements measured by MV gauges concerned in this study are shown in Figs. C.2 to C.8. These movements are plotted against the elevations of dam fill during construction. These information have been used to derive the incremental boundary displacements which are imposed in the analysis described in Chapter V. From Fig. C.2 where the movements at the surface and a depth of 30 feet in the bedrock

are shown, the compressibilities of the upper bedrock may be estimated and listed as in Table C.1.

TABLE C.1

COMPRESSIBILITY OF UPPER BEDROCK

Fill Elev. (ft.)	Overburden [*] Pressure (Ksf)	Compression of 30' Layer (ft.)	Compressive [†] Strain (%)	One-Dimensional Compressibility $\frac{\epsilon_v}{\sigma_v}$ (Ksf ⁻¹)	One-Dimensional Modulus $\frac{\sigma_v}{\epsilon_v}$ (Ksf)
1765	4.65	0.06	0.20	0.00043	2325
1980	37.98	0.08	0.267	0.00007	14224
2170	67.43	0.11	0.367	0.000054	18373
2210	73.63	0.11	0.367	0.00005	20063
2300	87.58	0.12	0.40	0.000046	21895

^{*}Bulk Density Multiplied by Height of Fill Around MV5

[†]Calculated Based on 30 ft. Thickness

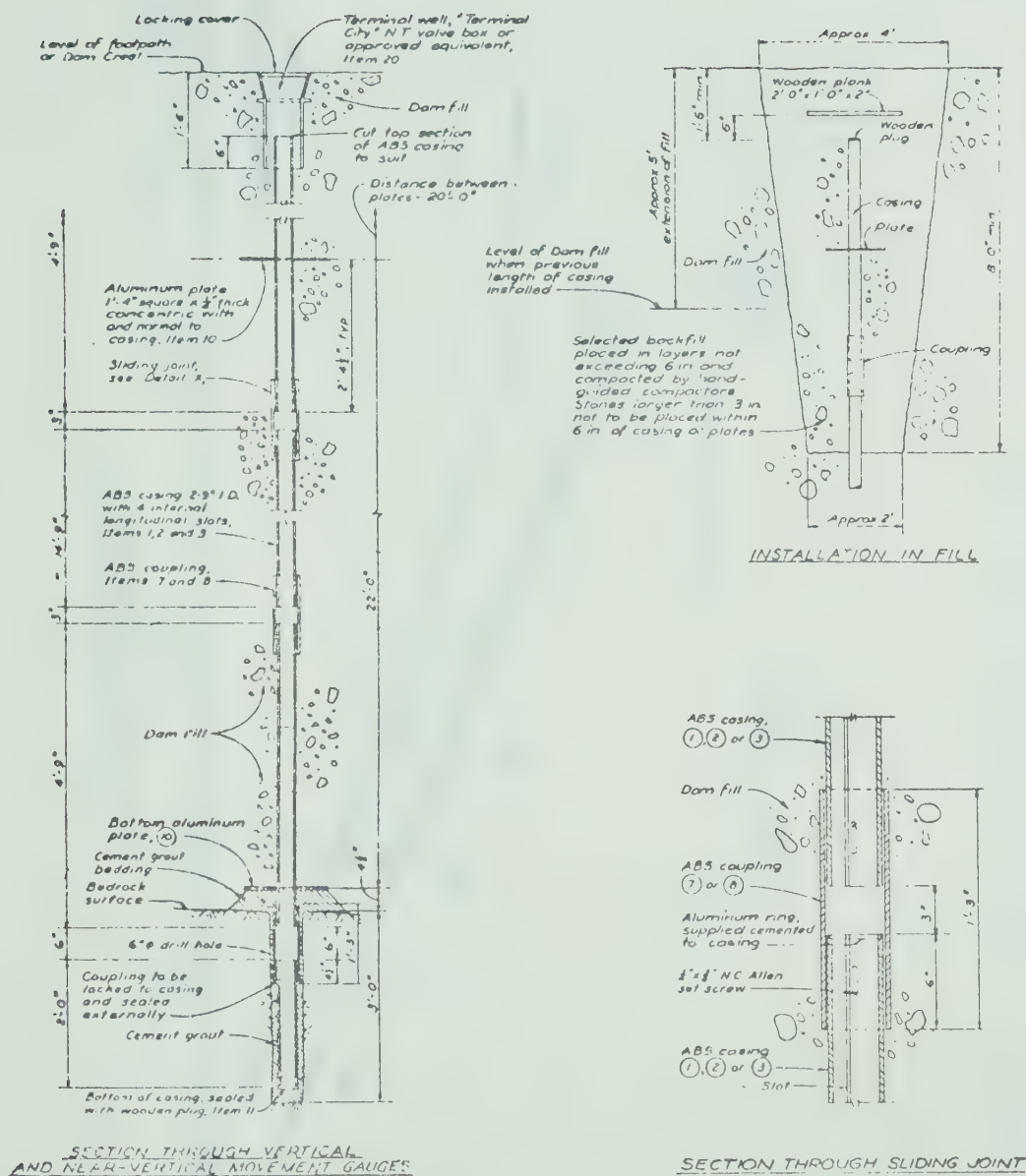


Fig. C.1 Details of Installment of a Typical MV Gauge (after CASECO report)

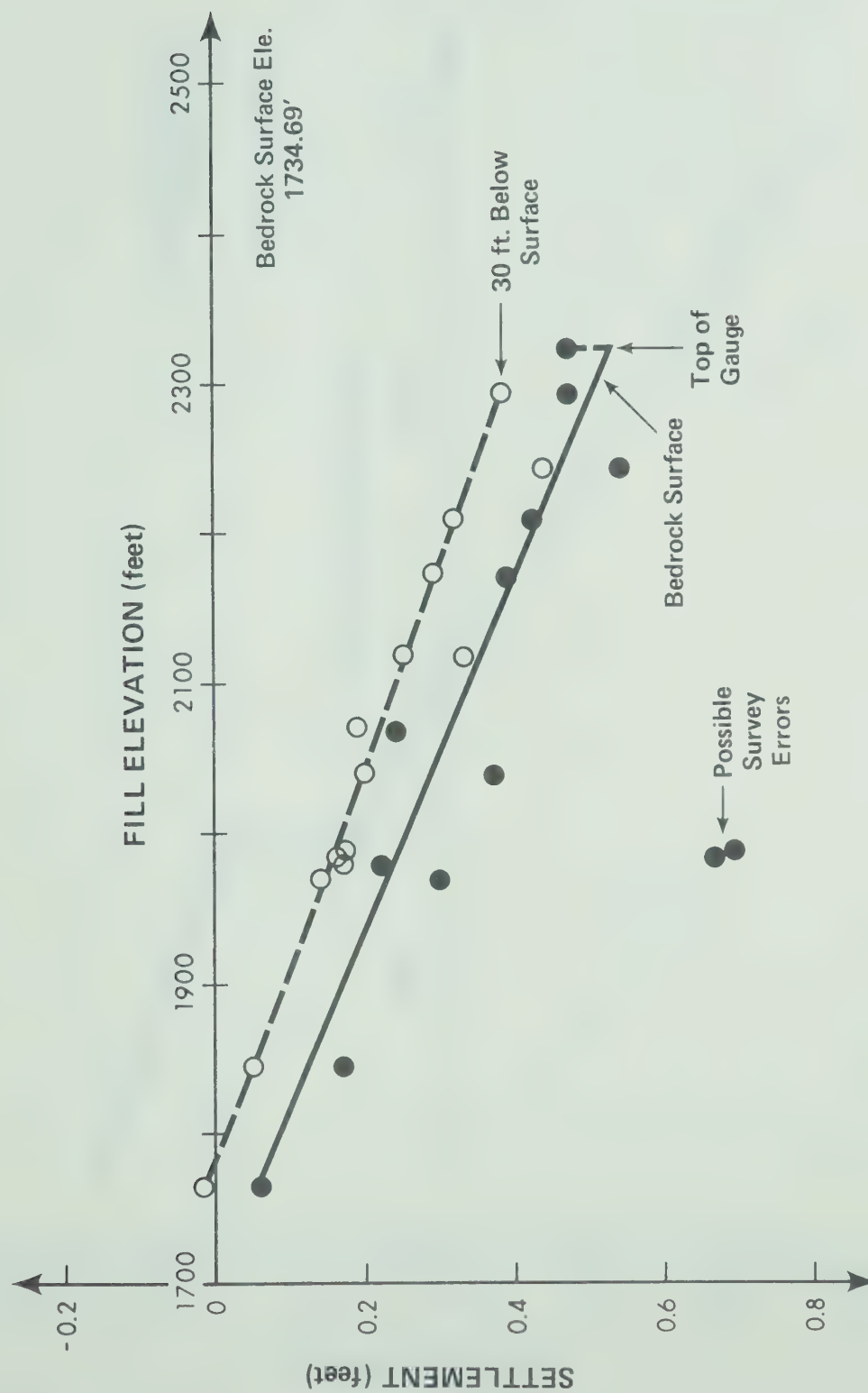


Fig. C.2 Bedrock Movement Under MV5

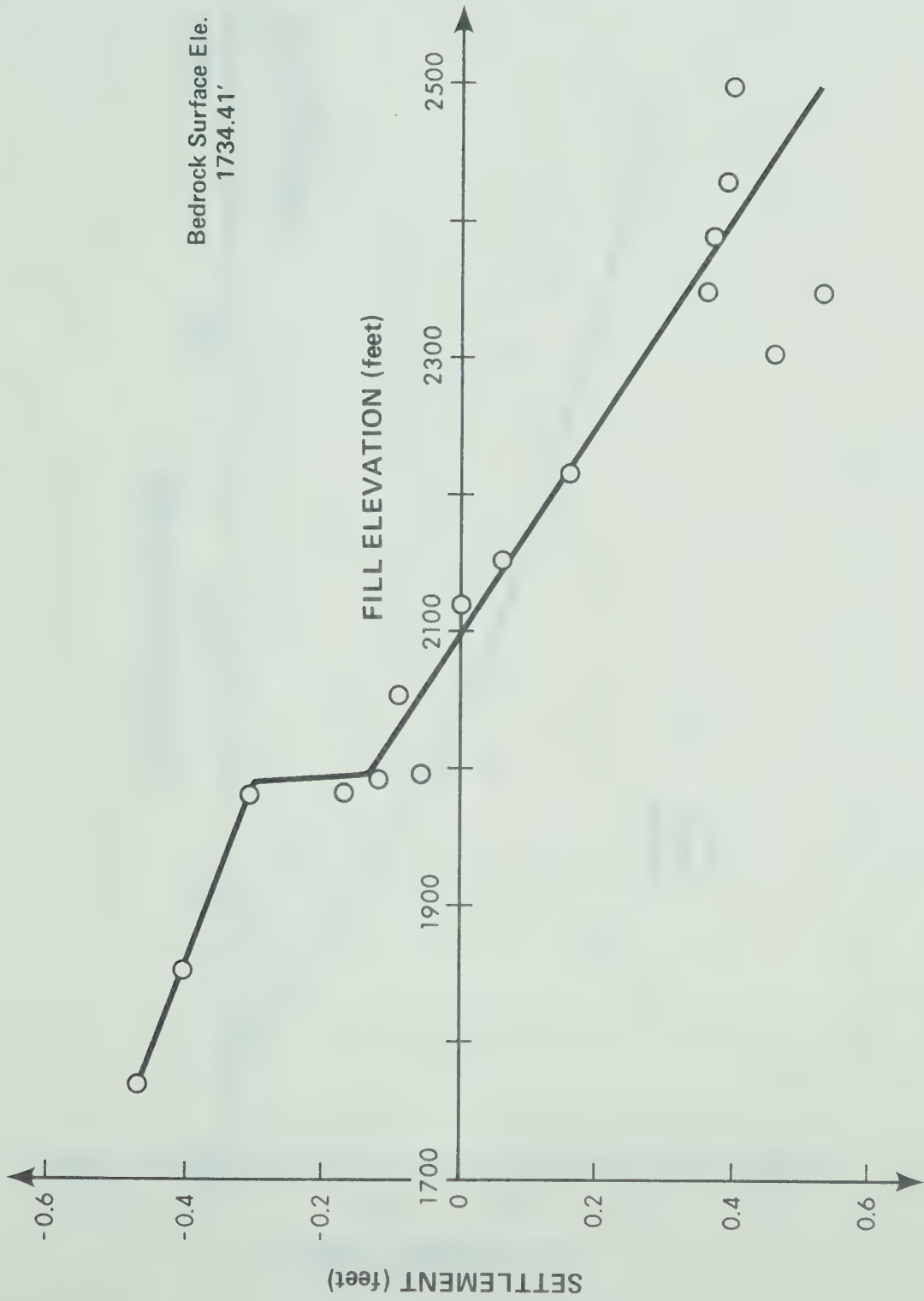


Fig. C.3.3 Bedrock Movement Under MV8

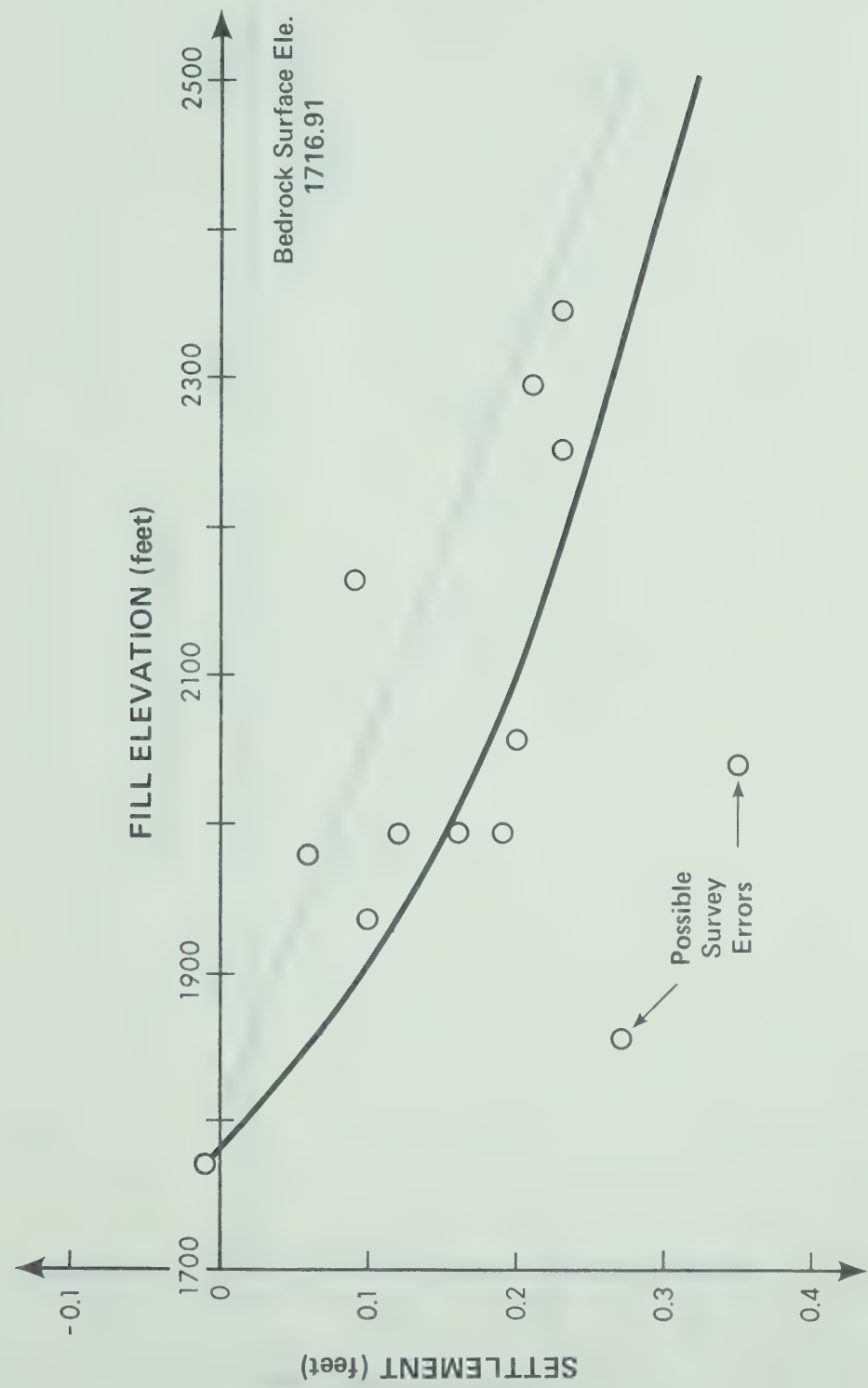


Fig. C.4 Bedrock Movement Under MV9

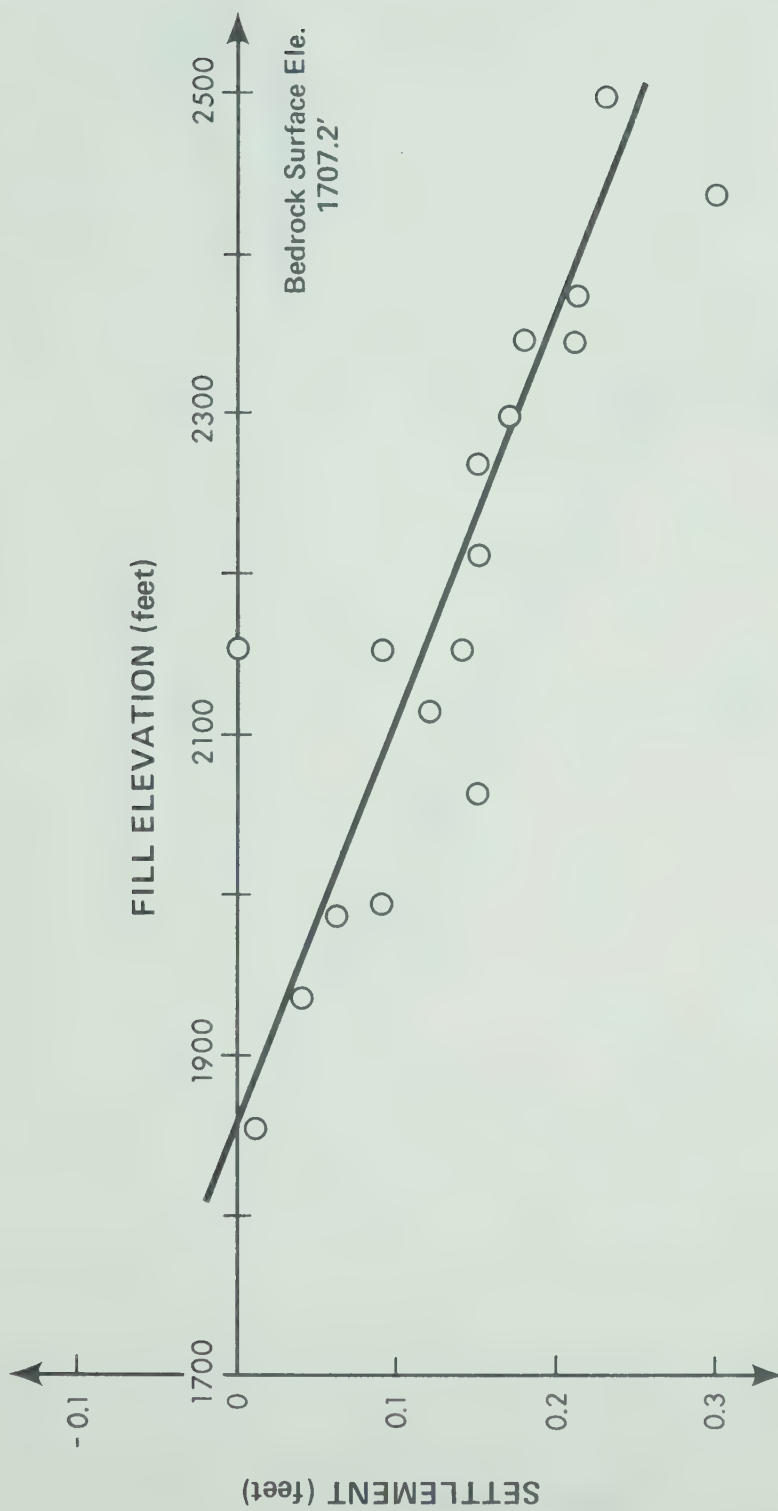


Fig. C.5 Bedrock Movement Under MV10

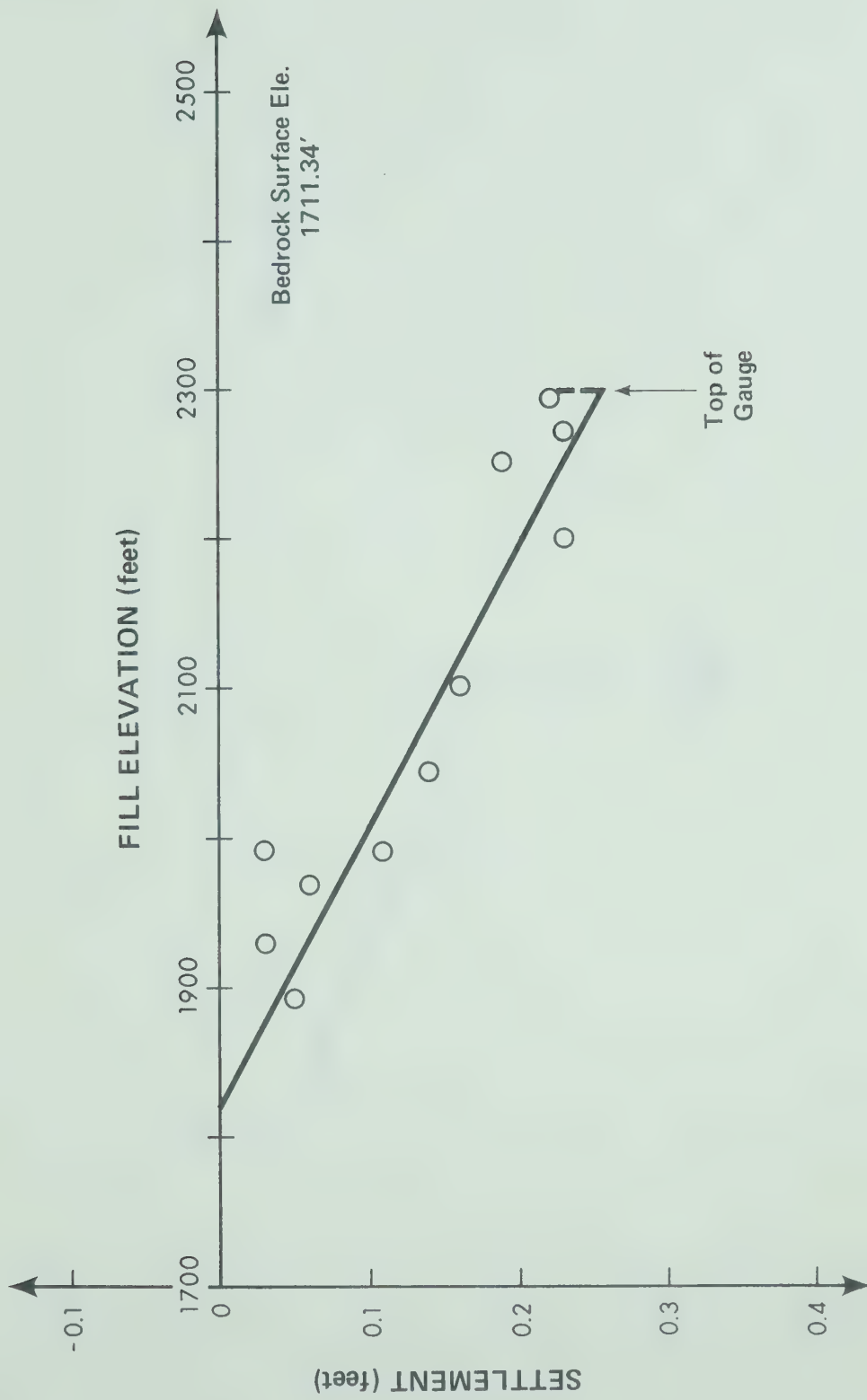


Fig. C.6 Bedrock Movement Under MV11

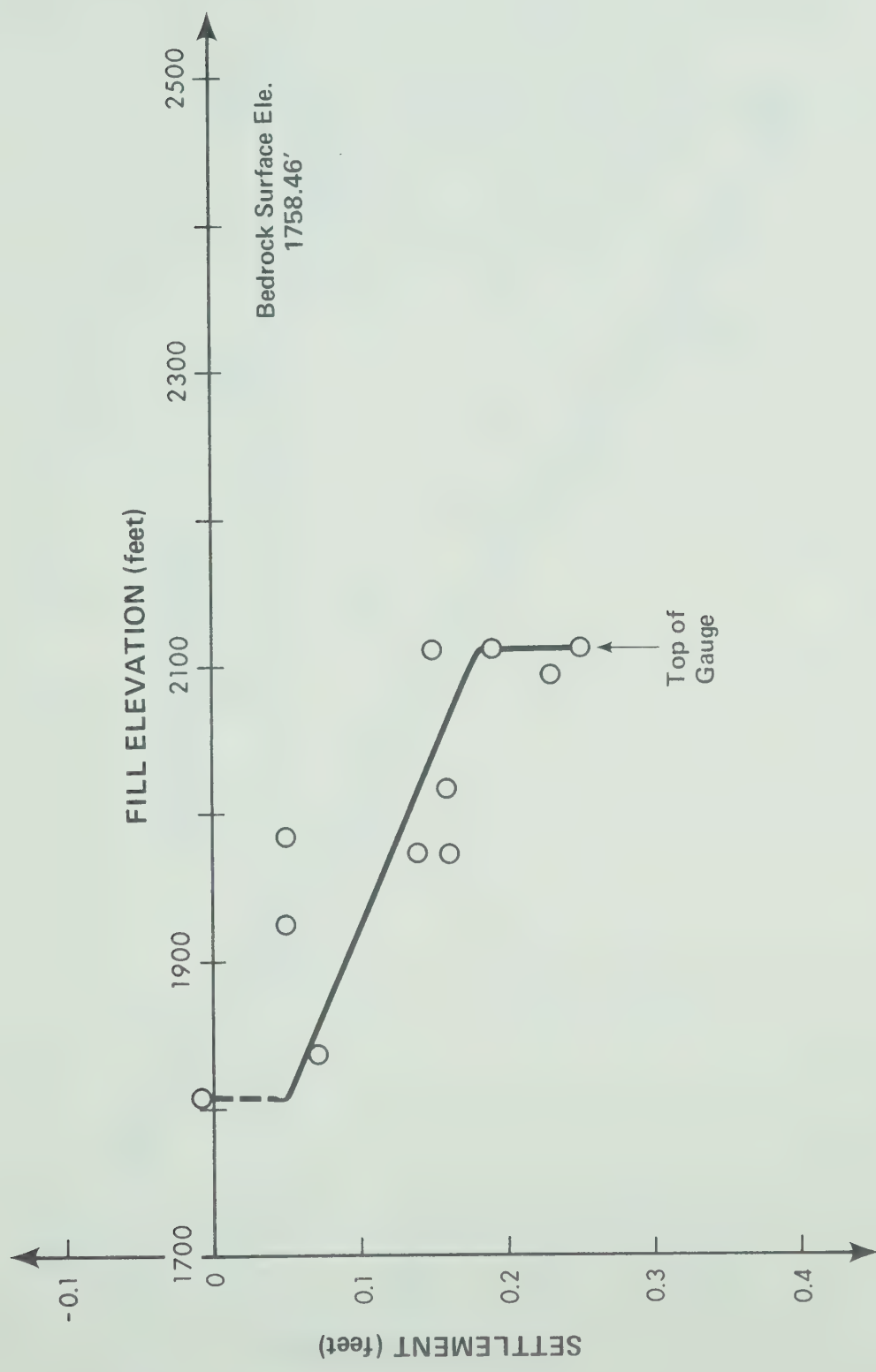


Fig. C.7 Bedrock Movement Under MV12

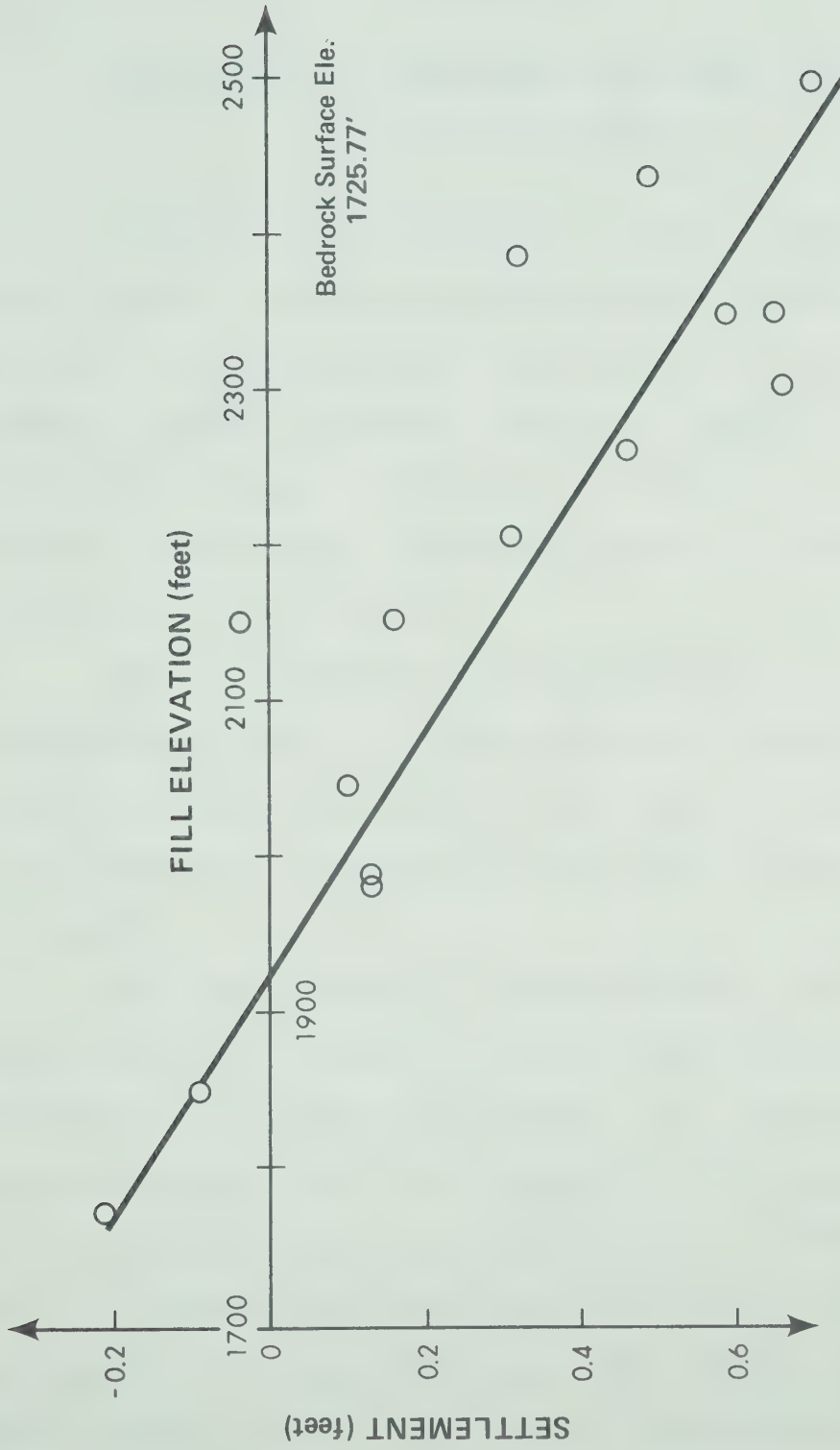


Fig. C.8 Bedrock Movement Under MV15

APPENDIX D

DERIVATION OF EMBANKMENT SETTLEMENT EXCLUDING THE BEDROCK MOVEMENT

Vertical or near-vertical movement gauges installed in the dam are generally anchored to the bedrock. The measured settlements, which are referred to the elevation changes of measuring points along the gauges, are the results of the compression of dam fill and bedrock. The general shape of the measured settlement profile is shown schematically as in (c) of Fig. D.1.

In simplified analyses, bedrock has often been assumed as undeformed media. In these cases the comparisons between analysis results and field data may be more appropriately made if the embankment settlements excluding the bedrock movements are known.

For illustration of the derivation a fill which has been placed to a height of h above bedrock surface is considered and shown in (a) of Fig. D.1. The variations of bedrock settlement with the height of fill are assumed as in (b) of Fig. D.1. The accumulative bedrock settlements when the fill reaches elevation A and the current height h are designated with $(\delta_B)_A$ and $(\delta_B)_h$ respectively. For measuring point A which initial elevation is established after the bedrock has deformed $(\delta_B)_A$, the elevation changes up to the

current height may have only included the bedrock movement of $[(\delta_B)_h - (\delta_B)_A]$. Thus, the embankment settlement excluding the bedrock movement for measuring point A may be approximately determined by subtracting $[(\delta_B)_h - (\delta_B)_A]$ from the measured settlement. The resulted embankment settlement profile is illustrated in (c) of Fig. D.1.

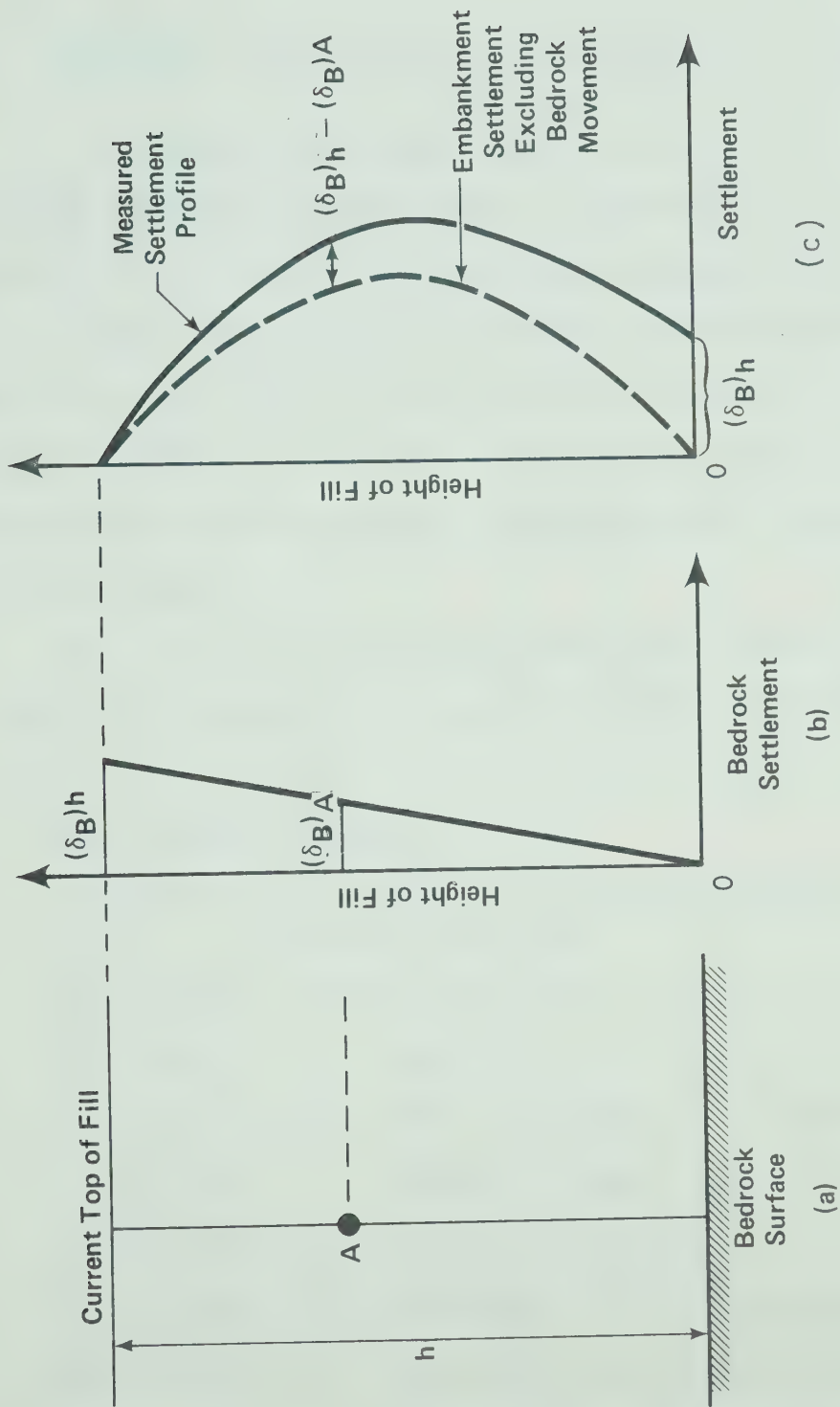


Fig. D.1 Embankment Settlement Excluding Bedrock Movement

APPENDIX E

HYPERBOLIC STRESS-STRAIN RELATIONSHIP PROGRAM

This appendix presents the subroutine used for describing nonlinear stress-strain behaviour of soil with hyperbolic relationship. The method proposed by Kulhawy et al., (1969) for deriving nonlinear tangent modulus and tangent Poisson's ratio from triaxial test data is used. By replacing this subroutine to subroutine DITEST in Appendix B, the analysis with hyperbolic stress-strain relationships can be performed.

For the case when this subroutine is used, item (13) of input data procedure in Appendix B has to be supplied as follows:

(a) Card 1 (F 10.0)

1-10 AP (Atmospheric pressure expressed in the same unit as stresses)

(b) Cards = NUMAT (8F 8.0)

1-8 HCR () (Cohesion C)

9-16 HIR () (Friction angle ϕ in degrees)

17-24 HKR () (Modulus number K_h)

25-32 HRR () (Failure ratio R_f)

33-40 HGR () (Poisson's ratio parameter (G_h))

41-48 HFR () (Poisson's ratio parameter F)

49-56 HDR () (Poisson's ratio parameter d)

57-64 HNR () (Modulus exponent n)


```

SUBROUTINE D1TEST(N1D)
COMMON/AREA2/ XORD(750),YORD(750),NFI(1400),NPJ(1400),NPK(1400),
1NPNUM(750),NUME(1400),NUMNP,NUMEL,NUMBC,NANLYS,JM,NSTEP
COMMON/AREA3/
1  ST(20,8),SL(20,8),SD(20,10,8),VS(20,10,8),NUMAT,
2NCELP,CONFAC,NSTRN
COMMON/AREA5/EBULK(1400),ESHEAR(1400),PA(1400),MAT(1400),RO(1400),
1XV(1400),YV(1400),XYV(1400),EPXV(1400),EPYV(1400),XMAX(1400),
2EMAX(1400),EMIN(1400),XVT(1400),YVT(1400),XYVT(1400),EPXVT(1400),
3EPYVT(1400),NELC(600),UEL(1400),OBFAC(1400),SIGM1,BULKM,SHEARM
4,SIGM2,SIGM3,XMIN(1400),XVT1(1400),YVT1(1400),XYVT1(1400)
COMMON/AREA6/NK,ITOPT,NITER,JEJ,AP,CCR(8),AR(8),XUR(8),
1CD(1400),AA(1400),XU(1400)
DIMENSION HCR(8),HIR(8),HKR(8),HRR(8),HGR(8),HFR(8),HDR(8),
1HNR(8)
IF (N1D.EQ.2) GO TO 5
READ (5,301) AP
301 FORMAT (F10.0)
DO 302 I=1,NUMAT
302 READ (5,303) HCR(I),HIR(I),HKR(I),HRR(I),HGR(I),HFR(I),HDR(I),
1HNR(I)
303 FORMAT (8F8.0)
DO 6000 M=1,NUMEL
IF (RO(M).LE.0.0) GO TO 6000
I=NPI(M)
J=NPJ(M)
K=NPK(M)
Y1=ABS(YORD(I)-YORD(J))
Y2=ABS(YORD(J)-YORD(K))
Y3=ABS(YORD(K)-YORD(I))
DEPTH=0.0
IF (Y1.GT.DEPTH) DEPTH=Y1
IF (Y2.GT.DEPTH) DEPTH=Y2
IF (Y3.GT.DEPTH) DEPTH=Y3
DEPTH=DEPTH/2.
NCOUNT=0
N=MAT(M)
HC=HCR(N)
HI=HIR(N)
HK=HKR(N)
HR=HRR(N)
HG=HGR(N)
HF=HFR(N)
HD=HDR(N)
HN=HNR(N)
OBP=DEPTH*RO(M)*OBFAC(M)
AVGSIG=OBP*0.5
18 NCOUNT=NCOUNT+1
SIGMM3=AVGSIG
XP=(HG-HF*ALOG10(SIGMM3/AP))/(1.-HD*( OBP -
1SIGMM3)/(HK*AP*((SIGMM3/AP)**HN)*(1.-HR*( OBP -
2SIGMM3)*(1.-SIN(HI*3.1416/180.)))/(2.*HC*COS(HI*3.1416/180.))+
32.*SIGMM3*SIN(HI*3.1416/180.)))))**2
IF (XP.GT.0.480) XP=C.480
CONST=XP/(1.-XP)

```



```

HPR=OBP*CONST
HPR=(HPR+AVGSIG)/2.
IF (NCOUNT.GE.21) GO TO 52
IF (ABS(HPR-AVGSIG).LT.0.01) GO TO 52
AVGSIG=HPR
GO TO 18
52 CONTINUE
ET=((1.-HR*(1.-SIN(HI*3.1416/180.)))*( OBP -
1 HPR )/(2.*HC*COS(HI*3.1416/180.))+2.*HPR *SIN(HI*3.1416/
2180.)))*2 )*HK*AP*(HPR /AP)**HN
ESHEAR(M)=ET/(2.*(1.+XP))
EBULK(M)=ESHEAR(M)*2.*(1.+XP)/(3.*(1.-2.*XP))
6000 CONTINUE
GO TO 6
5 IF (SIGM3.LE.0.300.AND.ITOPT.GT.0.AND.NITER.EQ.1) ESHEAP(JEJ)=0.
IF (SIGM3.LE.0.300.AND.ITOPT.GT.0.AND.NITER.EQ.1) SHEARM=0.0
IF (SIGM3.LE.0.300.AND.ITOPT.GT.0.AND.NITER.EQ.2) SHEARM=0.0
IF (SIGM3.LE.0.300.AND.ITOPT.GT.0.AND.NITER.EQ.1)
1BULKM=EBULK(JEJ)
IF (SIGM3.LE.0.300.AND.ITOPT.GT.0.AND.NITER.EQ.2) BULKM=EBULK(JEJ)
IF (SIGM3.LE.0.300) GO TO 6
HC=HCR(NK)
HI=HIR(NK)
HK=HKR(NK)
HR=HRR(NK)
HG=HGR(NK)
HF=HFR(NK)
HD=HDR(NK)
HN=HNR(NK)
XP=(HG-HF*ALOG10(SIGM3 /AP))/(1.-HD*(SIGM1 -
1SIGM3 )/(HK*AP*((SIGM3 /AP)**HN)*(1.-HR*(SIGM1 -
2SIGM3 )*(1.-SIN(HI*3.1416/180.)))/(2.*HC*COS(HI*3.1416/180.))+
32.*SIGM3 *SIN(HI*3.1416/180.)))))**2
IF (XP.GT.0.480) XP=0.480
ET=((1.-HR*(1.-SIN(HI*3.1416/180.)))*(SIGM1 -
1SIGM3 )/(2.*HC*COS(HI*3.1416/180.))+2.*SIGM3 *SIN(HI*3.1416/
2180.)))*2 )*HK*AP*(SIGM3 /AP)**HN
SHEARM=ET/(2.*(1.+XP))
BULKM=SHEARM*2.*(1.+XP)/(3.*(1.-2.*XP))
6 RETURN
END

```


B30135